Development of novel nucleating and clarifying agents for polypropylene

Entwicklung von neuartigen Nukleierungsmitteln und Transparenzverstärkern für Polypropylen

TECHNISCHE UNIVERSITÄT DARMSTADT

vom Fachbereich Chemie

der Technischen Universität Darmstadt

zur Erlangung des Grades

Doctor rerum naturalium

(Dr. rer. nat.)

Dissertation

von

Felix Budde

Erstgutachter:	Prof. Dr. Matthias Rehahn
Zweitgutachter:	Prof. Dr. Markus Busch

Darmstadt 2018

Tag der Einreichung: 18. Mai 2018

Tag der mündlichen Prüfung: 09. Juli 2018

Diese Arbeit wurde unter der Leitung von Herrn Professor Dr. Matthias Rehahn in der Zeit von Dezember 2014 bis Dezember 2017 am Fraunhofer LBF durchgeführt.

The following patent applications, based on the work of the present thesis, have been submitted:

EP 18163470	Polymer composition comprising diacetal derivatives	22.03.2018
EP 18163477	Diacetal derivatives and their use as clarifier	22.03.2018

Acknowledgment

The past three years have been an unforgettable and challenging time. Many people have contributed to the present thesis in different ways and for this I want to express my gratitude to them all. First of all, I would like to thank Prof. Dr. Matthias Rehahn and Dr. Rudolf Pfaendner for the support given and the chance to work on this interesting topic with Clariant as industrial partner.

In addition, I would like to thank all colleagues of the Additivation group at Fraunhofer LBF, for the warm welcome and support with several questions. Thanks to Dr. Elke Metzsch-Zilligen for your advice and the interest on the progress of this thesis.

I am grateful to Clariant, for offering me a challenging topic, access to state of the art laboratories and the financial support. I address a special thanks to Dr. Steffen Hofacker for the chance to join his Competence Center and to participate in his team meetings, which allowed me to understand the research organization of an international company.

Further, I would like to give special thanks to Dr. Thierry Muller and Dr. Stefan Hauck, you both have been great and patient mentors. In particular, I want to say thanks for all the valuable discussions, helpful advice and for sharing all your areas of expertise with me.

I would like to say my sincere thanks to all the members of the Competence Center Colorants & Functional Chemicals, in particular Dr. Fabian Schneider, Dr. Naveen Kumar Allampally, Dr. Andreas Endres, Junichi Tanabe, Lothar Fisch, Katrin Weber, Fabian Jessen and Christian Portaluppi. I really enjoyed working with all of you and I appreciated the fantastic working atmosphere. In addition, I would like to thank the members of the Competence Center Interface & Formulation Technology, in particular Dr. Simon Aben for insights into the French cuisine.

Furthermore, I want to express my gratitude to the Business Unit Additives, especially to Dr. Pascal Steffanut for support on this project. The BU Pigments Technical Marketing Plastics Lab is gratefully acknowledged for the training in extrusion and injection molding. I would like to thank Clariant Analytical Services for support in NMR, DSC and several other experiments. Thank you to Prof. Dr. Thomas Hellweg and Ramsia Sreij (Bielefeld University) for performing the WAXS measurements. Special thanks goes to my proof readers Dr. Erik Reuther, Dr. Dorothee Borchmann, Dr. Julie Murison for useful corrections and comments. Apart from this, I want to say thanks to the Clariant innovation community as a whole and to all my friends for their motivation.

Last but not least, I would like to thank my parents, my sister and my girlfriend for their constant love, support and belief in me. Without you I could have never come this far and I will always be grateful.

TABLE OF CONTENTS

1. Introduction

1.1. Preamble

Over the last decades a variety of plastic materials have replaced conventional materials like metal and wood, since they offer clear advantages. Apart from their low cost and ease of processing, the wide range of properties they potentially exhibit lead to a growing demand in many applications [1, 2]. The properties depend on the polymers' molecular structure and configuration, which direct the solid-state structure of the material. Amorphous polymers are typically transparent, whereas semi-crystalline polymers are opaque [3]. In order to transfer these advantages into as many application fields as possible, additives have been developed which adapt the plastic to the additional challenges during production and processing. Not only during processing, but also during service life plastic materials have to survive the exposure of harsh conditions, caused primarily by heat and light. Without suitable additives like plasticizers, flame retardants, antioxidants, UV-stabilizers, dyes and other processing aids, all these developments would not have been possible [2]. In particular, nucleating agents (NA) enable to influence the polymers' final structure and have gained increasing importance. A main driver in this field is the packaging industry, which is continuously striving to guarantee high-quality food, beverage and consumer packaging solutions for a constantly growing population (Figure 1-1). Polypropylene (PP), polyethylene (PE) and polyethylene terephthalate (PET) are the main resins used in these applications [1, 4–6].

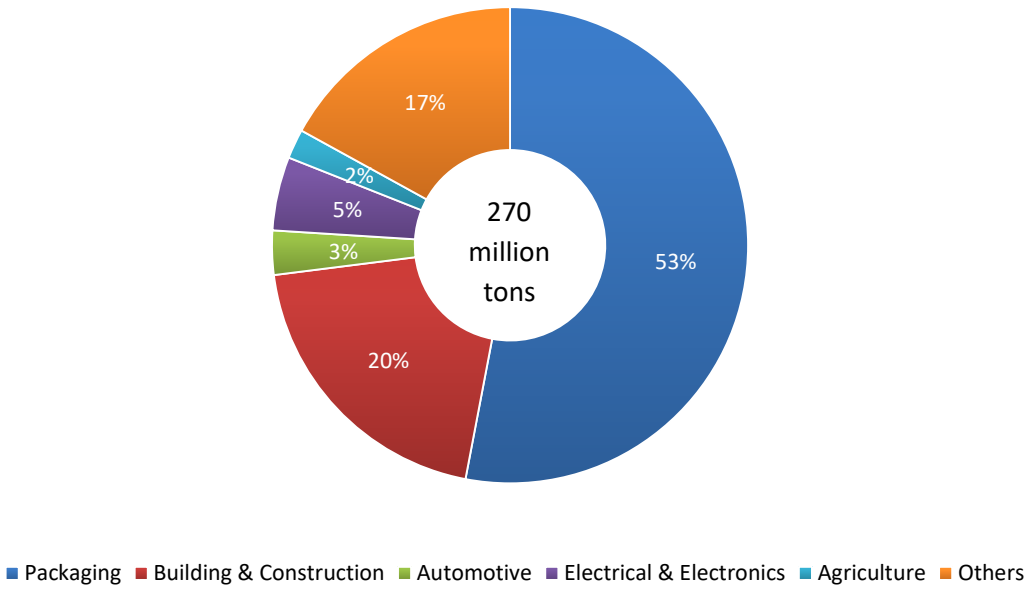

Figure 1-1 Worldwide plastics demand by segment in 2016 [7].

As a result of low costs, good recyclability, low density, good chemical and thermal resistance and good mechanical properties PP sees a growing demand in many applications. The use of nucleating and clarifying agents (CA) allows PP to overcome previous limitations, thus making it competitive against other polymers like PET, polyvinylchloride (PVC), PE, and polystyrene (PS) when it comes to improved optical and physical properties [1, 4–6].

Nucleating agents are used to reduce cycle times and improve physical properties. Clarifying agents, as a subcategory, can be used to affect the optical properties of the final products. The use of nucleating and clarifying agents is limited to semi-crystalline polymers. Due to its inherent low rate of crystallization (330 nm/s [8]) the main research activities on nucleating and clarifying agents for polyolefins focus on PP.

With a demand of around 60 million tons in 2016, PP is the second most important standard plastic after polyethylene, making up nearly 25 % of the global polymer demand [7]. The overall demand, especially for clear PP will increase, due to its use in applications like packaging, consumer products and the automotive sector.[9] 70 % of the global nucleating and clarifying agents market, which is estimated to reach USD 4.45 billion by 2026 [1], is used for PP, whereby 75 % of these are allocated for clarification and just 25 % for nucleation [10].

1.2. Polypropylene

Polypropylene is obtained by a catalyst mediated polymerization reaction of propylene, using either a Ziegler-Natta, or a metallocene catalyst. By the choice of catalyst and ligands, molecular mass distribution and stereospecificity are determined. Caused by the asymmetric propene monomer, PP can be produced in different stereochemical configurations. Figure 1-2 shows the three most common types. The stereo arrangement is controlled by the degree of branching (chain end or backbone addition), regiospecificity (head-to-tail) and stereospecificity (right or left handed) when adding the monomer unit [11]. The isomeric forms are depending on the orientation of the methyl groups attached to the alternating carbon backbone. Isotactic polypropylene (iPP) is the most common industrial form and all pendant methyl groups show the same configuration. Syndiotactic polypropylene (sPP) exhibits alternating methyl groups on opposite sides of the backbone, while in the atactic polypropylene (aPP) form the pendant methyl groups show a random orientation [12].

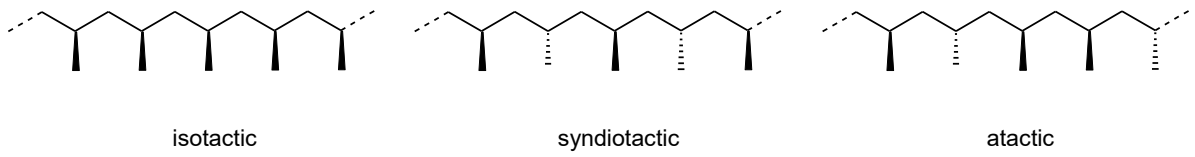

Figure 1-2 Isomeric forms of polypropylene.

Structure and stereochemistry of polypropylene have a major impact on its properties. Semi-crystalline iPP has the highest crystallinity, resulting in good mechanical properties. In contrast, sPP is still semi-crystalline, but less stiff than its isotactic form and therefore entails better impact strenght and clarity. The atactic form has the lowest crystallinity, resulting in an almost amorphous form due to its irregular structure. Compared to PE, PP shows higher tensile, flexural, compressive strength and higher moduli, due to its steric interaction of the pendant methyl groups [12].

Moreover, PP is commercially available in different forms, dependent on the desired properties. The homopolymer consists only of propene monomer units, whereas in the so called copolymers PP is copolymerized with ethylene or butene units [13].

The iPP molecules crystallize in form of a 3_1-helix. Steric repulsion of the methyl side groups in iPP let it arrange in an alternate trans/gauche conformation. In this way, there are two possible conformations, right- and left-handed forms to reach the energetic minimum. By this, both conformations built up a helix (Figure 1-3), where three repeating units are needed for one turn of the helix (6.5 Å)[12, 14]. Depending on the conditions, iPP can exist in different crystal modifications. Due to this fact, iPP can crystallize in different crystal polymorphs, a monoclinic α-phase, a hexagonal β-phase, a triclinic γ-phase and a forth modification which is named monomorphic or smectic phase. In all forms, the chain conformation is the threefold 3_1-helix; the only difference is resulting from the stacking geometries [11, 12, 14].

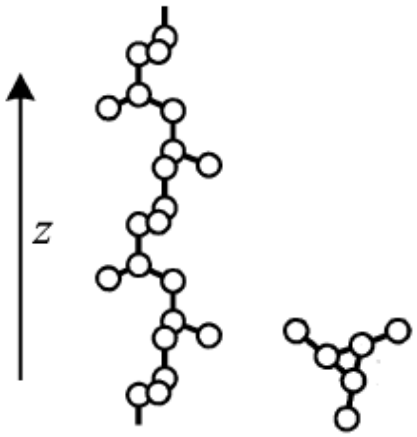

Figure 1-3 Three-fold helical chains of iPP with pendant CH_3 groups down with respect to the z-axis. Left parallel and right perpendicular to the chain axis. Reprinted from [15] with permission from American Chemical Society, Copyright 2006.

The dominant form is the α-form, which can be differentiated into its α_1- and α_2-species by two space group symmetries. The α-form is generated under normal processing conditions and is found to be the thermodynamically most stable form [16]. Different conditions, such as shearing [17–20], crystallization under a temperature gradient [21] and rapid quenching to isothermal temperatures [19, 21, 22], can force the iPP in its β-modification. The γ-form is only observed in small fractions and has been found during crystallization under high pressure [23, 24]. By mechanical or thermal treatment, both β- and γ-form change into the α-polymorph and thus they are just metastable. For some applications the β-polymorph is preferred, due to higher impact strength and toughness [25–27], while in other applications the better optical properties of the α-phase are more preferred [28, 29]. The induction of the polymorphs can be controlled by the use of different nucleating agents, which preferentially induce one or another phase or even a mixture thereof. By using these additives, the properties of the polymer can be controlled and a transformation into the other forms can be hindered [30–32].

All previously described characteristics influence the morphology of the polymer. During crystallization from the melt, the PP molecules associate to form supramolecular structures. In the melt the helical PP macromolecules exist in a random coil formation. When reaching the crystallization temperature, the macromolecules begin to arrange into crystals with ordered crystalline regions and disordered amorphous regions. This is caused by folding of the chains into thin ordered structures, called crystalline lamellae. Typically, lamellae exhibit a thickness of around 20-500 Å and around 10^5 Å in lateral dimension. Their thickness depends on processing methods and crystallization temperature. The lamellae plates arrange next to each other with distances of around 100-300 Å, forming lamellae blocks. The blocks are connected by amorphous ‘tie point’ regions, resulting from irregularities in the chain formation. The lamellae blocks grow in a radial direction to form spherulites building up spherical three-dimensional semi-crystalline structures. The size of the iPP spherulites themselves ranges from 1-50 μm. If the diameters of spherulites are greater than one-half of the wavelength of visible light and the densities and refractive indices of the crystalline and non-crystalline regions are different, objects appear opaque [11–13].

Figure 1.4 shows the morphology of the semi-crystalline iPP with its hierarchy in multiple scales. On the visual scale, which ranges from a few cm to mm, the macromorphology, such as particle shape and skin core structures, can be observed. On the next level, which is in the order of 1-50 μm, the above mentioned spherulitic structures can be made visible predominantly by optical microscopy under crossed polarizers, but also by small-angle light scattering (SALS). Moreover, Figure 1-4 shows the previously mentioned lamellae formation. This lamellar scale can be investigated by either small angle X-ray scattering (SAXS) or higher resolution electron microscopy. Furthermore, on the next finer scale, the lamellae are composed of the known crystallographically ordered regions (e.g. α, β, γ). The different stacking geometries and unit cell dimensions of the individual macromolecular chains build up the crystalline regions. The unit cell dimension of polypropylene's α-form is 6-20 Å and is schematically shown in Figure 1-4 Structures on this scale are commonly investigated by wide angle X-ray scattering (WAXS) and electron diffraction techniques [11].

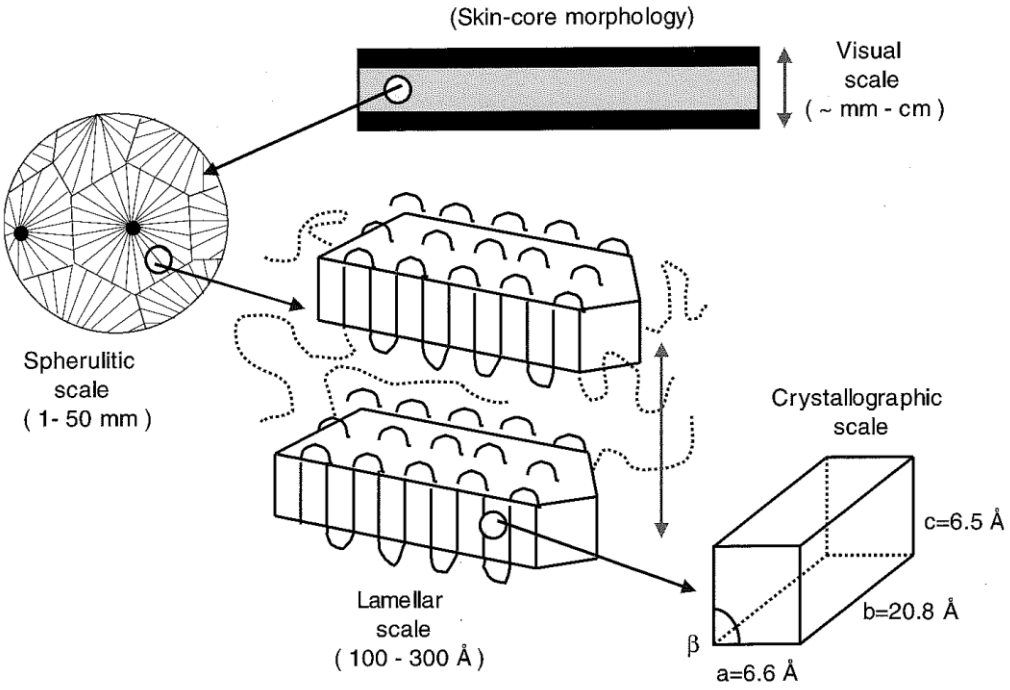

Figure 1-4 Characteristic hierarchy of morphological scales in PP. The skin-core morphology of injection molding is used to illustrate morphology on the visual scale. Reprinted from [11] with permission from Carl Hanser, Copyright 2005.

When investigating the spherulites with optical microscopy under crossed polarizers, characteristically a Maltese cross pattern is observed, caused by birefringence of the molecule alignment in the lamellae. The lamellae in the α-form of iPP grow mainly radially, but can also associate tangentially. Thus, positive, negative and mixed birefringence can be induced by the lamellae. Negative birefringence develops from spherulites with dominantly radial lamellae, whereas positive birefringence results from spherulites with predominantly tangential lamellae. Both forms appear as a Maltese cross pattern under crossed polarizers. In spherulites with mixed birefringence, neither of both lamellae forms is predominant. The characteristic feature is a

distinct Maltese cross. With an increasing crystallization temperature the tangential lamellae undergo premelting and by this the birefringence changes from positive to negative [11, 12].

The β-form of iPP is more disordered than the α-form and the parallel stacked lamella does not show cross-hatching, but more sheaf-like spherulitic structures have been observed. These show no distinct, but interconnected boundaries [11, 12, 16].

Moreover, α-, β- and γ-polymorphs can be distinguished, as seen in Figure 1-5 by using WAXS. Mixtures of α- and β-polymorphs are often present. Therefore, Turner-Jones et al. defined a relative index, describing the amount of β-crystallinity.[22]

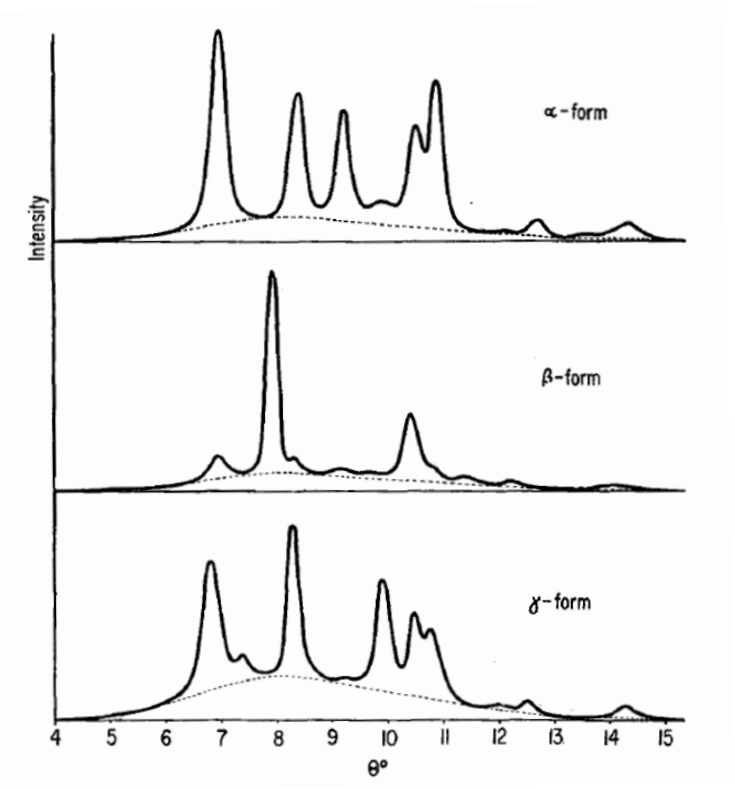

Figure 1-5 X-ray diffraction diagramms of polymorphs of isotactic polypropylene. Reprinted from [22] with permission from John Wiley and Sons, Copyright 1964.

The morphology of iPP affects the characteristics of polypropylene in different ways. The melting point of PP changes with the degree of crystallinity. At lower crystallinity the melting point decreases. Commercial iPP exhibits melting points in ranges from 160 to 166 °C. Typically, polymers, including PP, show no distinct melting point, but rather melt over a narrow temperature range, caused by slightly different lamellae thickness. The glass transition temperatures of PP resins vary around -10 °C. The mechanical properties vary as well with the degree of the crystallinity. Stiffness, yield stress and flexural strength increase with the crystallinity. In contrast, toughness and impact strength decrease. The transparency of PP is influenced by its crystallinity via the spherulites, which are larger than the wavelength of visible light and thus scatter light. The refractive index of the crystalline regions is higher than of the amorphous regions. Light scattering results in lower transparency and higher haze [12].

1.3. Crystallization

Macromolecules with a regular chain structure and sufficient flexibility associate to form supramolecular structures when cooled to temperatures below the melting point. At the crystallization temperature they start to organize in ordered crystalline regions and disordered amorphous regions [13]. Due to insufficient mobility, the polymer chains show deviations from ideal crystals and therefore do not crystallize completely. In general, the crystallinity of common PP ranges between 40 and 70 % and therefore it is called a semi-crystalline polymer [11]. The chain structure of these polymers forces them to crystallize at lower temperatures as they melt. To express this context, the degree of super-cooling / undercooling ($\Delta T = T_m^0 - T_c$) is often used [8].

The crystallization process of semi-crystalline polymers is well described in literature [33] and, due to this, hereinafter only most important aspects of the crystallization process will be defined. As described in chapter 1.2, during cooling from the melt molecules of semi-crystalline polymers, like iPP, organize in form of primary nuclei. This step initiates the crystallization process and is called primary nucleation. Starting from this focal nuclei, lamellae organize and subsequent spherulite growth begins. Spherulites grow until they impinge on an adjacent spherulite and growth is terminated. This schematic nucleation process is shown in Figure 1-6 [8, 34].

Figure 1-6 Nucleation process until impingement of spherulites (the temperature gradient is indicated by the direction of the arrows).

Both, the rate of nucleation and the rate of crystal growth determine the crystallization process. This temperature and polymer dependent process is schematically represented in Figure 1-7 for iPP. In the melt zone above the equilibrium melting point (T_m^0) crystallization cannot occur under normal conditions. If the polymer is cooled below this equilibrium, the rate of nuclei formation is very low, due to its nonexistent stability. In principle, crystallization is imaginable in this metastable region, but nuclei need to be present. In the super-cooled melt area, the rate of crystal growth first undergoes a maximum and subsequently approaches to zero. This means that, at a certain point, no more crystal growth can be observed. The same can be observed for the rate of nucleation, but is shifted to lower temperatures. Because of increasing viscosity of the polymer melt, the rate of nucleation decreases to become zero at the glass transition temperature (T_g). The polymer chain mobility is frozen at the glassy state and thus no more nucleation and growth can take place [6, 8, 35].

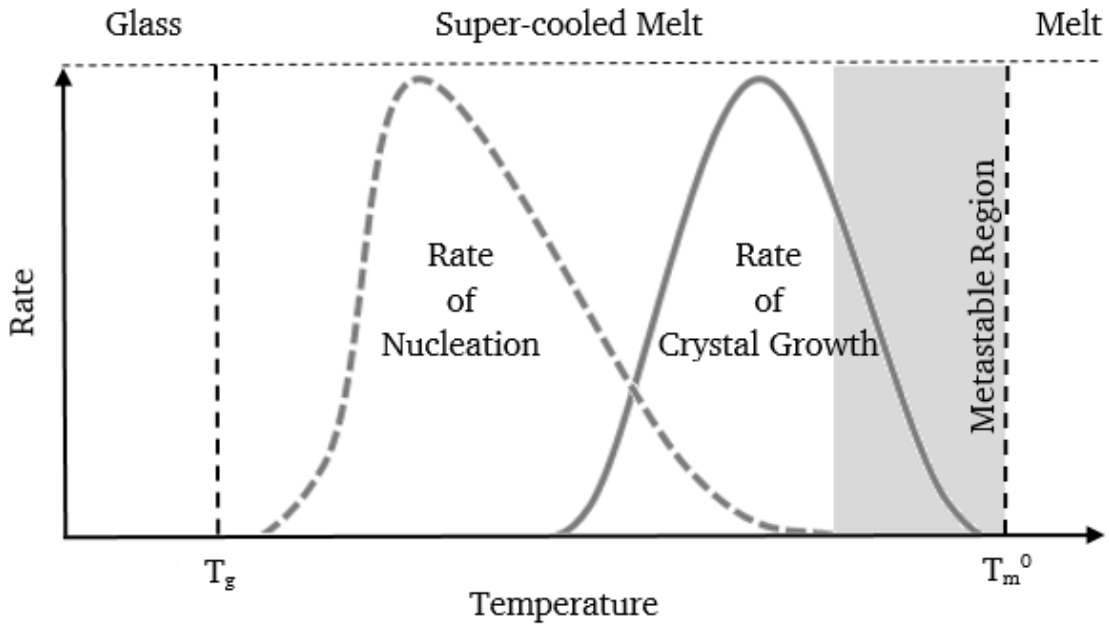

Figure 1-7 Schematic representation of the rate of nucleation and the rate of crystal growth as a function of temperature. Redrawn according to [35].

The crystal phase formation from melt is called primary nucleation, which is separated into three different types according to Binsbergen [6, 8]. The first one is the spontaneous nucleation, where homogenous nucleation only takes place under super-cooling conditions of the polymer melt, as described in the curve progression in Figure 1-7. This does not occur under typical processing conditions. The second type is the most important one regarding typical processing techniques. It is called orientation-induced nucleation and thus the nucleation process is induced by shear as a result of crystal alignment. Third, heterogeneous nucleation is induced by impurities at the surface of these foreign particles. Consequently, the addition of nucleating agents is a special case of heterogeneous nucleation. Secondary and tertiary nucleation describe the crystallization of a polymer chain either on the flat surface or on the edge of a polymer crystal. Heterogeneous nucleation is of particular interest due to its commercial importance for several applications [6, 8]. In the following chapter, several heterogeneous nucleating agents and their influence on physical and optical application properties are presented.

In general, the crystallization process of plastics is depending on the crystallization kinetics. In-depth aspects on the crystallization kinetics can be found in literature. It is important to note that isothermal and non-isothermal crystallization can be distinguished. Due to the fact that the determination of crystallization kinetics is laborious, other easily obtainable characteristic material values, like crystallization temperature and crystallization half time, are used in practice [8].

1.4. Nucleating and Clarifying Agents

By selection of different nucleating agents, it is possible to control the induction of one or another iPP polymorph. Most of the heterogeneous nucleating agents presented below induce the thermodynamically stable α-modification of isotactic polypropylene. Although there are specific nucleating agents inducing the β-modification, these are more or less neglected in the following. Moreover, it is necessary to distinguish between nucleating agents (NA) and clarifying agents (CA). "All clarifying agents are nucleating agents, but not all nucleating agents are clarifying agents" [36]. There are different classes of nucleating agents according to their chemical structure. Several thousands of structures with more or less potential as nucleating agents have been described in literature. The very first research on nucleating agents for polypropylene in particular was done by Beck and Ledbetter in 1965 [37], investigating more than 200 substances and their nucleating potential, as well as by Binsbergen and de Lange in 1970 [38], screening more than 2000 substances for latter purpose. This initial research builds up the fundamental insights for structural factors and types of nucleating agents. Only a limited number of molecules are known to influence the optical properties of the material as well. If some of these nucleating agents are known to improve optical properties, this will be mentioned explicitly in the following sections. In order to understand how difficult and versatile the search for new nucleating and clarifying agents is, examples of representative groups and substances are given hereafter. A comprehensive overview with references to original scientific papers can be found in literature [8, 39]. The mode of action of these nucleating and clarifying agents will be discussed in detail later on.

1.4.1. Classes of nucleating and clarifying agents

Inorganic Nucleating Agents

Most inorganic materials are used as filling materials in plastics. Beside this, it is known that some minerals, such as silica, clay and talc, can also be used at low concentrations to induce nucleation. Especially talc has a distinct impact on nucleation of PP. Furthermore, inorganic salts such as calcium carbonate have been investigated, but most of them show no or just a limited impact on nucleation of polymers. Their good price-performance ratio justified their use for a long time in some applications, but today they are mostly replaced by more recent and effective developments [8, 39].

Derivatives of carboxylic acid and their salts

Beck [37, 40] and Binsbergen [38, 41, 42] investigated several substances and screened different aromatic, aliphatic and cycloaliphatic carboxylic acid derivatives and their salts regarding their nucleating ability. They showed that most pure inorganics and hydrocarbons are poor nucleating agents and that organic acid derivatives and salts thereof are more effective nucleating agents. Moreover, they discovered that substituted benzoic acids were largely ineffective nucleating agents. The formation of analogous aluminum and sodium salts delivered much more powerful derivatives. Glutarate and succinate appeared to be the only performing structures out of the group of aliphatic dicarboxylic and monocarboxylic acid sodium salts. Cycloaliphatic carboxylates were characterized as moderate to good nucleators. The overall best

results were obtained with C_4-C_6 mono- and di-carboxylates and C_6-C_7 alicyclics. Aluminum carboxylates were also identified as effective nucleating agents. Several representatives out of the group of substituted benzoic acid salts, such as sodium and lithium benzoate as well as aluminum-monohydroxy-bis-(p-*tert*-butyl benzoate), are still sold as commercial products with a good price-performance ratio. A common feature for this group of molecules is the prerequisite of fine dispersion as small particles within the polymer matrix [8, 39].

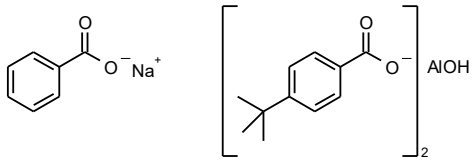

Figure 1-8 Structures of sodium benzoate (left) and aluminum-monohydroxy-bis-(p-*tert*-butyl benzoate) (right).

Even additives based on rosin acids and their derivatives have been found to be effective nucleating agents for polypropylene, most probably due to a fitting melting point of some derivatives, which allows for good dispersion in the polymer melt. Moreover, other natural products, such as derivatives of shellac, have been screened as nucleating agents.

A highly efficient class of nucleating agents are bicyclo acids and their derivatives. Unsaturated bicyclo [2.2.1] and [2.2.2] diacids, bicyclo [2.2.1] heptane dicarboxylic acid derivatives and analogous molecules have been investigated in detail. Bicyclo [2.2.1] heptane-2,3-dicarboxylic acid sodium salt has been identified as a highly efficient nucleating agent. This so called 'hypernucleator' provides a high nucleating performance combined with excellent stiffness, impact resistance and the ability to overcome anisotropic shrinkage [43]. It is commercialized by Milliken Chemical as Hyperform® HPN-68. A further development is based on salts of hexahydrophthalic acid, such as cis-1,2-cyclohexane dicarboxylic acid [44]. In combination with an acid scavenger it is commercially available as Hyperform® HPN-20E [8, 39].

Figure 1-9 Structures of calcium cis-1,2-cyclohexane dicarboxylic acid (left) and sodium bicyclo [2.2.1] heptane-2,3-dicarboxylic acid (NA 68) (right).

Carboxylic amides

Most of the amides of aromatic dicarboxylic acids are known as β-specific nucleating agents. Among others, Mohmeyer et al. [32] studied the effect of low molecular-weight 1,4-phenylene-bisamides as nucleating agents for iPP.

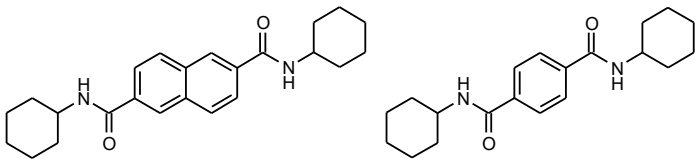

Figure 1-10 Structures of N,N'-dicyclohexyl-2,6-naphthalindicarboxamid (left) und N,N'-dicyclohexylterephthaldiamid (right).

A new class of nucleating agents was synthesized and investigated in detail by the research groups of H.-W. Schmidt and P. Smith [45]. This class is based on 1,3,5-benzenetrisamide derivatives and exhibits the general structure of a central benzene core, which is substituted with amide groups in the 1-,3- and 5-position [46]. The two main cores can consist of 1,3,5-benzene tricarboxylic acid or 1,3,5-trisamino benzene. The amide groups are capable of forming hydrogen bonds and contain aliphatic or cycloaliphatic substituents on the acid end. These determine the nucleating ability and the melting point of the molecules. Interestingly, this class induces the α-phase of iPP at very low concentrations. Furthermore, some derivatives enhance the transparency of polypropylene and thus can be described as clarifying agents. Depending on the substituents, the β-phase or even mixtures of α- and β-phase can be induced. As a result of this exceptional ability, this class can be called 'designer' nucleating agents. A major advantage of this class is the high thermal stability over a wide processing window. One derivative of these trisamides is commercially available from BASF as the clarifying agent Irgaclear® XT 386 [8, 39].

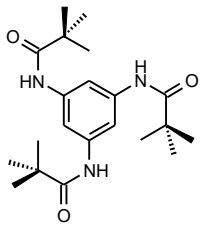

Figure 1-11 Structure of 1,3,5-Tris(2,2-dimethylpropanamido)benzene (Irgaclear® XT 386).

Organophosphorus derivatives and their salts

Nucleating agents based on organic phosphates are well known and several of them have been investigated by Adeka [47, 48] and are commercialized since the 1990's. Main representatives of this class are based on 2,2'-methylene-bis(4,6-di-tert-butylphenyl) phosphate salts, such as sodium 2,2'-methylene-bis(4,6-di-tert-butylphenyl)phosphate. These additives provide increasing stiffness and strength already at low concentrations. Furthermore, they can be applied in a wide processing window, due to their high thermal stability, and they are known to have an influence on optical properties. If iPP, nucleated with 2,2'-methylene-bis(4,6-di-tert-butylphenyl) phosphate salts, is processed under the right conditions, these nucleating agents can reach haze values that could previously only be achieved with clarifying agents [49]. Figure 1-12 shows the three main types of 2,2'-methylene-bis(4,6-di-tert-butylphenyl)

phosphate salts. The newest generations are in most cases formulations of these three derivatives, and they are optimized concerning their influence on optical properties [8, 39].

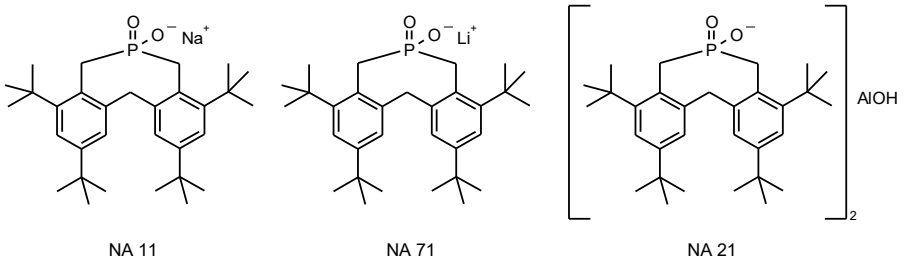

NA 11 NA 71 NA 21

Figure 1-12 Structures of sodium-2,2′-methylene-bis (4,6-di-tert-butylphenyl) phosphate (ADK STAB NA 11), lithium-2,2′-methylene-bis (4,6-di-tert-butylphenyl) phosphate (ADK STAB NA 71) and aluminumhydroxy-bis [2,2′-methylene-bis (4,6-di-tert-butylphenyl) phosphate] (ADK STAB NA 21).

Polymers

Polymers have been considered as nucleating agents in polypropylene as well. Addition of a polymer with a higher melting and higher crystallization temperature could force nucleation of the matrix polymer. A few studies have discovered different matrix / polymer additive pairings, but most of them show no or just a poor ability as nucleators. The pairing polypropylene/ polyvinylcyclohexane has been identified to work very well [50]. Most probably, the close two-dimensional lattice match of iPP and poly (vinylcyclohexane) (PVCH) is responsible for its effectiveness. This system has technical importance, because it is used as reactor nucleating agent during iPP polymerization. Several other systems with poor or moderate nucleating ability have been reported, such as polyamide (PA), PET or functionalized PP. Even oligomeric species have been screened as potential nucleating agents [39]. Moreover, Bernland et al. [51] investigated the ability of nanofibrils of poly(tetrafluoroethylene) (PTFE) to efficiently nucleate crystal growth in polymers like iPP [8, 39].

Pigments

Most pigments are acting as nucleating agents and nearly all of them induce the β-phase selectively. Pigments are rarely used as nucleators as they cause unwanted discoloration of the final articles. γ-Quinacridone is the best known β-nucleating agent and its formulation of *trans*-chinacridone and chinacrionchinone is a colorless nucleating agent used in PP-RACO pipe applications [8, 39].

Sorbitol based acetals

Sugars and sugar polyols have been screened as potential nucleating agents. Fructose and sucrose have been characterized as not very effective nucleating agents, whereas derivatives of sugar polyols such as sorbitol and xylitol delivered groundbreaking results. The reaction of sorbitol with aldehydes result in mono-, di- and tri-acetals, which were initially developed as gelling agents in cosmetic and pharmaceutical applications. These low-molecular-weight gelators have a history of over 100 years [52]. Dibenzylidene sorbitol (DBS) was identified as a highly effective nucleating and clarifying agent for polypropylene by Hamada et al. and subsequently commercialized as the first generation product of this class [53].

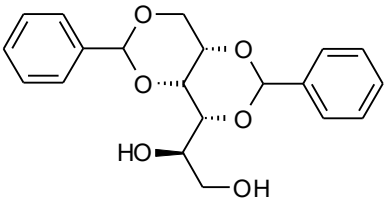

Figure 1-13 Structure of dibenzylidene sorbitol (DBS).

Concluding from its gelling behavior in liquids, a similar mechanism was held responsible for the nucleating efficiency of DBS. Monobenzylidene sorbitol (MBS) and tribenzylidene sorbitol (TBS) show less nucleating efficiency. One isomer of trinaphtylidene sorbitol has been identified to be an efficient nucleating agent and somehow refutes parts of common theories that free hydroxyl groups are necessary for effective nucleation of these kind of molecules. Even spiro-centered acetals have been synthesized and investigated with little success. The bad thermal stability of the DBS molecules is one major reason, why soon substituted analogues have been investigated and commercialized as effective clarifiers. These are second generation bis (4-methylbenzylidene) sorbitol (MDBS) [54], bis (4-ethylbenzylidene) sorbitol (EDBS) and third generation bis (3,4-dimethylbenzylidene) sorbitol (DMDBS) [55], which provided better thermal stability and improved nucleating performance. The initial shortcomings included odor and yellowing of the final products, through breakdown of the molecule and following benzaldehyde release. Nevertheless, stability has been improved as mentioned and all of the additives have food contact approval. The latest one, commercialized as Millad® 3988, has long been in a market leading position.

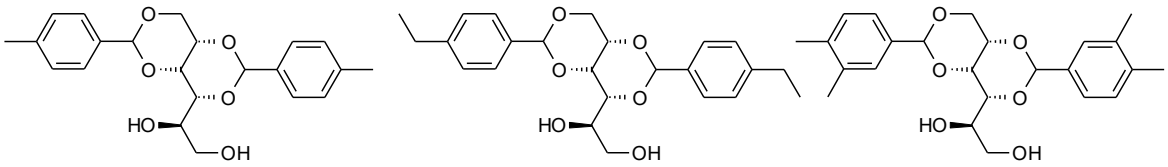

Figure 1-14 Structures of bis (4-methylbenzylidene) sorbitol (MDBS) (left), bis (4-ethylbenzylidene) sorbitol (EDBS) (middle) and bis (3,4- dimethylbenzylidene) sorbitol (DMDBS) (right).

A whole collection of symmetrically and asymmetrically substituted benzylidene sorbitols has been investigated. Apart from methyl substituted derivatives, other substituents were used, such as alkyl, alkoxy, halogen, ester, amide and nitro. Furthermore, functionalization of one of the free hydroxyl groups and 1-substituted sorbitols have been considered. Based on a 1-allylsorbitol, the latest fourth generation product of this class, 1,2,3-tridesoxy-4,6:5,7-bis-*O*-[(4-propylphenyl) methylene]-nonitol (TBPMN) [56], has been commercialized as Millad® NX 8000. The latter offers best in class performance when it comes to clarified polypropylene.

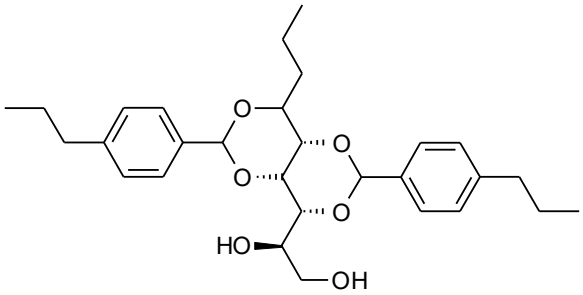

Figure 1-15 Structure of 1,2,3-tridesoxy-4,6:5,7-bis-*O*-[(4-propylphenyl) methylene]-nonitol (TBPMN).

In addition to sorbitol and xylitol based diacetals, dibenzylidene xylonates [57] have been investigated as potential nucleating and clarifying agents. By replacing both terminal free hydroxyl groups through a carboxylic acid, ester or amide group, improvements in nucleation and in optical properties could be observed [39].

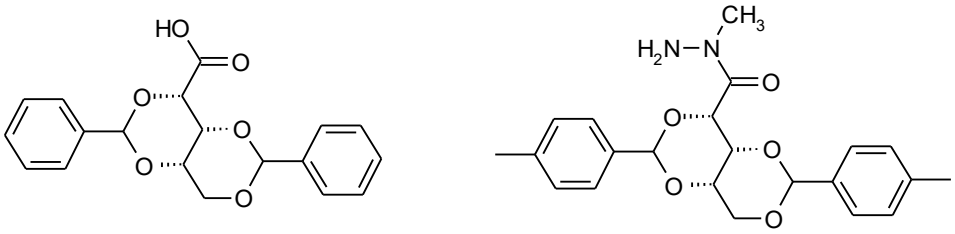

Figure 1-16 Structure of dibenzylidene xylonate derivatives, dibenzylidene xylonic acid (left) and 4,4′-dimethyldibenzylidene xylonic acid methyl hydrazide (right).

The major drawback of acetal based nucleating and clarifying agents is their poor thermal resistance and the resulting cleavage of benzaldehyde. Although this narrows the processing window of that class, the latest generation sorbitol clarifying agents offers state of the art performance with regard to optical properties. The lack of performance of substitutes and the continuing penetration of PP into higher-demanding applications, as well as the use of recycle-content PP grades, will intensify the need for new, durable and temperature resistant clarifying and nucleating agents. Considering this, several more structures will be investigated as potential nucleating and clarifying agents in the future.

In the following subchapter, the main characteristics, properties and the mode of action of the most important classes, such as organophosphorus and sorbitol derivatives, are discussed in detail. This allows to understand the main differences between these commonly used nucleating and clarifying agents.

1.4.2. Characteristics, properties and mode of action of nucleating and clarifying agents

'Dispersion' vs. 'Soluble' type nucleating agents

In general, the crystallization process of semi-crystalline polymers is initiated by primary nucleation. By incorporation of foreign particles, the amount of starting nuclei is much larger than by spontaneous self-nucleation. These common nucleators are normally high melting, insoluble materials in the polymer melt, such as previously presented talc, pigments and organophosphorus derivatives. The mode of action of these often so called 'dispersion' type nucleators is shown on the basis of optical micrographs in Figure 1-17 b). As they stay solid during the processing step, these types of additives have to be finely dispersed in the polymer matrix. Dispersed particles then act as starting sites and provide surfaces on which the polymer crystals growth can commence. In this way, the rate of crystallization is increased and this leads to a reduced spherulite size and a higher spherulite density. Consequently, a reduction in cycle times during processing is achieved. The nucleators allow the polymer to crystallize at higher temperatures and thus can lead to improved mechanical properties, such as modulus, tensile strength and heat deflection temperature by higher levels of crystallinity. The small size of the spherulites leads to reduced light scattering, which can result in improved optical properties. In general, however, only some representatives of this type of nucleating agents are able to improve optical properties and act as a sort of clarifying agents [58].

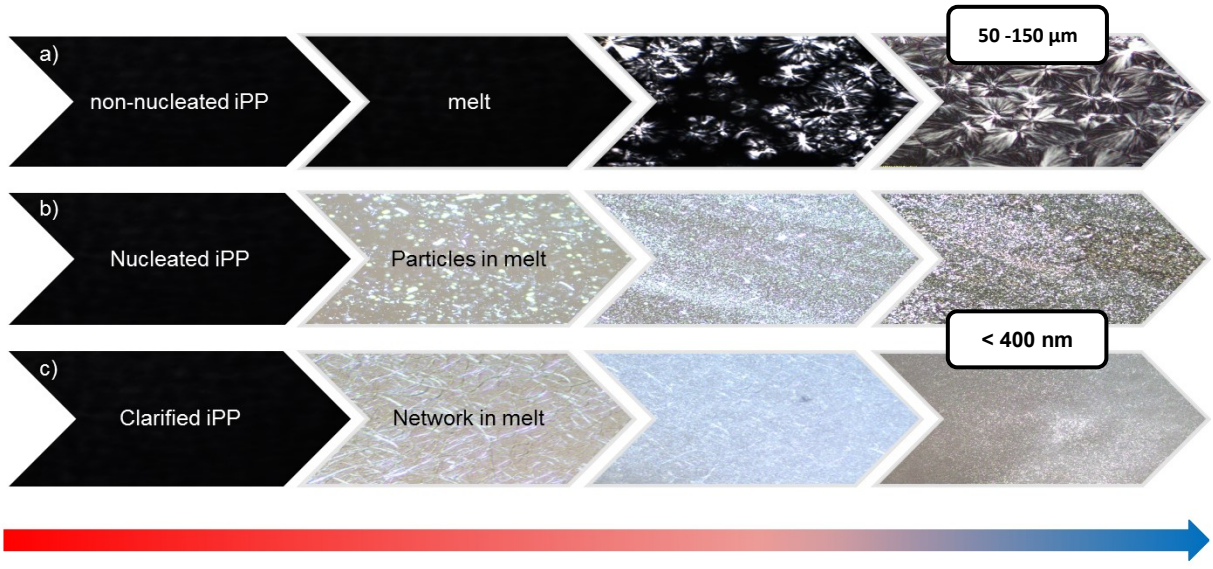

Figure 1-17 Mode of action of 'dispersion' type and 'solution' type nucleators. Illustration of nucleating process by polarized optical micrographs form melt of a) iPP; b) iPP/NA 11 (2.0 wt%); c) iPP/DMDBS (2.0 wt%).

'Solution' or 'melt-sensitive' nucleating agents typically have low melting points and become soluble in the polymer melt. Sorbitols [59] and trisamides [45] are the most prominent representatives of this class. Almost all do not only act as nucleating agents, but also as clarifying agents. In this case, the soluble additive crystallizes prior to the polymer melt during cooling in form of a finely distributed fibrillar network and thus acting as a large surface on

which nucleation occurs (Figure 1-17 c)). In principle, the working mechanism is similar to the particulate approach, the only difference is that the additive is soluble and by the formed network a by magnitudes larger surface is created. This three-dimensional network is formed in the melt, which can be detected by an increased complex viscosity prior to crystallization of the polymer itself [60]. This process is also known as 'physical gelation' [61]. The network surface provides an extremely high concentration of nuclei leading to very small spherulites. The network itself provides a higher density for resulting crystallization starting sites. The diameters of the network fibers themselves and the resulting spherulites are only a few nanometers; hence, they lie significantly under the wavelength of visible light. This results in lowest level of light scattering and improved optical properties regarding haze and clarity [58].

Exemplary 'design' of nucleating and clarifying agents and role of epitaxy

From the extensive screening of nucleating agents by Beck and Binsbergen [37, 38], a list of general characteristics a good nucleating agent should exhibit was deduced [42]. First of all, the NA should be capable of reducing interfacial free energies, which means that the molten PP should be able to adsorb onto the additive surface. The additive itself should have a melting point above that of PP and it should be insoluble in the melt near or below PP's melting point. Moreover, it should be stable and exhibit a crystalline structure close to that of PP. From this, it could be suggested that a 'model' additive needs to have two moieties, an apolar moiety, which makes it soluble above the polymers melting point, and a polar group, which makes it insoluble below the polymers melting point [6]. Later, some of these conclusions have been questioned and the exact mode of action is not yet resolved. Binsbergen [42] himself rejected the theory of epitaxial growth on the additive surface as the initiating nucleation step, but more recent research results by Wittmann, Lotz et al. [62–64] fostered exactly this mechanism. They observed that, in several cases, strong epitaxial interactions between polymer and additive occurred when the 'lattice matching criterion' [63] was fulfilled. Mathieu et al. [65] demonstrated that different nucleating agents with different crystallographic properties are able to nucleate iPP. This means that iPP and the additives interact over different crystallographic levels. Insights on the interaction of polymer and additive are quite valuable; nevertheless studies on this phenomenon are only possible with established working additives. This is why the development of novel nucleating and clarifying agents is still based on trial and error [8].

Mode of action – organophosphorus

Sodium 2,2'-methylene-bis-(4,6-di-*tert*-butylphenylene) phosphate (ADK STAB NA 11) has been found as one of the most effective nucleating agents for PP [66]. Yoshimoto et al. investigated its nucleation mechanism on iPP [67]. From various crystallization experiments of NA 11 and iPP and detailed crystallographic analysis, they found out that the rod-like NA 11 crystals show good fit with iPP's α-form. Moreover, they discovered that the c-cell dimension of iPP is very close to the b-cell dimension of NA 11 and the a-cell dimension of NA 11 is about four times the a-cell dimension of iPP. From this, they concluded that lattice matching can be performed between the two crystal lattices. Figure 1-18 shows that the iPP helix pitch matches the interval of NA 11's *tert*-butyl groups. The study showed that epitaxial growth is the nucleation mechanism which most of these organophosphorus NAs follow [68].

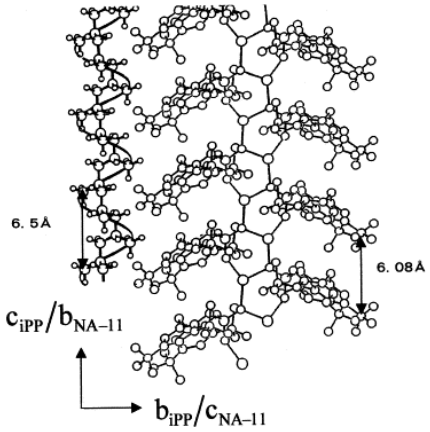

Figure 1-18 Molecular model of epitaxial relationship between NA 11 and iPP. Reprinted from [67] with permission from Elsevier, Copyright 2001.

Mode of action – sorbitols

Sorbitols are low molecular weight gelators, which are capable of forming a gel already at low (< 2.0 wt%) concentrations. These so-called organogelators are capable of forming fibrillar networks in organic solvents. Such molecules are amphiphilic; the lipophilic moiety enables its solubility in the organic solvent, whereas the polar moiety is responsible for the formation of the three-dimensional network by strong hydrogen bonding [69, 70]. As mentioned in chapter 1.4.3 some of these sorbitol based organogelators have been investigated as highly efficient clarifying agents [71]. 1,3:2,4-di(3,4-dimethylbenzylidene) sorbitol (DMDBS) is the third generation sorbitol clarifying agent and dissolves in the PP melt, which enables a homogenous dispersion and a uniform distribution of the additive. During cooling, DMDBS crystalizes in the form of a three-dimensional fibrillar network prior to PP. This nanoscale network acts as surface on which PP starts to crystallize. Straightforward the network creates a huge number of nucleation sites, which result in enhanced nucleation and significantly reduced spherulites. Finally by this, high degrees of clarification can be reached, since both, the fibrils and the spherulites, are below the wavelength of visible light.

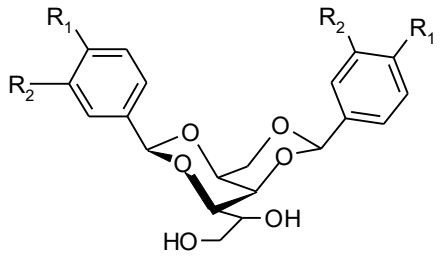

Figure 1-19 Chemical structure of 1,3:2,4-dibenzylidene-*D*-sorbitol (DBS) and its derivatives (R_1 = R_2 = H: DBS; R_1 = CH_3, R_2 = H: MDBS; R_1 = R_2 = CH_3: DMDBS).

Sorbitol derivatives, such as DMDBS, are chiral amphiphilic molecules and, as depicted in Figure 1-19, they adopt a 'butterfly' conformation. It is built up by an upgraded sorbitol hydrophilic 'backbone' and two hydrophobic benzene 'wings'. The two terminal hydroxyl groups enable intramolecular and intermolecular hydrogen bonds. In addition, the 'wings' contribute to the network formation via π-π interactions [68].

1.4.3. Investigations on the sorbitol family

The performance of DBS derivatives has been improved mostly by adjustments on the benzene 'wings'. As Table 1-1 provides an overview of the commercially available sorbitol-based clarifying agents, their performance increases from top to bottom of the table. Although there have been several research groups working on the nucleation and clarification ability of sorbitol derivatives, the very mechanism of clarification has not been fully understood. In the following, the most important outcomes will be described in order to better understand the working principle of this substance class. This will be outlined mostly on work based on the latest two generations.

Table 1-1 Overview of commercial sorbitol based clarifying agents, their abbreviations and their melting point.

Chemical Name	Abbreviation	T_m [°C]
Dibenzylidene sorbitol	**DBS**	225
Bis-4-ethylbenzilidene sorbitol	**EDBS**	235
Bis-4-methylbenzilidene sorbitol	**MDBS**	242
Bis-3,4-dimethylbenzilidene sorbitol	**DMDBS**	278
Tridesoxy-bis-*O*-[(4-propylphenyl) methylene]-nonitol	**TBPMN**	245

The performance of such additives is typically assessed by its crystallization temperature and haze value. Isotactic polypropylene commonly shows a crystallization temperature ($T_{c,p}$) of around 110 °C and a haze value of around 65 %. The incorporation of nucleating agents generally causes a shift of the crystallization temperature towards higher temperatures and with regard to an improvement in optical properties, the haze value is decreased. This shift is governed by a typical concentration dependency and increases by around 10 to 15 °C. Kristiansen et al. [72] differentiated between three main regions. The first region describes the concentration level of the additive/iPP mixture up to 0.1 wt% in which the additive shows no influence, in accordance with earlier investigations [36, 73]. In the second area between 0.1 and 0.5 wt% the crystallization temperature increases from 110 to 129 °C with an increasing loading level of DMDBS. At higher concentration levels exceeding the 0.5 wt% no changes in crystallization temperature have been recorded. Along with the latter, they observed an improvement in optical properties, which was explained by the reduction in spherulite size via an enhanced nucleation density [36, 74, 75]. Optical properties for those mixtures showed a typical behavior known for nearly all sorbitol derivatives. An optimal clarity of nearly 100 % was found between 0.2 and 1.0 wt%. At higher concentrations, the clarity dropped and at very low concentrations (< 0.1 wt%), clarity showed a little decrease to a value of around 40 %. Consistent with the initial clarity decrease, the haze value first showed an increase up to around 65 % (0.1 wt%). With increasing concentration levels the haze value decreased to reach a minimum value of about 20 % until no further improvement can be observed exceeding 1.0 wt% of additive concentration. Depending on the sorbitol derivative, while exceeding a certain concentration, often a downturn of optical properties can be observed, which can be related to the scattering of the nucleator itself [76].

Moreover, Kristiansen et al. established a simple binary eutectic phase diagram, which can be divided in four areas [72].

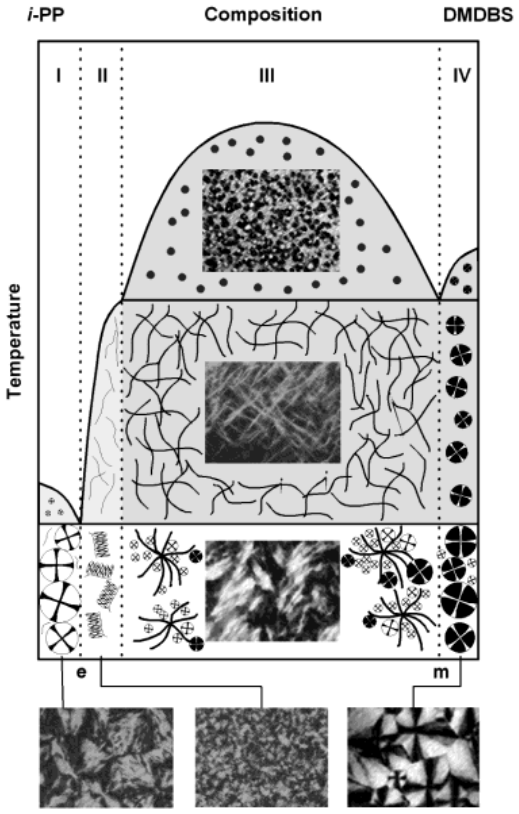

Figure 1-20 Schematic, monotectic phase diagram of the binary system iPP/DMDBS proposed by Kristiansen et al. including the four relevant composition ranges and sketches, as well as optical micrographs under crossed nicols of the various states of matter. Reprinted from [72] with permission of American Chemical Society, Copyright 2003.

In the low additive concentration regime I the polymer crystallizes before the additive. Here the additive shows no influence and a lower crystallization temperature is expected, due to the solubilized additive. Of greatest importance is regime II, where polymer and additive build a homogenous melt solution and the additive crystallizes prior to the polymer without preceding liquid phase separation upon cooling. The additive crystallizes in form of a fibrillar network in the melt. This network formation can be observed by an increase of complex viscosity [60, 69, 72]. Induced by the network, surface crystallization starts and thus an increase in crystallization temperature is observed. In the broad concentration regime III liquid-liquid phase separation is observed. During cooling, DMDBS crystallizes into large fibrillar structures, which can be observed in the optical microscope, followed by the polymer crystallization itself. Regime IV is the high concentration area, where the morphology of the mixture is dominated by the large primary structures of the additive. Details on this phase behavior can be found in the original literature [72].

Bernland et al. [77, 78] investigated a similar phase behavior for the binary system of iPP/TBPMN. In this case, the liquid-liquid phase separation has been observed exceeding 5.0 wt% of TBPMN. This was indicated as an enhanced miscibility of the new additive, compared to the DMDBS system [72] in which the separation was observed exceeding 2.5 wt%. Optical properties haze

and clarity progressively improved, starting at 0.1 wt% until the maxima was reached and phase separation started. The improved optical properties reached remarkable levels of haze with round about 10 % (~15 % for DMDBS [73]) and comparable levels of clarity. As a consequence of the enhanced solubility in iPP, the required concentrations for these haze levels are located at 0.6 wt%. This is a much higher activity concentration as known for previous members of the sorbitol family. An achieved advantage of this system is that it allows for its use in clarified products of higher thickness, which is an outstanding issue for many CAs [79]. A plateau of the peak crystallization temperature for the TBPMN system was recorded at 130 °C (0.4 wt%).

As mentioned, the sorbitol derivatives crystallize into large fibrillar structures, which can be observed by optical microscopy prior to polymer crystallization itself. An important difference between TBPMN and DMDBS has been mentioned by Bernland et al. in terms of the form of the fibrils upon crystallization of the mixtures. DMDBS fibrils could have been detected already at concentrations of 1.0 wt% under the optical microscope, whereas the TBPMN fibrils could not be detected even at high concentrations (4.0 wt%). The finer morphology of the TBPMN fibrils was considered as an indicator for a reduced lateral growth rate of the TBPMN additive, due to its more complex substituents.

Earlier, the mechanism of action of sugar acetals as nucleating agents for PP has been studied by Smith et al. [80]. With their data, they proposed a nucleation theory in which the nucleating agent forms in the shape of a cleft and then binds and stabilizes helical polypropylene. They speculated that the binding decreases the number of helices that return to a random conformation. Moreover they rejected the assumption of Titus and Millner [81], that dimer formation between two DBS molecules is critical for the nucleating ability, by showing that monomer energies correlated better than dimer energies and by proofing that trinaphthylidenesorbitol, which does not have a diol and thus cannot form a dimer, is a good nucleator.

1.4.4. Characteristic values for the evaluation of nucleating and clarifying agents

Material characteristic values like crystallization temperature and crystallization half time are used to determine the effectiveness of nucleating agents. The polymers' crystallization temperature ($T_{c,p}$) can be measured in a non-isothermal differential scanning calorimetry (DSC) cooling experiment. $T_{c,p}$ is dependent on the cooling rate and specific for each polymer resin. Moreover it is influenced by additive type and loading level. By applying DSC measurements, the nucleation effect can be investigated and is characterized by a typical temperature shift towards higher temperatures. Fundamentally, the higher the crystallization temperature compared to the non-nucleated polymer, the more effective the nucleating agent. Figure 1-21 shows an example of non-nucleated versus nucleated iPP [8].

The biggest advantage of the non-isothermal DSC experiment lies in its little effort, whereas its disadvantage is that the crystallization temperatures of many efficient nucleators do not differ significantly and thus lie in the range of the measuring error. In such cases, the use of the crystallization half-time ($t_{1/2}$), which can be determined from an isothermal DSC cooling experiment, can be valuable. The crystallization half-time is defined as the time at which the extent of crystallization is 50 % completed. The shorter the half-time, the faster the

crystallization rate. The crystallization half-time delivers a better resolution of nucleators with similar efficiency compared to $T_{c,p}$, but in general a more complex experimental setup is necessary.

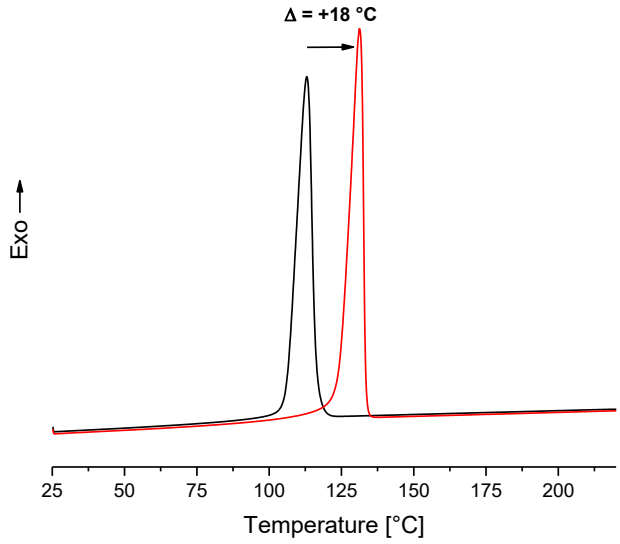

Figure 1-21 Non-isothermal cooling curve of non-nucleated (black) and with 0.3 wt% TBPMN nucleated (red) isotactic polypropylene homopolymer Moplen® HP 500 N.

Fillon et al. [71] established an improved nucleating efficiency scale, by using conventional differential scanning calorimetry (DSC) cooling runs. They made use of the crystallization temperature ($T_{c,p}$) of self-nucleated blank polymer. They studied the efficiency coefficients of different nucleating agents by defining the nucleation efficiency (NE) as the following ratio:

$$NE = 100\,\frac{T_{cNA} - T_{c1}}{T_{c2max} - T_{c1}} \qquad (1)$$

T_{c2max} and T_{c1} are the crystallization temperature of self-nucleated and non-nucleated iPP. NE is expressed as percentage, where 100 % stands for maximum nucleation efficiency and refers to ideally nucleated samples. This value is dependent on the cooling rate and the sample specific properties. Fillon et al. [71] determined the efficiencies of several nucleating additives and found efficiencies of around 50-60 % to be the best results. For DBS they determined a crystallization temperature of 123.2 °C and a NE of 41 %. Marco et al. [73] applied the same equation (1) and calculated an efficiency of 60 % for MDBS and 65 % for DMDBS. Their results showed that the efficiencies of the second and third generation were more than 20 % higher than earlier reported results for DBS at comparable concentrations.

Nucleating agents influence also mechanical and optical properties of the isotactic polypropylene. These are mainly influenced by the spherulite size and the polymer crystallization degree. The increased nucleation density, caused by the nucleating agents, results in a significant reduction in spherulite size [36]. Figure 1-22 shows polarized optical

micrographs of non-nucleated and nucleated isotactic polypropylene samples. Nucleated samples show an overall reduced spherulite size from a few hundred to just a few nm in square.

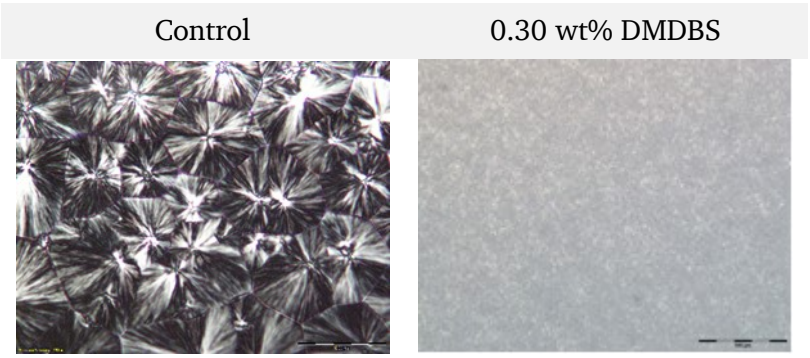

Figure 1-22 Polarized optical micrographs of melt-compression-molded iPP films without nucleating agent and containing 0.30 wt % DMDBS. Scale bar 100 µm.

Furthermore, the addition of nucleating agents can cause an increase of the crystallization degree. This can be measured by calorimetric or radiographical experiments. Detailed procedures can be found in literature [82, 83].

In literature, it is assumed that optical properties of semi-crystalline polymers are mainly influenced by the spherulite size [36]. The most important optical properties for plastic materials are transmission, haze and clarity. Transmission is defined as the ratio of the intensity of the transmitted light to the intensity of the incident light. In contrast, haze is a measure of the turbidity of a sample and is commonly defined according to ASTM D 1003 as the portion of visible light which is scattered at wider angles ($2.5° < \theta < 90°$) [3]. Clarity is related to the sharpness of an object and is defined as the amount of visible light that is scattered at small angles ($\theta < 2.5°$). As said, a result of nucleation is the reduction in spherulite size, haze can be reduced and clarity enhanced [58]. An essential prerequisite is that the particle size of the nucleating agents and clarifiers itself is so small that they do not scatter any light.

2. Aim and Objectives

Aim of the present PhD thesis was the design and development of new nucleating and clarifying agents as well as the establishment of the corresponding application tests to identify novel prototypes. The focus was put on a structure-activity relationship study, allowing to gain further insights into nucleating and clarifying phenomena. The understanding of the characteristics a good nucleating agent has to exhibit is limited until now. Moreover, the mechanism of clarification still remains poorly understood. The current understanding is that a good nucleating and clarifying agent needs to exhibit excellent dispersibility in the polymer melt. State of the art soluble clarifying agents provide a fine fibrillar network with a high surface area upon cooling [60, 61]. These criteria are not enough to induce polymer nucleation. It is known that, amongst others, the chemical structure of the additive is crucial for the nucleation behavior of the final resin. The provided surface must strongly promote nucleation of the polymer, which can be reached by fulfilling the 'lattice matching criterion' to enable epitaxial growth [63–65]. However, until now, a general statement on how an ideal clarifying agent structure has to look like and which functionalities it has to exhibit cannot be made.

Consequently, this study aims to reduce this knowledge gap by identifying a new class of clarifying agents with several modifiable functionalities. These functionalities should be varied systematically to derive potential new structure-property relations. The results may be used to provide insights into the structural "design" of new clarifying agents.

Sorbitol based derivatives, such as DMDBS (Figure 2-1) were chosen as a potential comparison system, as they are known as highly efficient clarifying agents. Beside the π-π interactions of the benzylidene 'wings', the two terminal hydroxyl groups enable intramolecular and intermolecular hydrogen bonds and seem to be crucial for the efficiency of this class [68].

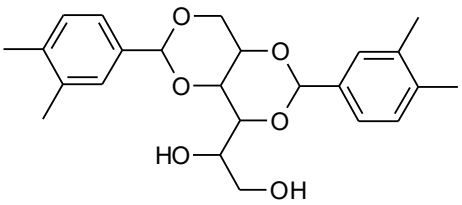

Figure 2-1 Structure of bis (3,4- dimethylbenzylidene) sorbitol (DMDBS).

The aim of the first part is the identification, synthesis and characterization of a new class of clarifying agents with additional functionalities. First of all, it should be investigated whether all polyols are capable of undergoing diacetalization reactions and whether their conformation is crucial for self-assembly [70]. The targeted molecules should consist of a C_6 'backbone', comprising two substituted benzylidene 'wings' and a different functionalized 'tail' with hydrogen bonding units to influence the self-assembly of the molecules. The schematic structure is shown in Figure 2-2.

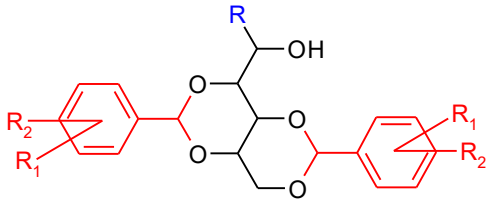

Figure 2-2 Generic structure of potential nucleating and/or clarifying agents.

In order to achieve this, the following issues have to be addressed:

- A potential model structure has to be identified with respect to its synthetic feasibility.
- To investigate structure-property relationships, the functionalization of the model structure at 'wings' and 'tail' has to be varied systematically. Consequently, all substitution patterns of the benzylidene 'wings' should be varied individually for each inserted 'tail', whereas the hydrogen boning 'tails' ought to be selected from the group of carboxylic acid, ester and amides, wherein the amides can be varied further in their alkyl chain length.
- Novel additives have to be characterized by standard methods, such as NMR spectroscopy, mass spectroscopy and thermal analysis.
- To gain a better understanding of the self-assembly potential of the molecules, their gelling behavior in organic solvents should be investigated.

The aim of the second part is to investigate the nucleation and clarification potential of a whole 'library' of derivatives. For the evaluation of these newly synthesized additives a reliable screening method has to be established. To study the novel additives, the following issues need to be addressed:

- All synthesized additives have to be screened in an iPP homopolymer in various concentrations.
- The melting and crystallization temperature of the prepared compounds have to be determined by DSC experiments and the optical properties have to be measured on injection molded plaques by applying standard procedures.
- To obtain a better insight in the solid-state morphology, the spherulite size has to be investigated with polarized optical microscopy and the crystal morphology of iPP has to be studied on injection-molded specimens by wide angle x-ray scattering.
- Initial melting and dissolution experiments, combined with rheology experiments should be applied to identify a potential network formation in the polymer melt, enabling the validation of the literature known mechanism of action ('dispersion' or 'soluble' type) for the novel additives.
- Attempts should be made to deduce universal tendencies, dependencies and correlations gained from the obtained results. These derived structure-property relations aim to provide insights on the structural "design" of new clarifying agents.
- Finally, the temperature dependency during compounding and the transferability into other polymer resins has to be investigated, at least for the lead structure, in order to ensure the effectiveness of the newly developed class of clarifying agents.

3. Strategy and selection of a suitable starting molecule

This section is meant to provide an overview on the identification process towards a lead structure, which enables to study the nucleation and clarifying process as defined in the aim of this thesis.

Strategic background

Major aim of this thesis is the identification of a new class of nucleating and clarifying agents, which exhibits additional structural functionalities in contrast to the established sorbitol based clarifying agents. This new class is intended to be used in order to better understand the crucial role of the chemical structure, which leads to the desired nucleating and clarifying effect. Although a lot of research on this topic has been conducted, there are still several unsolved issues. To the best of our knowledge, this is the first time that sorbitol like structures are systematically investigated regarding their nucleation ability, taking into account the influence of different functional 'tails'.

Even though numerous investigations on different dibenzylidene sorbitol derivatives in polymeric environments [53–56, 72, 77, 84] and their behavior as organogelators [85–93] have been performed, no study considered different functional moieties. Since the precise structure and the mechanism of DBS aggregation has been subject of controversial debate, it turned out that most probably an interplay of hydrogen bonding and π-π-stacking are the driving forces for its network formation [52]. Therefore it might be challenging, but informative at the same time, to investigate different 'tails' and the corresponding ability to nucleate especially iPP.

To derive potential structure-property relations, it was necessary to determine a model structure which is capable to provide the required functionalities.

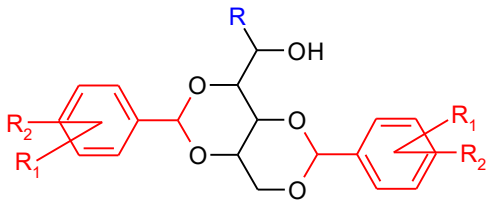

Figure 3-1 Generic structure of potential nucleating / clarifying agents.

The model structure of the potential nucleating and clarifying agent has to exhibit the appearance shown in Figure 3-1 and should consist of

- a central C_6 'backbone';
- two peripheral apolar benzylidene 'wings' with different substitution patterns, enabling stacking of the molecules and dissolution of the amphiphilic molecules in the molten, hydrophobic polymer;
- different hydrogen bonding 'tails', enabling the molecules to build up a fibrillar network – e.g. by ester, acid or amide functionalities.

Once an ideal substance class featuring above-mentioned modifications has been identified, the structural influence on the nucleation and clarifying abilities can be systematically studied.

Identification of structures, capable to act as model compound

The initial hurdle was to identify a potential structure, which at the end bore a different 'tail' and which was able to undergo a diacetalization reaction to form the desired dibenzylidene acetals.

First, *D*-glucamine and its *N*-methyl derivative (cf. Figure 3-2) have been considered as promising starting materials. By performing a diacetalization reaction with the derivatives presented in Figure 3-2, one would have obtained diacetals with an amino group modified 'backbone'. Due to the different hydrogen bonding strength and formation, most probably this would have influenced the molecules' self-aggregation behavior. Acetals are generally prepared by an acid catalyzed condensation of aldehydes with alcohols / polyols or by transacetalization. Fully aware of the reactivity of the primary and secondary amine group, which may result in the corresponding imine, the protection of the hydroxyl groups by benzylidene groups has been considered to be possible. The focus of this reaction was therefore put on the transacetalization reaction with dimethyl benzylidene acetal. Direct reaction of the benzylidene aldehyde has been tried as well. Owing to the basicity of the amino function the consumption of the acid catalyst has been considered too. Several experiments were conducted in which different amounts and types of catalytic systems and solvents, as well as temperatures and reaction-times were systematically varied. Combinations of the following catalysts and solvents were studied:

Catalysts:	p-Toluenesulfonic acid, Camphorsulfonic acid, Hydrochloric acid, Zinc chloride, Formic acid
Solvents:	Toluene, Dimethylformamide, Acetonitrile, Water, Methanol, Ethanol

Several experiments with the latter described conditions were performed with *N*-dimethyl-*D*-glucamine and *N*-acetyl-*N*-methyl-*D*-glucamine as well to avoid potential imine formation (cf. Figure 3-2).

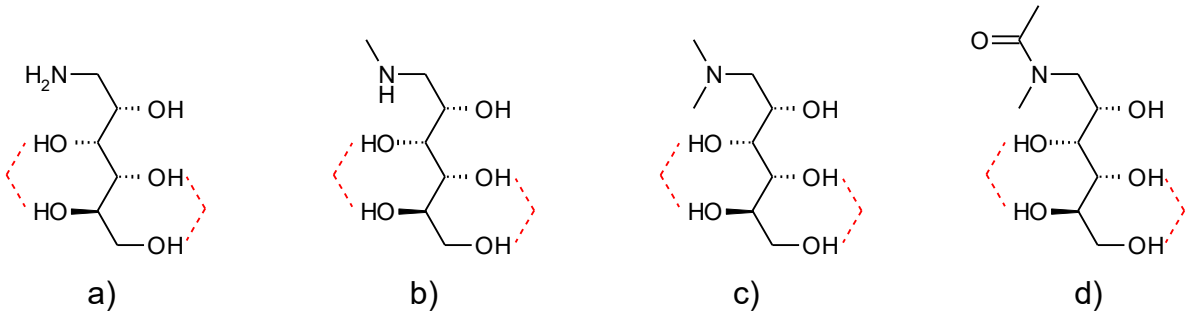

Figure 3-2 Structures of a) *D*-glucamine, b) *N*-methyl-*D*-glucamine, c) *N*-dimethyl-*D*-glucamine and d) *N*-acetyl-*N*-methyl-*D*-glucamine. Red dashed lines indicate potential acetalization pattern.

All these attempts to synthesize a dibenzylidene acetal turned out to be unfeasible. In some cases a reaction was observed, but in most cases the desired diacetal could not be isolated or

was just present in traces. Some reactions afforded the product among several by-products, but isolation attempts by means of column chromatography were not successful. Even reproduction of a published reaction [94] with *N*-acetyl-*N*-methyl-glucamine, shown in Figure 3-3, failed because isolation of the reported products was not possible. Apart from this, it would have been difficult to obtain enough pure substance for its intended use as a nucleating additive in a polymer system.

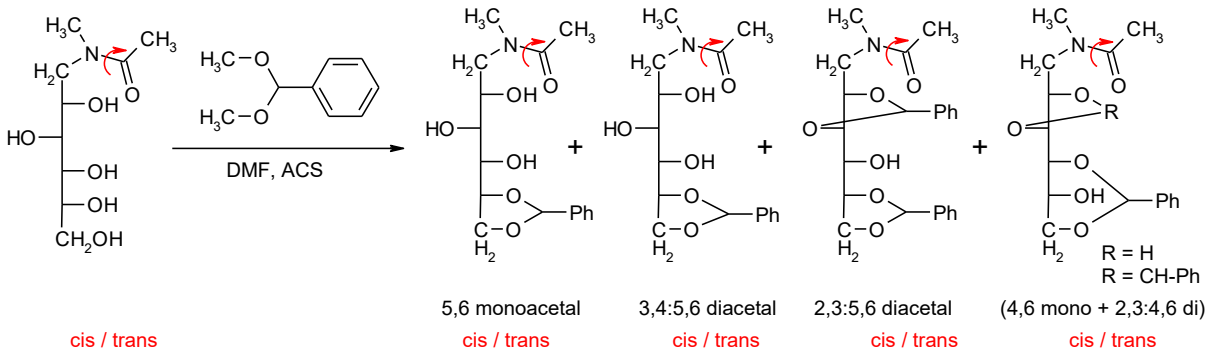

Figure 3-3 Reaction of *N*-acetyl-*N*-methyl-glucamine with dimethyl benzylidene acetal and the reported mono- and diacetals as reaction products. 5,6-*O*-benzylidene-*N*-acetyl-*N*-methylglucamine was reported as the major product and 2,3:4,6-di-*O*-benzylidene-*N*-acetyl-*N*-methylglucamine, 4,6-*O*-benzylidene-*N*-acetyl-*N*-methyl-glucamine and a mixture of 2,3:5,6- and 3,4:5,6-di-*O*-benzylidene-*N*-acetyl-*N*-methylglucamine as byproducts [94].

One conceivable explanation for the failure of all previous reactions is probably the stereochemistry of *D*-glucamine and its derivatives. Knowing that benzaldehyde preferably reacts with 1,3-dioles to form benzylidene acetals, the reacting hydroxyl groups should be arranged in syn-position. A closer look at the stereochemistry of *D*-glucamine and its derivatives reveals that the formation of a 3,5:4,6-dibenzylidene acetals is potentially hampered, due to an anti-arrangement of the 3,5-hydroxy groups (Figure 3-2). The crucial factor seems to be the alignment of the hydroxyl groups and a syn-arrangement turns out to be required.

In a further step, *L*-gulonic-1,5 lactone has been taken into consideration, as according to Yamasaki et al. it can be reacted with benzaldehyde dimethyl acetal to yield 3,5:4,6-diebenzylidene-*L*-gulonic acid methyl ester (Figure 3-4) [52, 85, 86].

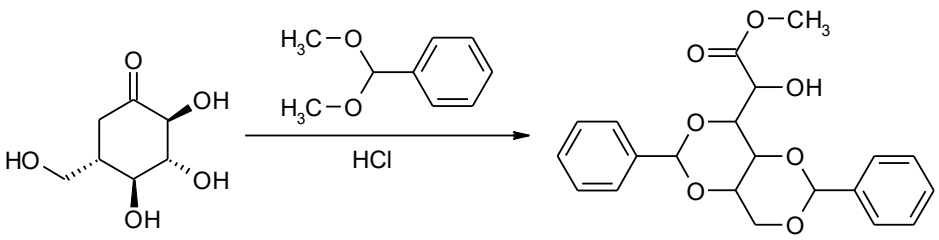

Figure 3-4 Scheme representing the reaction of *L*-gulonic-1,5 lactone with benzaldehyde dimethyl acetal to yield 3,5:4,6-diebenzylidene-*L*-gulonic acid methyl ester.

Functionalization of the terminal moiety of 3,5:4,6-dibenzylidene-*L*-gulonic acid methyl ester enables the accessibility to several other derivatives (e.g. acids, amides and amines). These derivatives most probably show different behaviors, due to different hydrogen bonding

strength. The only unsatisfying aspect has been the availability of *L*-glucono-1,5-lactone; it is only available in small quantities. That is why initial experiments were performed with *D*-glucono-1,5-lactone; being fully aware that the inverted stereochemistry might influence the described reactivity. In addition to that, the published stereochemistry of 3,5:4,6-dibenzylidene-*L*-gulonic acid methyl ester in the review article of Okesola et al. [52] is not correct and thus the open ring structure of the unreacted starting material looks like as follows in Figure 3-5.

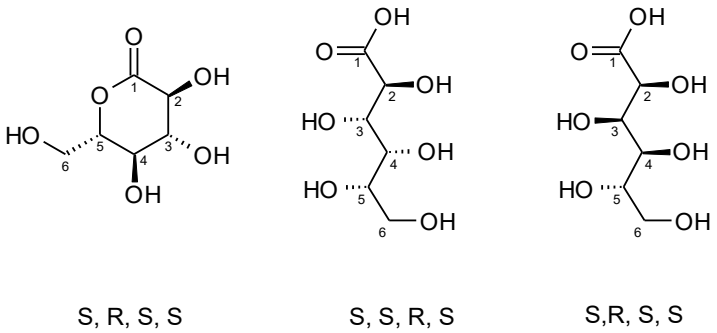

Figure 3-5 R/S configuration of *L*-glucono-1,5 lactone (left), incorrect (middle) [52] and correct configuration (right) of its open ring structure.

As expected, extensive analytical studies revealed that the initial trials with *D*-glucono-1,5 lactone presumably yielded only the 2,4-benzylidene-*D*-gluconic acid methyl ester (Figure 3-6) instead of the desired 3,5:4,6-dibenzylidene-*D*-gluconic acid methyl ester as described elsewhere [85]. Moreover, it is confusing that Yamasaki et al. [85] reported to yield 3,5:4,6-dibenzylidene-*L*-gulonic acid after the first step under described conditions. Normally, by applying these conditions the methyl ester is expected to form directly. Considering further the incorrect configuration, it is doubtful if the described procedure [85] is correct. A reproduction of the reported results [85] has not been possible.

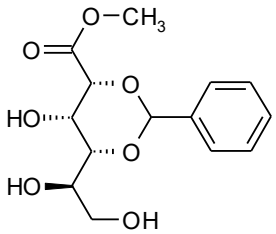

Figure 3-6 2,4-benzylidene-*D*-gluconic acid methyl ester.

Again, it turned out, that stereochemistry is crucial for acetal formation with 1,3-diols. In this case, only the 2,4- as well as the 4,6- hydroxyl groups are in a syn-configuration. The other existing possibility for 1,3-acetal formation between 3,5-hydroxy groups is arranged in an anti-configuration. As a result of the formed 2,4-monoacetal with no further accessible syn-configurated hydroxyl groups this approach was not pursued further.

Considering the importance of stereochemistry, *L*-gulonic acid gamma lactone (*L*-Gulono-1,4-lactone), which can be synthesized via a hydrogenation reaction out of *L*-ascorbic acid [95–98], had been considered as the most promising starting material.

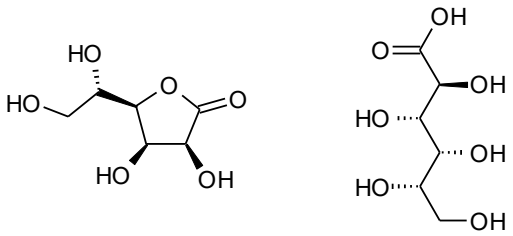

Figure 3-7 Configuration of *L*-gulonic acid gamma lactone (left) and its open structure (right).

The stereochemistry absolutely fits the requirements and exhibits syn-configurated hydroxyl groups in 4,6- and 3,5-positions (Figure 3-7). Literature research revealed that Crawford et al. followed exactly this approach, using *L*-gulono-1,4-lactone around 1977 [99, 100]. They converted *L*-gulono-1,4-lactone into ethyl-3,5:4,6-*O*-dibenzylidene-*L*-gulonate by treating it with 4 equivalents of benzaldehyde diethyl acetal and concentrated hydrochloric acid (Figure 3-8) [99, 100].

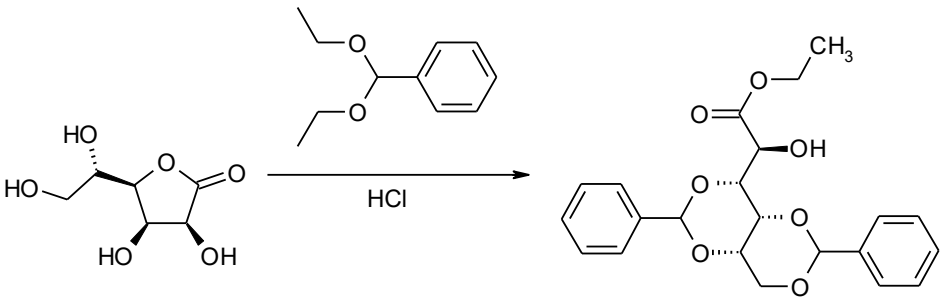

Figure 3-8 Synthesis of ethyl-3,5:4,6-*O*-dibenzylidene-*L*-gulonate by reacting *L*-gulono-1,4-lactone and benzaldehyde diethyl acetal in an acid catalyzed reaction.

Further promising derivatives, such as its acids, amides, substituted amides and amines were investigated in 1988 by researchers of Kao Corporation [101]. The intended application field of the dibenzylidenated polyhydric alcohol derivatives were emulsifiers.

Taking into account the mentioned reaction conditions, derivatization of 3,5:4,6-dibenzylidene-*L*-gulonic acid methyl esters enables to synthesize and finally investigate sorbitol like structures with different functional 'tails' [100, 101]. After successfully performing this reaction a feasible route with sufficient yields towards a model structure has become accessible. This model structure allows for the variation of the terminal moiety on the one hand, and for the substitution of the benzylidene 'wings' on the other. In this way an extensive library of potential nucleating and clarifying agents has become accessible. Building up this library by synthesizing several derivatives, in case of success, it might be possible to derive new structure-property relations in a for these derivatives unknown application field.

Conclusion

As a first outcome, one can conclude that not all polyols, consisting of a C_6 'backbone', are capable to undergo a diacetalization reaction. Most likely the configuration of the hydroxyl groups plays a crucial role. It has been found that syn-configurated hydroxyl groups are highly

favored to undergo acetalization reactions. Finally the new synthesized model structure ends up with an identical conformation as the sorbitol based dibenzylidene acetals.

4. Synthesis and characterization of a new nucleating and clarifying agent library

This section is divided into mainly two subparts. The first subpart comprises the synthesis strategy which has been used to build up the library of derivatives based on the model structure and its final synthetic route. Additionally, potential influences by the incorporated 'tails' are discussed. The second subpart is about the thermal properties of the newly synthesized additives, as their thermal characteristics have a crucial role in the intended application field of the additives. The additives gelling behavior is briefly discussed as well.

4.1. Synthesis of 3,5:4,6-dibenzylidene-*L*-gulonic acid derivatives

Synthesis strategy to afford a library of derivatives based on the model structure

After the quite challenging identification process of a potential model structure, it has been necessary to contrive the scope of the library of derivatives. Therefore, the most important aspect was getting access to different functional groups at the molecules' 'tail'. By derivatization of the model structure, several different 'tails' are accessible in theory; hence the scope was narrowed down to predominantly carboxylic acid derivatives, as well as some carboxylic amide structures. Figure 4-1 comprises a series of potential derivatives, which should be accessible.

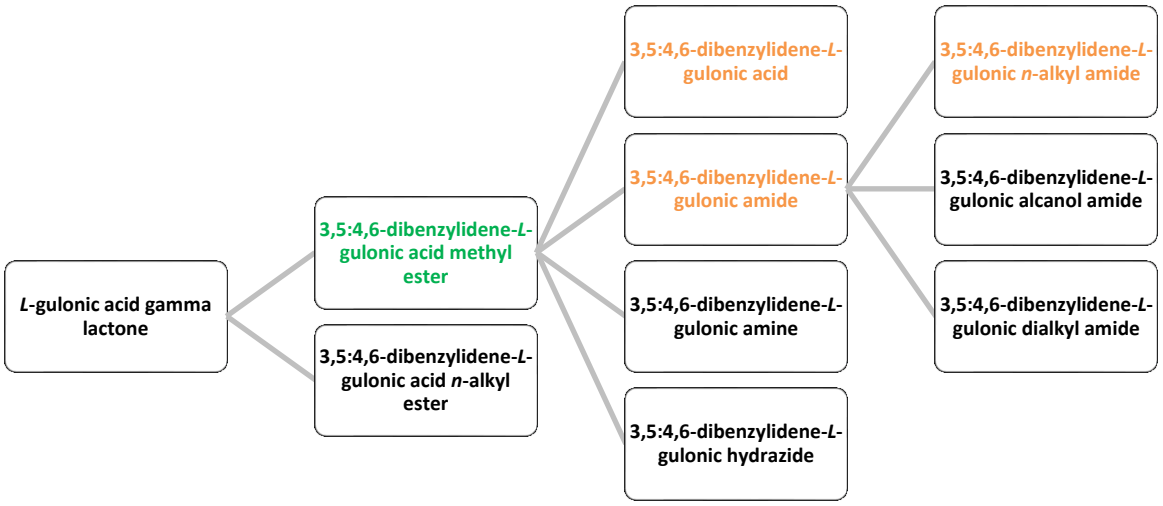

Figure 4-1 Pathway towards potential dibenzylidene-*L*-gulonic acid derivatives.

Particularly suitable for additional derivatization is the carboxylic amide moiety. For example, by introducing branched or unbranched alkyl chains of different length, the compatibility of the molecules in the polymer matrix will be influenced. By this, the previously polar 'tail' becomes more apolar and hydrogen bonding strength will be drawn off. Along with that, the melting and solubility behavior of the molecules might be affected. This may have a huge influence on the additives final aggregation behavior and nucleation potential. Some potential effects caused by the modification of the terminal moiety are briefly discussed later on.

If there is access to at least four of these derivatives, then in a second step the substitution of the benzylidene 'wings' has to be addressed. This step is straightforward as, in principle, only

the reactivity of the dibenzylidene acetal varies. Since there are several potential substitution patterns for the benzylidene 'wings', a selection was necessary. A decision was made to narrow down the amount of substitution patterns to nine. Mono- and dimethyl substituted analogues have contributed to an enormous efficiency increase in the development of sorbitol-based clarifying agents. For this reason, dimethyl substituted benzylidene acetals with different substitution patterns were used predominantly. Moreover, three mono alkyl substituted derivatives were used in addition to the unsubstituted benzylidene acetals. Details on the substituents used can be found in the synthesis description. It is likely, that the introduction of different substitution pattern causes conformational changes, as well as variations in the overall solubility of the molecules. These potential influences are briefly discussed later on.

Synthetic route towards dibenzylidene-*L*-gulonic acid derivatives

In the context of this work, derivatives of 3,5:4,6-dibenzylidene-*L*-gulonic acid were synthesized, based on *L*-gulonic acid gamma lactone (**2**) as a starting material. The latter can be synthesized by a simple hydration reaction of *L*-ascorbic acid (**1**). Different reaction conditions with different catalytic systems for this reaction can be found in the literature [95–98]. Beyond the literature-known catalysts Pd/C [95–97] and Rh/C [98], we found out that Ru/Al_2O_3 yielded the desired *L*-gulonic acid gamma lactone (**2**) stereo-selectively in nearly quantitative yield as well. Detailed procedures, yields and characterizations of all synthesized structures are given in the experimental part.

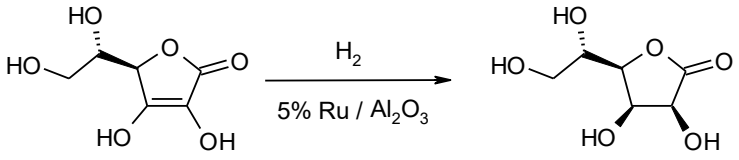

Figure 4-2 Synthetic route to *L*-gulonic acid gamma lactone (**2**) starting from *L*-ascorbic acid (**1**).

The main step in the synthetic route towards derivatives of 3,5:4,6-dibenzylidene-*L*-gulonic acid is a diacetalization reaction with two moles of aldehyde. The simple approach to conduct the acetalization reaction with the aldehyde (**3**) turned out to be challenging, because the reaction often stopped at the monoacetal stage and no further efforts were made to optimize this reaction. Therefore, it was necessary to perform a transesterification reaction with substituted benzaldehyde dimethyl acetal (**4**), following literature known procedures [102, 103].

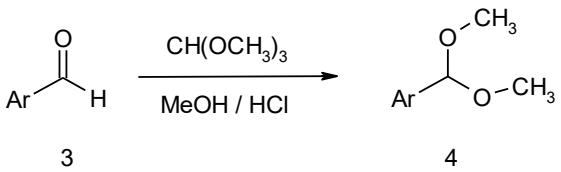

Figure 4-3 Synthetic route to substituted benzaldehyde dimethyl acetals (**4**) starting from substituted benzaldehyde (**3**).

For all synthesized derivatives shown in Table 4-1, the pure product was obtained in excellent yields.

Table 4-1 Derivatives of substituted benzaldehyde dimethyl acetals (4).

Ar =	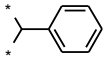	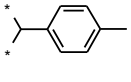	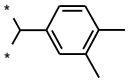	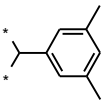	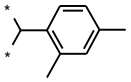
Abrr.	**4a**	**4b**	**4c**	**4d**	**4e**

Ar =	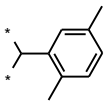	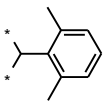	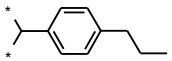	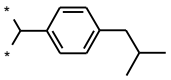
Abrr.	**4f**	**4g**	**4h**	**4i**

For ease of reading, the development of the 3,5:4,6-dibenzylidene-*L*-gulonic acid derivatives is divided into sets, according to the introduced carboxylic acid methyl ester, carboxylic acid, primary and secondary carboxylic amide 'tails' (Figure 4-4). Initially, feasibility of all synthetic steps was checked on the unsubstituted benzylidene derivative (**4a**).

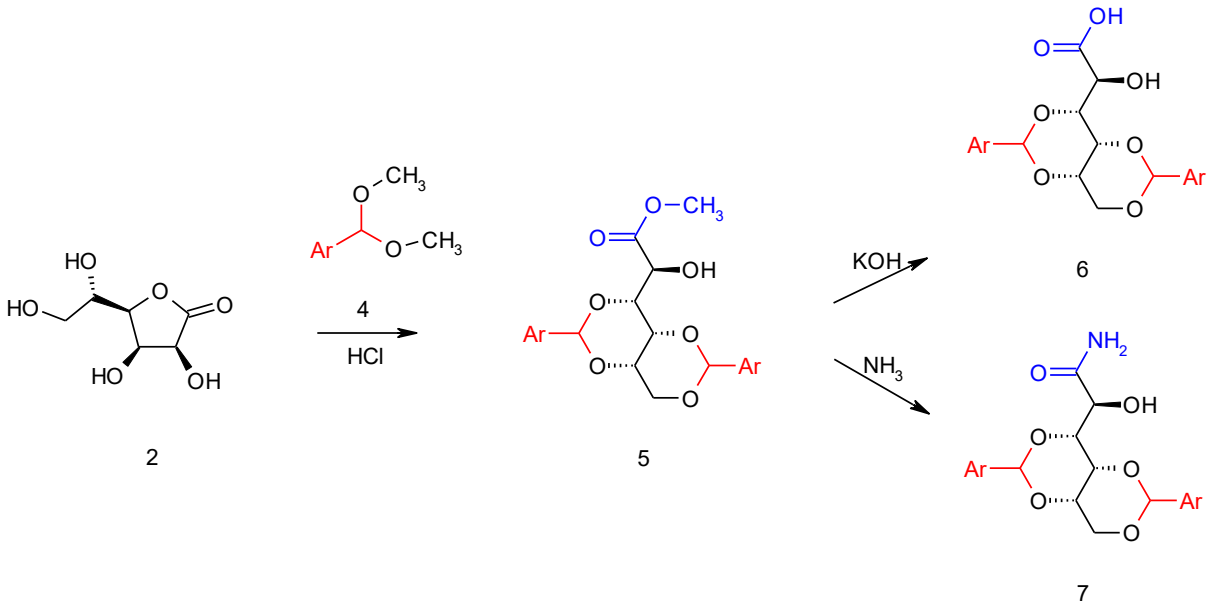

Figure 4-4 Synthetic route to derivatives of 3,5:4,6-dibenzylidene-*L*-gluconic acid methyl ester (**5**) starting from *L*-gulonic acid gamma lactone (**2**) and substituted benzaldehyde dimethyl acetal (**4**), as well as to 3,5:4,6-dibenzylidene-*L*-gluconic acid (**6**) and 3,5:4,6-dibenzylidene-*L*-gluconic amid (**7**) starting from 3,5:4,6-dibenzylidene-*L*-gluconic acid methyl ester (**5**).

All synthesized derivatives of 3,5:4,6-dibenzylidene-*L*-gluconic acid methyl ester (**5**) were obtained as pure, white products in very good to excellent yields via the reaction with substituted benzaldehyde dimethyl acetals (**4**). As mentioned, the reaction was only feasible following described conditions [99–101] with an excess of at least 4 equivalents of the respective

dimethyl acetal (**4**). Optimization attempts have not been conducted, because the goal was their investigation as potential nucleating and clarifying agents, rather than optimization of the synthesis. The reaction of *L*-gulonic acid gamma lactone (**2**) and 2,6-dimethylbenzaldehyde dimethyl acetal (**4g**) turned out to be unsuccessful. By applying the same reaction conditions as for all other derivatives, it was possible to observe the formation of mono-and diacetals via TLC. Nevertheless, no direct substance precipitation occurred. Several attempts to isolate the derivative **5g** failed. Neither variation of the reaction conditions (time, temperature, excess of acetal), nor column chromatography turned out to be successful. This reaction failed most probably due to steric and/or reactivity reasons.

Derivatives of 3,5:4,6-dibenzylidene-*L*-gluconic acid (**6**) were obtained in excellent yields. Since the workup step reported by Ohashi et al. [101] led to a high yield loss, some adjustments of that step were applied (cf. Experimental part). The reaction products **6g** and **7g** were not synthesized due to the missing precursor **5g**. Instead of performing the described amidation reaction described by Ohashi et al. [101], another approach using a solution of ammonia in methanol was compiled [104]. Consequently, all of the 3,5:4,6-dibenzylidene-*L*-gluconic amide (**7**) derivatives were obtained in excellent yields. All synthesized derivatives of 3,5:4,6-dibenzylidene-*L*-gluconic acid methyl ester (**5**), 3,5:4,6-dibenzylidene-*L*-gluconic acid (**6**) and 3,5:4,6-dibenzylidene-*L*-gluconic amide (**7**) can be found in Table 4-2.

Table 4-2 Derivatives of 3,5:4,6-dibenzylidene-*L*-gluconic acid methyl ester (**5**), 3,5:4,6-dibenzylidene-*L*-gluconic acid (**6**) and 3,5:4,6-dibenzylidene-*L*-gluconic amid (**7**).

Ar =	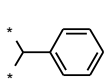	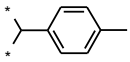	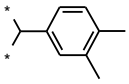	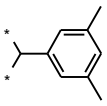	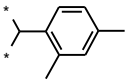
5-7	**a**	**b**	**c**	**d**	**e**

Ar =	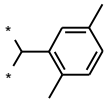	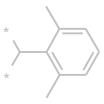	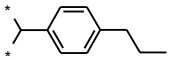	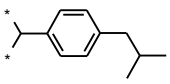
5-7	**f**	**g**	**h**	**i**

The simple approach to apply the reaction conditions, used in the synthetic step towards 3,5:4,6-dibenzylidene-*L*-gluconic amide (**7**) derivatives, for the synthesis of alkyl substituted amide derivatives (**8**) afforded the desired products (Figure 4-5). However, some of the derivatives required longer reaction times and a larger excess of the relevant amine derivative. Table 4-3 contains the derivatives obtained by this approach.

The reaction presented in Figure 4-5 is not limited to alkyl substituted derivatives of 3,5:4,6-dibenzylidene-*L*-gluconic amide (**8**). Initial trials showed that 3,5:4,6-dibenzylidene-*L*-gluconic *N*-alkanol amide derivatives can be synthesized as well. As a result of low yields, this approach was not considered further, because a certain amount (~ 3.5 g) of the additives was needed for the intended application test. Moreover, first trials to synthesize tertiary amides, applying

identical reaction conditions failed. Again, steric hindrance and/or reactivity was held accountable. No additional effort was put into optimization of this reaction.

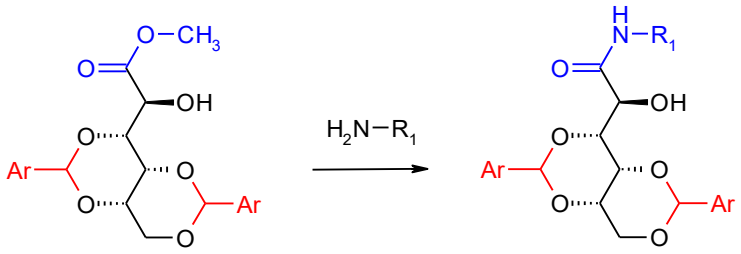

5 8

Figure 4-5 Synthetic route to derivatives of 3,5:4,6-dibenzylidene-*L*-gluconic alkyl amide (**8**) starting from 3,5:4,6-dibenzylidene-*L*-gluconic acid methyl ester (**5**).

Table 4-3 Derivatives of 3,5:4,6-dibenzylidene-*L*-gluconic alkyl amide (**8**)

R_1 =	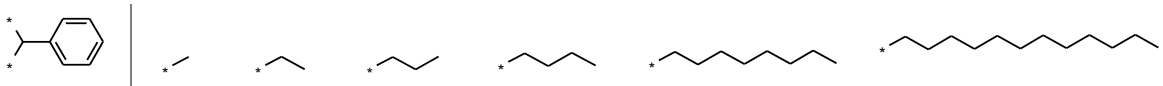					
Abrr.	**8.1a**	**8.2a**	**8.3a**	**8.4a**	**8.5a**	**8.6a**

R_1 =	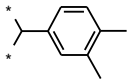	
Abrr.	**8.1c**	**8.2c**

R_1 =	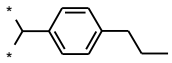	
Abrr.	**8.1h**	**8.2h**

Influence of terminal hydrogen bonding moieties and of 'wing' substitution pattern in dibenzylidene based acetal derivatives

Capturing the specific destinations of intermolecular hydrogen bonds among the newly synthesized additives is challenging. While it is in general possible to investigate the additive aggregation in organic solvents, it is almost impossible within a polymeric surrounding. Even the specific destination of the intermolecular hydrogen bonds of the sorbitol derivatives is not yet entirely resolved [52, 105]. It was proven, however, that the terminal hydroxyl group (6-OH) is critical as a hydrogen bond donor (HBD) for DBS self-assembly [86]. The 6-OH group is said to be intermolecularly hydrogen-bonded to an acetal oxygen and the 5-OH group is said to either hydrogen-bond intramolecularly to an acetal oxygen or intermolecularly to the surrounding solvent [86].

The tendency of functional groups to engage in hydrogen bonding with other targets (molecule or solvent) can be analyzed at a simple level, as illustrated in Figure 4-7.

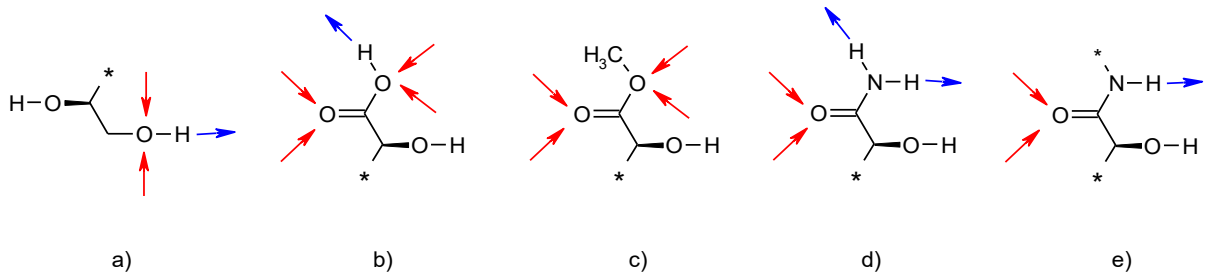

Figure 4-7 Potential HBD (→) and HBA (→) in different 'tails': a) 6-OH, b) acid, c) ester, d) prim. amide, e) sec. amide.

Primary alcohols (Figure 4-7a) are often involved in hydrogen bonding. Besides the hydrogen as a HBD, the oxygen can act as a hydrogen bond acceptor (HBA) as well. Conversion of the hydroxyl into an ether disrupts the HBD ability and may hinder the HBA process sterically or prevent it [86].

A carboxylic acid analogue (Figure 4-7b) acts as a HBD, but predominantly like a HBA, mainly through its carbonyl oxygen. Furthermore, carboxylic acid moieties are known to form head-to-tail hydrogen bonded dimers. Consequently, dibenzylidene derivatives bearing an acid 'tail' might aggregate in a completely different way than the DBS derivatives, which self-assemble over an acetal oxygen. An ester analogue (Figure 4-7c) which is devoid of HBD capacity can still act as an HBA. As a result, it can be assumed that these molecules in neither case self-assemble or dimerize.

Carboxylic amides may be involved in hydrogen bonding either as a HBA or as a HBD. The carbonyl oxygen acts as a HBA, forming two hydrogen bonds, whereas the nitrogen atom does not act as a HBA because the lone pair delocalizes into the carbonyl group. The N-H group of primary (Figure 4-7d) or secondary (Figure 4-7e) amides acts as HBD. The introduction of alkyl chains in the secondary amide leads to less hydrogen bonding strength and may hinder the ability to act as HBD via sterics or prevent it. In general, it must be considered that carboxylic acid, ester and amide groups are planar, and thus do not rotate because of their partial double bond character. This feature might influence self-assembly or dimerization additionally. Besides the terminal group, the substitution patterns of the aromatic 'wings' are likely to influence the aggregation behavior of the molecules as well. Intermolecular interactions between the 'wings' of at least two molecules, may twist the resulting fibrillar structures in a helical way to minimize energy [106]. Additionally, the solubility is influenced by the different substitution pattern and conformational changes might be a result from sterical effects [88, 89, 93]. Considering both effects, it is obvious that the aggregation process is strongly dependent on and sensitive to various different factors. Anyway, up to this point it was still unknown if, the dibenzylidene-*L*-gluconic acid derivatives will aggregate and finally influence the characteristics and morphology of iPP.

To gain first insights, if the synthesized molecules **5-8** are able to build up superstructures at all, their gelation ability was briefly screened. The results can be found in the following section.

4.2. The gelling ability of 3,5:4,6-dibenzylidene-*L*-gulonic acid derivatives

By performing gelation tests, typically known for low molecular mass organic gelators (LMOGs), the self-assembly of molecules into various network superstructures in organic solvents can be studied. Main driving forces are hydrogen bonding, π-π stacking, van der Waals interactions, coordination interactions, and other weak interactions [107]. However, it has to be noted that the main reason for the induction of gelation has not yet been identified [89].

Nevertheless, the conduct of gelling tests enables to gain first information on the differences in aggregation behavior of all synthesized 3,5:4,6-dibenzylidene-*L*-gulonic acid derivatives. *n*-Octanol is used often to perform gelation tests of LMOGs although it is not the best choice, since it is deemed not to represent the physico-chemical surrounding during crystallization from the apolar molten iPP. However, comparable superstructures formed in organic solvents have been found to develop in polypropylene as well [108]. Therefore, initial gelation tests were performed with all synthesized derivatives.

Table 4-4 and Table 4-5 comprise the results of gelation tests conducted with the additives in *n*-octanol. The investigated samples consisted of 1.0 wt% additive in *n*-octanol. Details can be found in the experimental part. Abbreviations are used to indicate the observed behaviors. Detailed photographs of the samples can be found in the appendix.

Table 4-4 Results of gelation test for derivatives **5-7** (1.0 wt% in Octanol)

	a	**b**	**c**	**d**	**e**	**f**	**h**	**i**
5	vS	G	G	vS	G	G	G	S
6	G	G	P	vS	G	vS	G	vS
7	vS	G	G	vS	G	G	G	G

G = gel; S = solution; P = precipitation; vS = viscous solution;

Five out of eight additives of the set of dibenzylidene *L*-gulonic acid methyl ester (DBGAcMeE, **5**) derivatives, half of the additives of the set of dibenzylidene *L*-gulonic acid (DBGAc, **6**) derivatives and six out of eight additives of the set comprising dibenzylidene *L*-gulonic amide (DBGA, **7**) derivatives form stable gels. Most of the derivatives which do not show gelation, form a viscous solution. Only two derivatives show a different behavior, **5i** and **6c**. Much more interesting is that for some substitution patterns the same behavior can be observed. All derivatives **b**, **e** and **h** form a stable gel independent of the 'tail', whereas all derivatives **d** form a viscous solution. The gels show different opacities, which result from the scattering of visible light [107]. The turbidity may be induced by structures larger than the wavelength of light and thus gives a hint on the size of the superstructure formed by the additives. The gel turbidity cannot be related to specific substitution patterns, but rather varies between milk-white and nearly transparent. It can be concluded that gels showing a milk-white appearance, most likely form superstructures which are greater than 380 nm within the xerogel. The turbidity of all mixtures forming a viscous solution has been found to be milk-white. Inability for gelation of some derivatives may result from steric effects, which disrupt the interaction between at least two molecules [93]. It is known, that especially meta-substituted DBS derivatives show no gelation [93]. This might be the reason for the additives **5-7d** as well, because they all exhibit a

3,5-dimethyl substitution. Thus having both methyl-substituents in meta-position might explain that in this case no gelation occurs and only viscous solutions are observed.

Table 4-5 Results of gelation tests for derivatives **8** (1.0 wt% in Octanol)

	8.1	**8.2**	**8.3**	**8.4**	**8.5**	**8.6**
a	vS	vS	vS	G	G	G
c	vS	G				
h	G	G				

G = gel; vS = viscous solution

Six out of ten dibenzylidene *L*-gulonic alkyl amide (DBGA-*n*, **8**) derivatives form stable gels. Secondary amide derivatives (**8.1-6a**) bearing unsubstituted benzylidene 'wings' induce gelation exceeding an alkyl chain length of four carbon atoms. Shorter chain lengths instead lead to viscous solutions. However, the behavior is strongly dependent on the substitution pattern of the benzylidene 'wings'. A changed substitution pattern enables gelation even for additives with shorter chain lengths, shown by the additives **8.1-2c** and **8.1-2h**. Nearly all samples exhibit a milk-white appearance. Unexpectedly, the additives containing C_8- and C_{12}-alkyl chains form more transparent gels, whereby the turbidity of the C_8 derivative changed within 24 h to milk-white.

Conclusion on the gelling ability of the novel additives

During preparation of the mixtures, the additives were found to exhibit different solubility in *n*-octanol, nevertheless all were soluble. DBGAcMeE (**5**) derivatives showed the best solubility and DBGAc (**6**) the worst. Nevertheless, most of the investigated additives (21 of 34) were found to form superstructures in *n*-octanol. The substitution pattern of the benzylidene 'wings' was found to have significant influence on the gelling and aggregation behavior of the additives [93]. Highlighting a difference resulting from the different 'tails' was by far more challenging. It seems, that the overall molecular architecture of the additives is even more important for the formation of stable gels [89]. Since DBGAcMeE (**5**) derivatives were able to form stable gels as well, it is questionable if the hydrogen bonding ability is of vital importance, at least for gelation in *n*-octanol. As a result of missing HBDs, no gelation ability has been expected. It is uncertain, if the additives show a similar behavior in the intended iPP surrounding. However, the hydrogen bonding strength derived from this experiment is expected to look like as follows: amide > acid > ester. Secondary amides were expected to show less gelation, because of less hydrogen bonding strength caused by sterically hindrance or the prevention to act as HBD. However this behavior was not observed, rather longer alkyl chains seem to favor the gelation process for unaccountable reasons [109].

All in all, the novel additives were found to aggregate and are capable to form networks. The morphology of the gels can be examined by scanning electron microscopy (SEM). Figure 4-8, exemplary shows that for additive **7c** smooth fibers with slight helical twisting can be observed. In contrast, **DMDBS** and **TBPMN** form more distinct ropelike helical structures with diameters of about 200 nm [106]. The morphology of all other derivatives **5-8** has not been investigated.

Self-assembly seems to result from a variety of driving forces and the overall molecular architecture [89, 107]. After screening the additives in their foreseen application field (Chapter 5), it turned out that there is no correlation between gelation and nucleation.

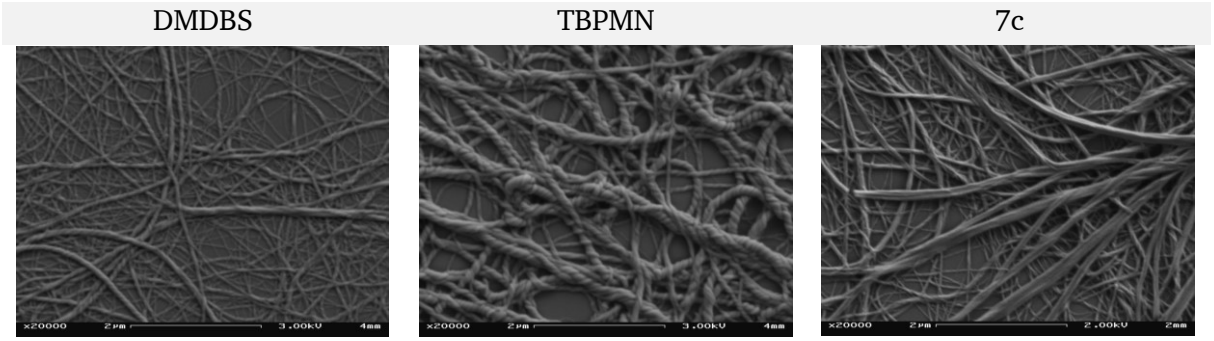

Figure 4-8 SEM images of xerogels from DMDBS, TBPMN and 7c in *n*-octanol (0.1 wt %). Scale bar 2 µm.

4.3. Thermal properties of 3,5:4,6-dibenzylidene-*L*-gulonic acid derivatives

Thermal properties are key characteristics of polymer additives. They have to withstand high temperatures, because they are being applied within the processing windows of the polymers. As potential nucleating and clarifying agents DBGAc derivatives have to endure these temperatures to a certain extent. In addition, peak melting and crystallization temperatures of the pure additive can provide insights into the dissolution and recrystallization behavior in the intended polymeric surrounding. For a better dispersibility, soluble additives should exhibit a melting temperature, which is at least in the range of the processing window of iPP (200-260 °C). The crystallization temperature should be above the crystallization temperature of the polymer (iPP: ~110 °C), as potential superstructures are supposed to provide a surface for polymer nucleation. For this reason it is important to examine key thermal properties of the pure additives upfront. Due to their different 'tails' the 'library' of additives is expected to exhibit different melting temperatures and behaviors. The thermal properties of the DBGAc derivatives were investigated using different analytical techniques. First, their melting and decomposition behavior was briefly investigated by a DSC and TGA decomposition run. The DSC experiment at 3 °C/min delivers the peak melting temperature (T_m) and the onset of the decomposition temperature ($T_{dec.}$), whereas the TGA experiment at 10 °C/min delivers the 5 % weight loss temperature ($T_{-5\ wt\%}$). In a second step, the detailed melting and crystallization behavior of the additives was studied by a two cycle DSC heating and cooling experiment at 10 °C/min. The experiment delivers peak melting (T_m^1, T_m^2) and crystallization (T_c^1, T_c^2) temperatures for the first and second heating and cooling cycle. Some of the two cycle DSC experiments only revealed partial results, due to decomposition of the substances during or after melting. In these cases, the reported melting temperatures refer to the values obtained from the decomposition experiment. If not stated otherwise, the melting temperature (T_m^1) of the two cycle experiment has been reported in the following. Slight deviations of the two observed melting temperatures result from the different heating rates applied (3 °C/min vs. 10 °C/min). Details on the experiment setups can be found in the experimental part.

Tables 4-6 – 4-11 comprise all chemical structures of DBGAc derivatives and their thermal characteristics. Each Table represents one set, according to the introduced 'tail'. With this view, the influence of the benzylidene substitution pattern can be compared and potential structure-property relations can be revealed. In addition it might be possible to draw conclusions on the hydrogen bonding strength as well.

Thermal properties of dibenzylidene-*L*-gulonic acid methyl ester (5) derivatives

All DBGAcMeE (**5**) compounds (Table 4-6) investigated show a defined melting point, which is followed by a gap where the compound exists as a liquid until decomposition starts. The only exception was found for additive **5d**, which shows direct decomposition after the melting peak. For the additives **5e**, **5f** and **5i** more than one melting endotherm was observed. This can be seen in Table 4-6, expressed by more than one reported melting temperature. Most of the additives show a melting temperature in the range between 200 and 240 °C. A recrystallization temperature (T_c^1) was detected for all derivatives, expect for additive **5d** and **5i**. In this case the measured temperatures were found in the range between 160 and 200 °C. The 5 % weight loss temperature of all additives was found to be above 265 °C.

Table 4-6 Thermal properties of 3,5:4,6-dibenzylidene-*L*-gluconic acid methyl ester (**5**) derivatives.

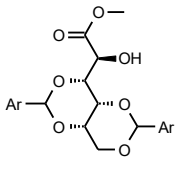

Ar =	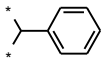	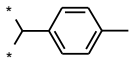	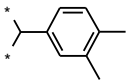	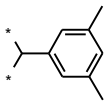
Abrr.	**5a**	**5b**	**5c**	**5d**
T_m [°C]	206	226	249	265[1)]
T_c [°C]	186	167	195	n.a.
$T_{-5\ wt\%}$ [°C]	269	281	292	277

[1)] T_m taken from DSC decomposition run; n.a. not available;

Ar =	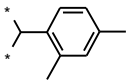	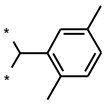	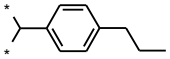	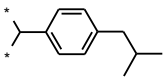
Abrr.	**5e**	**5f**	**5h**	**5i**
T_m [°C]	233 | 242	233 | 245	207	164 | 183 | 193
T_c [°C]	162	211	180	n.a.
$T_{-5\ wt\%}$ [°C]	296	284	289	310

[1)] T_m taken from DSC decomposition run; n.a. not available;

Figure 4-9 depicts the characteristic melting, decomposition and recrystallization behavior, in this case for substance **5a**. The peak melting temperature can be observed at 210 °C and decomposition starts at around 291 °C. This correlates to the measured 5 % weight loss temperature at 269 °C. Peak melting and crystallization temperature for the first heating and cooling cycle for substance **5a** can be observed at 206 °C and 186 °C. Deviations between the two melting temperatures result from the different applied heating rates applied.

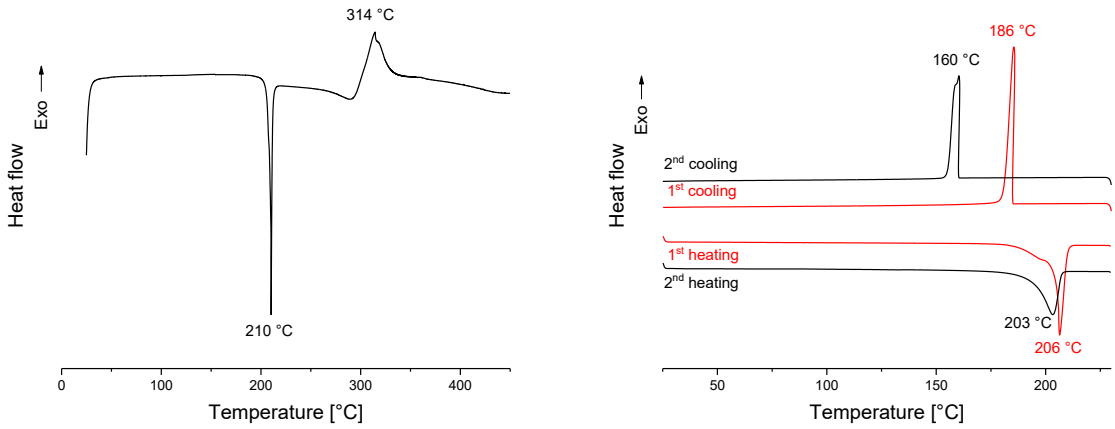

Figure 4-9 Melting, decomposition and recrystallization behavior of substance **5a**. DSC decomposition run with 3 K/min (left) and two cycle DSC experiment at 10 K/min (right).

Comparison of the two heating and cooling cycles reveals that the melting and crystallization temperatures of the 1st and 2nd cycle are gradually shifted towards lower temperatures with an increasing number of scans. Regarding the molecule's structure, it is reasonable to attribute such behavior to the decomposition of the molecule. Acetal cleavage is caused by hydrolysis and results in the undesired release of benzaldehydes [55, 110].

The relatively high 5 % weight loss temperature of over 265 °C allows the application of all additives at the commonly used processing temperatures, as iPP nucleating agents. It was found, that the additives' $T_{-5\ wt\%}$ can be increased slightly by insertion of additional substituents to the benzylidene 'wings'. Depending on the induced substitution pattern, the molecules are more or less stable. Apart from this, the substitution patterns were found to increase the melting temperature when dimethyl substituted benzylidene 'wings' (**5c-5f**) were studied. In case of additive **5d**, direct decomposition has to be linked to the meta-substitution pattern. However, this needs to be reviewed with the aid of the following sets. Interestingly, additive **5i** shows no recrystallization upon cooling, although the molecule was not found to decompose after melting. For the intended application, this might cause the loss of iPP nucleation, as no surface is provided. The existence of more than one melting peak, which has been observed for three additives, might be a result of phase transitions.

Thermal properties of dibenzylidene-*L*-gulonic acid (6) derivatives

The thermal behavior of all DBGAc derivatives (**6**) is adversely affected by the saponification step. After melting, the additives readily decompose. As can be seen in Table 4-7, all of the additives of this set exhibit 5 % weight loss temperatures that are below 240 °C or, in most cases, even below 215 °C. In addition, the overall melting range is reduced significantly and was found to be below 200 °C for five out of eight additives. As a consequence of direct decomposition after melting, for none of the additives a recrystallization temperature could be measured.

Table 4-7 Thermal properties of 3,5:4,6-dibenzylidene-*L*-gluconic acid (**6**) derivatives.

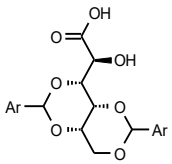

Ar =	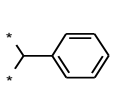	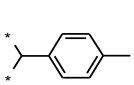	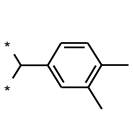	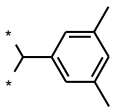
Abrr.	**6a**	**6b**	**6c**	**6d**
T_m [°C]	207	192[1)]	187[1)]	219[1)]
T_c [°C]	n.a.	n.a.	n.a.	n.a.
$T_{-5\ wt\%}$ [°C]	213	214	213	236

[1)] T_m taken from DSC decomposition run; n.a. not available;

Ar =	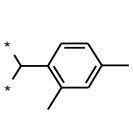	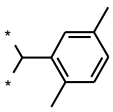	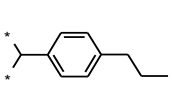	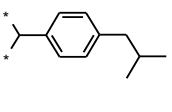
Abrr.	**6e**	**6f**	**6h**	**6i**
T_m [°C]	177[1)]	209[1)]	189[1)]	186[1)]
T_c [°C]	n.a.	n.a.	n.a.	n.a.
$T_{-5\ wt\%}$ [°C]	208	223	214	202

[1)] T_m taken from DSC decomposition run; n.a not available;

The melting, decomposition and recrystallization behavior of substance **6a** is shown as example in Figure 4-10. The peak melting temperature can be observed at 189 °C and decomposition starts according to its onset temperature at around 222 °C. This correlates reasonably with the 5 % weight loss temperature at 213 °C, due to the difficulty to determine onset of decomposition. The first heating cycle reveals a melting temperature of 207 °C. In this case a

greater discrepancy (T_m vs. T_m^1) of the two detected melting temperatures is observed and crystallization cannot be detected.

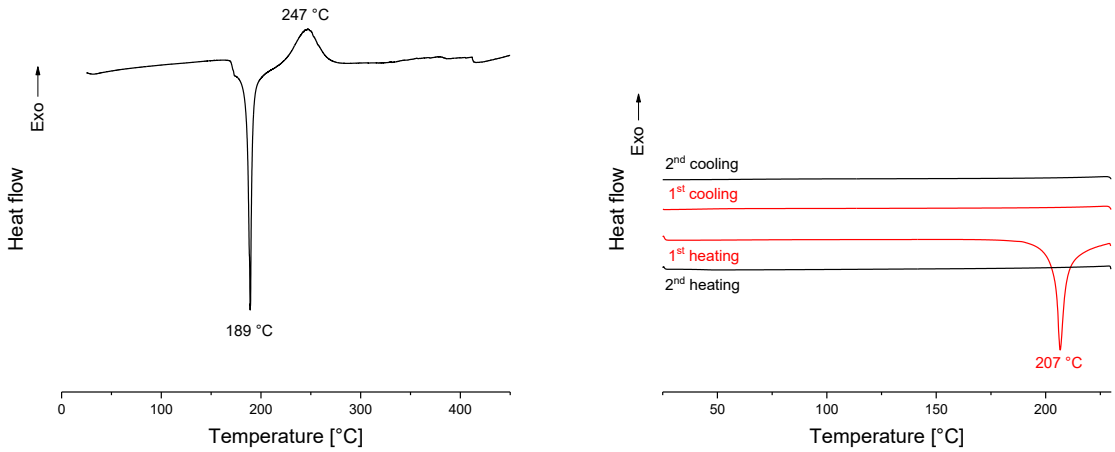

Figure 4-10 Melting, decomposition and recrystallization behavior of substance **6a**. DSC decomposition run with 3 K/min (left) and two cycle DSC experiment at 10 K/min (right).

In this case, comparison of the two heating and cooling cycles does not reveal a change of the melting and crystallization temperatures with an increasing number of scans, because the additive decomposes after melting at the end of the first heating cycle. In several cases, it was difficult to select an appropriate endset temperature for the DSC experiment.

The significantly reduced thermal stability of the DBGAc derivatives is unexpected. As the intermolecular forces of DBGAc and DBGAcMeE derivatives are in principle similar, the different thermal behavior should have a different cause. A reasonable explanation could be the potentially different crystalline arrangement of the molecules, due to head-to-tail hydrogen bonded dimers. Nevertheless, these low weight loss temperatures may cause serious problems when such additives are compounded into iPP at around 220 °C. No further structure-property relations could be identified through analysis of thermal behavior.

Thermal properties of dibenzylidene-*L*-gulonic amide (7) derivatives

The thermal properties of the DBGA (**7**) derivatives (Table 4-8) show predominantly a similar behavior as observed for the DBGAc (**6**) derivatives, expressed by a direct transition from melting into decomposition. Only the derivatives **7h** and **7i** were identified as an exceptions. Both show a defined melting point, which is followed by a gap until decomposition starts. For four additives (**7a**, **7c**, **7d** and **7f**), melting temperatures above 255 °C were measured, while the other four derivatives show a melting temperature above 215 °C. The recorded recrystallization temperatures are in the range between 165 and 205 °C. By skilled selection of the endset temperature, it was possible to measure a crystallization temperature for the additives **7a** and **7b**, although direct decomposition was observed after melting. All eight additives exhibit high 5 % weight loss temperatures of above 285 °C.

The DBGA (**7**) derivatives show improved thermal properties compared to the DBGAcMeE (**5**) derivatives, as was expected by the greater HBD ability of the amide moiety. In addition, the results reveal that the derivatives with longer alkyl substituents on the benzylidene 'wings' induce slightly lower melting points and prevent direct decomposition after the melting process.

Table 4-8 Thermal properties of 3,5:4,6-dibenzylidene-*L*-gluconic amide (**7**) derivatives.

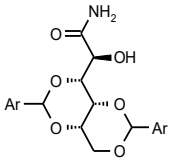

Ar =	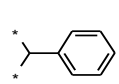	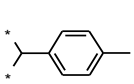	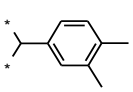	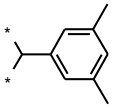
Abrr.	**7a**	**7b**	**7c**	**7d**
T_m [°C]	258	226	261[1)]	278[1)]
T_c [°C]	202	167	n.a.	n.a.
$T_{-5\ wt\%}$ [°C]	292	291	297	309

[1)] T_m taken from DSC decomposition run; n.a not available;

Ar =	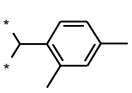	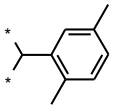	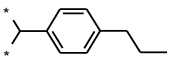	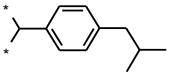
Abrr.	**7e**	**7f**	**7h**	**7i**
T_m [°C]	230	272	225	205 | 216
T_c [°C]	n.a.	n.a.	171	172
$T_{-5\ wt\%}$ [°C]	285	297	288	295

[1)] T_m taken from DSC decomposition run; n.a.not available;

Thermal properties of dibenzylidene-*L*-gulonic alkyl amide (8) derivatives

Table 4-9 comprises the thermal properties of the set of DBGA-*n* (**8.1-6a**) derivatives, which bear only unsubstituted benzylidene 'wings'. Here again, all of the additives show a distinct gap between melting and decomposition. The melting temperature is in the range of 190 – 260 °C, and for all additives, a recrystallization temperature between 225 °C and 165 °C was detected. The weight loss temperature is quite high with $T_{-5\ wt\%} > 265$ °C and in the cases of longer alkyl chains even above 320 °C.

The delta of temperatures between melting and decomposition is influenced by the alkyl chain length and increases with longer chain lengths. In contrast to the primary amide derivatives (**7**), secondary amide derivatives (**8**) show a gap between melting and decomposition. In conclusion, the insertion of alkyl substituents causes a change in the thermal behavior of the additives. Moreover, longer linear aliphatic substituents result in lower melting temperatures and the molecules exhibiting an even number of carbon atoms show slightly lower melting points as the ones with an odd number. This effect is known as an odd-even correlation. When considering the recrystallization temperatures of the additives, it can be concluded that short chain alkyl derivatives show higher crystallization temperatures.

Table 4-9 Thermal properties of 3,5:4,6-dibenzylidene-*L*-gluconic alkyl amide (**8**) derivatives.

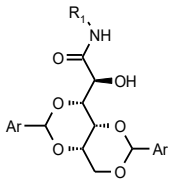

R_1 =	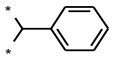				
Abbr.	**8.1a**	**8.2a**	**8.3a**	**8.4a**
T_m [°C]	263	259	260	243
T_c [°C]	263	222	219	214
$T_{-5\ wt\%}$ [°C]	278	284	269	296

[1] T_m taken from DSC decomposition run; n.a. not available;

R_1 =	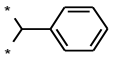		
Abbr.	**8.5a**	**8.6a**
T_m [°C]	206	193
T_c [°C]	168	166
$T_{-5\ wt\%}$ [°C]	321	321

[1] T_m taken from DSC decomposition run; n.a. not available;

Table 4-10 comprises the thermal properties of DBGA-C_1 and -C_2 (**8.1-2**) derivatives for two different substitution patterns of the benzylidene 'wings'. Both 3,4-dimethyl benzylidene substituted derivatives (**8.1-2c**) show direct decomposition and can be seen as exceptions out of all structures **8**. They exhibit both high 5 % weight loss temperatures of around 300 °C and very high melting points (> 300 °C). Recrystallization could not be observed, due to the direct decomposition after melting. The 4-propyl benzylidene (**8.1-2h**) derivatives show a gap between melting and decomposition, which fits to the overall behavior of the other secondary amides except for the derivatives described previously. The additives reveal a 5 % weight loss temperature of around 300 °C and high melting temperatures of above 250 °C as well. The relatively high recrystallization temperature of 231 °C for the derivative **8.1h** is rather surprising.

Table 4-10 Thermal properties of 3,5:4,6-dibenzylidene-*L*-gluconic methyl / ethyl amide (**8**) derivatives.

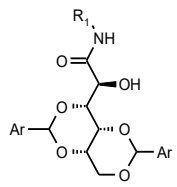

R_1 =	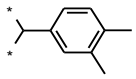		
Abbr.	**8.1c**	**8.2c**
T_m [°C]	315[1]	303[1]
T_c [°C]	n.a.	n.a.
$T_{-5\ wt\%}$ [°C]	306	297

[1] T_m taken from DSC decomposition run; n.a. not available;

R_1 =	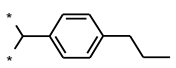		
Abbr.	**8.1h**	**8.2h**
T_m [°C]	251	241
T_c [°C]	231	173
$T_{-5\ wt\%}$ [°C]	299	315

[1] T_m taken from DSC decomposition run; n.a. not available;

The tendency that the melting point decreases with longer alkyl chains can be confirmed for both methyl and ethyl derivatives (**8.1-2c, 8.1-2h**). Unexpectedly, the 3,4-dimethyl substitution pattern of the benzylidene 'wings' induces a different thermal behavior than the one found for all other derivatives out of this set. On the other hand, the increase of gap width between melting and decomposition, as well as the increase of $T_{-5\ wt\%}$, could be confirmed for derivatives **8.1-2h** with increasing alkyl chain lengths.

Thermal properties of commercial nucleating and clarifying agents

Owing to their structural similarity, the thermal properties of the commercial nucleating and clarifying agents **DMDBS** and **TBPMN** were studied to ensure comparability. Both derivatives exhibit a thermal behavior with a distinct gap formation between melting and decomposition. In addition, decomposition with an increasing number of scans can be confirmed for these additives. Clear structure-property relations for different substitution patterns could not be drawn, even though data on the melting temperatures of the different derivatives are accessible through the literature [55, 110]. The other commercial nucleating agents, most known to be insoluble, reveal very high melting and decomposition temperatures or could not even be subjected to thermal analysis. The measured values can be found in Table 4-11.

Table 4-11 Thermal properties of commercial nucleating and clarifying agents.

Abrr.	DMDBS	TBPMN	NA 11	NA 71	XT 386
T_m [°C]	275	245	n.a.	384[1)]	427[1)]
T_c [°C]	214	201	n.a.	n.a.	n.a.
$T_{-5\ wt\%}$ [°C]	302	316	n.a.	358	337

[1)] T_m taken from DSC decomposition run; n.a. not available;

Discussion and conclusions on the thermal behavior of novel additives

The thermal properties of the newly synthesized additives can be described by mainly two different behaviors. The DBGAcMeE (**5**) and DBGA-*n* (**8**) derivatives predominantly exhibit a distinct melting and crystallization point, whereas most of the DBGAc (**6**) and DBGA (**7**) derivatives decompose following the melting process. While melting and recrystallization represent desired properties to induce nucleation in polymers, early decomposition shall be avoided.

Melting and/or solubility of the additive in principal enable a good dispersibility of the additives in the polymer melt. Subsequent crystallization of the additive upon cooling, ideally as a fine fibrillar network prior to crystallization of iPP, provides large surfaces that induce the iPP crystallization [69, 70]. Therefore, most of the DBGAcMeE (**5**) and DBGA-*n* (**8**) derivatives might be ideal candidates to nucleate iPP. However, for several other additives it had not been possible to determine a recrystallization temperature. In these cases, it was interesting to study their behavior in the polymer melt. In particular, several of the DBGA (**7**) derivatives exhibit melting points far above the foreseen processing temperature of 220 °C and thus it can be expected that they either exist as finely dispersed crystal particles or that they dissolve in the polymeric surrounding. For all additives that exhibit higher $T_{-5\ wt\%}$ values, than the processing temperature (220 °C) of iPP, it is likely that they can serve as nucleating agents. In contrast, most of the DBGAc (**6**) derivatives showed weight loss temperatures below 220 °C and therefore, it is

questionable if they endure these temperatures. Most probably, decomposition occurs and acetal cleavage can be expected [55, 110]. Even though this is a knockout criterion in general, these additives have been investigated to understand their behavior in the polymer melt. If DBGAc (**6**) derivatives are soluble in the polymer melt, they could be protected somehow. Anyway, the additives behavior is different in the polymer melt compared to surrounding air, as in the underlying DSC experiments.

It was found that the overall thermal behavior could be influenced by selection of the 'tail' and additional alkyl substituents. Variation of the substitution pattern on the benzylidene 'wings' revealed only minor differences, like slight stability improvements. However, the possibility to influence the crystallization temperature of the secondary amides by variation of its alkyl chain length or potential other substituents might enable nucleation of iPP at different crystallization temperatures.

Since particulate additives are known as effective nucleating agents as well, melting and/or solubility do not seem to be a required prerequisite. For this reason, the thermal behavior of selected additives in the polymer melt has been investigated in detail under the optical microscope. By this, the dissolution, melting and recrystallization behavior of the additives in iPP surrounding was studied. The previous thermal examinations may aid in understanding the behavior of the additives in the following screening experiments as nucleating and clarifying agents.

5. Screening of nucleating and clarifying agents for isotactic polypropylene

This section is divided into three main parts. The first part describes the screening setup and the methods which were used to investigate the nucleation and clarifying ability of the additives. The second part explains the state of the art to verify the screening method and to have valid values of commercial nucleating and clarifying agents under comparable experimental conditions. The third part contains the results of the screening tests on the extensive 'library' of dibenzylidene-*L*-gulonic acid derivatives with respect to their nucleating and clarifying potential. This part comprises four sets, each set representing a different 'tail' of the derivatives.

5.1. Screening setup

In order to study and evaluate the large number of potential nucleating and clarifying agents a screening method was established. The screening method needed to be reliable, efficient and, if possible rapid. This section describes the development of these methods.

Nucleation

To investigate if a particular new additive is capable of inducing nucleation of isotactic polypropylene, first the peak crystallization temperature ($T_{c,p}$) has to be determined. To perform this measurement samples containing different concentrations of the additive are required. These are obtained by dry blending, mixtures of powdery iPP, stabilizers and additive. In a second step the powders were compounded on a single-screw extruder at 220 °C, and iPP compounds containing between 0.03 and 0.60 wt% of the respective additives were obtained as granules. Using these samples a two cycle DSC heating and cooling experiment (10 °C/min) with the obtained granules delivered the peak melting temperature ($T_{m,p}$) and $T_{c,p}$ at the respective concentrations. $T_{c,p}$ was taken from the first cooling cycle and is known to be an appropriate first indication for nucleation in the case the incorporated additive shows a temperature shift towards higher temperatures (cf. Figure 1-21). Because the amount of additive is small compared to the polymer $T_{c,p}$ is treated as the crystallization temperature of the polymer. In strict terms, this temperature reflects the crystallization temperature of the eutectic iPP/additive mixture, however for screening purposes the approximation is valid. Additionally, $T_{m,p}$ also provides further valuable information on the obtained mixtures, as for example the existence of different crystal modifications.

Clarification

The clarifying ability of the additives is determined by measuring the optical properties of 1.0 mm thick plaques. The optical properties of interest are transmission, haze and clarity. The plaques were made from previously obtained granules, with different amounts of additives and processed with an injection molding step. The measured values of total transmission, haze and clarity are commonly used to evaluate polymers' optical properties. Improved optical properties are considered to decrease in haze values and to increase in clarity values.

These two screening methods, DSC for nucleation, and optical property measurements for clarification are complemented by the earlier measured thermal properties of the pure additives. This allows structure-property relationships to be made.

Evaluation of the screening setup

The first necessary step is to determine the general parameters of the used isotactic polypropylene homopolymer system, and any potential impacts of the processing steps. The used isotactic polypropylene homopolymer contains a minimal unknown basic stabilization. This grade is named "neat" (**I**, Table 5-1) throughout the rest of this thesis. Due to the applied three-cycle compounding step in a single screw extruder, a decision was made to add a further stabilization package (0.1 wt% Irganox 1010; 0.1 wt% Irgafos 168 and 0.1 wt% Calcium Stearate). This grade is named "control" (**II**, Table 5-1).

Table 5-1. Characteristic values of isotactic polypropylene homopolymer and the influence of additional stabilization.

Nr.	stabilization grade	Rep. #	$T_{m,p}$ [°C]	$T_{c,p}$ [°C]	Transmission [%]	Haze [%]	Clarity [%]
I	neat	1	161.2	114.5	90.1	61.1	47.0
		2	160.5	115.0	90.0	62.1	47.7
II	control	1	165.6	112.9	89.3	62.4	43.0
		2	165.3	113.9	90.0	65.3	45.1

$T_{m,p}$ = peak melting temperature, polymer; $T_{c,p}$ = peak crystallization temperature, polymer; Transmission, Haze and Clarity were measured on 1.0 mm plaques.

The experiments shown in Table 5-1 compare the two different stabilization packages. These investigations on the effect of further stabilized polymer were necessary due to the applied three-cycle extrusion steps, allowing sufficient distribution of the nucleating agents on the single-screw extruder at a later stage. Typically, the standard deviation of the three measured samples was below 0.5 % for all optical property values and below 0.5 °C for the crystallization temperature. However, in this case slightly higher deviations of up to 2.0 % can be observed between the independent repeated trials of the 'control' sample. The most significant difference, which can be drawn is that the 'neat' resin was exposed to higher thermal stress. This is confirmed by a slightly lower M_w of 354 kg/mol for the 'neat' sample (**I**) compared to the 'control' sample (**II**, M_w = 383 kg/mol). This also explains the slightly lower melting temperature. Therefore it can be seen that adding additional process stabilizers was an appropriate measure. The impact of the compounding step itself was checked by comparing the results from the single screw extruder with the results of a laboratory mini twin-screw extruder. The obtained results were in the typical range of the standard deviation.

Based on these results, decision was taken that for the screening setup the combination of additional stabilized, powdery isotactic polypropylene homopolymer compounded on a single-screw extruder (**II**, Table 5-1) is sufficient to ensure thermal stability of the polymer. All developed potential nucleating agents were screened under the same conditions and have been compared against the 'control' (**II**) material, with an average $T_{m,p}$ of 165.5 °C, $T_{c,p}$ of 113.4 °C, transmission of 89.7 %, haze of 63.9 % and clarity of 44.1 %. Having now developed the

screening methods for the additives, the next important factor is the quality of the dispersions. The quality of the dispersion was investigated by means of the commercial nucleating and clarifying agents in the next section.

5.2. Verification of screening method using commercial additives

The screening methods described in the previous subsection were verified by measuring five commercial nucleating and clarifying agents (Table 5-2). By measuring the properties of known additives on our setup we were able to verify the reliability of our method and produce comparative values for benchmarking the novel additives.

Table 5-2. Chemical names and abbreviations of the commercial nucleating and clarifying agents.

Chemical Name	Abbreviation
1,3:2,4-bis(3,4-dimethylbenzylidene)sorbitol	**DMDBS**
1,2,3-trideoxy-4,6:5,7-bis-*O*-[(4-propylphenyl)methylene]-nonitol	**TBPMN**
Sodium 2,2'-methylene-bis-(2,4-di-tert-butylphenyl)-phosphate	**NA 11**
Lithium 2,2'-methylenebis(2,4-di-tert-butylphenyl)phosphate	**NA 71**
1,3,5-tris(2,2-dimethylpropionylamino)benzene	**XT**

The sorbitol based clarifying agents **DMDBS** and **TBPMN** are of most interest, due to their similarity to the newly developed structures. The previously established screening methodology was applied and the details can be found in the experimental part (chapter 10). Table 5-3 shows the screening results of the different compounds. Values above a crystallization temperature of 120 °C are marked green, indicating a distinct nucleation effect. Values below 55 % haze and above 55 % clarity are marked green and values above 70 % haze and below 40 % clarity are marked red, indicating improved or worsened optical properties. These limits have been set arbitrarily to underline significant changes.

Compared to the 'control' sample, the **DMDBS** containing compounds show increased crystallization temperatures reaching a concentration level of 0.15 wt%. A $T_{c,p}$ of 113.4 °C indicates that **DMDBS** is not active at the minimum applied concentration [72]. A maximum $T_{c,p}$ of 131.6 °C, is reached at a concentration of 0.60 wt%. The decreasing haze value with a minimum of 14.2 % and the increasing clarity value with a maximum of 94.8 % at certain concentration levels confirms **DMDBS** effectiveness as a clarifying agent. A similar behavior can be observed for **TBPMN**, reaching an increased crystallization temperature of 132.8 °C, an increased clarity of 94.7 % and a decreased haze value of 9.2 % at 0.60 wt%. The determined values for **TBPMN** fit to the literature known behavior [77], whereas the values for **DMDBS** show a slightly different behavior than previously reported [72]. In our results the minimum haze value is already reached at 0.30 wt%. The organophosphate based nucleating agent **NA 11** and its related clarifying agent **NA 71** show increased crystallization temperatures of above 130 °C as well. At low concentrations they already have an influence on iPP's crystallization behavior. **NA 11,** as a pure nucleating agent, has a moderate effect on the optical properties. Minimum haze values of 45.1 % and clarity values of around 93 % are reached. In contrast its clarifying analogue **NA 71** reaches 24.1 % in haze and increases clarity to 91.5 %. Comparison of the sorbitol and the organophosphorus based additives confirms that the soluble sorbitol derivatives are far better clarifying agents. The trisamide based clarifying agent (**XT**), shows a completely different behavior from all other tested. Highest efficiency is reached at very low concentrations, between 0.01 and 0.03 wt %. In this range the highest crystallization temperature is 126.7 °C

and haze decreases to 20.0 %, whereas clarity increases to 94.6 %. By employing higher concentrations, no improvement occurred, but rather the opposite [45].

Table 5-3. Screening results of commercial nucleating and clarifying agents.

Nr.	Additive	T_m [°C]	T_c [°C]	$T_{-5\ wt\%}$ [°C]	Conc. [wt%]	$T_{m,p}$ [°C]	$T_{c,p}$ [°C]	Trans. [%]	Haze [%]	Clarity [%]
iPP	-	-	-	-	-	165.5	113.4	89.7	63.9	44.1
I	DMDBS	275	214	302	0.03	166.3	113.4	90.3	59.4	45.3
					0.15	165.5	129.6	89.8	32.3	94.1
	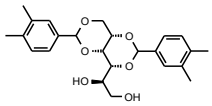				0.30	166.1	130.7	89.5	14.2	94.8
					0.45	166.1	131.0	89.5	16.8	94.2
					0.60	166.1	131.6	89.2	18.5	94.0
II	TBPMN	245	201	316	0.03	163.9	114.3	89.8	60.2	41.2
					0.15	164.4	120.2	90.3	47.2	92.6
	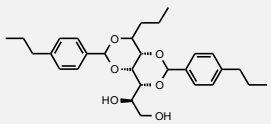				0.30	165.2	131.2	88.8	18.6	94.5
					0.45	166.5	132.5	89.6	11.2	94.6
					0.60	166.5	132.8	89.7	9.2	94.7
III	NA 11	n.a.	n.a.	n.a.	0.03	165.2	124.8	90.8	66.9	87.7
					0.15	166.3	128.9	90.3	52.3	92.7
	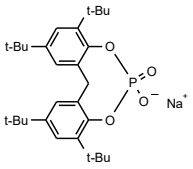				0.30	166.6	130.0	89.4	47.2	93.0
					0.45	166.6	130.4	88.9	45.1	92.5
					0.60	166.2	131.0	88.5	45.8	92.2
IV	NA 71	384[1)]	n.a.	358	0.03	165.6	122.8	90.8	61.8	90.2
					0.15	166.3	130.1	89.4	33.1	93.7
	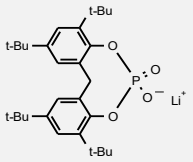				0.30	166.9	130.9	88.6	26.2	93.1
					0.45	166.8	132.3	88.5	24.4	92.0
					0.60	166.2	132.9	88.4	24.1	91.5
V	XT	427[1)]	n.a.	337	0.01	165.4	125.9	89.5	30.0	94.4
					0.02	164.7	126.1	89.0	20.0	94.6
	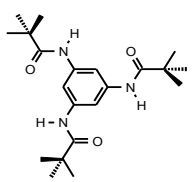				0.03	165.5	126.7	89.0	22.6	94.4
					0.15	165.2	123.3	88.7	34.2	92.5
					0.30	165.0	124.9	88.7	47.6	89.8
					0.45	164.4	125.8	88.8	58.2	87.6
					0.60	165.4	125.4	89.0	68.4	83.8

T_m = melting temperature, additive; T_c = crystallization temperature, additive; $T_{-5\ wt\%}$ = 5 % weight loss temperature, additive; $T_{m,p}$ = peak melting temperature, polymer $T_{c,p}$ = peak crystallization temperature, polymer, n.a. = not available, Transmission, Haze and Clarity were measured on 1.0 mm plaques; [1)] T_m taken from DSC decomposition run.

Quality of dispersion

To verify the method and to check the quality of dispersion of the incorporated additives a comparative experiment was conducted on a twin-screw extruder. Twin-screw extrusion delivered comparable results and thus the screening setup delivers reliable values.

Morphology of nucleated and clarified isotactic polypropylene

If nucleation is induced by nucleating agents, the overall spherulite size of iPP drastically decreases. This behavior can be observed with the aid of polarized optical micrographs (Figure 5-1) of the respective iPP/additive mixtures. This process is concentration dependent and a drastic decrease in spherulite size can be observed at concentration levels exceeding 0.30 wt%. The spherulite size is consistent with the calculated nucleation efficiencies (NE). The 'control' sample shows the typical appearance of 'mixed' α-spherulites [111] with no distinct Maltese cross pattern and spherulite sizes of around 50 to 120 μm. Significant differences between the nucleated samples are difficult to judge. The sample containing **NA 11** shows the existence of additive agglomerates. The mixture containing additive **XT** shows a slightly coarser morphology as the other samples.

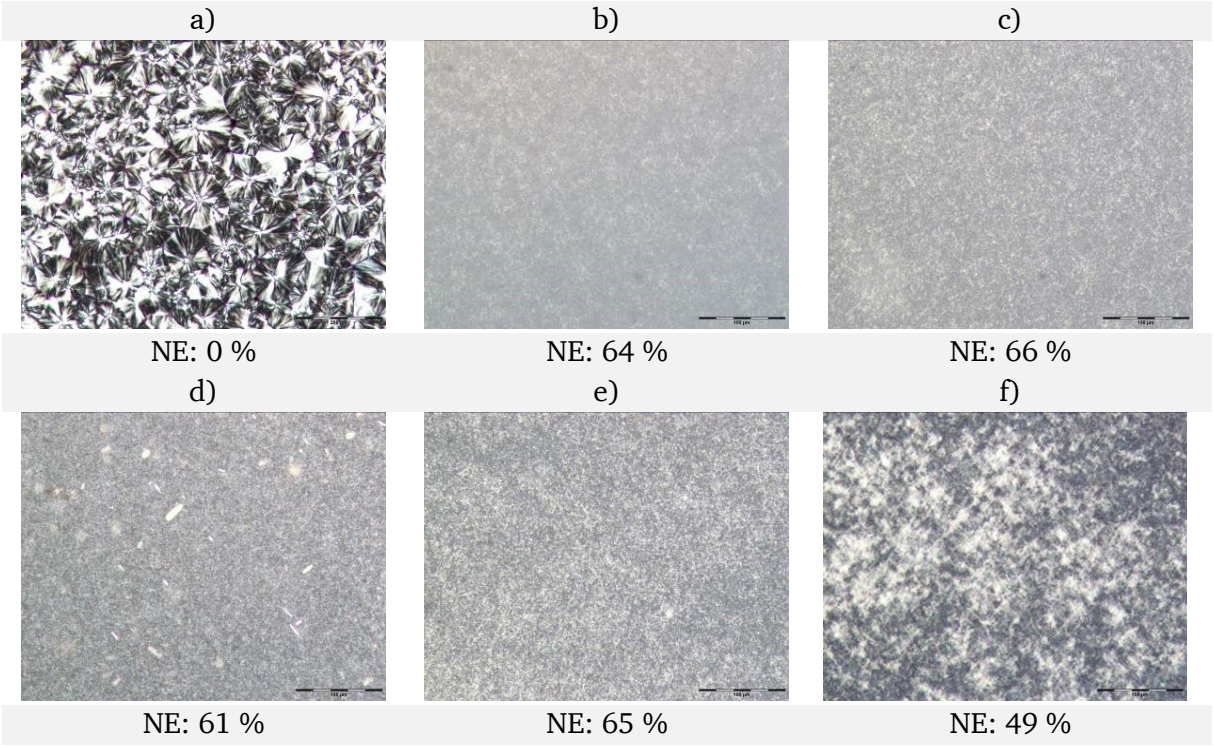

Figure 5-1 Polarized optical micrographs of melt-compression-molded iPP films containing a) no nucleating agent, b) 0.30 wt% **DMDBS**, c) 0.30 wt% **TBPMN**, d) 0.30 wt% **NA 11**, e) 0.30 wt% **NA 71** and f) 0.03 wt% **XT**. Nucleation efficiencies are given in percent and are calculated according to literature known procedures [71]. Scale bar 100 µm.

In general smaller spherulites result in improved optical properties of the nucleated parts. However, in several cases nucleation and reduced spherulite sizes alone are not enough to reach highly clarified materials [58]. An illustrative example for nucleated and clarified iPP is shown in Figure 5-2, for 1.0 mm injection-molded plaques with an increasing amount of **NA 11** and **TBPMN**.

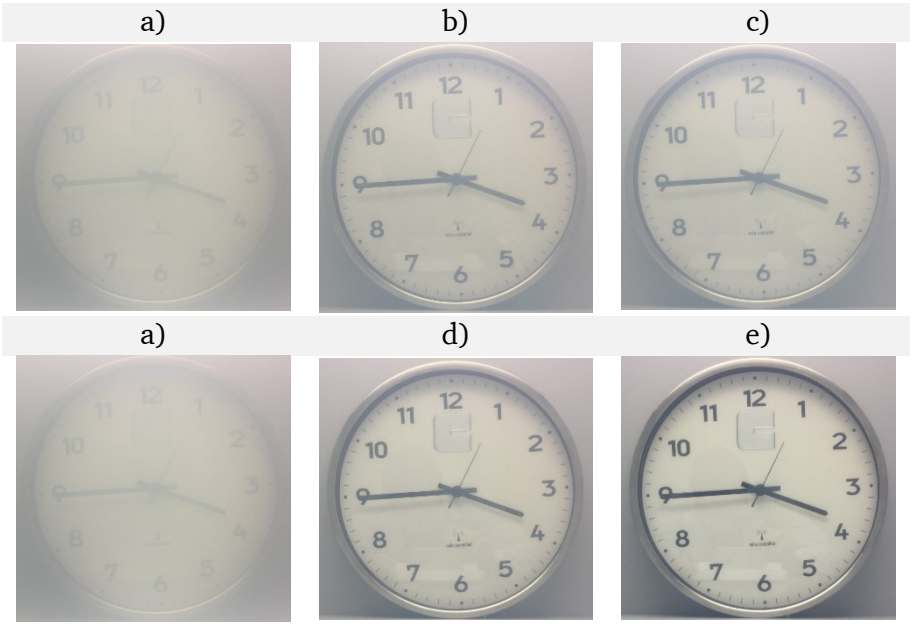

Figure 5-2 Illustration of nucleating and clarifying effect. Photograph through 1.0 mm thick injection-molded iPP plaques. a) Control sample, b) containing 0.30 wt% **NA 11**, c) containing 0.60 wt% **NA 11**, d) containing 0.30 wt% **TBPMN** and e) containing 0.60 wt% **TBPMN**.

Conclusion

In general the findings made for the tested series of commercial nucleating and clarifying agents correspond to the common literature [45, 72, 77]. Slight deviations from reported crystallization temperatures and haze values may result from a different iPP polymer type or a different compounding and injection molding setup. Nevertheless, the established screening setup delivers reliable values and can be used for the extensive 'library'.

5.3. Screening of 3,5:4,6-dibenzylidene-*L*-gulonic acid derivatives as nucleating and clarifying agents for isotactic polypropylene

In this section the dibenzylidene-*L*-gulonic acid derivatives are systematically studied in sets to reveal structure-property relations with respect to nucleation ability and impact on optical properties of iPP. The previously validated screening methodology was applied and the properties are discussed as a function of additive concentration. The first set compares the DBGAcMeE (**5**) derivatives, which vary in their alkyl substitution pattern at the aromatic 'wings'. The second set compares the DBGAc (**6**) derivatives, which contain the same alkyl substituents on the aromatic 'wings' as the previous derivatives. The third and fourth set discusses the DBGA (**7**) derivatives and the DBGA-*n* (**8**) derivatives, which vary both in their alkyl substituents on the aromatic 'wings' and predominantly the DBGA-*n* (**8**) derivatives in their 'terminal' chain length in the range from C_1 to C_4, C_8 and C_{12}.

5.3.1. 3,5:4,6-Dibenzylidene-*L*-gulonic acid methyl ester derivatives (5)

As can be seen from the data summarized in Table 5-4 most of the newly synthesized additives from set **5**, act as nucleating and in some particular cases as well as clarifying agents. Depending on the substitution pattern of the aromatic 'wings', some additives show efficient nucleation of iPP and some provide improved optical properties with regard to haze and clarity as well. Six out of eight compounds show nucleation of iPP at a certain concentration. A haze improvement of more than 10 % compared to the 'control' sample, is achieved by only four compounds. In comparison a change in clarity values is recognized for six compounds.

Additive **5a** increases the crystallization temperature of iPP up to 126.6 °C at a concentration level of 0.60 wt%, whereby haze and clarity remain unchanged. The $T_{c,p}$ for compounds containing additive **5b** reaches a maximum temperature of 125.8 °C and haze and clarity values are slightly improved. The lowest measured haze value is 45.2 % and the highest clarity value 88.2 %. Comparable values are found for iPP samples containing additive **5c**. The crystallization temperature reaches a plateau value of 128.6 °C and haze and clarity are improved to 45.6 %, respectively 88.7 %. An increase of the loading level leads to further improved optical properties. Compounds containing additive **5d** nucleate already at a low concentration level of 0.15 wt% and induce the highest crystallization temperature of this set of 131.0 °C. Haze and clarity are improved moderately, to 41.7 % and respectively 82.9 %. Additive **5e** increases the $T_{c,p}$ of iPP up to around 123.0 °C, whereby haze and clarity are only improved marginally. Compounds containing additive **5f** show an increased crystallization temperature only at the highest applied concentration level and haze remains unaffected, whereas clarity slightly improves to a value of 58.6 %. The compounds containing additive **5h** or **5i** show only insignificantly improved crystallization temperatures by around 2.0 °C. Haze values of compounds comprising additive **5h** deteriorate, but clarity improves. Haze and clarity of samples containing additive **5i** remain unaffected.

Table 5-4. Screening results of 3,5:4,6-dibenzyliedene *L*-gulonic acid methyl ester (**5**) derivatives.

Nr.	Substitution pattern	T_m [°C]	T_c [°C]	$T_{-5\ wt\%}$ [°C]	Conc. [wt%]	$T_{m,p}$ [°C]	$T_{c,p}$ [°C]	Trans. [%]	Haze [%]	Clarity [%]
iPP	-	-	-	-	-	165.5	113.4	89.7	63.9	44.1
5a	-	206	186	269	0.03	162.4	114.0	89.9	61.5	44.5
	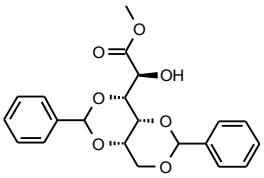				0.15	165.2	114.1	90.0	59.4	45.3
					0.30	163.9	114.4	89.7	59.5	45.1
					0.45	163.9	120.3	87.8	63.0	43.0
					0.60	164.2	126.6	86.4	63.3	44.5
5b	4-Me	226	167	281	0.03	165.2	115.8	90.1	63.6	46.1
	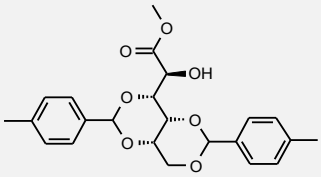				0.15	164.9	115.5	90.1	69.2	55.7
					0.30	163.4	123.3	89.9	69.0	63.0
					0.45	163.5	125.8	89.6	59.8	81.9
					0.60	165.2	124.1	89.0	45.2	88.2
5c	3,4-DiMe	249	195	292	0.03	164.6	114.3	86.4	65.8	45.5
	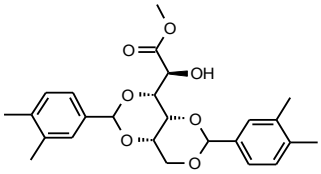				0.15	164.3	115.9	86.2	65.4	45.8
					0.30	164.9	128.6	83.1	67.3	54.1
					0.45	166.3	127.7	89.8	61.2	73.9
					0.60	165.7	128.6	89.0	45.6	88.7
					0.75	165.1	128.6	89.1	38.1	92.5
5d	3,5-DiMe	265[1)]	n.a.	277	0.03	163.7	116.3	90.1	64.2	45.3
	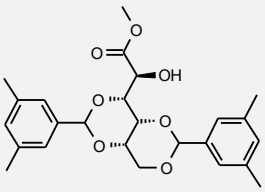				0.15	163.2	128.4	90.1	63.5	44.3
					0.30	162.9	131.0	89.8	72.5	48.0
					0.45	163.7	130.8	85.3	55.9	70.6
					0.60	165.5	125.9	85.7	41.7	82.9
5e	2,4-DiMe	242[2)]	162	296	0.03	163.5	114.3	90.2	62.5	42.1
	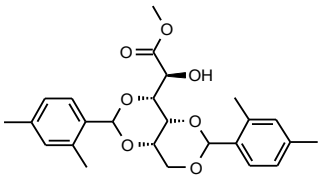				0.15	165.3	113.6	90.3	60.6	42.0
					0.30	164.1	119.6	90.1	64.0	43.6
					0.45	165.1	123.4	90.1	62.2	50.5
					0.60	165.2	122.4	89.7	50.6	65.2

T_m = melting temperature, additive; T_c = crystallization temperature, additive; $T_{-5\ wt\%}$ = 5 % weight loss temperature, additive; $T_{m,p}$ = peak melting temperature, polymer $T_{c,p}$ = peak crystallization temperature, polymer, n.a. = not available, Transmission, Haze and Clarity were measured on 1.0 mm plaques. [1)] T_m taken from DSC decomposition run; [2)] main melting point from several.

Table 5-4. Continued.

Nr.	Substitution pattern	T_m [°C]	T_c [°C]	$T_{-5\ wt\%}$ [°C]	Conc. [wt%]	$T_{m,p}$ [°C]	$T_{c,p}$ [°C]	Trans. [%]	Haze [%]	Clarity [%]
5f	2,5-DiMe	245[2)]	211	284	0.03	165.5	115.4	90.0	70.4	52.3
	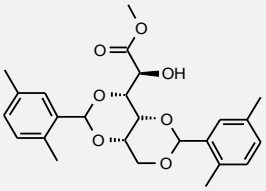				0.15	163.9	115.4	90.0	64.9	50.4
					0.30	164.3	115.1	90.1	65.0	52.2
					0.45	163.9	116.1	90.0	65.5	55.7
					0.60	164.2	124.0	89.9	65.0	58.6
5h	4-Pr	207	180	289	0.03	163.3	114.7	89.9	63.7	46.2
	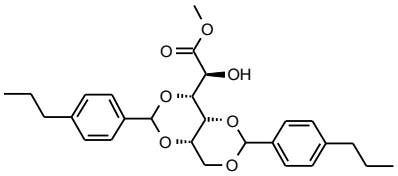				0.15	164.2	114.7	89.7	66.4	44.1
					0.30	163.9	115.0	89.7	67.9	49.6
					0.45	164.8	115.4	89.8	72.1	69.2
					0.60	162.7	115.5	89.8	72.5	82.1
5i	4-Isobu	193[2)]	n.a.	310	0.03	163.9	114.4	90.3	61.3	42.5
	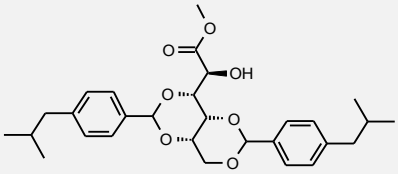				0.15	161.6	115.1	90.2	64.4	40.8
					0.30	163.6	114.7	90.2	62.2	42.1
					0.45	161.6	115.1	90.2	63.0	41.8
					0.60	162.6	114.9	90.1	63.0	43.3

T_m = melting temperature, additive; T_c = crystallization temperature, additive; $T_{-5\ wt\%}$ = 5 % weight loss temperature, additive; $T_{m,p}$ = peak melting temperature, polymer $T_{c,p}$ = peak crystallization temperature, polymer, n.a. = not available, Transmission, Haze and Clarity were measured on 1.0 mm plaques. [1)] T_m taken from DSC decomposition run; [2)] main melting point from several.

As a general observation it can be noted that all derivatives show different efficiencies. The onset of the increase of the crystallization temperature and the improvement of the optical properties are independent of each other. The concentration levels, at which these values are influenced by the different additives can be taken from Table 5-4.

Detailed investigations on compound 5c

Considering the good performance regarding the improvement of optical properties, additive **5c** was selected as the lead candidate out of the set **5**. Therefore, the concentration dependence of the crystallization temperature and the optical properties of this additive were investigated and discussed in more detail.

The left diagram in Figure 5-3 shows the dependence of the peak crystallization temperature as a function of additive concentration. Below an additive concentration of 0.30 wt%, the crystallization temperature increases negligible to around 116 °C. Above this concentration, nucleation starts and reaches a plateau value of a $T_{c,p}$ around 128 °C. This concentration is reached at around 0.30 wt%. The right diagram in Figure 5-3 shows the effect of the additive on the optical properties. The haze values run counter to the clarity values. Clarity starts to increase and haze starts to decrease exceeding 0.30 wt%. By increasing the loading level up to 0.75 wt% haze and clarity values of 38.1 % respectively 92.5 % are reached.

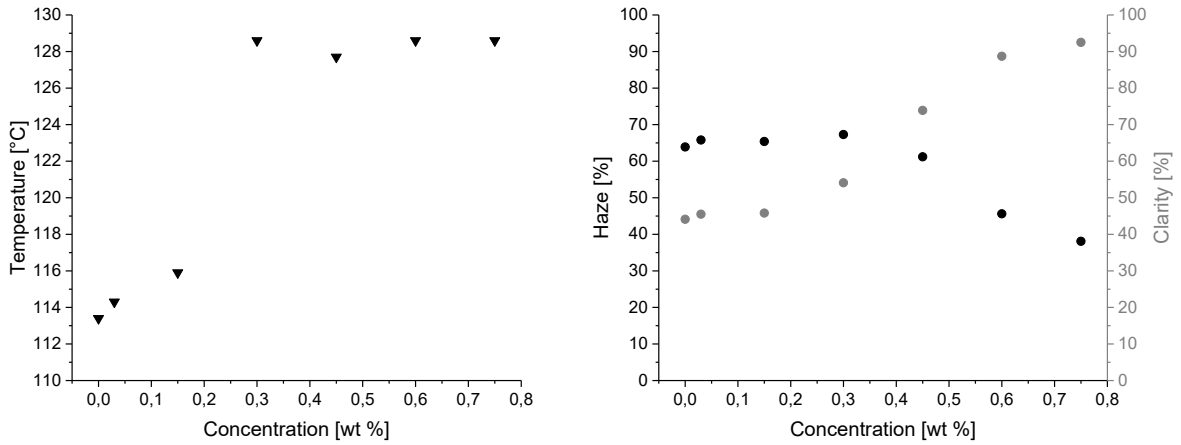

Figure 5-3 Crystallization temperature ($T_{c,p}$ ▼) and values for haze (•) and clarity (•) in relation to additive concentration for compounds containing additive **5c**.

The step height, by which the haze value decreases, represents its efficiency and is often said to be dependent on the solubility limit of the respective additive in the polymer [84, 112]. Differences in effectiveness result from the chemical structure of the additives. As already stated and in contrast to $T_{c,p}$, the optical properties, particularly with regard to haze improve with further additive concentration beyond 0.60 wt%. In several cases, especially for the earlier sorbitol based derivatives, it is known that haze increases again above a threshold of 0.50 wt% [72]. This is understood by the limited solubility of the additive, which results in larger additive crystals which scatter light [113]. The solubility limit of additive **5c** is not reached until a concentration of 0.75 wt%. This indicates an overall good solubility of the additive.

Conclusions and impact of substitution pattern of the 'wings'

Six out of eight additives were found to act as nucleating agents for iPP at a certain concentration level, whereas only three additives (**5b-d**) were found to improve optical properties by more than 20 % haze.

As the 'methyl ester tail' was common to all tested additives described above, it can be concluded that the substitution pattern of the benzylidene 'wings' has an impact on the additives nucleation and clarification behavior. The results indicate, that derivatives showing less or even no effects might be sterically hindered by their substituents. As a result, different stacking geometries of the aromatic 'wings' might disfavor potential network formation. Additionally, the substituents might trigger a different lattice match between additive and polymer. Definitely, the different substitution patterns and especially the longer alkyl chain substituents lead to improved solubility of the additives and may prevent the formation of supramolecular structures below a threshold concentration upon cooling. Below this threshold solubility is high and no network forms. As the surface of the network or the additives themselves are necessary to induce nucleation, for highly soluble additives nucleation does not occur below the threshold [112]. However, the additives acting as moderate clarifying agents (**5b-d**) become effective exceeding concentrations of 0.60 wt%. This is to be contrasted with **DMDBS** and its derivatives, which are employed commercially at concentrations of about 0.25 wt%, delivering significant improved transparencies [36, 72].

These results demonstrate that the nucleation and clarification ability of polymer additives depend on the individual chemical structure and their potential to provide a nucleation surface. To eludiate if nucleation of this set is induced by the surface of the additives themselves or by the formation of superstructures due to self-assembly, additional experiments were necessary. Considering the fact that the methyl ester is devoid of HBD capacity it is likely that the molecules of this set do not self-assemble by the formation of intermolecular hydrogen bonds. This suggests that a potential network formation is mainly based on π-π interactions between the benzylidene 'wings'. Based on these findings, dissolution and crystallization experiments with selected examples (**5c** and **5h**) in order to better understand the structural differences on the solubility, self-assembly and efficiency at the same time, were conducted and are presented in chapter 6.

5.3.2. 3,5:4,6-Dibenzylidene-*L*-gulonic acid derivatives (6)

The results from the screening of additive set **6** are summarized in Table 3-5. Most of the additives were found to be more or less effective nucleating agents for iPP. In particular cases the additives provide slightly improved optical properties. All additives increase the crystallization temperature, and five out of eight derivatives enabled an increase above 120 °C. Interestingly, only two derivatives have been found to improve optical properties in terms of haze by 10-20 %, whereas clarity values are improved by all derivatives.

Compounds containing additive **6a** reach a crystallization temperature of 124.5 °C at the highest applied concentration level. Haze values deteriorate up to 83.8 % with increasing additive loading level and clarity values increase as well. Additive **6b** increases the crystallization temperature of iPP up to 122.5 °C at a concentration level of 0.45 wt%. The haze value remains nearly unaffected, but the clarity value increases up to around 92.0 %. The $T_{c,p}$ value for compounds containing additive **6c** reaches a maximum value of 124.8 °C and only the clarity value is improved up to 92.7 %. Compounds containing additive **6d** induce the highest crystallization temperature of this set with a value of 125.3 °C at a loading level of 0.45 wt%. Haze and clarity values are improved to 45.5 %, respectively 93.8 %. Comparable values are found for iPP samples containing additive **6e**, but all values undergo a maximum at a concentration of 0.30 wt%. The crystallization temperature reaches 124.1 °C, haze decreases to 44.8 % and clarity increases to 94.2 %. The compounds containing additive **6f**, **6h** or **6i** show only marginal improved crystallization temperatures of around 6.0 °C. The haze values of compounds containing additive **6f** or **6h** deteriorate slightly, whereas the addition of additive **6i** reduces the haze value negligible. However, the clarity values of the three compounds increase above 80.0 %.

Table 5-5. Screening results of 3,5:4,6-dibenzylidene *L*-gulonic acid (**6**) derivatives.

Nr.	Substitution pattern	T_m [°C]	T_c [°C]	$T_{-5\ wt\%}$ [°C]	Conc. [wt%]	$T_{m,p}$ [°C]	$T_{c,p}$ [°C]	Trans. [%]	Haze [%]	Clarity [%]
iPP	no additive	-	-	-	-	165.5	113.4	89.7	63.9	44.1
6a	-	207	n.a.	213	0.03	165.6	114.1	89.1	66.1	43.7
	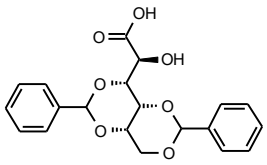				0.15	164.8	117.1	88.0	70.3	71.9
					0.30	163.2	119.4	89.1	72.0	80.5
					0.45	164.0	123.9	89.0	74.7	82.2
					0.60	164.2	124.4	87.4	83.8	68.0
6b	4-Me	192[1)]	n.a.	214	0.03	163.6	114.7	89.7	64.1	48.5
	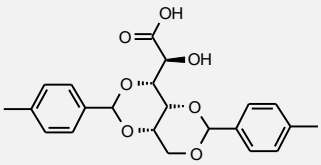				0.15	165.4	115.9	89.1	59.5	84.9
					0.30	163.7	120.5	89.6	59.5	92.0
					0.45	163.6	122.5	88.9	61.3	91.6
					0.60	165.6	121.1	87.3	68.7	88.7
6c	3,4-DiMe	187[1)]	n.a.	213	0.03	161.7	115.8	89.7	66.4	58.3
	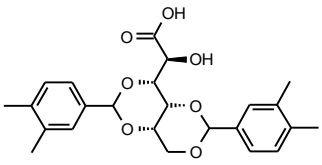				0.15	161.4	116.7	89.8	61.5	86.7
					0.30	164.7	121.7	89.6	56.1	92.7
					0.45	163.5	124.8	88.9	57.1	92.2
					0.60	164.0	124.0	87.5	65.0	91.0
6d	3,5-DiMe	219[1)]	n.a.	236	0.03	164.9	115.1	89.8	64.7	48.6
	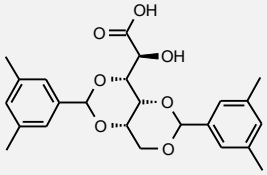				0.15	162.8	116.1	89.7	64.3	80.9
					0.30	164.5	121.9	89.9	56.0	92.6
					0.45	163.5	125.3	89.6	46.0	93.7
					0.60	163.3	125.0	88.6	45.5	93.8
6e	2,4-DiMe	177[1)]	n.a.	208	0.03	164.2	114.9	89.9	64.1	45.8
	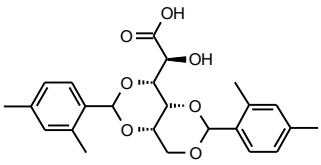				0.15	164.6	122.6	89.4	51.6	93.3
					0.30	164.3	124.1	89.4	44.8	94.2
					0.45	164.0	123.6	88.6	51.2	93.5
					0.60	163.3	119.2	83.4	76.8	77.9
6f	2,5-DiMe	209[1)]	n.a.	223	0.03	164.4	115.2	89.9	68.8	49.4
	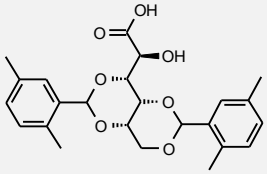				0.15	162.8	116.7	87.3	66.9	68.2
					0.30	162.1	117.1	84.5	70.1	72.4
					0.45	161.4	117.7	84.6	69.6	79.7
					0.60	164.1	118.2	86.8	63.2	88.5

T_m = melting temperature, additive; T_c = crystallization temperature, additive; $T_{-5\ wt\%}$ = 5 % weight loss temperature, additive; $T_{m,p}$ = peak melting temperature, polymer $T_{c,p}$ = peak crystallization temperature, polymer, n.a. = not available, Transmission, Haze and Clarity were measured on 1.0 mm plaques. [1)] T_m taken from DSC decomposition run; [2)] main melting point from several.

Table 5-5. Continued.

Nr.	Substitution pattern	T_m [°C]	T_c [°C]	$T_{-5\ wt\%}$ [°C]	Conc. [wt%]	$T_{m,p}$ [°C]	$T_{c,p}$ [°C]	Trans. [%]	Haze [%]	Clarity [%]
6h	4-Pr	189[1)]	n.a.	214	0.03	164.5	115.2	89.7	66.4	48.6
	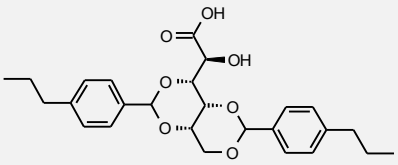				0.15	165.0	116.5	86.8	67.7	66.8
					0.30	162.4	117.3	78.8	69.2	71.5
					0.45	163.0	117.4	81.0	69.6	78.9
					0.60	162.5	118.2	81.2	72.1	80.9
6i	4-Isobu	186[1)]	n.a.	202	0.03	164.9	115.7	89.7	72.4	48.7
	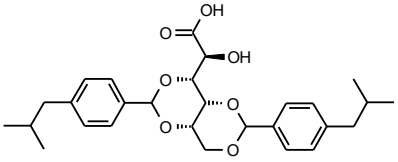				0.15	164.2	116.4	85.7	69.2	71.7
					0.30	161.2	117.4	80.1	67.7	78.7
					0.45	162.8	120.8	83.6	64.8	86.9
					0.60	161.0	118.0	86.0	56.6	92.0

T_m = melting temperature, additive; T_c = crystallization temperature, additive; $T_{-5\ wt\%}$ = 5 % weight loss temperature, additive; $T_{m,p}$ = peak melting temperature, polymer $T_{c,p}$ = peak crystallization temperature, polymer, n.a. = not available, Transmission, Haze and Clarity were measured on 1.0 mm plaques. [1)] T_m taken from DSC decomposition run; [2)] main melting point from several.

All derivatives of this set induce different efficiencies. Table 5-5 reveals the concentrations at which the crystallization temperatures or the optical properties are influenced. In addition, as with set **5**, the results show that an increased crystallization temperature does not necessarily correspond to improved optical properties.

Detailed investigations on compound 6d

Additive **6d** was chosen as this sets lead candidate, because iPP compounds containing additive **6d** yielded good optical properties. The concentration dependence of the crystallization temperature and the optical properties of this additive are illustrated in the following Figure 5-4 in more detail.

The left diagram in Figure 5-4 shows the dependence of the peak crystallization temperature as a function of the loading level. Here as well, below a certain additive amount of 0.15 wt%, the crystallization temperature increases negligibly by only 3 °C and remains nearly constant. Above a concentration of 0.30 wt%, nucleation starts and reaches a plateau at around 125 °C. The right diagram in Figure 5-4 shows the effect of additive content on the optical properties of the polymer. Haze and clarity values cross each other exceeding a concentration of 0.15 wt% of the respective additive **6d**. Haze and clarity values develop in complete agreement with the observed crystallization temperatures. Clarity increases up to a value of 93.8 % and haze decreases to a minimum value of 45.5 %. The overall smaller step height of the haze values, especially between 0.15 and 0.30 wt% indicates a reduced efficiency, but might be characteristic for a reduced solubility of the additive as well [84, 112, 113].

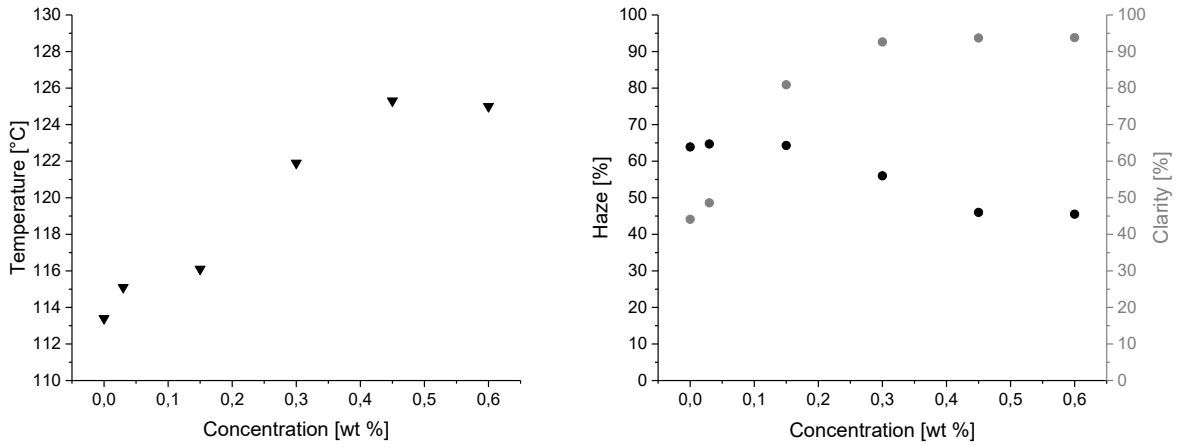

Figure 5-4 Crystallization temperature ($T_{c,p}$ ▼) and values for haze (•) and clarity (•) in relation to additive concentration in iPP for compounds containing additive **6d**.

Conclusion and impact of substitution pattern of the 'wings'

All eight additives were found to act as nucleating agents for iPP at a certain concentration level. At least two additives (**6d** and **6e**) were found to improve optical properties with respect to haze by around 20 %. The fact haze values were less reduced and lower crystallization temperatures have been achieved, reveals that molecules bearing a terminal acid moiety are less efficient than those bearing a terminal methyl ester moiety. However, as in the case of previous additive classes, it is difficult to draw a complete structure-property relationship for this set of additives.

As a consequence of the fixed 'acid tail', it can be seen that the efficiency of this set is dependent on the substitution pattern of the 'wings'. Again, longer alkyl chains on the benzylidene 'wings' lead to a decline of the additives nucleation efficiency. Most probably due to steric hindrance, different stacking geometries or influenced lattice parameters. The fact that all additives induce nucleation but only a limited number of additives improve the optical properties, suggests a different underlying mode of action. A conceivable reason might be an overall different aggregation behavior, such as the formation of head-to-tail hydrogen bonded dimers. This might influence the solubility of the additives as well. Consequently, less soluble or even insoluble additives need to be finely dispersed in the polymer melt to be capable to provide a surface and act as nucleating agent. To reveal the mode of action, dissolution and crystallization experiments were conducted with selected derivatives (cf. chapter 6.3).

5.3.3. 3,5:4,6-Dibenzylidene-*L*-gulonic amid derivatives (7)

The screening results of additive set **7**, summarized in Table 5-6, reveal that these additives are efficient nucleating and clarifying agents for iPP. All eight additives were able to increase the crystallization temperature above 120 °C at a certain concentration. Unexpectedly, all of the additives were also found to be reasonable clarifying agents.

Table 5-6. Screening results of 3,5:4,6-dibenzylidene *L*-gulonic amid (**7**) derivatives.

Nr.	Substitution pattern	T_m [°C]	T_c [°C]	$T_{-5\ wt\ \%}$ [°C]	Conc. [wt%]	$T_{m,p}$ [°C]	$T_{c,p}$ [°C]	Trans. [%]	Haze [%]	Clarity [%]
iPP	-	-	-	-	-	165.5	113.4	89.7	63.9	44.1
7a	-	258	202	292	0.03	162.6	115.2	90.1	61.3	47.7
	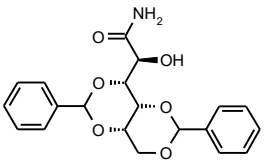				0.15	163.9	119.5	89.4	65.4	50.8
					0.30	164.2	126.3	87.7	70.2	55.8
					0.45	164.4	120.4	85.0	63.3	69.3
					0.60	164.9	123.2	85.3	49.3	90.4
7b	4-Me	226	167	291	0.03	163.0	115.0	90.0	63.1	45.1
	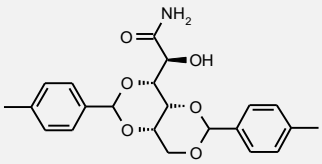				0.15	163.7	121.8	89.9	38.9	93.8
					0.30	163.5	123.1	88.9	26.6	93.3
					0.45	162.8	123.1	88.2	35.5	88.7
					0.60	163.2	122.4	87.7	48.5	81.8
7c	3,4-DiMe	261[1)]	n.a.	297	0.03	164.9	113.4	90.1	62.9	43.9
					0.15	164.3	124.3	89.7	34.1	94.2
	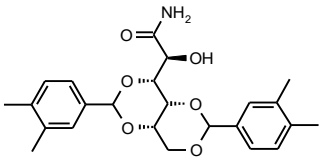				0.225	164.5	124.5	89.0	24.8	94.6
					0.30	164.8	124.0	88.8	22.8	94.4
					0.375	164.8	123.4	88.4	22.8	93.9
					0.45	164.3	123.3	88.2	22.7	93.6
					0.60	164.9	122.6	87.8	25.7	92.7
7d	3,5-DiMe	278[1)]	n.a.	309	0.03	163.2	114.4	90.2	61.7	46.6
	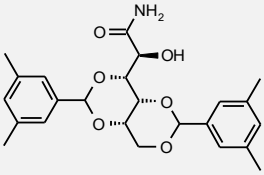				0.15	164.2	122.0	90.0	40.9	93.1
					0.30	164.2	122.5	88.9	27.9	94.0
					0.45	164.8	124.3	88.5	35.4	92.2
					0.60	165.0	123.8	88.3	80.5	71.9
7e	2,4-DiMe	230	n.a.	285	0.03	161.0	112.8	90.2	60.4	41.3
	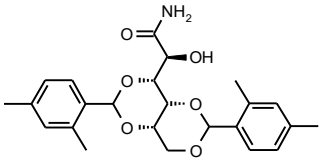				0.15	165.4	113.5	90.4	64.6	82.1
					0.30	165.2	122.2	90.1	46.1	93.6
					0.45	162.9	122.2	88.9	40.3	92.1
					0.60	163.1	128.6	88.4	39.9	90.7

T_m = melting temperature, additive; T_c = crystallization temperature, additive; $T_{-5\ wt\%}$ = 5 % weight loss temperature, additive; $T_{m,p}$ = peak melting temperature, polymer $T_{c,p}$ = peak crystallization temperature, polymer, n.a. = not available, Transmission, Haze and Clarity were measured on 1.0 mm plaques. [1)] T_m taken from DSC decomposition run; [2)] main melting point from several.

Table 5-6. Continued.

Nr.	Substitution pattern	T_m [°C]	T_c [°C]	$T_{-5\ wt\%}$ [°C]	Conc. [wt%]	$T_{m,p}$ [°C]	$T_{c,p}$ [°C]	Trans. [%]	Haze [%]	Clarity [%]
7f	2,5-DiMe	272	n.a.	297	0.03	164.3	115.4	90.0	63.7	48.1
	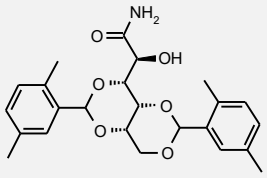				0.15	164.4	116.0	89.9	66.7	57.4
					0.30	164.9	118.7	89.9	62.7	87.4
					0.45	164.2	122.4	89.1	63.5	83.1
					0.60	163.6	116.9	87.9	41.7	92.6
7h	4-Pr	225	171	288	0.03	164.9	114.4	90.2	61.5	44.4
	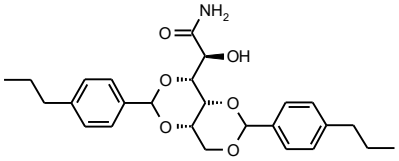				0.15	165.6	117.5	90.7	59.2	91.6
					0.30	163.7	122.3	89.2	30.6	94.3
					0.45	163.2	121.4	88.4	26.2	94.8
					0.60	163.1	122.0	88.0	26.2	94.5
7i	4-Isobu	217[2)]	172	295	0.03	164.5	114.6	90.3	75.9	48.5
	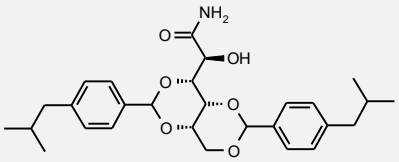				0.15	163.9	115.5	90.0	66.5	46.2
					0.30	165.1	115.7	90.2	61.0	90.0
					0.45	165.8	123.1	89.2	37.4	94.2
					0.60	165.2	126.8	88.1	29.9	94.6

T_m = melting temperature, additive; T_c = crystallization temperature, additive; $T_{-5\ wt\%}$ = 5 % weight loss temperature, additive; $T_{m,p}$ = peak melting temperature, polymer $T_{c,p}$ = peak crystallization temperature, polymer, n.a. = not available, Transmission, Haze and Clarity were measured on 1.0 mm plaques. [1)] T_m taken from DSC decomposition run; [2)] main melting point from several.

Additive **7a** increases the crystallization temperature of iPP up to a maximum of 126.3 °C at a concentration level of 0.30 wt%. Haze decreases only negligible, but clarity increases significantly. Some of the earlier sorbitol derivatives are known to show a rebound in haze exceeding a certain amount of additive loading [113]. A similar curve progression can be observed for the additives **7b-d**, which all run through a slight haze minimum at around 0.30 wt%. Compounds containing additive **7b** increase $T_{c,p}$ up to 123.1 °C. The lowest measured haze value is 26.6 % and the highest clarity value is 93.8 %. Additive **7c** induces a crystallization temperature of around 124.0 °C and reduces haze by more than 41 % to the lowest haze value of the set with 22.8 %. In addition, clarity reaches a value of nearly 95.0 %. Compounds containing additive **7d** reach a maximum crystallization temperature of 124.3 °C, haze decreases to 27.9 % and clarity increases to 94.0 %. At a concentration level of 0.60 wt% the haze value soars form 35 % to over 80 %. Additive **7e** nucleates iPP and induces the highest crystallization temperature of this set with 128.6 °C. Haze and clarity are improved to 39.9 % and respectively 90.7 % at a concentration level of 0.60 wt%. The $T_{c,p}$ for compounds containing additive **7f** reaches a maximum value of 122.4 °C and optical properties are improved. Haze decreases to a value of 41.7 %, whereas clarity increases to a value of 92.6 %. Unexpectedly, the compounds containing additive **7h** or **7i** show a significant decrease in haze at higher loading levels. Additive **7h** induces a crystallization temperature of 122.0 °C. Haze and clarity values improve significantly to 26.2 % and respectively 94.8 %. Additive **7i**, shows a similar

behavior and increases the crystallization temperature up to 126.8 °C. Haze decreases to a value of 29.9 % and clarity increases to a value of 94.6 %.

This set of additives had different efficiencies, but in this case most of the substitution patterns lead to significant improved optical properties. Once again, the additives induce their best performance in different concentration regions. Table 5-6 reveals these regions. Surprisingly, five out of eight additives achieve haze values below 30 % and thus reduce haze by more than the half compared to the control material. Even though the optical properties are not yet comparable to the sorbitol based clarifying agents, **TBPMN** and **DMDBS**, which were found to show remarkable levels of haze with values below 15 % (cf. Table 5-3), this set is more effective than the previous ones.

Detailed investigations on compound 7c

Additive **7c** was selected as lead candidate of the current set of derivatives. Figure 5-5 comprises concentration dependent illustrations of the peak crystallization temperature as well as of the optical properties.

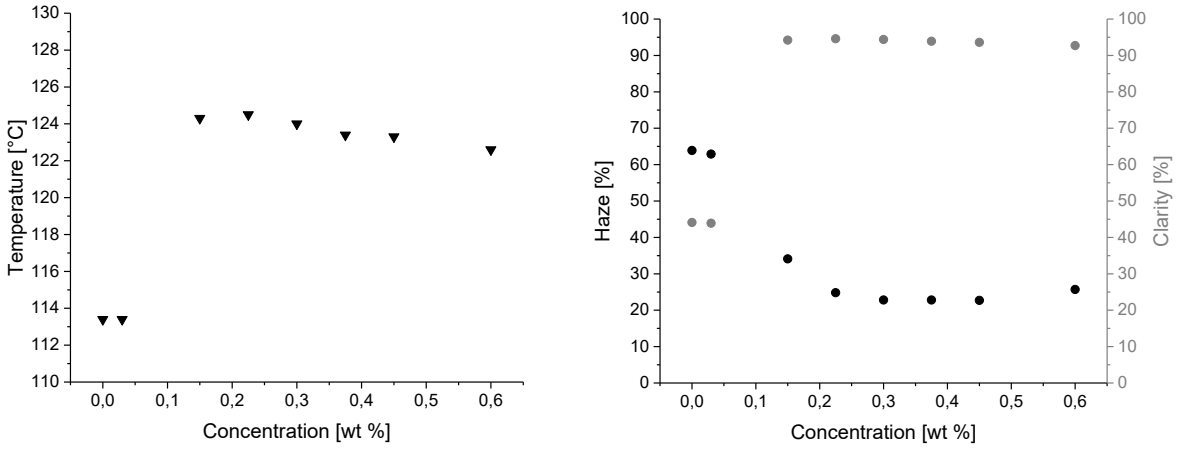

Figure 5-5 Crystallization temperature ($T_{c,p}$ ▼) and values for haze (•) and clarity (•) in relation to additive concentration in iPP for compound **7c**.

The diagram on the left in Figure 5-5 illustrates the crystallization temperature as a function of additive concentration. Below a concentration of 0.15 wt% no increase of the crystallization temperature can be observed, represented by a constant value of 113.4 °C. This constant development can be explained by the existence of a eutectic temperature at low additive concentrations [72, 113]. The threshold, below which the additive ceases to function as a nucleating agent is consequently below 0.15 wt%. Above this concentration, nucleation starts and reaches a plateau value of around 124.5 °C. Exceeding a concentration of 0.30 wt% the crystallization temperature slightly decreases. The right diagram of Figure 5-5 shows the haze and clarity values as a function of additive concentration. Both values are consistent with the crystallization temperature. Haze reaches a minimum value of 22.7 % and clarity increases up to 94.4 %. Due to the fact, that both values, $T_{c,p}$ and haze undergo a maximum respectively a minimum at 0.30 wt%, additional concentrations before and after this extremum have been tested with less success. Therefore it can be expected that no better performance will be reached

with raising the additive level above 0.60 wt%. Additive **7c** shows a slight rebound in haze after its maximum at 0.30 wt%, which is most probably due to a efficiency loss caused by additive overloading [72]. In that case, a limited solubility results in larger additive crystals and thus in light scattering by the additive itself [113]. Compared to the previous sets **5** and **6**, additive **7c** has a much higher efficiency.

Detailed investigations on compound 7h

Additive **7h** has been identified to provide the second best results and additionally did not show a haze and clarity extremum up to a concentration of 0.60 wt%. Therefore, it was also selected to be investigated in more detail.

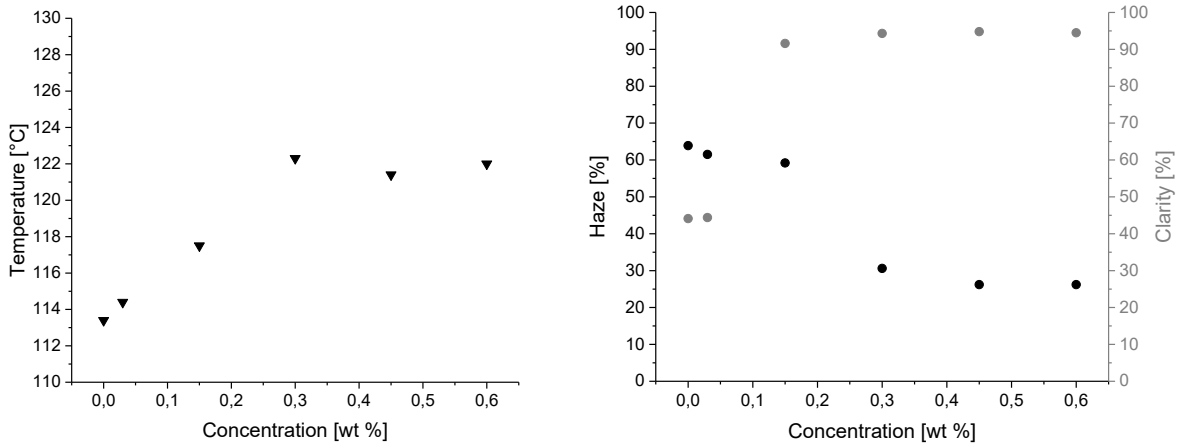

Figure 5-6 Crystallization temperature ($T_{c,p}$ ▼) and values for haze (•) and clarity (•) in relation to additive concentration in iPP for compound **7h**.

The left diagram in Figure 5-6, shows the development of the crystallization temperature depending on the concentration level of additive **7h**. In this case, the crystallization temperature already shows at 0.15 wt% an increase up to 117.5 °C and reaches the plateau at around 122 °C. Consequently, the threshold below which the additive ceases to function as a nucleating agent is below 0.15 wt%. The development of the optical properties is shown in the right diagram in Figure 5-6. Exceeding a concentration of 0.30 wt%, haze decreases significantly and reaches a plateau at 26.2 %. The clarity value changes already at 0.15 wt% and is more sensitive to the additive. Unexpectedly, these overall good optical properties coincide with relatively low crystallization temperatures. The fact, that the crystallization temperature as well as haze pass over into constant values, exceeding 0.45 wt% may be an indication that the threshold concentration of additive **7h** is reached.

Conclusion and impact of substitution pattern of the ‘wings’

All eight additives of the current set were found to be efficient nucleating and clarifying agents for iPP. The efficiency of each additive depends highly on the applied concentration level and is influenced by the substitution pattern of the benzylidene ‘wings’. Five additives induce improved haze values of at least 34 % at a certain additive concentration. Additive **7c** reduces the haze value of iPP by even 41 % from 64 % to a level below 23 %.

The present set of additives achieved significantly greater haze improvements in comparison to the previous investigated sets **5** and **6**. Therefore, it is likely that the 'amide tail' is responsible for the significantly increased efficiency. Nevertheless, drawing conclusions on how the efficiency of the additives is influenced by the substitution pattern of the benzylidene 'wings' is still challenging. It can be observed, that reduced haze values do not necessarily imply high crystallization temperatures. The fact that the efficiency of some compounds undergo an extremum and that the efficiency of other compounds is shifted towards higher concentration levels, strongly suggest that solubility is an important aspect [112, 113]. In case of a network formation process, the aggregation and thus surface formation is only possible in concentration regimes where the network is fully developed. Consequently the thresholds below which the additives ceases to function are different. The threshold concentration of additive **7c** is below 0.15 wt%. Whereas additive **7h** for example exhibits a threshold below 0.15 wt%, but is most effective with regard to haze improvement above 0.45 wt%. This has to be contrasted with the sorbitol based nucleating and clarifying agents, which exhibit different maxima and thresholds as well. **DMDBS** and **TBPMN** cease to function as nucleators and clarifiers below 0.10 wt% [36, 72, 77]. **DMDBS** is claimed to be most effective above 0.25 wt% [114] and **TBPMN** above 0.60 wt% [77]. In this case, it might be worth to compare the mole fraction instead of the mass fraction of the additives.

Based on the findings, sterical hindrance due to the longer alkyl chains in para-position and a resulting disfavor during network formation can be excluded for this set of derivatives. To reveal potential differences in solubility, dissolution and crystallization, additional experiments especially for the additives **7c** and **7h** were studied in depth. The results are presented in chapter 6.

5.3.4. 3,5:4,6-Dibenzylidene-*L*-gulonic alkyl amid derivatives (8)

This subsection on set **8** is further subdivided in three parts. The main focus was put on the variation of the alkyl substituents which have been incorporated to the amide moiety in combination with completely unsubstituted benzylidene 'wings'. The alkyl substituents have been selected from the set of the following chain length, C_1 to C_4, C_8 and C_{12}. Besides the variation of the alkyl chain length, two different 'wing' substitution pattern have been investigated in combination with the DBGA-C_1 and -C_2 core. The following three tables will summarize the screening data of these derivatives.

Impact of varying the *n*-alkyl chain length

Table 5-7 summarizes the screening data of the synthesized additives of subset **8.1-6a**. Most of the additives act as nucleating agents and some act as moderate clarifying agents as well. Four out of six additives significantly increase the crystallization temperature above 120 °C at a certain concentration, but only two improve the haze value in a moderate way.

Additive **8.1a** increases the crystallization temperature of iPP up to around 128.0 °C, and the optical properties show a moderate improvement. Haze decreases to a value of 41.7 % and clarity increases up to a value of 77.3 %. The $T_{c,p}$ of compounds containing additive **8.2a** reaches only around 123.0 °C, whereby haze and clarity are improved in a moderate way to values of

42.1 %, respectively 83.1 %. The additives **8.3a** and **8.4a** induce nucleation as well. Compounds comprising additive **8.3a** increase the crystallization temperature up to 124.8 °C, but haze is only slightly reduced to 55.9 %. Clarity improves to a value of 71.5 %. Compounds containing additive **8.4a** reveal crystallization temperatures of around 126.0 °C. Haze is again only slightly reduced to 52.5 % and clarity improves to 78.0 %. The additives, bearing longer alkyl chains (**8.5-6a**), only slightly nucleate iPP by 3-4 °C. They show constant haze values, with only a slight increase compared to the 'control' sample. In contrast, clarity is only improved to 53.6 % by additive **8.5a**, whereas additive **8.6a** improves it to a value of 84.1 %.

Table 5-7. Screening results of 3,5:4,6-dibenzylidene *L*-gulonic alkyl amide (**8a**) derivatives.

Nr.	Substitution pattern	T_m [°C]	T_c [°C]	$T_{-5\ wt\ \%}$ [°C]	Conc. [wt%]	$T_{m,p}$ [°C]	$T_{c,p}$ [°C]	Trans. [%]	Haze [%]	Clarity [%]
iPP	-	-	-	-	-	165.5	113.4	89.7	63.9	44.1
8.1a	-; R=C1	263	263	278	0.03	163.8	116.7	89.8	64.5	61.9
	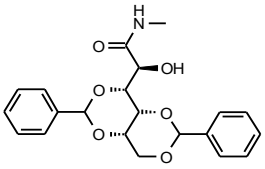				0.15	164.9	117.1	89.7	65.6	66.8
					0.30	165.8	128.3	89.6	61.5	79.5
					0.45	164.8	127.7	88.7	53.7	78.8
					0.60	164.5	127.8	88.6	41.7	77.3
8.2a	-; R=C2	259	222	284	0.03	167.3	114.3	89.6	63.0	46.5
	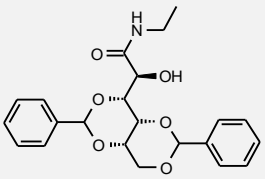				0.15	164.2	115.9	89.6	66.3	55.3
					0.30	162.1	116.2	89.4	67.6	67.6
					0.45	164.2	123.2	89.4	49.3	71.1
					0.60	164.4	123.1	89.2	42.1	83.1
8.3a	-; R=C3	260	219	269	0.03	163.0	115.0	89.7	64.6	45.5
	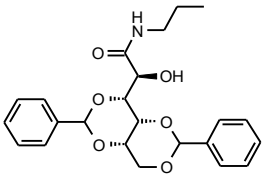				0.15	163.9	116.1	89.6	65.2	52.3
					0.30	163.4	121.7	89.3	68.6	58.6
					0.45	164.1	124.8	89.3	69.0	70.0
					0.60	164.2	124.2	88.7	55.9	71.5
8.4a	-; R=C4	243	214	296	0.03	164.9	115.0	89.6	62.9	45.0
	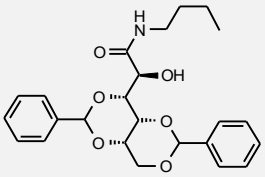				0.15	163.9	116.0	89.6	65.9	52.2
					0.30	163.1	116.3	89.3	68.0	62.0
					0.45	164.3	126.2	89.3	64.9	78.0
					0.60	164.3	125.7	88.8	52.5	77.1

T_m = melting temperature, additive; T_c = crystallization temperature, additive; $T_{-5\ wt\%}$ = 5 % weight loss temperature, additive; $T_{m,p}$ = peak melting temperature, polymer $T_{c,p}$ = peak crystallization temperature, polymer, n.a. = not available, Transmission, Haze and Clarity were measured on 1.0 mm plaques. [1)] T_m taken from DSC decomposition run; [2)] main melting point from several.

Table 5-7. Continued.

Nr.	Substitution pattern	T_m [°C]	T_c [°C]	$T_{-5\ wt\ \%}$ [°C]	Conc. [wt%]	$T_{m,p}$ [°C]	$T_{c,p}$ [°C]	Trans. [%]	Haze [%]	Clarity [%]
8.5a	-; R=C8	206	168	321	0.03	163.2	115.6	90.0	66.2	51.2
	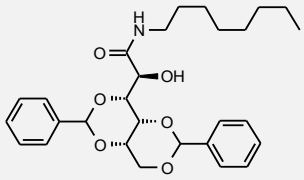				0.15	165.4	116.0	90.1	65.6	57.0
					0.30	166.3	116.1	90.0	67.3	59.9
					0.45	164.0	116.2	90.0	64.7	53.6
					0.60	166.4	115.1	89.7	62.4	59.3
8.6a	-;R=C12	193	166	321	0.03	166.1	114.2	90.1	63.1	47.7
	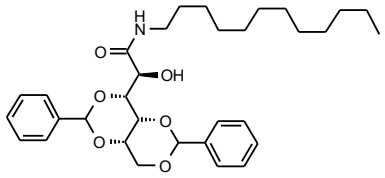				0.15	165.1	116.0	90.1	66.3	54.5
					0.30	165.2	116.8	90.1	67.2	63.1
					0.45	165.0	117.8	89.9	67.0	84.1
					0.60	164.1	117.9	89.9	67.2	81.1

T_m = melting temperature, additive; T_c = crystallization temperature, additive; $T_{-5\ wt\%}$ = 5 % weight loss temperature, additive; $T_{m,p}$ = peak melting temperature, polymer $T_{c,p}$ = peak crystallization temperature, polymer, n.a. = not available, Transmission, Haze and Clarity were measured on 1.0 mm plaques. [1] T_m taken from DSC decomposition run; [2] main melting point from several.

In this special case, the efficiency depends significantly on the introduced alkyl chain at the amide 'tail'. The appearance of the nucleation effect is dependent on the loading level and the introduced alkyl chain length. In addition, moderate improvements of the optical properties are only reached for additives with shorter alkyl chain length.

Detailed investigations on compound 8.2a

The structure **8.2a** was selected as lead candidate of the current subset and has been investigated in more detail. Figure 5-7 comprises concentration dependent illustrations of the peak crystallization temperature and of optical properties.

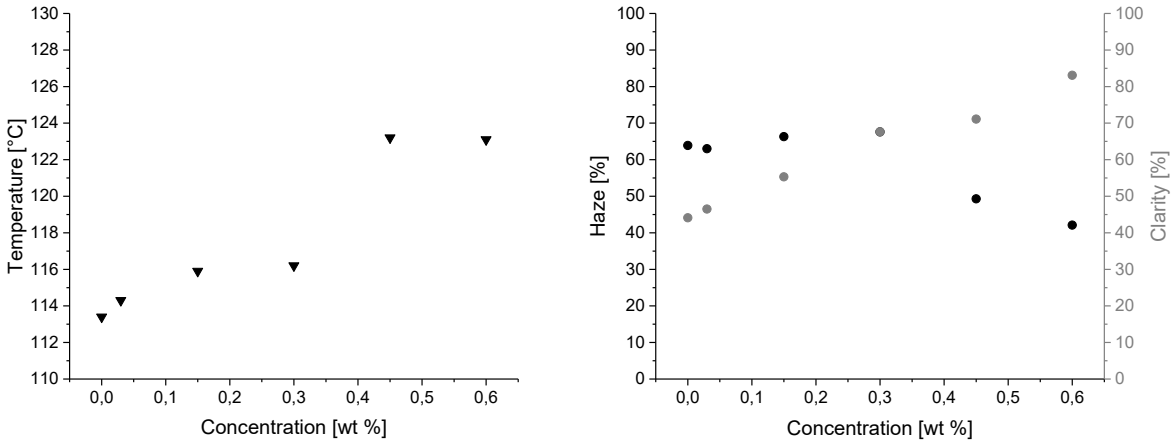

Figure 5-7 Crystallization temperature ($T_{c,p}$ ▾) and values for haze (•) and clarity (•) in relation to additive concentration in iPP for compound **8.2a**.

The current compounds display a completely different behavior compared to the previously discussed derivatives from set **5**, **6** and **7**. Below an additive concentration of 0.45 wt% only a

slight increase of the peak crystallization temperature can be observed. Towards higher concentrations, nucleation starts and reaches a plateau at 123 °C. On the other hand, if one considers the haze and clarity values as a function of additive concentration, it can be observed that clarity continuously improves up to a value of 85 %. In contrast, haze at first glance shows a slight increase up to around 68 %. Exceeding a certain amount of additive loading the haze value drops below 50 % haze. The fact, that haze drops at a certain point of additive loading combined with the steady increase of clarity suggests, that a higher loading level may be favorable to further improve optical properties. Based on the results one might expect a higher solubility of the additive 8.2a in the iPP matrix [84, 112, 113].

Conclusion and impact of varying *n*-alkyl chain

Four additives have been found to significantly increase the crystallization temperature. The highest crystallization temperature of around 128 °C has been found for the compounds containing the derivative with the shortest alkyl chain length (C_1) at the secondary amide moiety. No tendency can be identified, that shorter alkyl chains increase the crystallization temperature. For molecules bearing C_2 to C_4 alkyl chains, the opposite has been identified. The crystallization temperature increased from 123 °C for the C_2 derivative to 126 °C for the C_4 derivative. Longer alkyl chains (C_8 and C_{12}) induced lower nucleation efficiencies. The fact that they still induce nucleation to a certain extent is unexpected. Typically, the network formation is favored by strong hydrogen-bonding moieties and has been expected to be hampered by longer alkyl chains. Again the assumption might arise, that hydrogen bonding interactions are less important for the nucleation process of the additives. Consequently, π-π interactions would be more important or even no aggregation is needed to nucleate iPP. If no aggregation occurs, lattice matching and epitaxial growth on the molecules themselves may be the main driving force [62–64].

Looking at the haze values reveals that a moderately improvement is only induced by molecules bearing methyl and ethyl substituted amides. The primary amide derivative (**7a**) shows less haze improvement as the secondary methyl and ethyl derivatives. These results could emphasize the importance of increased solubility. A completely different approach might be that the insertion of the methyl and ethyl chains influences the stacking distance of the molecules in the self-assembly process. Resulting in a better lattice match between additive and iPP [63]. To study these questions in more details dissolution and crystallization experiments were conducted on mixtures containing additives **8.1a** or **8.2a**. The results are presented in the following chapter.

Impact of varying the substitution pattern of the ‘wings’ at a constant C_1-amide ‘tail’

The screening results of compounds containing additives of set **8.1** are summarized in Table 5-8. The additives vary only in their substitution pattern of the benzylidene ‘wings’ and bear a secondary methyl amide ‘tail’. All three additives induce nucleation and two of them act as relatively good clarifying agents.

As already discussed, the crystallization temperature of compounds containing additive **8.1a** reaches a plateau of around 128.0 °C, beginning at a concentration of 0.30 wt%. Haze and

clarity are improved to 41.7 %, respectively 77.3 %. A remarkably different behavior can be observed for compounds containing additive **8.1c**. The crystallization temperature reaches a plateau of around 124.0 °C and haze increases to a final value of around 100 %. Unexpectedly, the clarity value first improves and then after exceeding a threshold significantly decreases below 20 %. Whereas additive **8.1h** induces a crystallization temperature of 126.5 °C and shows a continuous improvement in haze exceeding 0.30 wt%. At higher loading levels, the additive is highly efficient in improving optical properties. Haze is reduced to a minimum value of 29.8 % and clarity improves to a value of 94.2 %.

Table 5-8. Screening results of 3,5:4,6-dibenzylidene *L*-gulonic methyl amide (**8.1**) derivatives.

Nr.	Substitution pattern	T_m [°C]	T_c [°C]	$T_{-5\ wt\ \%}$ [°C]	Conc. [wt%]	$T_{m,p}$ [°C]	$T_{c,p}$ [°C]	Trans. [%]	Haze [%]	Clarity [%]
iPP	-	-	-	-	-	165.5	113.4	89.7	63.9	44.1
8.1a	-; R=C1	263	263	278	0.03	163.8	116.7	89.8	64.5	61.9
	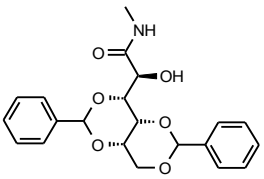				0.15	164.9	117.1	89.7	65.6	66.8
					0.30	165.8	128.3	89.6	61.5	79.5
					0.45	164.8	127.7	88.7	53.7	78.8
					0.60	164.5	127.8	88.6	41.7	77.3
8.1c	3,4-DiMe; R=C1	315[1)]	n.a.	306	0.03	159.6	115.1	89.9	66.5	50.4
	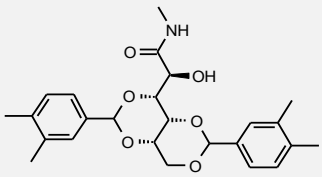				0.15	162.5	124.1	89.6	61.7	93.4
					0.30	162.3	124.7	88.8	86.5	67.6
					0.45	161.6	123.3	89.0	97.4	29.8
					0.60	163.0	124.5	88.3	99.5	16.9
8.1h	4-Pr; R=C1	251	231	299	0.03	163.5	115.0	89.9	65.5	47.4
	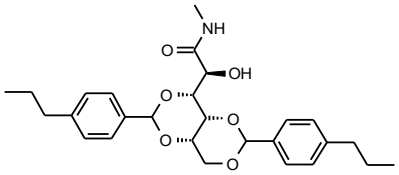				0.15	164.8	115.1	89.9	65.9	54.5
					0.30	164.5	125.7	90.4	60.3	91.3
					0.45	163.8	126.9	89.5	38.9	94.3
					0.60	163.8	126.5	89.0	29.8	94.2

T_m = melting temperature, additive; T_c = crystallization temperature, additive; $T_{-5\ wt\%}$ = 5 % weight loss temperature, additive; $T_{m,p}$ = peak melting temperature, polymer $T_{c,p}$ = peak crystallization temperature, polymer, n.a. = not available, Transmission, Haze and Clarity were measured on 1.0 mm plaques. [1)] T_m taken from DSC decomposition run; [2)] main melting point from several.

As a result of the unchanged C_1-amide 'tail' the efficiency changes drastically, depending on the substitution pattern of the aromatic 'wings'. This is most visible by the change observed for the optical properties. Little changes in the overall molecular structure result on the one hand in improved optical properties and on the other hand in strong deterioration. In addition, the strongest influence on the optical properties is observed at high additive concentrations.

Detailed investigations on compound 8.1h

The structure **8.1h** was selected as lead candidate of the current subset, due to the good haze results and was investigated more precisely. Figure 5-8 comprises concentration dependent illustrations of the peak crystallization temperature and of optical properties.

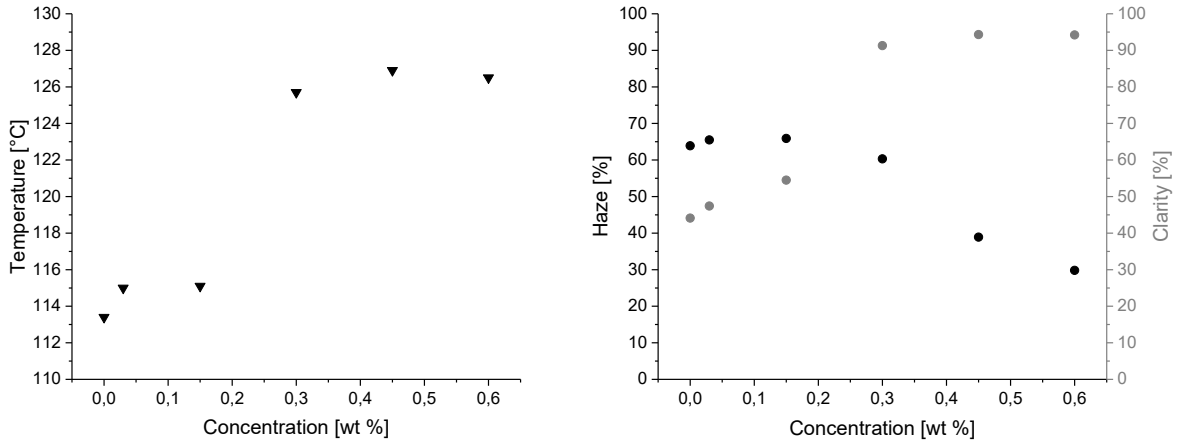

Figure 5-8 Crystallization temperature ($T_{c,p}$ ▼) and values for haze (•) and clarity (•) in relation to additive concentration in iPP for compounds containing additive **8.1h**.

The present compounds display a behavior, where optical properties are significantly influenced at a relatively high concentration level. Below an additive concentration of 0.30 wt% only a slight increase of the crystallization temperature can be observed. Exceeding this threshold, the crystallization temperature suddenly increases and reaches a plateau at around 126 °C. Haze does not improve continuously with increasing concentration, but rather improves suddenly at a certain loading level. In fact, additive **8.1h** needs higher loading levels and acts above 0.45 wt% as a clarifying agent. Clarity in contrast to haze, increases in accordance with the observed crystallization temperature and reaches values of above 90 % at 0.30 wt%. In general, a high loading level reflects a high solubility of the additive in the polymer and thus might explain the effectiveness in reducing haze only at higher concentrations [84, 112].

Detailed investigations on compound 8.1c

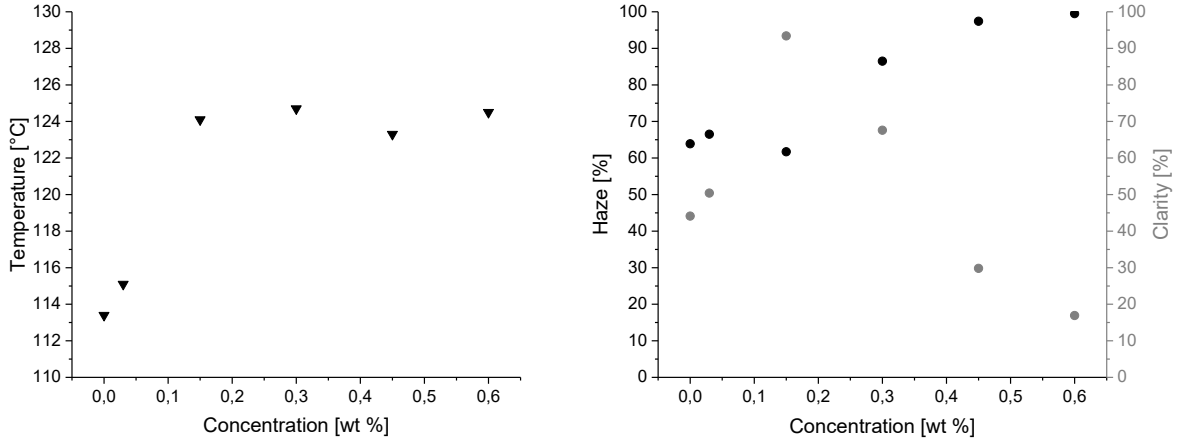

Figure 5-9 Crystallization temperature ($T_{c,p}$ ▼) and values for haze (•) and clarity (•) in relation to additive concentration in iPP for compounds containing additive **8.1c**.

As already stated, additive **8.1c** does not improve the optical properties, but rather worsens the results compared to the 'control' sample. Based on this completely different findings, detailed considerations have been performed on this compound as well. The crystallization temperature does not show a difference to other nucleated compounds. At a certain additive level, here 0.15 wt%, the crystallization temperature increases and stays nearly constant at a plateau value of around 124 °C. As can be seen in Figure 5-9 exceeding a concentration of 0.15 wt%, haze increases significantly and approaches a maximum value of nearly 100 %. Clarity in contrast shows first a significantly improvement above 93 % and subsequently decreases below 20 %. Figure 5-10 illustrates the optical properties of injection-molded samples containing different amounts of additive **8.1c**. The optical properties of the 'control' material, which are already poor, become more opaque with an increasing additive concentration.

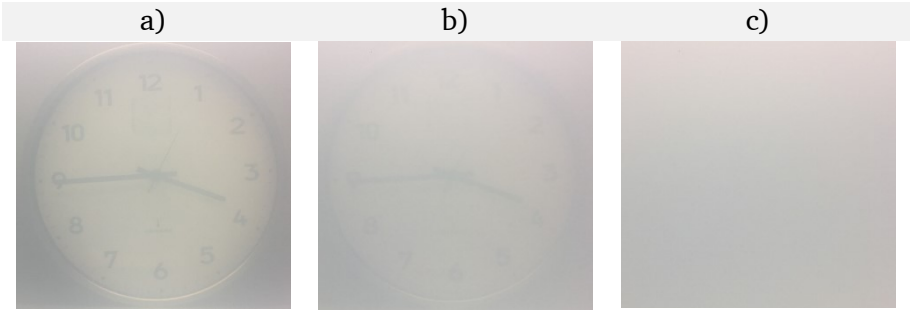

Figure 5-10 Illustration of increasing haze value and accompanying opaqueness. Photograph through 1.0 mm thick injection-molded iPP plaques. a) Control sample, b) containing 0.30 wt% **8.1c** and c) containing 0.60 wt% **8.1c**.

Such a change in optical properties might be the result of different crystal modifications. For example an increased β-crystal content might result in a higher opaqueness, due to highly birefringent spherulites [8, 115]. In general, β-crystals have a melting point that is typically around 10-15 °C below that of the α-form [116]. iPP samples containing both crystal forms typically show a double melting peak which can be detected in DSC analytics. The melting temperature of compounds containing additive **8.1c** is minimally decreased, but the DSC curves do not show a double melting peak. A conclusive explanation may be that the β-phase is only minimally induced and the α-phase is still the predominant phase. This would explain why the β-peak cannot be detected.

Conclusion and impact of varying the substitution pattern of the 'wings' at a constant C_1-amide 'tail'

All three additives were found to nucleate iPP, but with diverse effects on the optical properties. Two additives improve haze, but the third deteriorates the optical properties, resulting in a completely opaque material. It can be suggested, that the additive **8.1c** induces the β-phase of iPP at least to a certain extent. However, it had not been possible to confirm this by DSC experiments. To reveal this issue, detailed WAXS investigations on compounds containing additive **8.1c** have been conducted and are presented in chapter 6.2.

On the basis of the collected data presented in Table 5-8 it is evident that both the substitution pattern of the benzylidene 'wings' and the 'tail', are of paramount importance. Most probably,

the molecules do not just provide a surface to promote epitaxial growth of iPP, but determine the polymers' crystal modification as well. As before, the stacking behavior and the solubility of the molecules is highly influenced by the aromatic substituents [84, 112, 113]. Therefore, initial experiments on the phase behavior are presented in chapter 6.

Impact of varying the substitution pattern of the 'wings' at a constant C_2-amide 'tail'

The screening results of compounds containing additives of set **8.2** are summarized in Table 5-9. Again, the additives vary only in their substitution pattern of the benzylidene 'wings', but bear a secondary ethyl amide 'tail'. All three additives efficiently induce nucleation and act as moderate to good clarifying agents. Additive **8.2a** induces nucleation and increases the crystallization temperature to a plateau at 123.0 °C. Haze and clarity are improved to 42.1 %, respectively 83.1 %. Compounds containing additive **8.2c** show significant nucleation and the $T_{c,p}$ is found in the range between 122 and 126 °C. Optical properties undergo an extremum, whereby haze reaches a minimum of 43.1 % and clarity increases to a maximum value of 90.2 %. Additive **8.2h** induces the highest measured crystallization temperature of 130.9 °C. Haze reaches a minimum value of 36.0 % at the highest applied concentration and clarity is improved to a value of 93.5 %.

Table 5-9. Screening results of 3,5:4,6-dibenzylidene *L*-gulonic ethyl amide (**8.2**) derivatives.

Nr.	Substitution pattern	T_m [°C]	T_c [°C]	$T_{-5\ wt\ \%}$ [°C]	Conc. [wt%]	$T_{m,p}$ [°C]	$T_{c,p}$ [°C]	Trans. [%]	Haze [%]	Clarity [%]
iPP	no additive	-	-	-	-	165.5	113.4	89.7	63.9	44.1
8.2a	-; R=C2	259	222	284	0.03	167.3	114.3	89.6	63.0	46.5
	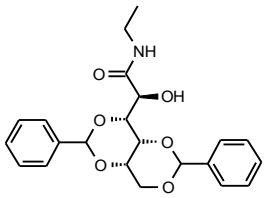				0.15	164.2	115.9	89.6	66.3	55.3
					0.30	162.1	116.2	89.4	67.6	67.6
					0.45	164.2	123.2	89.4	49.3	71.1
					0.60	164.4	123.1	89.2	42.1	83.1
8.2c	3,4-DiMe; R=C2	303[1)]	n.a.	297	0.03	163.7	114.9	89.9	66.1	50.7
	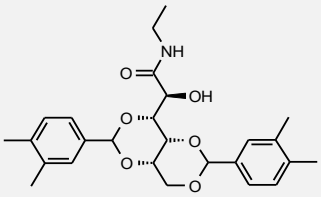				0.15	164.4	126.0	90.2	65.9	86.6
					0.30	164.3	122.5	89.3	45.1	90.2
					0.45	165.2	124.2	89.0	43.1	85.4
					0.60	165.4	122.1	87.3	59.5	88.6
8.2h	4-Pr; R=C2	241	173	315	0.03	164.5	116.3	89.8	64.7	61.2
	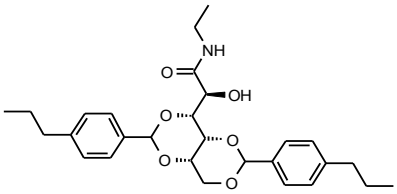				0.15	163.9	116.6	89.8	65.7	64.5
					0.30	164.0	121.1	89.9	64.1	78.9
					0.45	164.8	130.3	89.9	57.4	91.9
					0.60	165.1	130.9	89.2	36.0	93.5

T_m = melting temperature, additive; T_c = crystallization temperature, additive; $T_{-5\ wt\%}$ = 5 % weight loss temperature, additive; $T_{m,p}$ = peak melting temperature, polymer $T_{c,p}$ = peak crystallization temperature, polymer, n.a. = not available, Transmission, Haze and Clarity were measured on 1.0 mm plaques. [1)] T_m taken from DSC decomposition run; [2)] main melting point from several.

Here again, due to the unchanged C_2-amide 'tail', the efficiency is influenced significantly by the substitution pattern of the aromatic 'wings'. Functionalization towards more apolar derivatives resulted in higher nucleation efficiencies and better optical properties. Nevertheless, the best results have been found at high additive concentrations.

Detailed investigations on compound 8.2h

The structure **8.2h** was selected as the lead candidate of the current subset, due to the good haze results. Therefore, it was investigated in more depth. Figure 5-11 comprises concentration dependent illustrations of the peak crystallization temperature and of the optical properties.

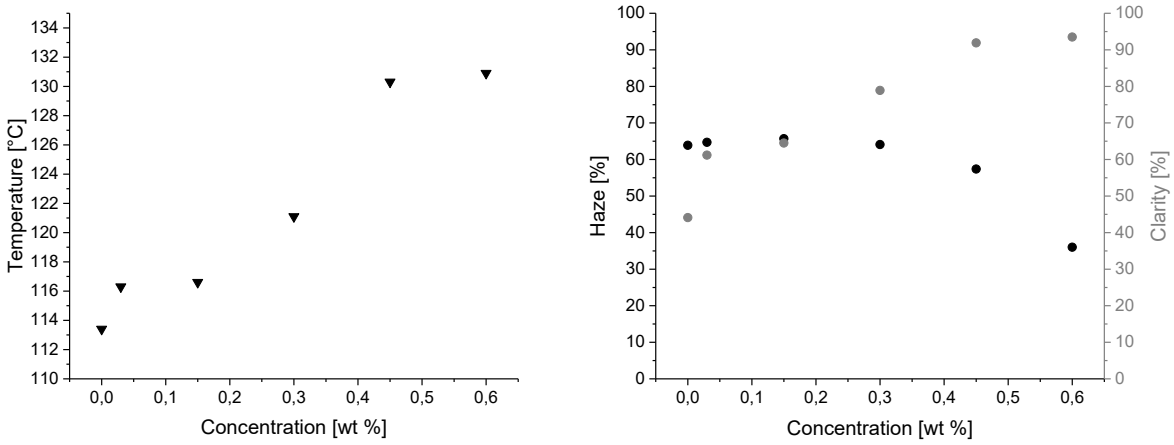

Figure 5-11 crystallization temperature ($T_{c,p}$ ▼) and values for haze (•) and clarity (•) in relation to additive concentration in iPP for compound **8.2h**.

The optical properties of these compounds are significantly influenced at relatively high concentration levels, whereas the crystallization temperature indicates an earlier change. Below an additive concentration of 0.45 wt% only a moderate, stepwise increase of the crystallization temperature can be observed, reaching an intermediate level of around 121 °C. Exceeding this threshold the crystallization temperature suddenly increases and reaches a plateau above 130 °C. The value of haze responds not before exceeding this threshold concentration of 0.45 wt. In contrast, clarity increases constantly in accordance with the observed crystallization temperature and reaches values of 93.5 % at 0.60 wt%.

Conclusion and impact of substitution pattern of 'wings' with C_2-amide 'tail'

All three additives of the current set were found to clarify iPP at concentration levels exceeding 0.45 wt%. The results reveal that different substitution patterns have a major influence on the additives efficiency to increase the crystallization temperature and improve the optical properties. Nucleation is not inhibited by insertion of an ethyl chain at the terminal amide moiety. The derivative, which is bearing propyl substituents on the benzylidene 'wings' even induced drastically increased crystallization temperatures. It is likely that the solubility of the additives is increased by both structural changes, as the additive becomes more apolar. Due to the efficiency increase at higher concentrations, it can be suggested that aggregation and surface formation requires a specific concentration level [84, 112, 113]. The results of dissolution and crystallization experiments of these additives are presented in chapter 6.

5.4. Discussion and conclusion on the new 'library' of nucleating and clarifying agents

A class of novel nucleating and clarifying agents for isotactic polypropylene has been successfully identified. The screening results of this new class, the identification process, as well as the synthesis pathway, have been presented in this chapter. The possibility to combine different functionalities by choosing different 'wings' and 'tails' enables the design of molecules with desired properties and different efficiencies on crystallization temperature and optical properties. In the following, the main results of the screening process are summarized.

Correlation between crystallization temperature and optical properties

The developed additives cover a large range of induced crystallization temperatures, but not all have been found to improve PPs optical properties. The scattering of light in polypropylene is mainly caused by the lamellae in the space-filling spherulitic structures and the intensity is dependent on the total spherulite size [117–121]. Consequently, several attempts to improve the optical properties of iPP have aimed at decreasing the overall size or disturbing the order within the spherulites. It is often claimed that good optical properties result from high crystallization temperatures and reduced spherulite sizes [37]. Although there are commonly no clear correlations between these two parameters, in Figure 5-12 they have been plotted against each other for two concentrations of all new additives [112, 122].

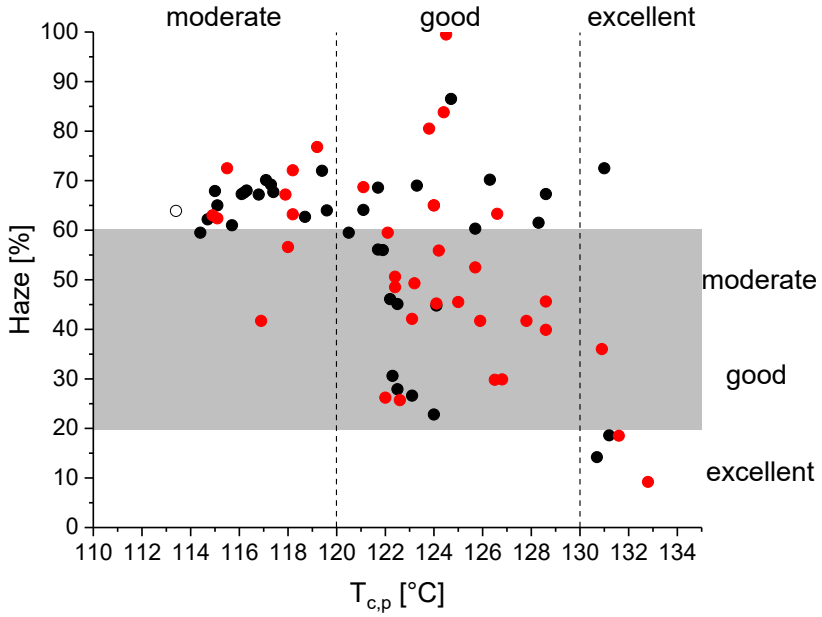

Figure 5-12 Crystallization temperature vs. value of haze for all tested compounds at two concentrations (○ control sample, • 0.30 wt% and • 0.60 wt%. **DMDBS** and **TBPMN** are shown in lighter shade.

As expected, the values were found to be widely spread over the chart and no sound correlation was found. To facilitate reading, the diagram is divided arbitrary into three areas each, indicating moderate to excellent nucleation and clarification. The majority of the new additives show moderate to good nucleating properties and the additives providing moderate to good optical properties act at high loading levels. The results emphasize that the different introduced functional moieties of the additives are of crucial significance in the nucleating and clarifying process.

By narrowing the number of additives and by comparing them setwise as shown in Figure 5-13, it is possible to draw a general trend on the sets' efficiency to clarify iPP.

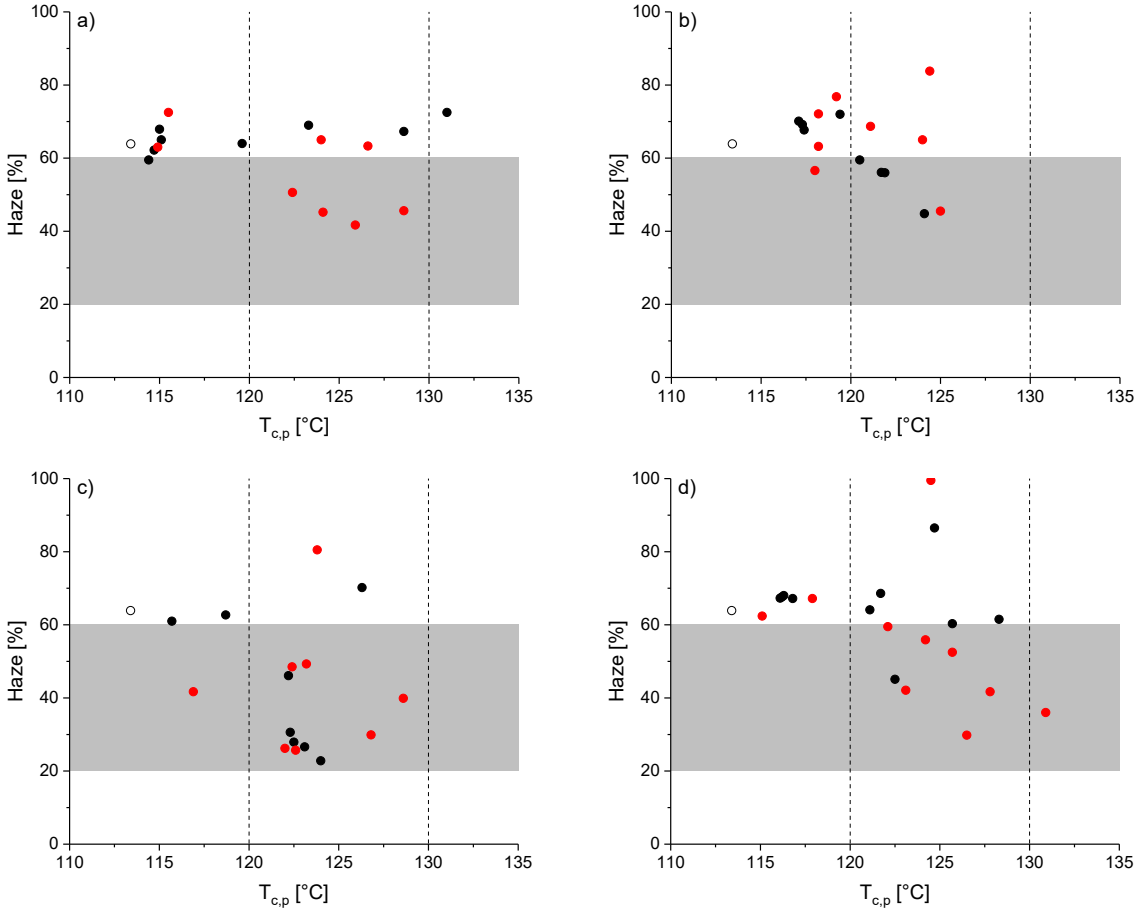

Figure 5-13 Crystallization temperature vs. value of haze for compounds containing the additives of set a) **5**, b) **6**, c) **7** and d) **8**. Concentration: ○ control, • 0.30 wt% and • 0.60 wt%.

The primary amide derivatives (**7**) deliver the best optical properties and the acid derivatives (**6**) are predominant nucleating agents. Additionally, it can be seen that most of the additives (**5** and **8**) become effective at higher concentrations. Figure 5-14 illustrates the trend resulting from the introduced terminal functional groups.

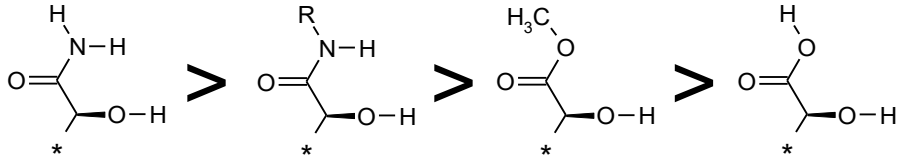

Figure 5-14 Clarifying efficiencies of functional moieties and total number of nucleating / clarifying additives.

In addition, the alkyl chain length of the DBGA-*n* (**8**) derivatives influence the additives efficiency as well. In certain cases, specific derivatives show an improvement of the optical properties with a decreasing alkyl chain length. However, the positive effect depends on the substitution pattern of the benzylidene 'wings'. For example, 4-propylbenzylidene derivatives revealed that the primary amide performs best, followed by the secondary methyl amide and the secondary ethyl amide derivative (Figure 5-15). The haze values at the highest applied concentration (0.60 wt%) showed the following tendency for the three mentioned additives (26.2 % < 29.8 % < 36.0 %).

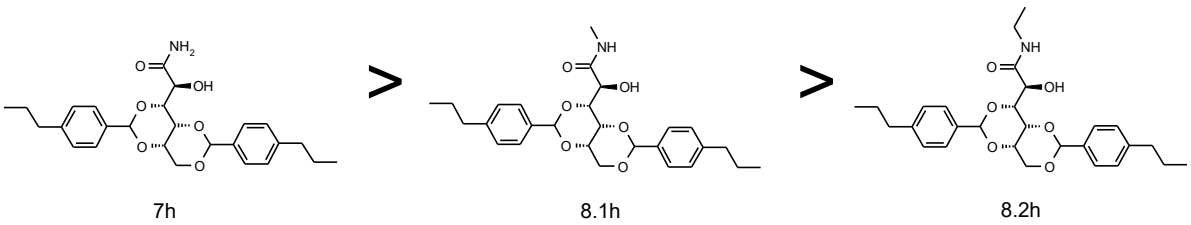

7h > 8.1h > 8.2h

Figure 5-15 Clarifying efficiencies induced by the additives **7h**, **8.1h** and **8.2h**. Arrows indicate increasing haze values.

Unexpectedly, nucleation is induced to a certain extent by secondary amide derivatives with longer chain lengths and methyl ester derivatives as well. The hydrogen bonding ability of the molecules to form intermolecular hydrogen bonds is strongly influenced, hindered or even prevented by modifications on the primary amide moiety. Consequently, this suggests that π-π interactions are more important than assumed or that even no aggregation is needed to nucleate iPP. In any case, the stacking geometries and stacking distances resulting from the different 'tails' influence the molecules ability to nucleate iPP by 'lattice matching' [63].

Influence of modifications on the benzylidene 'wings' by variation of the substitution pattern on the nucleation and clarification efficiency

Besides the influence of the terminal functional groups, the nucleating and clarifying performance of the additives depends strictly on the substitution patterns of the benzylidene 'wings'. Attempts to narrow the number of additives by comparing sets of the same substitution pattern do not reveal appropriate relations between the substituents and the resulting performance. Figure 5-16 demonstrates this, as an example, for 3,4-dimethylbenzylidene and 4-propylbenzylidene substituted derivatives. The diagrams emphasize that no general behavior can be assigned to a specific substitution pattern or to specific combinations. This again confirms that the overall efficiency is defined by the 'tail', the substitution pattern significantly influences the final performance.

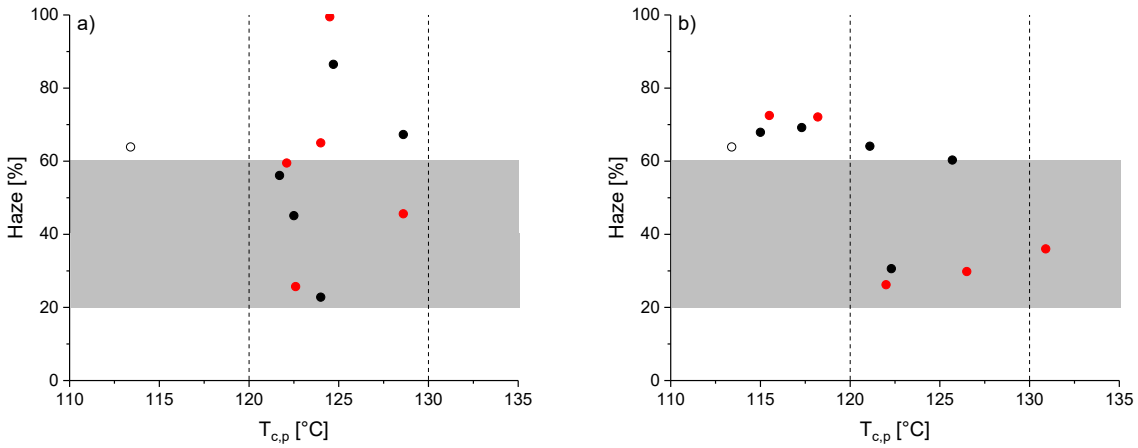

Figure 5-16 Crystallization temperature vs. value of haze for compounds containing a) 3,4-dimethylbenzylidene and b) 4-propylbenzylidene substituted additive derivatives. Concentration: ○ control, • 0.30 wt% and • 0.60 wt%.

Influence of the overall molecule solubility on the nucleation and clarification efficiency

In several cases, increased crystallization temperatures and improved optical properties were observed at higher concentration levels. It is likely that these derivatives exhibit a high solubility. The solubility of the molecules is heavily influenced by the overall chemical structure and thus by the modifications on the 'wings' and 'tail'. In general, one would expect a very small solubility for these molecules in PP, because intermolecular interactions with each other are preferred to interactions with the polymer [113]. As a result, molecules becoming more apolar by their substituents can be expected to exhibit a higher solubility in the apolar polypropylene.

Influence of the overall molecular structure on the nucleation and clarification efficiency

The results confirm the common findings that there is a lack of a correlation between clarifying and nucleating ability [112, 113, 122]. Elevated crystallization temperatures and reduced spherulite sizes do not necessarily imply improved optical properties. However, it is demonstrated that the individual chemical structure of the additive is crucial. The additives performance is influenced by little modifications on the 'wings' and on the 'tail', but the total efficiency is the result of a combination of both. Earlier research revealed that rather the nucleation density correlates with the improved optical properties [112]. Improved optical properties only occur if the additives are capable to provide a nanofibrillar network with ultra-high density of nucleation sites [72, 78, 112, 113]. Unfortunately, detailed aspects between the formed additive superstructures, the induced changes in the polymer solid-state structure and the clarifying effect are still largely unknown. Therefore, the following sections may provide additional insights to reveal the underlying mechanism of the different additive sets.

6. Detailed studies on the nucleation and/or clarification behavior of dibenzylidene-*L*-gulonic acid derivatives

There is still not a clear understanding of how and why clarifying agents work, and what morphological changes in the polymer give rise to an increased transparency. In order to gain a deeper understanding of the structure-property relationship of the new additive class, it is necessary to compare the different subclasses with each other. The main focus was put on 3,4-dimethylbenzylidene and 4-propylbenzylidene substituted derivatives, but in some cases it has been necessary to include further derivatives. The main part of this section covers the melting and dissolution behavior of the additives as well as morphological investigations on the nucleated and/or clarified isotactic polypropylene.

6.1. Investigations on the crystal modification of injection-molded iPP plaques

Wide-angle X-ray scattering (WAXS) experiments were applied to determine the crystal phase modification induced by the various new additives. Measurements have been conducted on 1.0 mm thick iPP plaques. The k-value is calculated according to standard procedures as described in the literature [22]. This value represents the β-phase content. Typical α-nucleating and clarifying agents exhibit k-values below 0.10, this means that the β-phase is present below 10 %. The measurements revealed as expected, that the 'control' sample and the commercial clarifying agents only induce the α-polymorph [45]. In addition, the new additives from all four sets (**5**, **6**, **7**, and **8**) induce the α-polymorph predominantly. Therefore, the selected samples presented in Figure 6-1 exhibit reflections only of the α-phase and thus have k-values below 0.10. A detailed list of the measured k-values for all compounds can be found in the appendix.

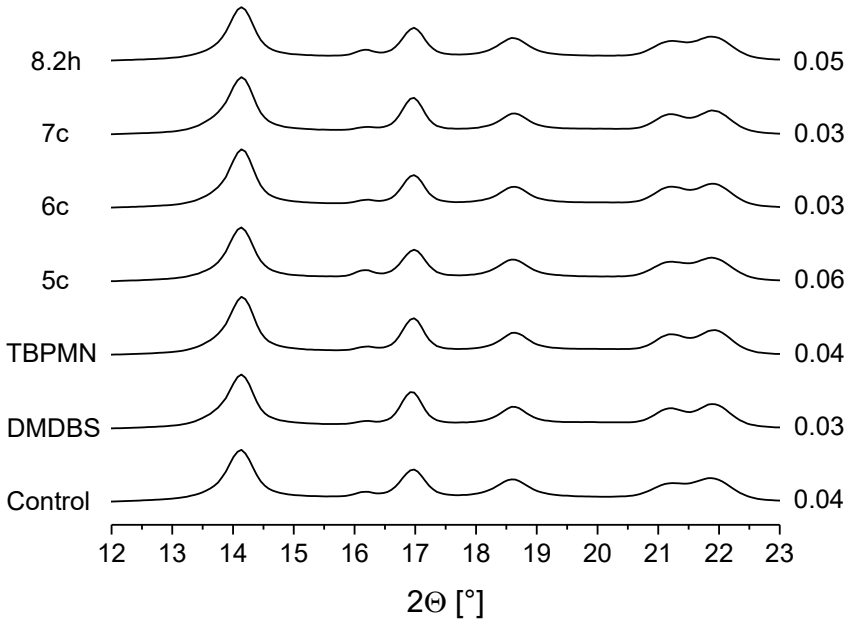

Figure 6-1 Wide angle X-ray diffractograms of 1.0 mm injection-molded samples containing different amounts of the selected additive (left) and the respective k-value (right).

The only exception has been found for additive **8.1c**, which shows a slightly increased k-value of 0.18 at a concentration of 0.30 wt%. This indicates that the sample contains both crystal forms, but still the α-phase is the predominant one. As reported in the previous chapter, it was not possible to detect the β-content in the DSC experiments. Having a second glance on the optical properties of samples containing additive **8.1c** (Table 5-8), the obtained values absolutely fit to these new observations. The formation of both crystal phases leads to increased light scattering, due to differences in birefringence and refractive index between the two polymorphs [27, 30]. As shown in Figure 6-2, the k-value increases up to a value of 0.30 with increasing additive concentration.

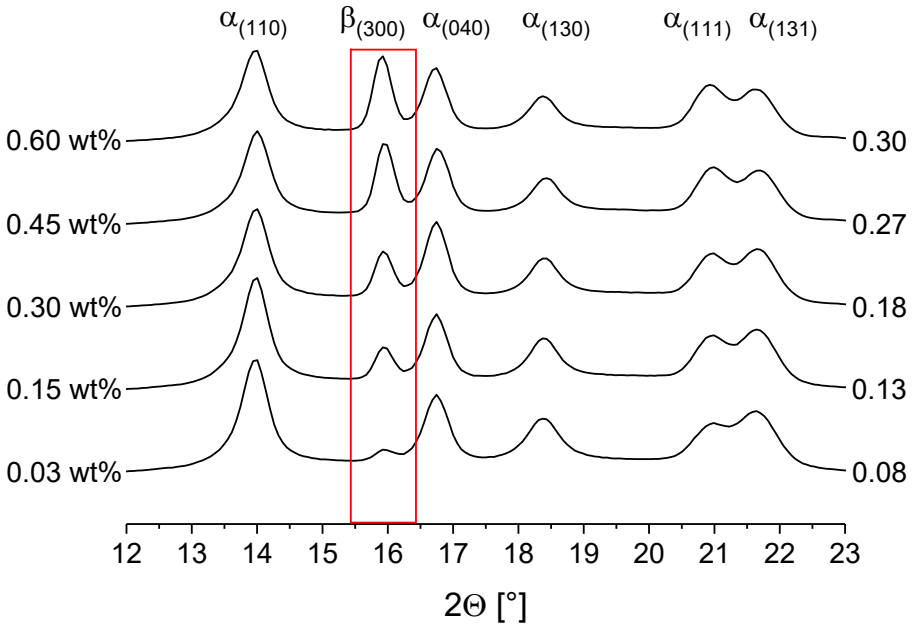

Figure 6-2 Wide angle X-ray diffractograms of 1.0 mm injection-molded samples containing different amounts of additive **8.1c** (left) and the respective k-value (right).

In addition to typical α-nucleating and clarifying agents, additive **8.1c** has been found to be a 'hybrid' nucleating agent, inducing a mixture of both polymorphs (α and β). This in turn is a highly unexpected development. Until now, only a limited number of nucleating agents which preferentially nucleate the beta crystal phase of iPP are known [30]. Moreover, to our knowledge, it is the first time that a dibenzylidene acetal based nucleating agent induces the β-phase. A further advantage of this new nucleating agent could be a potentially better solubility compared to common β-inducing nucleating agents. These are often not soluble in the polymer melt and thus are difficult to disperse [123–125]. The following experiments give rise on the dissolution behavior of additive **8.1c**.

6.2. Investigations on the solubility and dissolution ability of the additives in iPP and on the overall phase behavior of compounds by polarized optical microscopy and rheology experiments

It is well known, that the sorbitol based derivatives **DMDBS** and **TBPMN** are designed to dissolve and recrystallize in the molten polymer, enabling the formation of a finely dispersed, large surface, fibrillar network [60, 61]. Moreover, it was shown earlier that the nucleating and clarifying abilities are strongly dependent on the additive concentration. This is the result of a underlying phase behavior of the binary iPP/additive system and of its solidification kinetics [72, 126]. The fibrillar network formation of sorbitol derivatives in polymer melts was investigated by rheological studies and the phase behavior by optical microscopy studies on a heating stage [60, 72, 77]. These investigations enabled to readily understand the concentration dependence of the nucleating and clarifying effect of the sorbitol class [72].

The newly synthesized additives aimed to have similar structural features and properties as the sorbitol derivatives. Thus studying these parameters with described techniques enables to better understand the underlying mode of action of the novel additives. Therefore, initial investigations on the phase behavior of selected mixtures are presented and attempts to establish relationships with regard to the resulting optical properties are made.

Selected species of all four sets with different 'tails' have been chosen as model compounds in order to better understand the differences in their performance. Therefore, temperature dependent optical microscopy was applied and the melting and in addition the crystallization temperatures of the initial obtained DSC results have been used. To study the melting, dissolution and recrystallization temperature of the newly synthesized additives, a known method has been adapted [127]. For this purpose a compression-molded iPP film was placed on a microscope slide and a small amount of the additive was positioned in the middle of the film. Subsequent heating and cooling experiments on a hot stage, showed the melting, dissolution and recrystallization process of the additive. This experimental setup somehow covers the concentration regimes I-III of the phase diagram presented in chapter 1, Figure 1-20 [72]. In the case, superstructures are formed by the additives the complex viscosity of the mixtures increases. Thus rheological studies help to support these findings. Therefore, selected species (**5c**, **5h**, **6c**, **6d**, **6h**, **7c**, **7h** and **8**) are discussed setwise at first. Afterwards salient differences between the systems are discussed separately.

Dissolution and crystallization behavior of DBGAcMeE derivative 5c

Figure 6-3 contains optical micrographs of an iPP/**5c** mixture, taken at different temperatures on a hot stage. The investigations revealed that the additive slowly dissolves and diffuses into the polymer matrix. At 240 °C the additive is completely molten and liquid-liquid phase separation can be observed in high concentrated regions. Upon cooling the phase-separated liquid recrystallizes at around 205 °C. In less concentrated regions, fibrillar structures develop at around 195 °C. In the less concentrated homogenous one-phase liquid regions the fibrillar structures are of finer size, which can be seen in the picture taken at 145 °C. The formed surface induces nucleation, at around 128 °C, in accordance with earlier DSC experiments. Nucleation is only observed within the 'diffusion zone' of the additive. Outside of this area, large spherulites

develop [72]. Repeated heating reveals the dissolution of the fibrillar structures by disappearance of the birefringence structures, between 215 and 230 °C. In lower concentration regimes the network dissolution starts earlier.

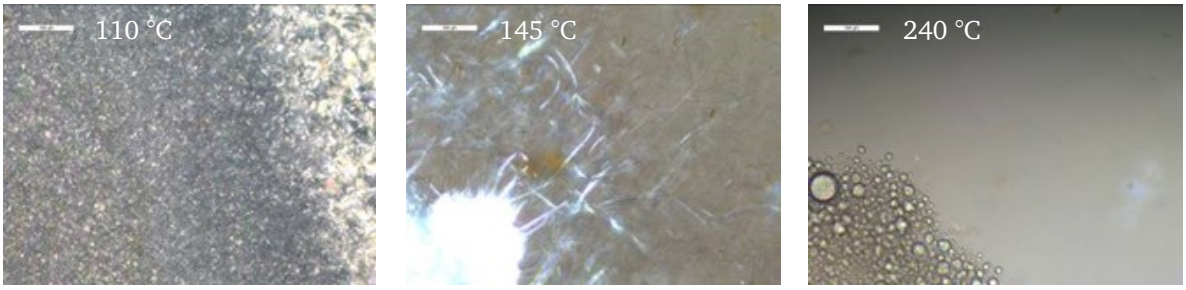

Figure 6-3 Polarized optical micrographs of additive **5c** at different temperatures and different positions of the sample. Scale bar 100 µm.

In addition, Figure 6-4 (red) shows the complex viscosity as a function of temperature, recorded during cooling from the melt, for samples containing different concentrations of additive **5c**. Here, the formation of the fibrillar structures can be followed by a relatively small, but distinct increase in viscosity prior to nucleation and subsequent crystallization of the polymer. At low additive concentrations, in the concentration range between 0.03 and 0.45 wt%, the complex viscosity increases gradually with decreasing temperature to the onset of crystallization. This shape is comparable to that of the 'control' sample, but with another crystallization onset. At higher concentration levels (0.60 wt%) a shoulder formation can be observed, which can be assigned to the formation of the fibrillar network [60, 72]. The onset of network formation increases with increasing additive concentration [60]. This finding is in accordance with the observations made in the hot stage experiment, where presumably higher concentrations have been studied. Additionally, the onset of crystallization can be observed by a final sharp increase in complex viscosity. The higher onset and endset temperature compared to DSC results is due to a lower cooling rate and shearing.

Dissolution and crystallization behavior of DBGAcMeE derivative 5h

Similar investigations have been made for compounds containing additive **5h**. In this case, the complex viscosity did not reveal a network development by the additive (Figure 6-4, blue). In contrast, the heating stage experiment delivered a completely different observation (Figure 6-5). At around 190 °C dissolution of the additive starts and at around 205 °C phase separation is observed. Recrystallization of the additive can be observed at around 160 °C, whereas earlier DSC experiments delivered a recrystallization temperature of 180 °C for the pure additive. A network formation in form of coarse fibrils is only observed around the additive center below a temperature of 160 °C. In the lower concentrated regions the network could not be detected. However, for unknown reasons it has not been possible to confirm the network development by rheological studies. Though, this is consistent with the initial findings that only little nucleation and no clarification is induced by this additive derivative (cf. Table 5-4). Oddly enough the heating stage experiment revealed nucleation at around 120 °C, at an identical heating rate of 10 °C/min, as applied in the DSC experiment.

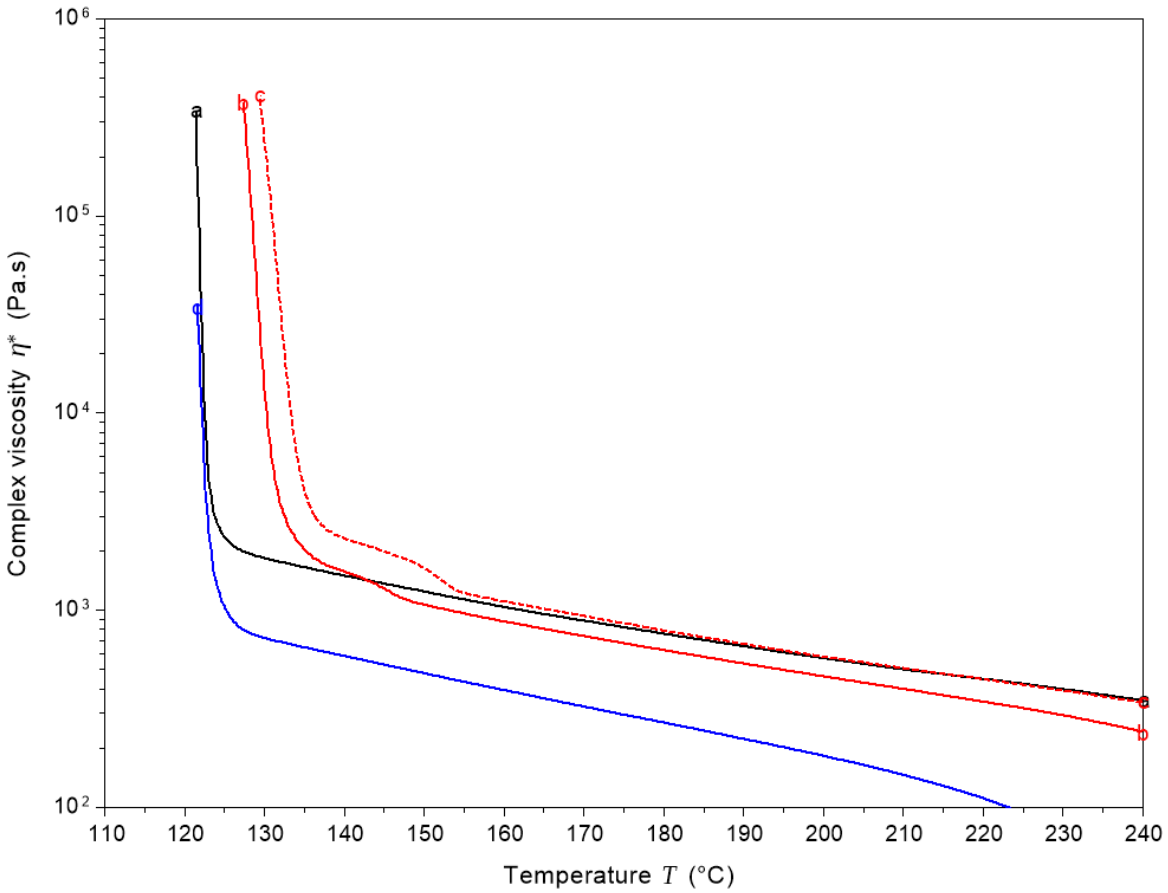

Figure 6-4 Complex viscosity as a function of temperature upon cooling at 2 °C/min of compounds containing additive **5c** (red) and **5h** (blue). Concentration: a) Control, b) 0.60 wt% and c) 0.75 wt%.

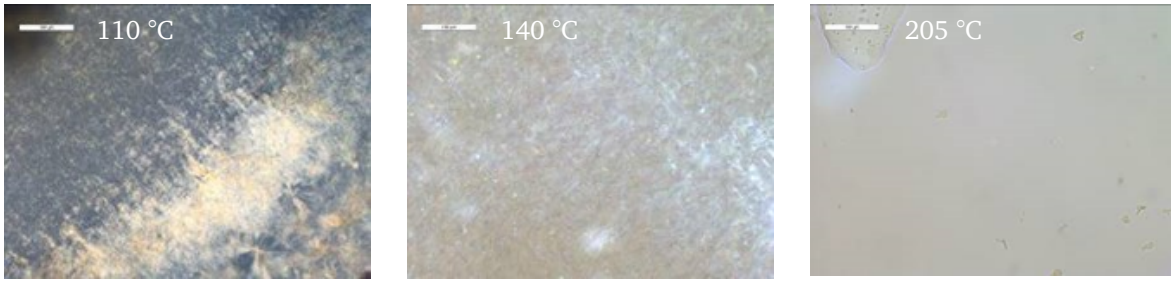

Figure 6-5 Polarized optical micrographs of additive **5h** at different temperatures and different positions of the sample. Scale bar 100 µm.

Conclusion with regard to additive 5c and 5h

Both additives dissolve in iPP, but show different solubility. Even liquid-liquid phase separation occurs at different temperatures. Recrystallization upon cooling in form of fine fibrillar networks has been observed for both derivatives, but however for additive **5h** only in high concentrated regions. In the case of additive **5c**, the developed network provides a surface for crystallization of the polymer and induces its nucleation. The fact, that nucleation by additive **5h** was observed only in the high concentrated additive center suggests that the necessary threshold for a sufficient network formation has not been reached up to a concentration of

0.60 wt%. That might explain, why no network formation was observed on the basis of rheological studies.

Dissolution and crystallization behavior of DMBGAc derivatives 6c, 6d and 6h

Figure 6-6 contains the development of the complex viscosity for three compounds (**6c**, **6d** and **6h**) with a loading level of 0.60 wt%. Based on the low 5 % weight loss temperatures of this set, it is likely that the additives are very vulnerable to heat. For this reason, the maximum applied temperature in the experiments was chosen below the decomposition temperature of the relevant additive. As found in the previous chapter, additive **6d** was the only derivative improving the optical properties to a certain extent and therefore only exemplary micrographs of this mixture are presented in Figure 6-7.

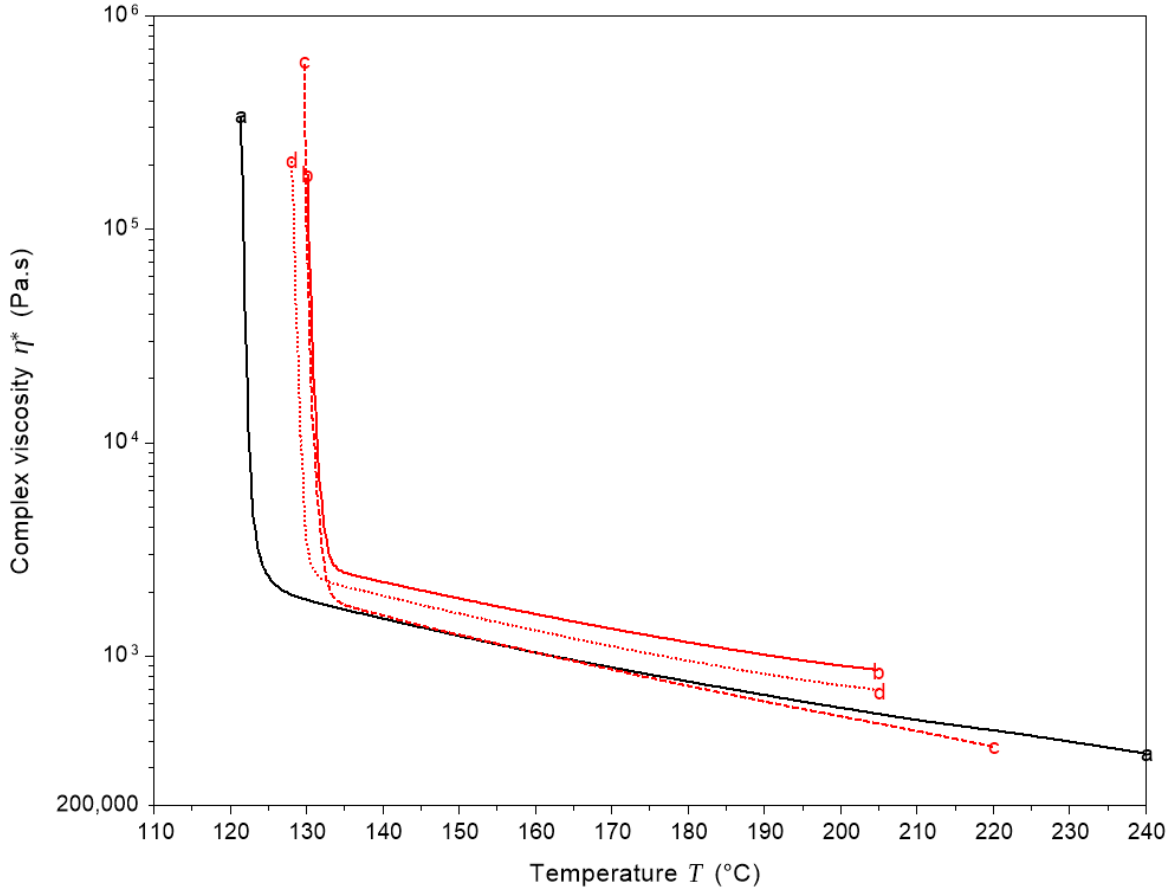

Figure 6-6 Complex viscosity as a function of temperature upon cooling at 2 °C/min of a) 'control' sample and compounds containing 0.60 wt% of additive b) **6c**, c) **6d** and d) **6h**.

The curve shapes of the complex viscosity reveal that all three additives do not form a network upon cooling of the polymer melt. This suggests the additives to act in a different way, which can be proven by the micrographs presented in Figure 6-7. Additive **6d** does not dissolve upon heating and only a few additive particles diffused out of the core region. Upon cooling, no network formation occurred and nucleation started at around 120 °C in regions, where additive particles have been present. Consequently nucleation only occurs on the particles surface. The micrograph at 115 °C shows that nucleation occurs, but subsequently the nucleated melt has been observed to be overgrown by the surrounding non-nucleated melt. The higher

crystallization temperature of 125 °C observed in DSC experiments can be explained by a better particle distribution as a result of shear forces during compounding. By this, the resulting surface is larger and the little improved haze values can be traced back to a slight reduction in spherulite size.

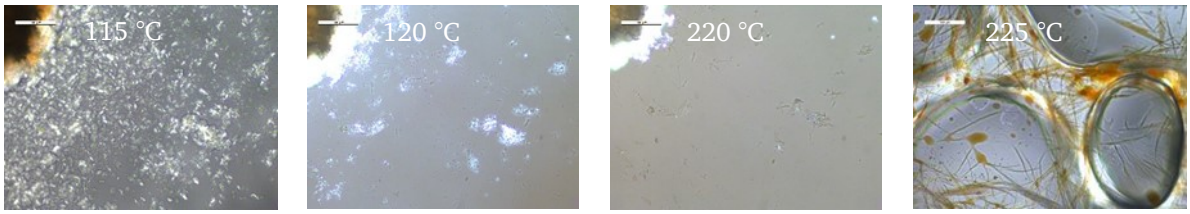

Figure 6-7 Polarized optical micrographs of additive **6c** at different temperatures and different positions of the sample. Scale bar 100 µm.

For the additives **6c** and **6h** comparable behaviors have been determined, but due to their lower $T_{-5\ wt\%}$ the experiments have been studied at a temperature of 200 °C. In both cases no melting of the additives has been observed. The bulk of needles stayed as they have been incorporated into the polymer. Upon cooling, nucleation was observed at expected temperatures, but only in regions where additive particles have been present. However, the nucleated areas have been quickly overgrown by non-nucleated polymer melt.

Heating the mixtures slightly above the respective $T_{-5\ wt\%}$ of the additive caused its decomposition, as indicated by browning of the needles and even droplet formation and subsequent phase separation. This is exemplary shown in Figure 6-7 for derivative **6c**. Most probably the decomposition process results in acetal cleavage [55, 110]. However, some of the particles withstand these temperatures for a certain time. Based on these results, it seems reasonable that some of the additives do not survive the harsh processing conditions at 220 °C, as described in the previous chapter.

Conclusion with regard to studied derivatives of set 6

The experiments demonstrated that nucleation of the DBGAc (**6**) set of additives is not induced by the formation of a fibrillar network, but rather by the surface of the additive particles. The fact that only additive **6d** has been found to improve iPPs optical properties moderately, can be explained by the additives slightly higher $T_{-5\ wt\%}$ of 236 °C. Compared to the 5 % weight loss temperatures of the other additives, the one of additive **6d** is above the applied compounding temperature of 220 °C. Therefore, it is likely that the other derivatives do not withstand the processing step completely. Parts of the additive particles survive higher temperatures for a certain time. This explains why the compounded mixtures (Table 5-5) still showed an increase in crystallization temperature after processing at 220 °C and even after deletion of the 'thermal history' at 230 °C in the DSC experiment. Nevertheless, the marginal increased yellowness indices (YI) with values above 3.50 at a concentration level of 0.60 wt% is a first sign that decomposition occurs. If parts of the introduced additive particles decompose they are not available to induce nucleation and consequently the nucleation density is reduced. This supports why only slight nucleation can be observed, but the optical properties are not affected.

Dissolution and crystallization behavior of DBGA derivative 7c

Additive **7c** dissolves upon heating, but the solid state changes prior to dissolution as shown in Figure 6-8. Reaching a temperature of 240 °C the additive bulk still exists, but shrinks over time. At this temperature the additive shows no phase-separation. Upon cooling the additive starts to crystallize briefly below 200 °C in form of a fine fibrillar network, which is hardly to detect. Nucleation is induced by the formed surface at a temperature of around 124 °C. Heating the sample above the earlier detected melting temperature of 261 °C shows that melting subsequently changes into decomposition of the additive. At 285 °C phase separation can be observed in the core region, but unlike the additives of set **5**, in this case the formed droplets show a brown color due to decomposition.

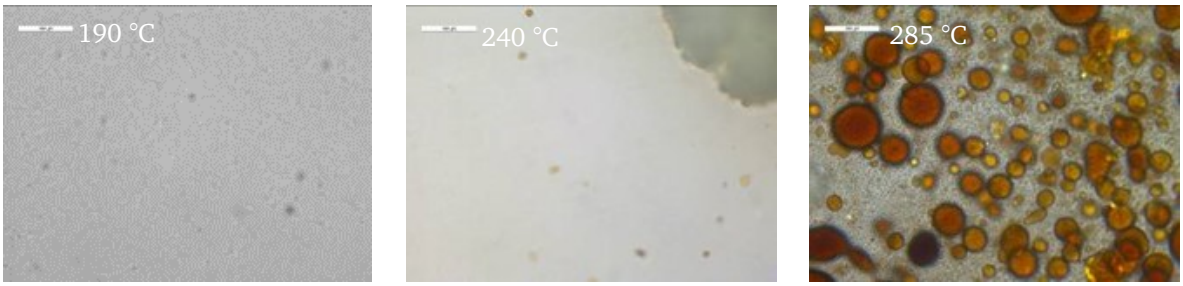

Figure 6-8 Polarized optical micrographs of additive **7c** at different temperatures and different positions of the sample. Scale bar 100 µm.

The network development is confirmed by the rheological experiments, on compounds containing additive **7c**. In this case, a less pronounced shoulder formation can be observed in Figure 6-10 (red).

Dissolution and crystallization behavior of DBGA derivative 7h

Similar investigations on additive **7h** revealed a slightly different behavior. The additive shows liquid-liquid phase separation at around 220 °C in the high concentrated regime (Figure 6-9). This additive does not directly decompose after melting and therefore distinct melting can be observed. The liquid droplets recrystallize at a temperature of 195 °C, which is earlier as expected (T_c of pure additive: 171 °C). A network formation can be just presumed in the micrographs, but with the help of the rheological investigations the network formation can be revealed (Figure 6-10, blue). The provided surface induces nucleation at around 124 °C.

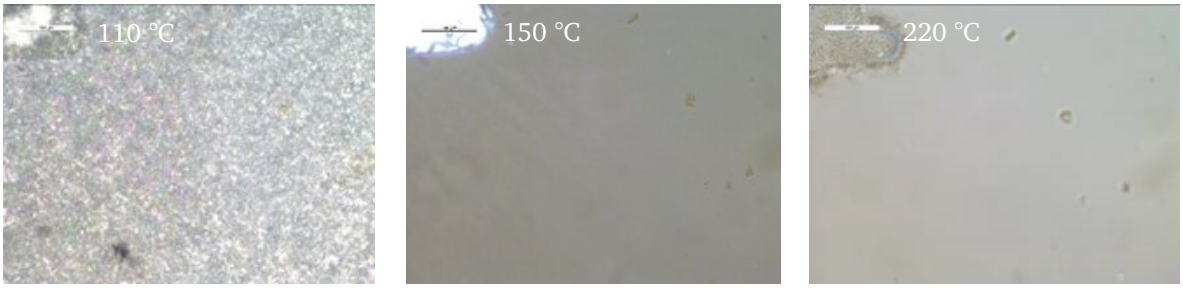

Figure 6-9 Polarized optical micrographs of additive **7h** at different temperatures and different positions of the sample. Scale bar 100 µm.

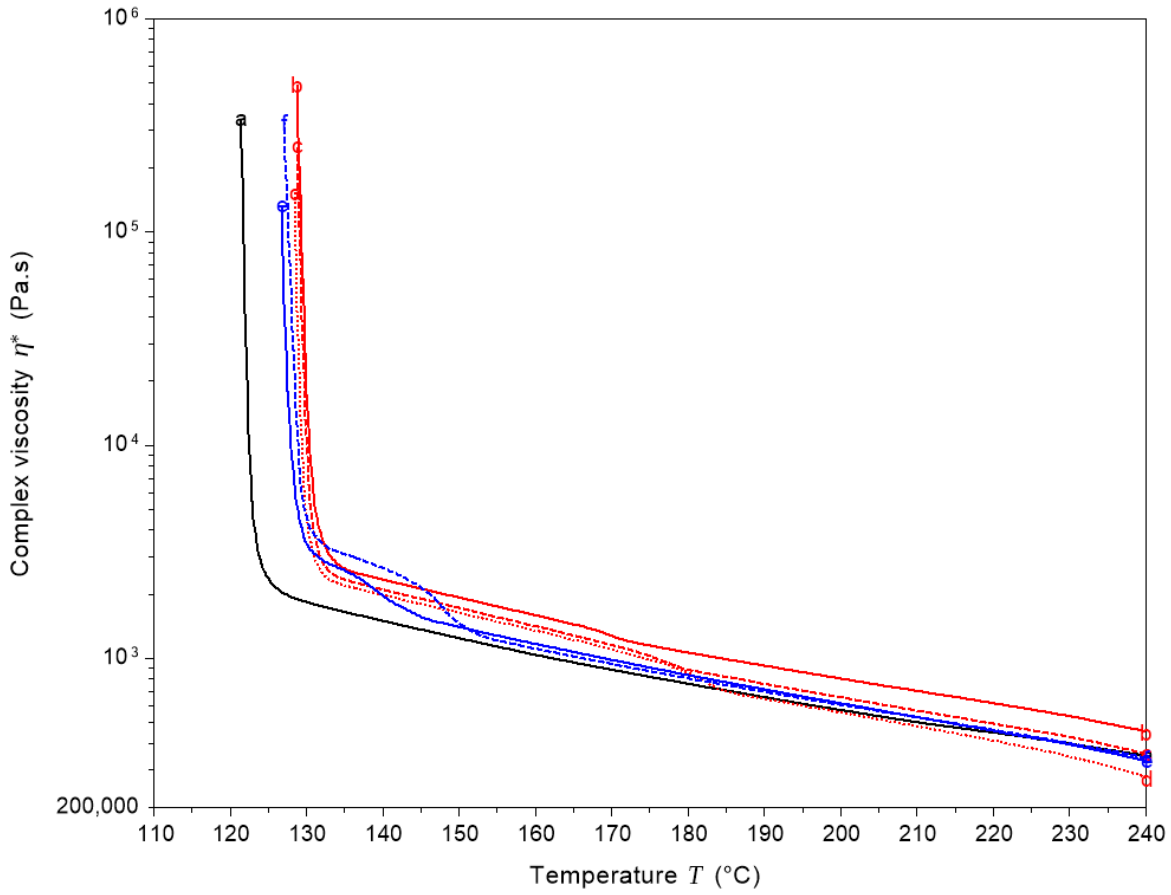

Figure 6-10 Complex viscosity as a function of temperature upon cooling at 2 °C/min of compounds containing additive **7c** (red) and **7h** (blue). Concentration: a) Control, b) 0.30 wt%, c) 0.45 wt%, d) 0.60 wt%, e) 0,45 wt% and f) 0.60 wt%

Conclusion with regard to additives 7c and 7h

The experiments revealed, that both investigated additives are highly soluble in iPP. Additive **7h** even better than additive **7c**, most probably due to the propyl substituents on the benzylidene 'wings'. The additives form fine fibrillar networks upon cooling, which are difficult to determine. Therefore, larger surfaces can be expected, which are provided by these fine networks. The observed fibrils are by orders of magnitude thinner as the ones provided by derivatives of set **5**. This results in an overall higher nucleation density and consequently smaller spherulites. It seems, as if a nearly invisible network, may it be due to the finer structures and/or a higher similarity in refractive index, is necessary to achieve minimum haze values. The finer morphology is likely to be the result of a reduced lateral growth rate of the present additive due to different substituents [77].

Dissolution and crystallization behavior of DBGA-*n* derivatives (8)

The focus of this set was put on the methyl and ethyl amide derivatives, as they showed the most interesting changes with regard to the optical properties. Figure 6-11 illustrates the progression of the complex viscosity of compounds comprising 0.60 wt% of the additives **8.1a** or **8.2a** (red), **8.1c** or **8.2c** (blue) and **8.1h** or **8.2h** (green). Network formation is confirmed

for all compounds containing 0.60 wt% of the respective additive. However, the shoulder shape varies to different degrees.

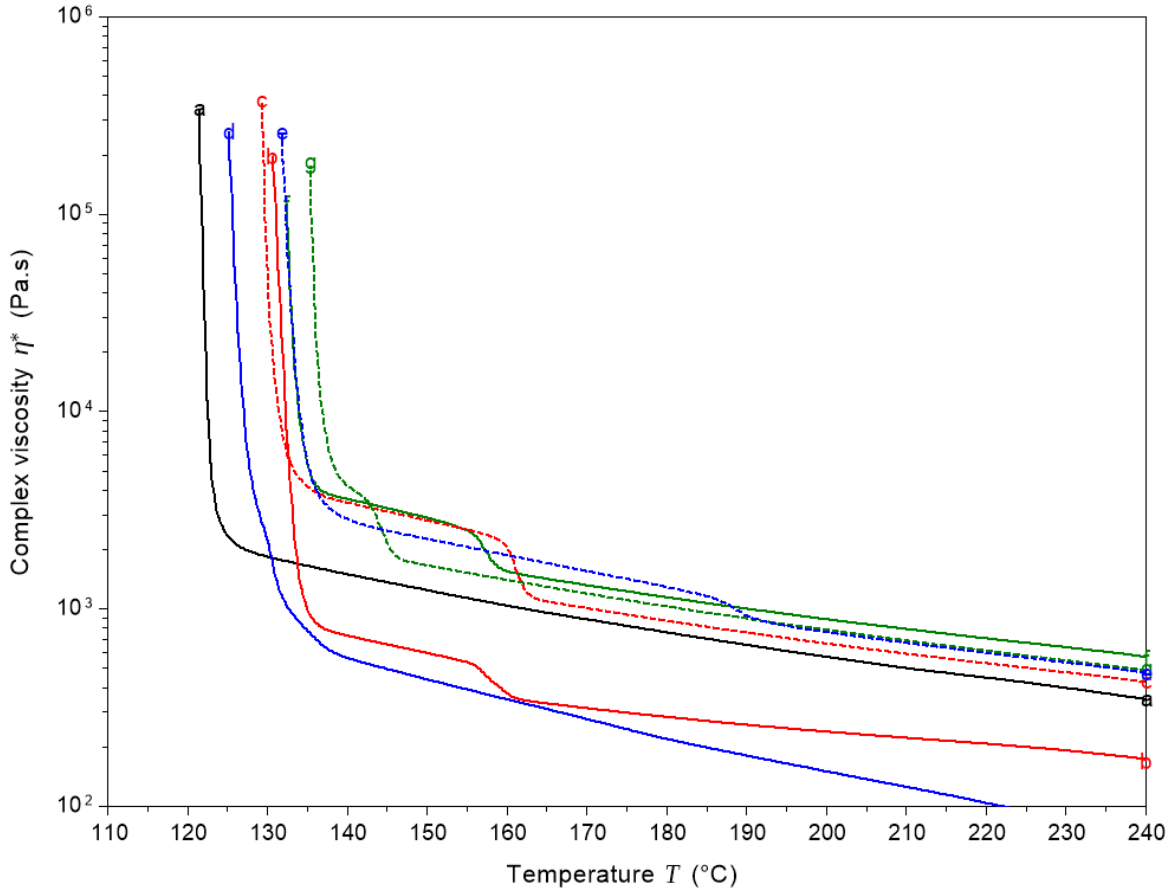

Figure 6-11 Complex viscosity as a function of temperature upon cooling at 2 °C/min of a) 'control' sample and compounds containing 0.60 wt% of additive b) **8.1a**, c) **8.2a**, d) **8.1c**, e) **8.2c**, f) **8.1h** and g) **8.2h**.

The micrographs of the derivatives **8.1a**, **8.2a**, **8.2c**, **8.1h** and **8.2h** are not presented, as the dissolution and recrystallization behavior is nearly identical to the previously discussed derivatives of set **5**. The additive crystals slowly dissolve upon heating and the bulk region shows liquid-liquid phase separation at some point. Subsequent cooling leads to recrystallization and in lower concentrated regions thicker fibrillar networks start to develop. Disappearance of the network, due to dissolution, was observed in the same temperature range. Nucleation is induced by the network at different temperatures, depending on the additive derivative in accordance with earlier DSC results. A reduced spherulite size was only observed in the dissociation zone of the additives. The spherulites in the non-nucleated region were by magnitudes larger.

Dissolution and crystallization behavior of DBGA-*n* derivatives 8.1c

Figure 6-12 shows the micrographs of mixtures containing additive **8.1c**, which has been found to partly induce the β-crystal phase of iPP. The additive slowly dissolves above a temperature of 210 °C, but up to a temperature of 250 °C the fine crystalline needles do not show phase separation. The dissolution process is accelerated with increasing temperature. On the basis of earlier experiments liquid-liquid phase separation is expected at temperatures above 300 °C.

Below a temperature of 170 °C the formation of a network can be perceived, but is hardly visible. In addition, conformation of the network development on the basis of rheological studies, was hardly possible. However, an apparent formed shoulder, directly in front of the onset of nucleation indicates a network formation process (Figure 6-11). With occurrence of nucleation at around 125 °C the very fine split up network can be observed in the micrograph.

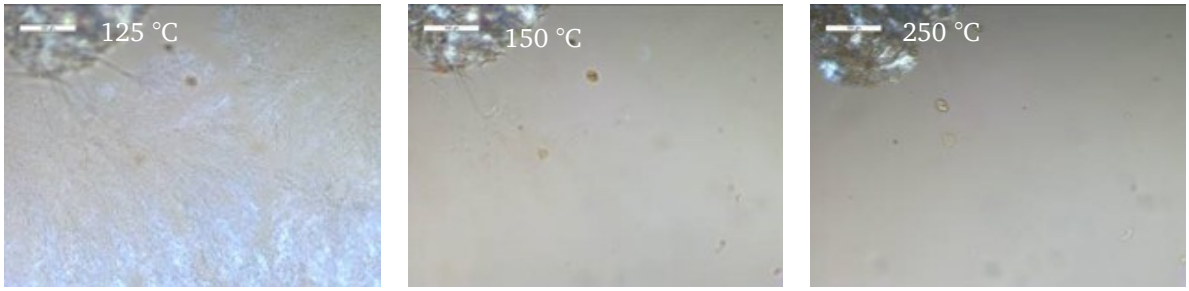

Figure 6-12 Polarized optical micrographs of additive **8.1c** at different temperatures and different positions of the sample. Scale bar 100 µm.

Conclusion with regard to the studied derivatives of set 8

All additives developed fibrillar structures in the polymer melt and thus provide nucleation surfaces. The shape of the fibrils and the observed shoulders cannot be related to characteristic properties, but most probably, the coarser structures are triggered by the induced alkyl chains on the 'tail'. The discussed additives are soluble in iPP, but it turned out that the degree of solubility depends on the overall chemical structure. Different dissociation distances around the additive core in the microscopic experimental setup supported this finding. However, this observation might be a result of different applied additive amounts. The fact that the maximal applied temperature in the rheological experiment (240 °C) and in the compounding step (220 °C) was below the additives melting temperatures suggests that melting is not strictly necessary. Unexpectedly, the additives revealed lower crystallization temperatures when incorporated in the polypropylene matrix compared to its pure form.

Additive **8.1c** revealed the formation of a very fine fibrillar network and unexpectedly a relatively good solubility in iPP, although the sample preparation for NMR measurements pointed out substantial problems to find an appropriate solvent. The main concern, why especially this additive is inducing the β-phase cannot be resolved by observations of its dissolution and crystallization behavior in the polymer melt. It is likely that in this case lattice matching plays a decisive role.

Comparison against state of the art sorbitol derivatives

Figure 6-13 compares rheological measurements of the sorbitol based clarifying agents **DMDBS** and **TBPMN** with the new developed additives **7c**, **7h**, **8.1h** and **8.2h**. For all additives, a network formation is observed and confirmed by the rheological results. However, contrary to literature, the sensitivity of the measurement only allowed to uncover the network formation of the commercial additive **DMDBS** starting at a concentration of 0.30 wt% [72].

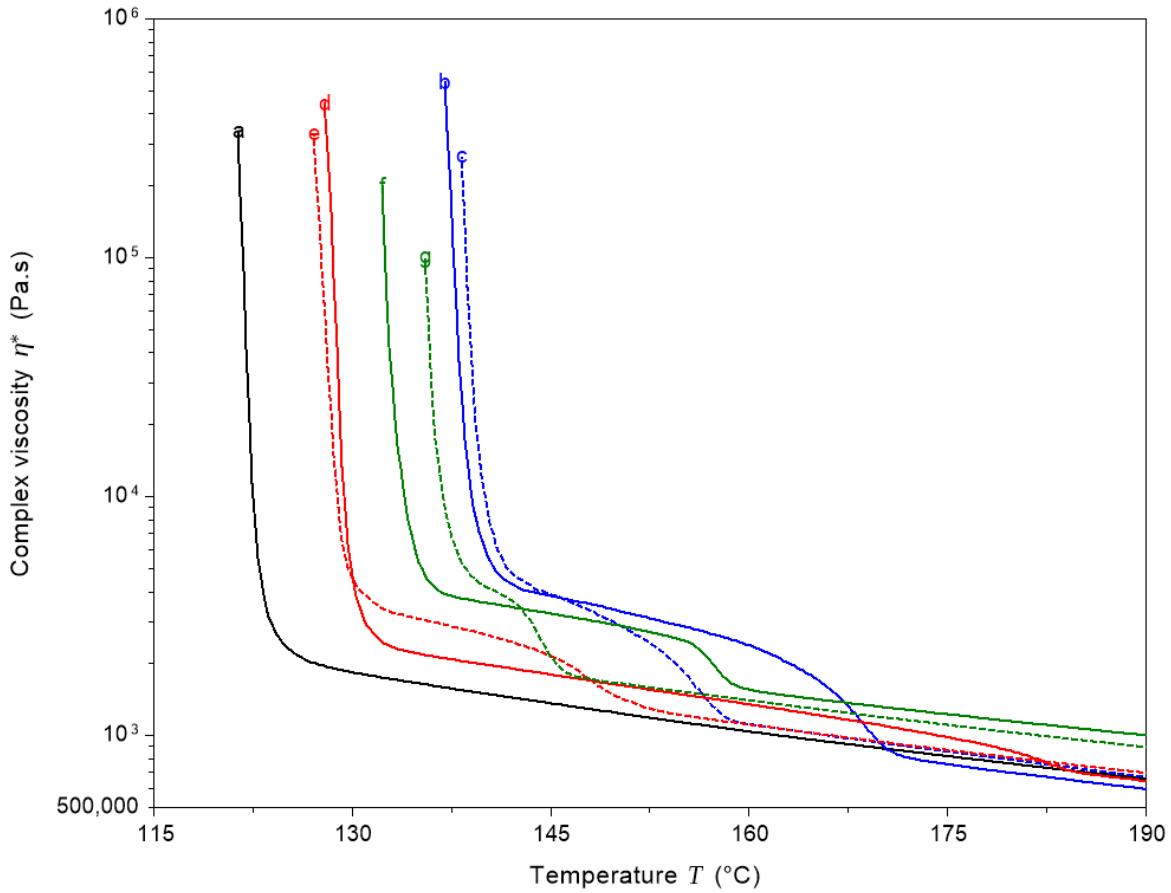

Figure 6-13 Complex viscosity as a function of temperature upon cooling at 2 °C/min of a) 'control' sample and compounds containing 0.60 wt% of additive b) **DMDBS**, c) **TBPMN**, d) **7c**, e) **7h**, f) **8.1h** and g) **8.2h**.

The amplitude (η*) of the formed shoulder is much higher for both sorbitol based clarifying agents and the onset of iPP crystallization starts earlier as well. The latter is well known from previous DSC results. The amplitude height might express the strength of the network. Whereas an earlier onset of sol-gel formation, which can be observed for additive **7c**, might express earlier separation from iPP melt. Both arguments are plausible, but they are simply hypotheses that remain to be further evaluated. It is challenging to link these findings of an earlier onset of network formation or even a greater magnitude of the increase in η* with increasing concentration to a better nucleation and/or clarifying efficiency [60]. Moreover, in the case of **7c** and **DMDBS**, the best optical properties have been found for concentrations at around 0.30 wt%. At these concentrations the network is still not significant detectable in terms of complex viscosity. Consequently, at least the amplitude height can be excluded as a valuable indicator.

In the experimental setup, the iPP/additive mixtures have not been investigated on the hot stage over the whole concentration range. As a result of this, it is unknown at which concentration level liquid-liquid phase separation of the new additives occurs. Nevertheless, determination of the threshold concentration could give rise to more details of the additives compatibility in iPP [77].

Conclusion on dissolution experiments

The investigated sets of additives showed different melting, recrystallization and nucleation behaviors. The results demonstrate, that the magnitude of the fibrils and the resulting surface plays a key role in clarifying iPP. In addition, based on these results, the efficiency of the different novel nucleating and clarifying agents can be roughly explained. First of all, the surface provided by particles is by orders of magnitude smaller than the one provided by a fibrillar network. This results in a lower nucleation density and consequently larger spherulite sizes for particulate nucleated iPP. It explains why haze is only slightly decreased by some of the particulate acting derivatives of set **6**. The particle size and distribution of the additives themselves plays a decisive role in that process. Apart from this the diameter of the formed fibrils, which have been observed for additives of set **5**, **7** and **8** is decisive. Some derivatives showed finer fibrils, as for example the derivatives **7c** and **7h**. Additives of set **8** revealed in initial experiments coarser fibrils, which nevertheless resulted in good optical properties. In general the derivatives, which showed finer nearly invisible fibrillar structures delivered the best optical properties. The fact that some of the networks could be hardly detected expresses that the diameter of these fibrils has to be very small. It can be assumed that the network formation follows a simple approach. First at high temperatures the molten or dissolved molecules are finely dispersed in the polymer matrix. Upon cooling they aggregate to isolated fibrils, which grow with a constant diameter by increasing concentration. In particular at higher concentrations also thicker fibrils can be formed. Changes in the overall chemical structure, such as different substituents, lead to a finer morphology most probably by a reduced lateral growth rate. These results can be evidenced by earlier developments, which showed that DMDBS was a better nucleating agent when it was given less time for its gelation process [128]. This means that the formation of secondary structures, by means of bundles of thicker fibrils, result in a decrease of the surface area which is available for nucleation. Consequently, the formation of fine and nearly invisible networks is a key feature for the additive to act as a highly efficient clarifying agent. The network induces significant nucleation of the polymer, so that large-scale spherulitic structures do not have sufficient volume to develop and therefore leads to reduced scattering of light. This in the end supports that nucleation density is of huge importance. Hence the solubility and the dispersibility of the additives are of paramount importance, it is likely that a homogenously distributed additive provides a more regularly spread surface upon cooling.

In total the results of this section (Chapter 6.2) confirm the initial thoughts on the importance of nucleation density and emphasize the lack of correlation between crystallization temperature and the haze value. Thus once more improved optical properties come along with the capability of the additives to provide a nanofibrillar network with ultra-high density of nucleation sites.

6.3. Polarized optical microscopy studies on the morphology of nucleated and clarified compounds

In the previous subchapter, nucleation density was suggested to play an essential role in improving optical properties [3, 112]. Typically ,an increased nucleus density results in a significant decreased average spherulite size, which usually improves the optical properties. Depending on the nucleation density and the spherulite size induced by the different nucleating agents, iPP samples possess a wide variety of spherulitic textures. For a quick determination of nucleation densities, samples were observed through an optical microscope. The samples have been prepared by mainly two methods. On the one hand compression-molded samples and on the other hand thin-sections have been prepared. With both methods it was possible to compare the obtained textures of the additives. Compression-molded samples gave rise to the relative number of spherulites formed. Fully aware that exceeding a certain size it is difficult to determine differences. However, it has been tried to correlate the textures to the nucleation efficiency (NE) calculated according to literature. Therefore, the efficiency scale established by Fillon et al. [71] has been applied. The NE has been calculated for all new additive/iPP mixtures and can be found in the appendix. The self-nucleation temperature of the polypropylene homopolymer Moplen HP 500 N has been determined according to literature known procedures and accounts for 140.5 °C [129]. For the commercial clarifying agent **DMDBS** an efficiency of 64 % at a concentration of 0.30 wt% has been calculated, which fits pretty well to the 65 % reported in literature [73]. Figure 6-14 exemplarily shows the concentration dependency of the additives and the effect caused by the nucleating additives on the basis of compression-molded samples. Spherulite size drastically decreases with increasing additive content. The control sample shows the typical 'mixed' α-spherulites with no distinct Maltese cross pattern and spherulite sizes of about 60 to 120 μm [111]. With increasing nucleation efficiency, which is calculated from the crystallization temperature, the spherulite size is decreasing and spherulite texture is becoming finer (< 400 nm). Even the threshold concentration can be identified, as the sample containing 0.15 wt% shows a coarser texture. However, a reliable differentiation between samples exceeding a concentration of 0.30 wt% is not possible at this level.

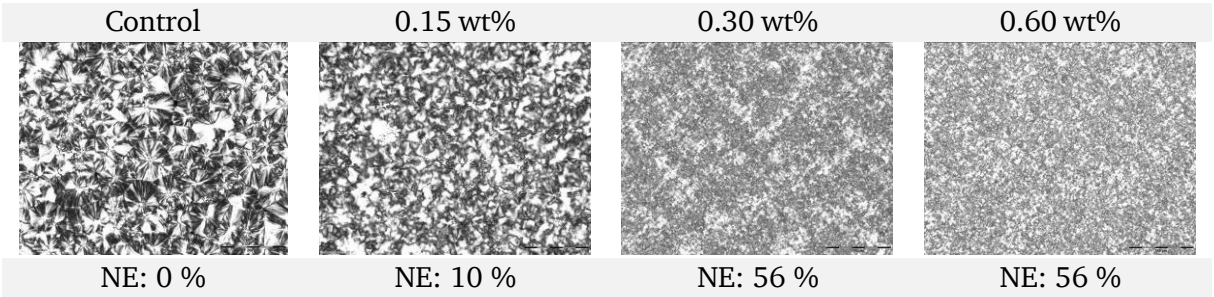

Figure 6-14 Polarized optical micrographs of melt-compression-molded iPP films, containing different amounts of additive **5c**. Scale bar 100 µm.

In general, there are other possibilities to calculate or measure the nucleation density [130–133]. Nevertheless, it is questionable if these methods deliver more reliable results. One of the easiest techniques is the estimation of nucleus density by optical microscopic experiments [134, 135]. Under isothermal conditions, normally it is possible to count the number of nuclei, but the method is imprecise and works only within special temperature ranges. Often the induced

spherulite number is too large to be counted reliably. Another approach is to determine the nucleus density from calorimetric experiments based on kinetic equations [136, 137]. Typically the method of Lamberti is applied [112, 138].

Additionally, using the thin-sections which are taken from injection-molded plaques are worth to be investigated, as the morphology and the spherulites in the final article at least influence the optical properties. The sections have been cut parallel to the flow direction and have been investigated under an optical microscope with crossed polarizers. The micrographs show half of the cross section of the injection-molded parts (Figure 6-15).

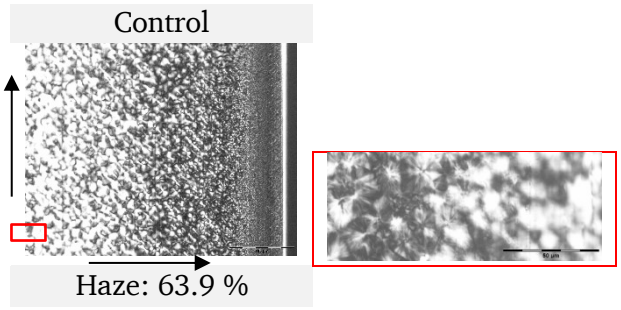

Figure 6-15 Polarized optical micrographs of 10 µm thin-sections of 1.0 mm injection-molded iPP plaques; ↑ indicates cutting direction and → points from middle to outside of the sample. Scale bar 100 µm resp. 50 µm.

In these thin-sections skin–core structures can be observed, which on a finer scale reveal spherulitic structures in the order of 1–50 μm. The spherulites do no look like the typical α-spherulites with a 'mixed' birefringence. They look like α_I-spherulites described by Padden and Keith [111]. They exhibit a positive sign of birefringence with a simple Maltese cross pattern. The bright, often serrated edge on the surface of the skin is assigned to a cutting artifact. The surface shows a highly oriented none spherulitic skin zone in flow direction. This zone changes into a micro-spherulitic structure at a certain depth, where the large number of spherulites are nucleated and are of nearly identical size. The size of the spherulites increases with increasing distance from the skin zone. The core, which usually makes up the major part of the volume in injection-molded specimen, contains larger, randomly sized spherulites. In some cases, a shear zone can be identified between skin and core zone [139]. Moreover, the skin zone is said to increase significantly with decreasing melt temperature [139]. The determination of precise values for the spherulite size is nearly impossible. Therefore, only some general statements and assumptions can be made and correlated to the resulting haze values. In the following, compression-molded samples and thin-sections of selected samples will be discussed. The micrographs of all other samples can be found in the appendix.

Morphological studies on DBGAcMeE derivatives (5)

Figure 6-16 represents the micrographs taken from samples containing 0.60 wt% of the additive **5c** or **5h**. As expected the compression-molded sample of additive **5c** shows significantly reduced spherulites and a quite high nucleation efficiency of 56 %. The effect of the nucleating agent becomes apparent in the thin-sections as well. The presence of the nucleating agent influences the spherulite size distribution of iPP in the different zones significantly [140]. The samples show a by far finer texture and the spherulites are drastically reduced. Comparing the

melt compression-molded samples of **5c** and **5h** reveals at first glance no substantial difference. Both show significantly reduced spherulites, but on a second glance the texture of **5h** is a little bit coarser. This becomes apparent by the thin-sections. Compared to the non-nucleated sample, sample **5h** shows smaller spherulites, but compared to sample **5c** the spherulites are not that fine and a different spherulite distribution can be observed as well. Sample **5c** looks very homogenous, as the transition from the skin to the core zone is harder to identify. Unexpectedly, despite of the clearly reduced spherulite size only a very low nucleation efficiency of 8 % has been calculated. Even though the investigations on the hot stage, in previous section, determined a slightly higher crystallization temperature of around 120 °C, it is uncertain why the haze value of sample **5h** even increases.

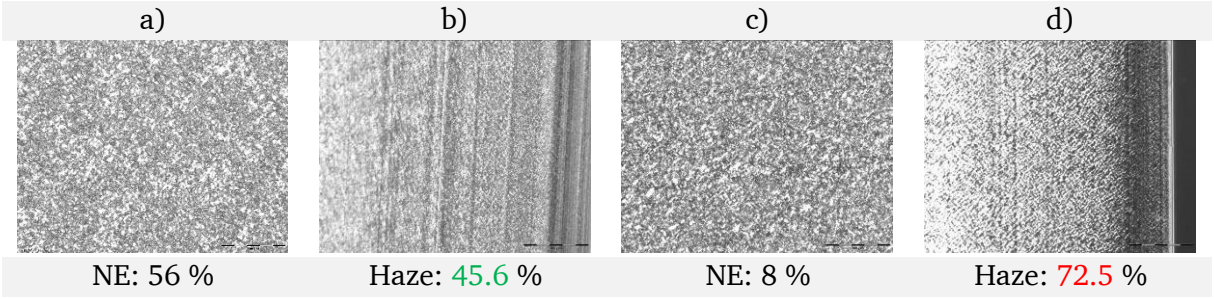

Figure 6-16 Polarized optical micrographs of melt-compression-molded iPP films and 10 µm thin-sections of 1.0 mm injection-molded iPP plaques containing 0.60 wt% of a-b) **5c** and c-d) **5h**. Scale bar 100 µm.

Conclusion with regard to DBGAcMeE derivatives (5)

Observations on the remaining additives revealed that no sound correlations can be drawn between the chemical structure and the efficiency of the additives. In both cases (compression-molded and thin-sections) several samples showed reduced spherulite sizes. In some cases the spherulites appear coarser and some inexplicable behaviors have been observed as well. For example the coarser structure of the compression-molded sample **5d** could be a result of large crystalline additive domains or an artefact caused by crystallization under the glass surface. Unexpectedly, a strange behavior has been observed for samples containing additive **5a.** The compression-molded sample showed in some areas diffuse spherulitic domains with a distinct Maltese cross. This phenomenon will be taken up again later in this subchapter.

Moreover, the skin layer of thin-sections of all samples showing reduced haze values, has been found to disappear. The nucleation effect and the resulting higher solidification rate are presumed to cause a more uniform distribution of small spherulites in the whole sample.

Morphological studies on DBGAc derivatives (6)

As was noted in the previous subchapter the additives of set **6** do not form a network, but in most cases the additive particles itself act as nucleation sites. Consequently, this type of additive needs to be finely dispersed in the polymer matrix. The samples **6c**, **6d** and **6h** show all reduced spherulite size, but the textures vary in their fineness (Figure 6-17). Sample **6d** shows the finest texture and exhibits the highest nucleation efficiency with 43 % of the present set. Additive **6h** reduces the spherulite size compared to the ‘control’ sample as well, but has a much coarser texture and a NE of only 18 %. Most of the spherulites can be assumed to be in the range of 5-

15 μm. The micrographs of the thin-sections exactly reflect the overall reduced spherulite size of the different zones [140]. However, differences of the samples can be observed and relations to the haze values can be drawn. Sample **6d** which improves moderately the haze value and shows a fine and homogenous spherulite distribution. In contrast, sample **6h** has a coarser texture and a broader skin zone. Sample **6c** illustrates, that a reduced spherulite size does not inevitably lead to an improvement of the optical properties, in particular haze.

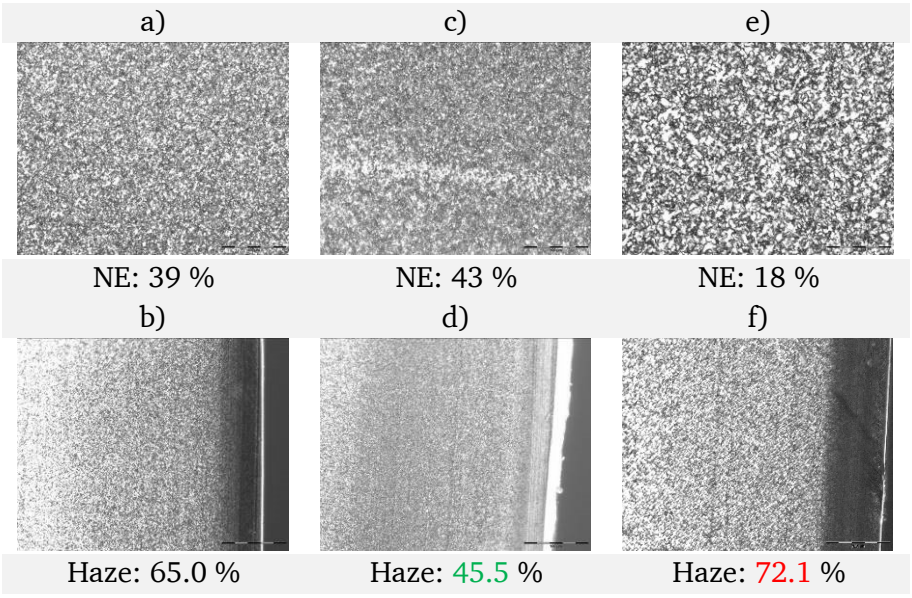

Figure 6-17 Polarized optical micrographs of melt-compression-molded iPP films and 10 µm thin-sections of 1.0 mm injection-molded iPP plaques containing 0.60 wt% of a-b) **6c**, c-d) **6d** and e-f) **6h**. Scale bar 100 µm.

The presumption that the width of the skin zone correlates with the haze values can be approved by the thin-section of additive **6d** at a concentration of only 0.30 wt%. The sample has a higher haze value of 56 % and shows a slightly darker skin zone compared to the sample at a concentration of 0.60 wt%.

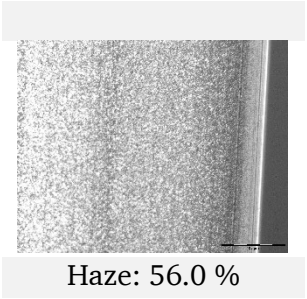

Figure 6-18 Polarized optical micrograph of 10 µm thin-sections of 1.0 mm injection-molded iPP plaques, containing 0.30 wt% of additive **6d**. Scale bar 100 µm.

Conclusion with regard to DBGAc derivatives (6)

Observations on the additional additive samples reveal that all additives reduce the overall spherulite size significantly. The nucleation efficiency does not correlate with the induced spherulite size. The thin-sections of the samples from the present set, which do not improve the

haze value, exhibit all a clearly visible skin zone. The moderately improved haze value of additive **6i** and a smaller width of the skin layer confirm these findings.

Morphological studies on DBGA derivatives (7)

Figure 6-19 represents the micrographs of the melt compression-molded samples and the thin-sections containing an additive concentration of 0.30 wt%. As known from the previous subchapter, the clarifiers **7c** and **7h** form fine fibrillar networks. The nucleation efficiency is moderate with a value below 40 %, but optical properties have been found to be best of all new additives. Both nucleating agents show an enormous influence on the morphology of the different zones in the thin-sections[140]. This is consistent with the results obtained from the melt-compression-molded samples, which show significant reduced spherulite sizes. Again, it can be concluded that finer and better distributed spherulites result in better optical properties. In both cases in which good optical properties are reached, nearly no skin zones have been observed.

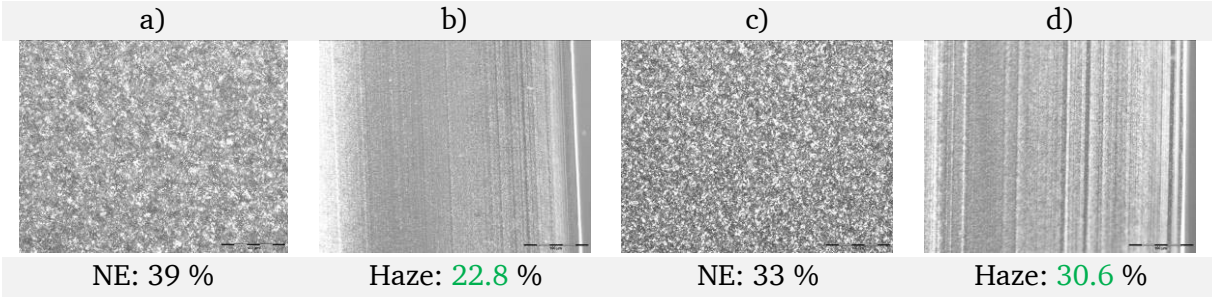

Figure 6-19 Polarized optical micrographs of melt-compression-molded iPP films and 10 µm thin-sections of 1.0 mm injection-molded iPP plaques containing 0.30 wt% of a-b) **7c** and c-d) **7h**. Scale bar 100 µm.

From the initial screening experiments it is known that increasing additive contents have different effects on the performance of these two additives. While mixtures containing additive **7c** undergo an extremum at 0.30 wt%, mixtures containing **7h** show further improvement with increasing concentration. Figure 6-20 comprises the thin-sections of samples containing a higher loading level of the two additives.

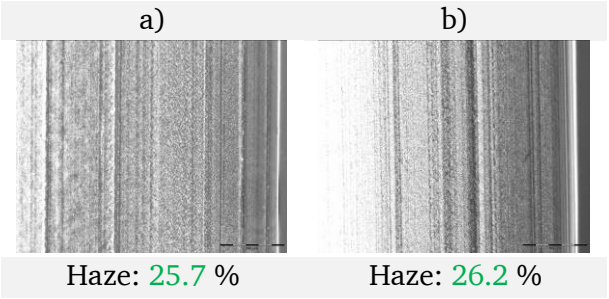

Figure 6-20 Polarized optical micrograph of 10 µm thin-sections of 1.0 mm injection-molded iPP plaques, containing 0.60 wt% of additive a) **7a** and b) **7h**. Scale bar 100 µm.

Two opposite effects can be observed. Increasing the loading level of **7c** leads to a more heterogeneous, coarser texture and a more visible skin zone. On the other hand, increasing the

amount of **7h** results in a more homogenous texture and additionally improved optical properties.

Conclusion with regard to DBGA derivatives (7)

Having a look on the additional samples (cg. Appendix) reveals that all melt compression-molded samples show reduced spherulite sizes. The corresponding NEs are ranged between 30 and 40 %. Only the additives **7f** and **7i** exhibit lower NEs and the texture appears slightly coarser. All the corresponding thin-sections show overall reduced spherulites, but in some cases unexpected textures. The samples **7a**, **7f** and **7i** show coarser textures and consequently no improved optical properties. However, by increasing the additive loading level their morphological texture becomes finer and their haze values improve from moderate to good. The biggest difference is observed for compounds **7i**. In that case, the haze value changes from 61.0 % to 29.9 % by increasing the concentration from 0.30 wt% to 0.60 wt%. Again a disappearance of the skin layer was observed, accompanied by a change from a coarser to a finer morphology.

Morphological studies on DBGA-*n* derivatives (8)

In this section, first the methyl amide derivatives will be discussed and the ethyl amide derivatives afterwards. Longer alkyl amide derivatives have been neglected due to inconspicuous findings; their micrographs can be found in the appendix.

Figure 6-21 comprises micrographs of compounds containing 0.60 wt% of the respective nucleating additive **8.1a**, **8.1c** or **8.1h**. The samples show all different behaviors, although the structures only differ in their substitution pattern on the benzylidene 'wings'. Compression-molded samples containing additive **8.1c** show reduced spherulites which are much more luminous. That is the result of the induced β-crystal phase. Beta crystals can be easily distinguished optically, by their highly luminous appearance amidst of the less bright α-spherulites [141]. The thin-sections of the injection-molded plaques exhibit brighter spherulites as well, but unexpectedly the whole texture is much coarser. Typically these spherulites crystallize as the hexagonal β-structure and show a strong negative birefringence. However, in case of reduced spherulite sizes this is even challenging.

The sample containing additive **8.1a** exhibits a relatively high nucleation efficiency, but the observed homogenous grain structure of the compression-molded sample (Figure 6-21 a) shows only moderately reduced spherulite sizes in the range of 10 to 20 μm. In accordance with these results, the corresponding thin-section shows a coarser texture, even though the haze value was found to be moderately reduced. In this case, the results do not fit to the common observations.

The compression-molded sample containing additive **8.1h** revealed an unexpected effect. The additive has been found to deliver a relatively high nucleation efficiency, but contrary to expectations the major part of the investigated sample shows a distorted texture with spherulites of not determinable size. The texture is not comparable to the previous samples, which showed significant reduced spherulites. In this case, even some parts of the sample show the development of large (>100 μm) diffuse spherulitic structures (Figure 6-22, right).

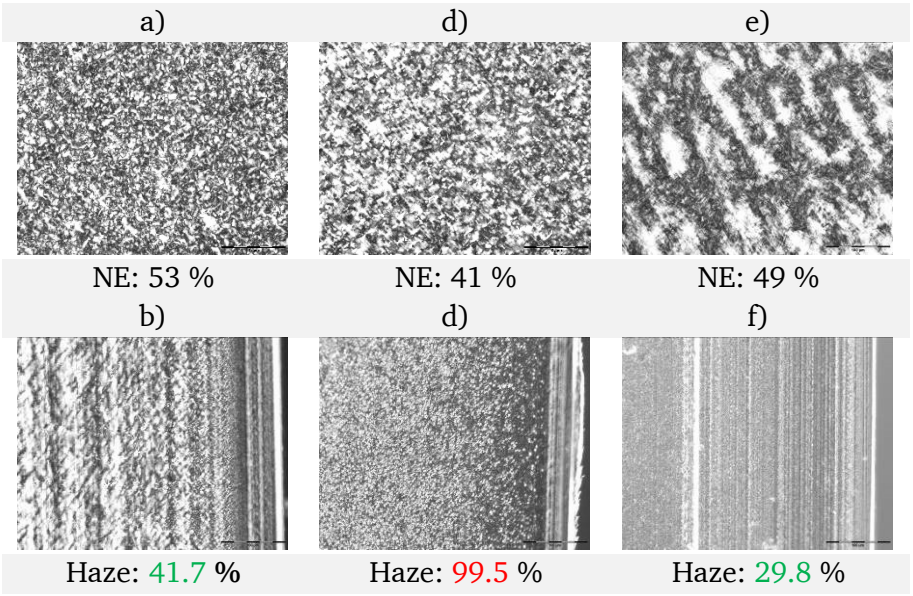

Figure 6-21 Polarized optical micrographs of melt-compression-molded iPP films and 10 µm thin-sections of 1.0 mm injection-molded iPP plaques containing 0.60 wt% of a-b) **8.1a**, c-d) **8.1c** and e-f) **8.1h**. Scale bar 100 µm.

Figure 6-22 shows the two different textures at a magnification of 100 μm, but in larger images. Again the spherulites are not of the 'mixed' type, but they look like α_1-spherulites with a simple Maltese cross pattern [111]. Surprisingly, these diffuse spherulitic structures have not been found in the thin-sections of the injection-molded plaques. As can be seen in Figure 6-21 f), the thin-section shows a fine, homogenous spherulitic texture and even good haze values (< 30 %) can be assigned. The reason for the development of this diffuse spherulite formation in the compression-molded samples is still unsolved. However, the phenomenon has been observed for other derivatives as well. Therefore, possible reasons will be discussed later in this chapter in more detail.

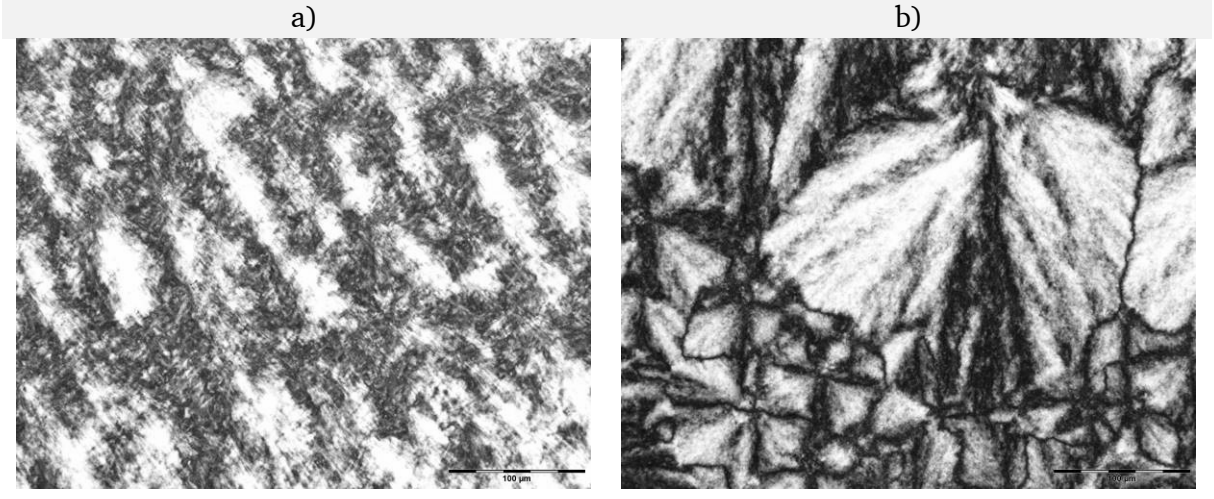

Figure 6-22 Polarized optical micrographs of melt-compression-molded iPP films and 10 µm thin-sections of 1.0 mm injection-molded iPP plaques containing 0.60 wt% of additive **8.1h** at different positons of the sample a) and b). Scale bar 100 µm.

Figure 6-23 comprises micrographs of samples containing 0.60 wt% of the additives **8.2a**, **8.2c** or **8.2h**. The compression-molded samples containing the additive **8.2a** or **8.2c**, show reduced spherulite sizes and moderate nucleation efficiencies have been calculated. The texture of samples containing additive **8.2a** looks coarser and comprises several bright colored areas. The bright colored areas are likely to result from α_1-type spherulites. The related thin-sections of both samples show a different behavior. Both samples show reduced spherulites compared to the 'control' material. Even though the first quarter of the sample **8.2a** shows a really fine spherulite distribution, the large part of the sample comprises larger spherulites with a bright white color. The isolated spherulites, which can be found upfront the dense white zone, do not look like α_1-type spherulites. The assignment of the visual appearance to a known spherulite type is challenging, however the observed appearance can be best described as a 'chessboard' like pattern [111, 142, 143]. A schematic illustration of this 'chessboard' pattern is presented in Figure 6-23.

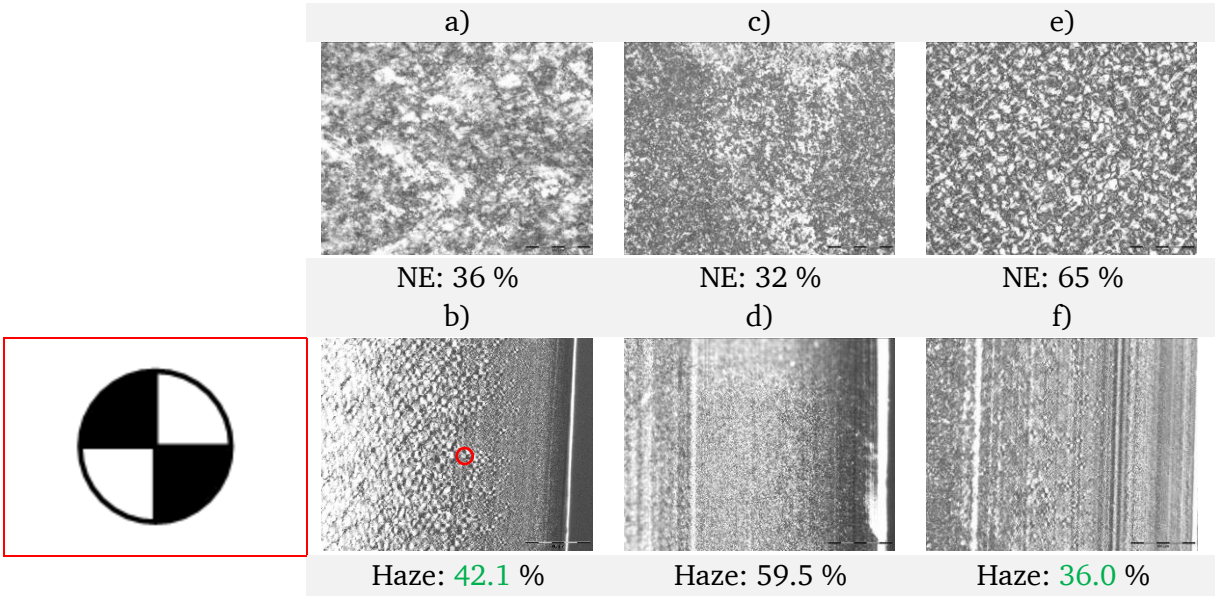

Figure 6-23 Polarized optical micrographs of melt-compression-molded iPP films and 10 µm thin-sections of 1.0 mm injection-molded iPP plaques containing 0.60 wt% of a-b) **8.2a**, c-d) **8.2c** and e-f) **8.2h**. Schematic illustration of the observed extinction pattern of compound **8.2a**. Scale bar 100 µm.

However, the sample containing additive **8.2c** looks more uniform and spherulites are again of the α_1-type. Nevertheless, the measured haze value is not reduced significantly. For the compression-molded sample containing additive **8.2h** the phenomenon of diffuse spherulites occurred only in some areas of the sample. Although it exhibits the highest measured nucleation efficiency, several of the spherulites are larger than 100 μm. The related thin-sections show homogeneous fine grain textures with similar size distributions in the skin and core zone. However, the compression-molded samples revealed diffuse spherulites here and there, optical properties of the injection-molded samples have been found to improve. This finding makes this phenomenon much more difficult to explain and therefore a few considerations will be discussed in the following.

The diffuse spherulite development, which has been observed for some of the melt-compression-molded samples has been found for several other additive derivatives as well. Besides the two reported examples, samples containing 0.30 wt% of the additives **8.1a**, **8.2a** and **8.3a** showed the phenomenon as well. In addition to the typical grain like texture in some areas of the sample, diffuse α_I-like spherulites with a distinct Maltese cross pattern have been found. The appearance was similar to the reported one and is therefore not shown. The strongest effect was found for samples containing additive **8.2h** and therefore, the sample has been investigated in more detail on a heating stage. A sample containing a concentration of 0.60 wt% was heated up to 230 °C and subsequently cooled with a cooling rate of 10 °C/min. The development of diffuse α_I-type spherulites was observed under these conditions as well. It can be almost excluded that the observed phenomenon is caused by the fast cooling (quenching) used for sample preparation of the compression-molded films. Unexpectedly, the dissolution experiments in the previous subchapter haven't revealed the development of such diffuse spherulitic structures and only a granular texture around the core region was observed. Apart from that, one could imagine a concentration dependent effect and indeed, for mixtures containing additive **8.2h** a concentration dependency has been found. Figure 6-24 shows the morphological change with increasing additive content. The diameter of the observed diffuse structures increases by simultaneous occurrence of increasing nucleation efficiency. Because the effect occurs at relative low concentrations (~ 0.60 wt%), it can be excluded that the diffuse spherulite morphology in the solidified mixture is dominated by primary structures of the additive itself [72]. At higher concentrations, when phase-separated domains may develop, it is possible that PP crystallizes in form of diffuse spherulites in these areas. In some cases the effect is more or less pronounced. Even though the solubility threshold is not exceeded, the spherulite growth rate and the overall crystallization rate of iPP might be influenced by the little dilution effect of the additive. The additive may retard the crystallization of iPP and thus leads to the decrease of both values, resulting in more diffuse morphologies.

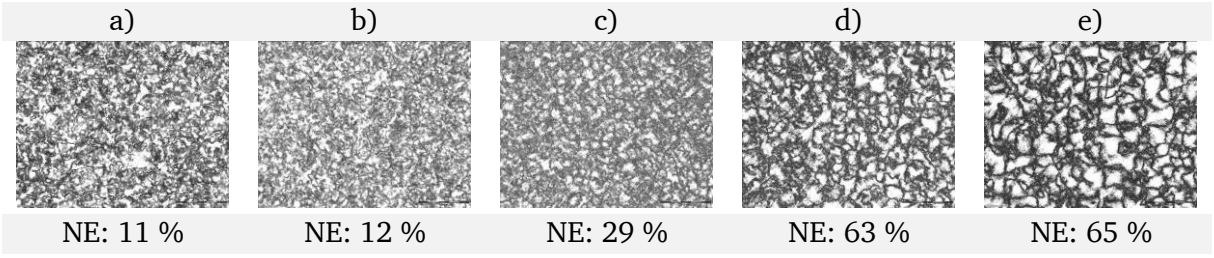

Figure 6-24 Polarized optical micrographs of compression-molded samples containing a) 0.03 wt%, b) 0.15 wt%, c) 0.30 wt%, d) 0.45 wt% and e) 0.60 wt% of additive **8.2h**. Scale bar 100 µm.

In addition, surface nucleation by the cover glass may be another possible reason for the formation of large diffuse spherulites [144]. However, in that case other samples should show the development as well and repetition of the experiment under identical conditions should deliver somehow different results. At least repetition without the cover glass showed a less pronounced effect, but some diffuse spherulites have still been identified.

The observed behavior remains suspicious. In general, one expects unaffected optical properties and nucleation efficiencies for samples containing larger and diffuse spherulitic morphologies. Anyhow the opposite can be observed. Figure 6-25 comprises the thin-section prepared of samples containing additive **8.2h** in different magnifications. As mentioned, the sample shows predominantly drastically reduced spherulites of hardly determinable size. However, the sample shows in some areas larger diffuse spherulites, which appear to show the 'chessboard' like extinction pattern. At lower concentrations (0.30 wt%) the sample **8.2h** shows only the formation of space filling α_I-like spherulites. Therefore, the observation fits to the corresponding increased haze value.

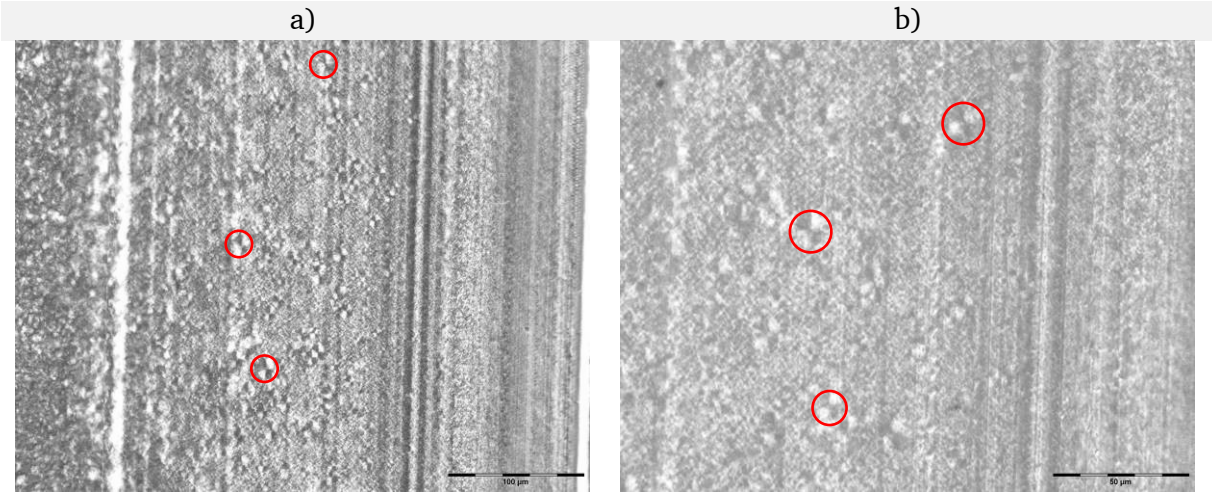

Figure 6-25 Polarized optical micrographs of 10 µm thin-sections of 1.0 mm injection-molded iPP plaques containing 0.60 wt% of additive **8.2h** at magnifications a) 20x, Scale bar 100 µm and b) 40x, Scale bar 50 µm.

The phenomenon in the compression-molded samples is likely to be an artefact, but was found to be caused by some special derivatives only. What all these additives have in common are either unsubstituted or propyl substituted benzylidene 'wings'. Additionally, the 'tail' exhibits a C_1 to C_3 substituted amide functionality.

Conclusion with regard to DBGA-*n* derivatives (8)

Attempts have been made to find correlations between the additive structures and the induced iPP morphologies. The morphology, as a measure for the induced nucleation density, has been studied on the basis of thin-sections and compression-molded samples. In addition, nucleation efficiency and optical properties have been used in order to better understand the observed differences.

Non-nucleated iPP in compression-molded films revealed space-filling spherulitic structures with mixed Maltese cross pattern. The morphology of all samples has been influenced by the additives and exceeding 0.15 wt% reduced spherulite sizes have been observed. Depending on the additives efficiency more or less fine morphologies could be revealed. However, these fine morphologies only differ in the appearance of their grain structure. The tendency observed for the NE somehow correlated with the spherulite sizes, but in some cases finer morphologies have

been found for lower NEs. Unexpectedly, a few samples revealed diffuse α_1-spherulites with distinct Maltese crosses.

Thin-sections of samples of unaffected optical properties revealed similar morphological textures as the non-nucleated 'control' sample. More or less visible skin-core morphologies and spherulites in the core region with typical α_1-spherulites with a distinct Maltese cross have been detected. The nucleation effect was clearly visible and much finer spherulite sizes have been revealed as fine textures.

The finest morphologies and thus the smallest spherulite sizes have been induced by the additives of set **7**. In accordance with the previous investigations, most probably the fine, narrow network serves as a high density nucleation surface. The fundamental difference to the other derivatives with regard to their haze values becomes clearly visible by the thin-sections. Samples with haze values between 30 and 50 % exhibit clearly reduced spherulite size, but nevertheless samples with haze values below 30 % show significant finer textures.

It has not been possible to uncover the occurrence of the diffuse spherulite development in some compression-molded samples. Most probably this effect is triggered by a combination of the overall chemical structure of the additive and the preparation conditions. This can be supported by the thin-sections of injection-molded samples, because they do not show this effect.

The general observed tendency fits the common known theories. The nucleation density seems to be an important factor. The provided fine fibrillar network provides a larger surface and induces nucleation. The finer the network, the larger the surface and thus the smaller are the induced spherulites. The homogenous dispersion of the additives is as well a decisive factor and this is likely the reason, why some injection-molded parts reveal less improved optical properties. The occurrence of non-nucleated layers leads to different light scattering effects. In addition, the overall nucleation efficiency in terms of higher crystallization temperatures plays still a role, as faster cooling leads to better performance [128].

Finally, the results confirm earlier observations that not necessarily high nucleation efficiencies are needed to obtain good optical properties.

6.4. Influence of the additives on the crystallinity of isotactic polypropylene

Additionally, the degree of crystallinity (X_c) of the samples was calculated from DSC experiments. The values were evaluated from the second DSC heating endotherms, calculated on the basis of 209 J/g [145] for 100 % crystalline iPP and corrected for the presence of the additive. The degree of crystallinity has been considered for the sake of completeness. In general, this value is known to be only poorly affected by the use of nucleating agents. Therefore, only a few observations will be discussed and a detailed list of all calculated values can be found in the appendix.

As expected no significant differences can be found. All mixtures show only slight deviations from the non-nucleated 'control' sample with a value of 44 %. Crystallinity of most iPP/additive mixtures increases only slightly with increasing additive concentration. As can be seen in Figure 6-25, the values differentiate within the known uncertainty of the measurements. Most values varied between 45 and 50 %. Efficient nucleated samples exhibited tendencies towards higher values (50-51 %).

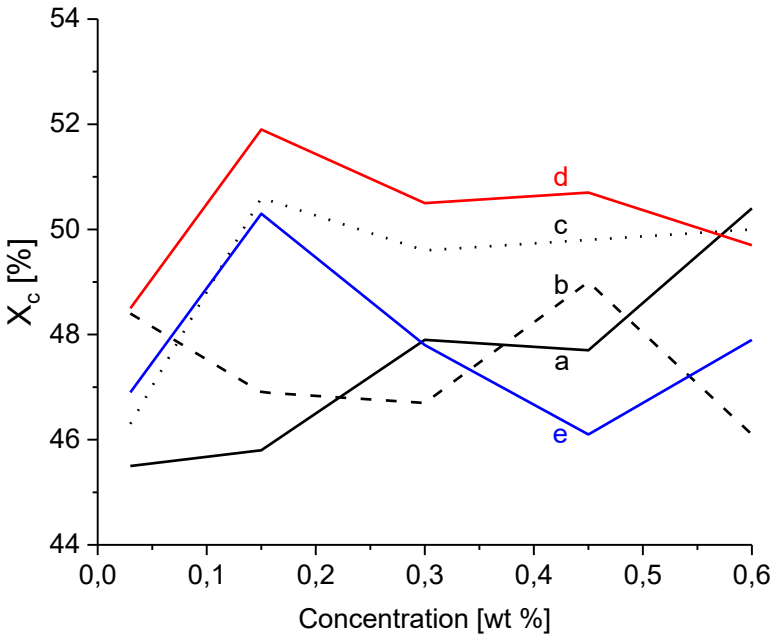

Figure 6-25 DSC crystallinity as a function of the concentration of a) **5c**, b) **6c**, c) **7c**, d) **8.1c** and e) **8.2c** in iPP.

6.5. Influence of the additives on the color of isotactic polypropylene

The yellowness index (YI) has been investigated, as discoloration of iPP can be caused by a variety of factors. Besides process-related factors, the type of the additives themselves in conjunction with the thermal history of the polymer play a key role in inducing or minimizing discoloration. Additionally, decomposed additives influence the final optical properties. To achieve excellent optical properties of the final products, the YI should be influenced as little as possible by the incorporated additives. Thus it is worth having a closer look on the yellowness indices of the additives. A detailed list of the YI values can be found in the appendix of this thesis.

The 'control' iPP samples exhibit YI values of 2.20. The material is negligible aged after the compounding and injection molding steps at 220 °C, but positively affected by the process stabilizers. Having a look on the commercial additives, mainly **DMDBS** and **TBPMN**, it can be observed that the incorporation of the additive shows no negative effect on the YI. Especially the sorbitol based additives, with their sugar-based chemical structure tend to decompose during processing. However, the 5 % weight loss temperatures of this two additives demonstrate, that decomposition does not occur during the processing conditions applied. **DMDBS** shows just slightly increased values of around 2.40 over the whole concentration range and thus no dramatic change. Interestingly, for **TBPMN** very low YI values (~1.00) have been identified. The reason for this very low YI values is connected to the fact, that the applied **TBPMN** is the finished commercial grade Millad NX 8000® from Milliken Chemical. By further optical and analytical investigations, an optical brightener and an inorganic violet pigment have been identified. These are used to mask inherent yellowness of the discolored polymer due to the processing conditions [146]. Discoloration is a major issue to some derivatives out of the sorbitol family owing to their sugar-based chemical structure and therefore, potential decomposition of some additive molecules needs to be prevented [55].

Since all novel additives exhibit a sugar-based chemical structure as well, it seems beneficial to have an initial look on the yellowness indices of the compounds. Most of the additives show no significant influence and only slightly increased values can be observed. The YI values for compounds of set **5** varied between 1.70 and 2.70, whereas the values of compounds from set **7** varied between 1.55 and 3.85. Nearly all compounds of set **8** exhibit YI values between 2.50 and 3.30, and some even showed lower values. In some cases higher YI values have been measured (**5a**, **5d**, **7a** and **7f**). Due to the fact that all of these additives exhibit a $T_{-5\ wt\%}$, which is above the applied processing temperature, decomposition of the additives can be excluded. Therefore, the increased values have to be connected to the high loading levels. The only exception has been found for the additive set **6**. In this case, most of the additives showed $T_{-5\ wt\%}$, which were below the applied processing temperature. This consequently implies that most probably the additives do not endure the processing step and discoloration is most probably caused by a complete or at least a partial collapse of the additive. This collapse can be either the cleavage of the benzylidene 'wings' or by a decarboxylation reaction, which results in chain shortening of the additive. As no foaming has been detected, the latter one can be excluded.

6.6. Influence of processing temperature and particle size on the crystallization temperature and optical properties of the lead structure

The influence of processing temperature and particle size on crystallization temperature and optical properties in the final articles have been investigated for the lead structure (**7c**) of the novel nucleating and clarifying agents. As the initial experiments revealed, the thermal properties of several additives of the DBGA set (**7**) have been found to directly decompose after melting. For additive **7c**, a melting temperature of 261 °C and an onset of decomposition at 263 °C have been determined. The 5 % weight loss temperature accounts for 297 °C. Therefore, in principal the additive should withstand the processing steps without any problems up to a temperature of 250 °C. However, the dissolution experiments showed that exceeding a temperature of 260 °C the additive starts to decompose. Nevertheless, the additive is soluble in the iPP melt and can be easily distributed. Several parameters like crystalline structure, particle size and processing temperature are known to influence the efficiency of the clarifying agent [147, 148]. Therefore, it was interesting to investigate, if the distribution of the additive is influenced by its initial processing temperature or by its particle size.

Influence of the processing temperature

In a first step the influence of the processing temperature on the crystallization temperature has been studied. The different initial compounding temperatures may deliver different qualities of additive distributions and consequently the crystallization temperature is directly affected. Mixtures containing different amounts of additive **7c** have been compounded at four different temperatures between 200 and 260 °C. The left diagram in Figure 6-26 reveals that the crystallization temperature is nearly not affected by changing the compounding temperature. The curve progression of the samples compounded at 220 °C and 260 °C show hardly any difference. The difference is within the range of the standard deviation. Interestingly, the samples compounded at 260 °C showed no larger deviations even though the applied temperature is located in the range of melting and decomposition of the pure additive.

Slight deviations towards higher crystallization temperatures have been observed for the samples compounded at lower processing temperatures (200 °C). The measured crystallization temperatures have been found to be 1-2 °C higher as for the samples processed at higher temperatures. A possible interpretation of this finding is that the solubility of the additive is already good enough at lower temperatures and no melting of the additive is necessary. However, it is not clear why the performance is slightly improved. In addition, slightly increased crystallization temperatures are found for the samples containing 0.15 wt%, but no sound explanations can be made. Most probably the values represent a plateau value with typical fluctuations in the range of the standard deviation (0.5°C). Based on these results it can be noted, that the additive is soluble in the polymer resin at least until the maximal applied concentration of 0.60 wt%.

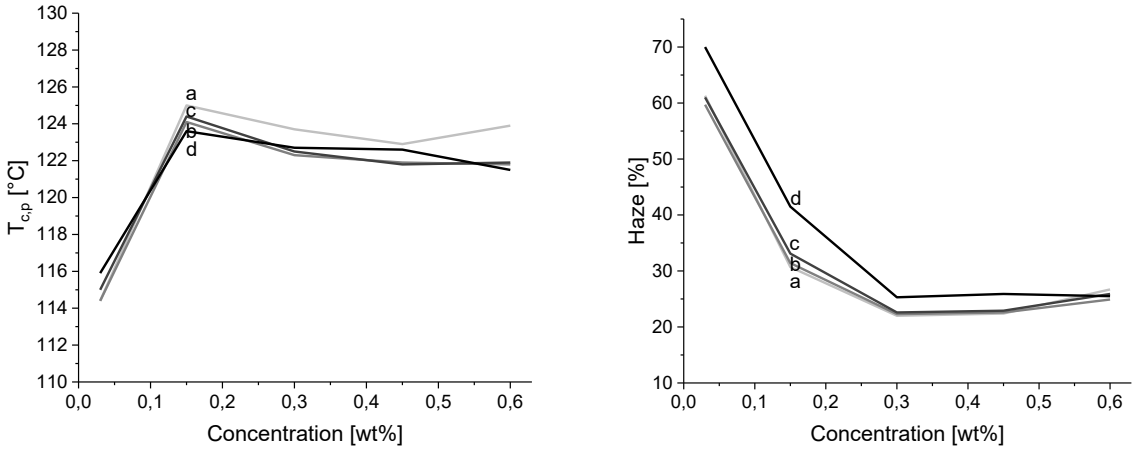

Figure 6-26 Effect of compounding temperature on the nucleation efficiency (left) and haze values (right) of **7c** as a function of additive concentration. Compounding temperature: a) 200 °C, b) 220 °C, c) 240 °C and d) 260 °C.

In a second step the granules produced at different compounding temperatures were used in the subsequent injection molding step at a constant temperature of 220 °C. The values gained by haze measurements on 1.0 mm thick plaques are compared in Figure 6-26 (right). As can be seen, haze is hardly affected by the initial different compounding temperatures. The deviation of the plaques prepared of granules compounded between 200 and 240 °C is negligible. The only deviation has been found for samples containing compounds prepared at 260 °C. This finding results of the high compounding temperature prior to the injection molding step. It is likely that the additive partly starts to decompose at the applied temperature, which in the end results in increased scattering of light and slightly increased haze values. However, investigations of the yellowness index haven't confirmed this assumption in the low concentration range. In general, all samples independent of the compounding temperature, exhibit higher YI values with increasing additive content.

Influence of particle size

The nucleating efficiency depends on the particle size of the incorporated additive as well [149–151]. A potential agglomeration of the particles results in a reduced availability of the additive and a smaller surface area. The solubility of the additive should overcome this issue, but the dissolution process might need more time to dissolve larger agglomerates. For this reason it is advisable to use as small as possible particles. In the next step the influence of different particle size portions of additive **7c** have been compared. In general, the additives have been briefly grinded after the isolation step. Figure 6-27 shows the particle size distribution analyzed by a sieve analysis of the additive after a quick grinding step with a mortar. As can be seen nearly 50 % of the particles are larger than 250 μm. The efficiency of the additive has been compared by testing two fractions of different particle sizes. The first fraction comprised a random sample directly after briefly grinding and thus represents the distribution presented below. In a second fraction only particles with a particle size below 125 μm have been used.

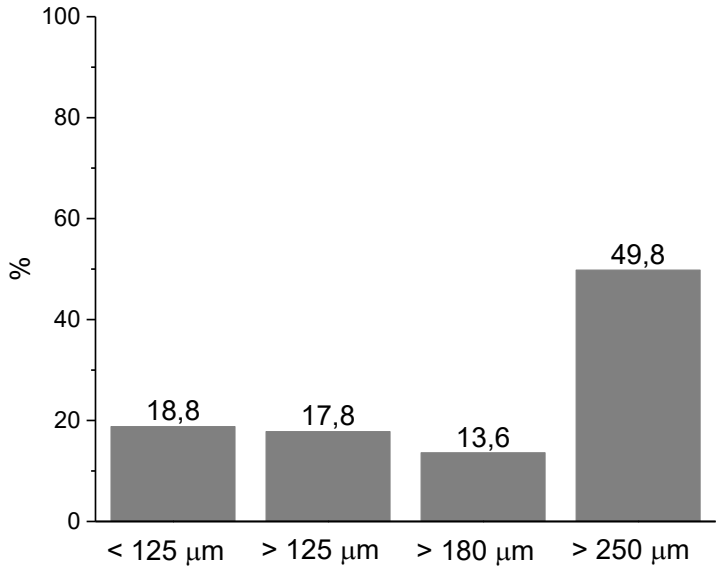

Figure 6-27 Particle size distribution of additive **7c** after roughly grinding past isolation.

Figure 6-28 reveals that neither the crystallization temperature, nor the haze value is influenced significantly by the different additive particles. The largest deviation of the crystallization temperature has been recognized for the small particle fraction ($< 125\,\mu$m). However the difference is almost negligible. In the case of the larger particle fraction, in some injection-molded plaques additive particles have been observed at higher loading levels, but optical properties have not been affected.

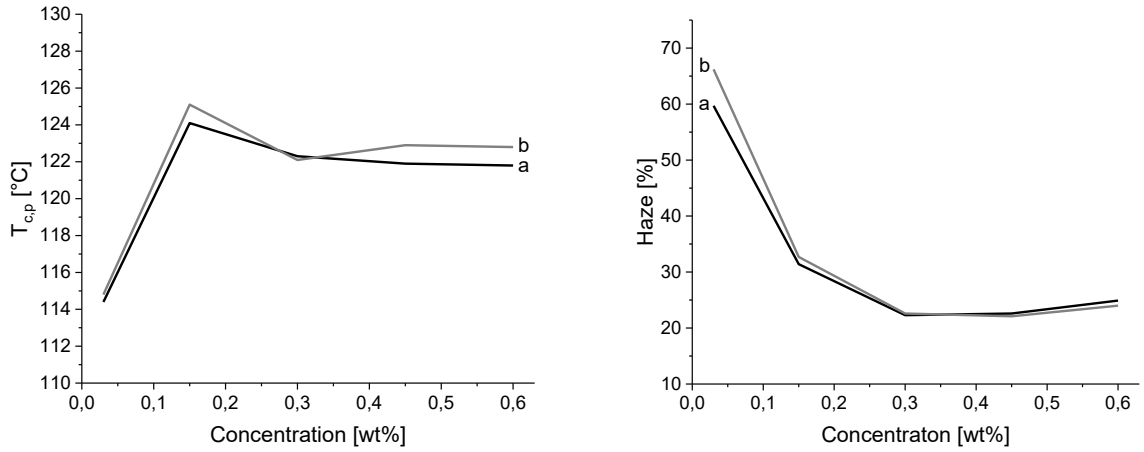

Figure 6-28 Effect of particle size on the nucleation efficiency (left) and haze values (right) of **7c** as a function of additive concentration. Processing at 220 °C of a) ground and b) sieved (<125 µm) additive powder.

Conclusion on compounding temperature and particle size

In principle the obtained results demonstrate that the efficiency of the novel additive is hardly affected by the change of compounding temperature and particle size. This supposes a good solubility of the additive or at least a transformation process of the additive upon heating in the polymer melt. By this, the common poor dispersibility of crystalline clarifiers can be overcome.

The fact that the processing temperature is below the melting temperature of the additive and good transparency is reached anyway, supports this assumption. The haze values, which have been determined at the maximal applied concentration of 0.60 wt% are above the smallest measured value. This reveals a solubility limit of the additive (> 0.30 wt%), leading to increased haze due to light scattering. In addition, the observation of additive particles at higher loading levels at constant optical properties shows, that saturation occurs and thus exceeding this threshold further added additive remains unused. However, using a fine particulate morphology of the additive improves this issue and enhances the overall dispersibility at the same time.

The temperature dependence of the additive at different injection molding temperatures has not been considered yet. In the underlying experiment the temperature was kept constant at 220 °C. This question offers room for future research. Potentially the earlier onset of gelation, observed in the rheological experiments for additive **7c** in combination with lower compounding temperatures could result in thinner fibrillar structures, because they have less time to form the network and consequently less lateral growth occurs.

6.7. Efficiency of dibenzylidene-*L*-gulonic acid based nucleating and clarifying agents in polypropylene random copolymer

As is known, objects produced of PP appear opaque and face restrictions in applications that require excellent optical properties [152]. Lots of research aimed to reduce the overall spherulite size or the order within, to improve the optical properties of PP. One possible approach is the use of copolymers with ethylene and butene comonomer fractions. However, the degree of crystallinity and its mechanical properties are significantly influenced. Another possibility is to use nucleating and clarifying agents to reduce the overall spherulite size. A combination of both consequently results in further improved optical properties, making nucleated PP copolymers the material of choice when it comes to highly transparent materials [152–155].

For this purpose, the initial applied screening setup has been used to screen the additives in a PP copolymer. First, the screening results of two commercial additives are compared against the 'control' sample. In a second step two additives of the initial presented 'library' of novel nucleating and clarifying agents, which have been proven to nucleate iPP homopolymer will be investigated. Their results are compared against the produced state of the art benchmark. In a final step the screening results of the homopolymer are contrasted with those of the copolymer.

Impact of copolymer resin

Table 6-1 comprises the screening results of the 'control' sample and PP copo mixtures containing known amounts of **DMDBS** and **TBPMN**. The additionally stabilized PP copo type Moplen RP 310 M exhibits a crystallization temperature of 109.6 °C and haze measurements of 1.0 mm thick plaques revealed a haze value of 55.1 %. As expected the haze value is already 10 % lower as for the homopolymer.

Table 6-1. Screening results of commercial nucleating and clarifying agents.

Nr.	Additive	T_m [°C]	T_c [°C]	$T_{-5\,wt\%}$ [°C]	Conc. [wt%]	$T_{m,p}$ [°C]	$T_{c,p}$ [°C]	Trans. [%]	Haze [%]	Clarity [%]
iPP	-	-	-	-	-	153.0	109.6	90.30	55.10	71.30
I	DMDBS	275	214	302	0.03	152.7	109.1	90.10	55.90	69.10
					0.15	154.6	123.3	89.50	16.90	95.30
	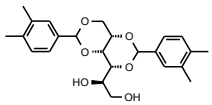				0.30	155.0	124.4	89.80	10.30	95.40
					0.45	155.4	124.1	89.60	13.40	94.90
					0.60	155.4	124.0	89.40	14.10	94.80
II	TBPMN	245	201	316	0.03	148.7	108.9	90.20	54.40	66.70
					0.15	153.7	121.6	90.10	26.00	95.20
	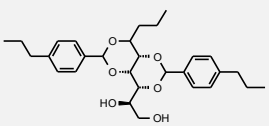				0.30	155.0	124.1	89.70	10.60	95.40
					0.45	155.0	125.2	90.30	7.40	95.40
					0.60	153.1	125.2	90.30	7.20	95.40

T_m = melting temperature, additive; T_c = crystallization temperature, additive; $T_{-5\,wt\%}$ = 5 % weight loss temperature, additive; $T_{m,p}$ = peak melting temperature, polymer $T_{c,p}$ = peak crystallization temperature, polymer, n.a. = not available, Transmission, Haze and Clarity were measured on 1.0 mm plaques. [1)] T_m taken from DSC decomposition run.

The results of **DMDBS** and **TBPMN** show comparable tendencies as observed for the homopolymer mixtures. **DMDBS** containing samples reach a plateau value of around 124 °C for the crystallization temperature and undergo a minimum haze value of 10.3 % at a concentration of 0.30 wt%. In contrast, the values of **TBPMN** containing samples constantly improve with increasing concentration. The crystallization temperature reaches around 125 °C and haze values improve up to a level of nearly 7.0 %. Clarity improves for all mixtures to a level of around 95.0 %.

The screening results of two novel additives out of the DBGAcMeE (**5**) and DBGA (**7**) sets are presented in Table 6-2. Focus has been put on compounds containing additive **7c**, as it has been identified as the lead structure out of all novel additives. Here as well the measured values represent identical tendencies as found for homopolymer mixtures. Copolymer compounds containing additive **5c** increase the crystallization temperature to a level of around 120.5 °C and improve haze constantly with increasing loading level. Haze reaches a value of 28 %, but the maximal threshold concentration is probably not reached at 0.75 wt%. Conversely, mixtures containing additive **7c** undergo an extrema at 0.30 wt%, exceeding this threshold the efficiency decreases. The crystallization temperature reaches a maximum value of around 120 °C and haze can be improved to a level of 16.8 %.

Table 6-2. Screening results of 3,5:4,6-dibenzylidene *L*-gulonic acid methyl ester (**5c**) and amid (**7c**) derivatives.

Nr.	Substitution pattern	T_m [°C]	T_c [°C]	$T_{-5\ wt\%}$ [°C]	Conc. [wt%]	$T_{m,p}$ [°C]	$T_{c,p}$ [°C]	Trans. [%]	Haze [%]	Clarity [%]
iPP	-	-	-	-	-	153.0	109.6	90.30	55.10	71.30
5c	3,4-DiMe	249	195	292	0.03	150.2	109.9	90.30	56.40	70.70
	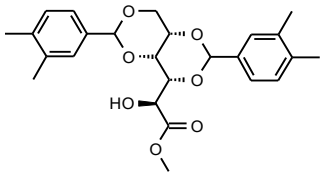				0.15	152.1	121.0	89.90	55.40	96.10
					0.30	153.3	120.2	90.10	55.80	84.30
					0.45	154.3	120.6	89.70	39.40	91.90
					0.60	154.5	120.6	89.30	32.20	94.10
					0.75	153.0	120.8	88.30	28.00	94.90
7c	3,4-DiMe	261[1)]	n.a.	297	0.03	152.7	108.7	90.30	54.30	77.60
	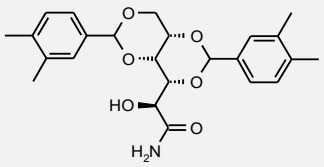				0.15	153.7	120.3	89.60	20.60	95.30
					0.30	154.2	120.0	89.00	16.80	95.00
					0.45	153.8	119.2	88.00	19.50	94.20
					0.60	153.4	117.1	86.80	20.10	94.00

T_m = melting temperature, additive; T_c = crystallization temperature, additive; $T_{-5\ wt\%}$ = 5 % weight loss temperature, additive; $T_{m,p}$ = peak melting temperature, polymer $T_{c,p}$ = peak crystallization temperature, polymer, n.a. = not available, Transmission, Haze and Clarity were measured on 1.0 mm plaques. [1)] T_m taken from DSC decomposition run.

Figure 6-29 contrasts the results of homopolymer mixtures with copolymer mixtures containing additive **7c**. The curve shape of crystallization temperature and of the optical properties of both PP grades are nearly identical and differ only in their absolute values. The crystallization temperatures of the copolymer compounds are around 4 °C lower as for the homopolymer. The

difference in haze is found to be in the range of 5 to 10 %, whereas clarity only shows a deviation below a concentration of 0.15 wt%.

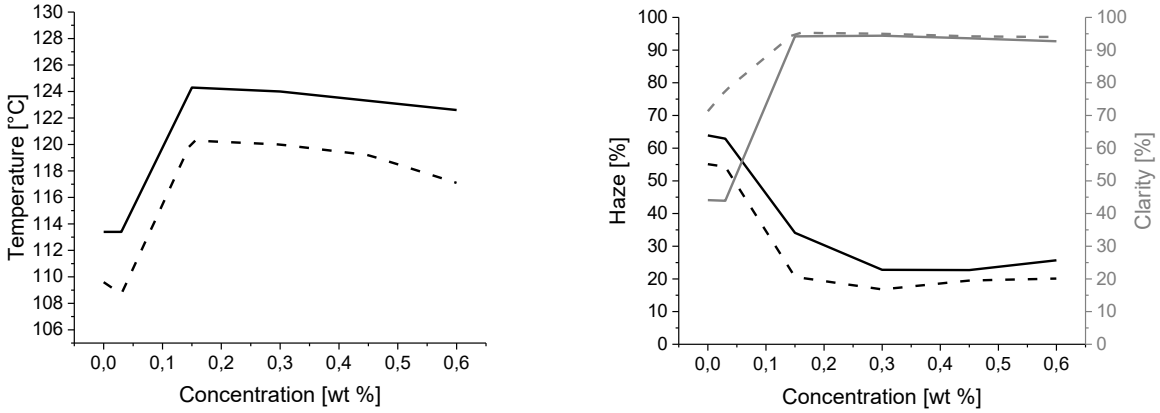

Figure 6-29 Crystallization temperature (left) and values for haze and clarity (right) against additive concentration of PP homopolymer (full line) and PP copolymer (dashed line) mixtures containing additive **7c**.

Conclusion on type of polymer resin

Some derivatives of the novel 'library' of nucleating and clarifying agents have been screened in a PP copolymer to demonstrate their usability in more market relevant PP resins. Comparable results, as determined for the iPP homopolymer, have been revealed for the additives **5c** and **7c**. In both cases the crystallization temperatures measured for the copolymer compounds, were below those of the homopolymer. Haze values of the copolymer compounds are slightly improved by around 5 %, but clarity remained on a constant level. The improved optical properties are the result of the inherent better values of the copolymer resin.

In principle, the novel derivatives are expected to deliver comparable performance in other PP resins. Beyond that it is obvious that dibenzylidene-*L*-gulonic acid based nucleating and clarifying agents could be useful in other polymer resins as well.

6.8. Conclusions on detailed studies of the additives behaviors based on structure property relations

In this chapter, attempts were made to better understand the mode of action and to reveal correlations between crystallization temperature and haze in dependence of the introduced functionalities of the additives. In addition, the additives influence on the induced crystal modification has been investigated. The focus was put on the phase behavior and on the morphology of the nucleated and/or clarified isotactic polypropylene samples. Finally, the influence of compounding temperature, particle size and polymer resin has been investigated for the identified lead structure.

The wide-angle x-ray scattering measurements gave rise to the induced crystal morphology by the additives. All newly developed additives are typical α-nucleating and clarifying agents, but one special derivative has been found as a 'hybrid' nucleating agent inducing a mixture of α- and β-polymorphs. To our knowledge, this is the first time a dibenzylidene acetal based nucleating agent induces the β-phase to a certain extent. Further modifications might give access to a desired soluble, easy dispersible and exclusively β-nucleating agent.

The dissolution, melting and recrystallization behavior of selected derivatives of the different sets has been investigated in order to understand the underlying mode of action. Mainly two different behaviors have been revealed. The DBGAcMeE (**5**), DBGA (**7**) and DBGA-*n* (**8**) derivatives have been found to form fibrillar networks upon cooling, whereas DBGAc (**6**) derivatives do not dissolve or melt and consequently exist as fine particles in the polymer melt. The differences are mainly caused by the 'tails', which influence the additives solubility in the polymer melt. Unexpectedly, DBGAcMeE (**5**) derivatives showed a clearly visible network in the polymer melt, although the molecules are not able to build up hydrogen bonds via their ester 'tail'. Thus, other stacking forces are accountable for the network formation. In contrast, the DBGAc (**6**) derivatives and their acid 'tail' revealed that they heavily disfavor the solubility and prevent network formation by a different stacking mechanism. In addition, the dispersibility and the density of the developing surface is influenced by the substituents and the overall chemical structure as well. Reduced lateral growth rates lead to fine and high density networks. The experiments confirmed that the magnitude of the fibrils and the resulting surface plays a key role in clarifying iPP. A higher nucleation density consequently causes smaller spherulites and improves the optical properties.

By the simple method of reviewing compression-molded samples and thin-sections, the nucleation density induced by the novel additives has been studied. Reduced spherulite sizes have been observed for all samples. Depending on the efficiency of the additive more or less fine morphologies have been revealed. Unexpectedly, a few samples showed diffuse α_I-spherulites with distinct Maltese crosses, whose origin has not been fully understood. As the diffuse appearance was only visible in compression-molded samples, it is likely that a combination of the overall chemical structure and the sample preparation conditions can be made responsible. The thin-sections revealed more or less visible skin-core morphologies. The nucleation effect was clearly visible and finer spherulite sizes have been revealed as fine textures. Moreover, the disappearance of the clearly visible skin zone has been observed for all samples significantly improving the optical properties. In general, samples with haze values

between 30 and 50 % exhibit clearly visible reduced spherulite sizes, but nevertheless samples with haze values below 30 % show significant finer textures. The general observed tendencies fit to the common known theories and nucleation density seems to be an important factor. Additionally, the homogenous dispersibility of the additives seems to be as well a decisive factor and this might be the reason, why some injection-molded parts show less improved optical properties. Overall, it has not been possible to determine structure property relationships, but previous findings can be confirmed that not necessarily high nucleation efficiencies are needed to obtain good optical properties.

The degree of crystallinity was investigated based on DSC melting endotherms. The crystallinity of the nucleated samples is not significant and shows a typical slight increase up to values of around 50 %. The samples color is in most cases only negligibly affected. Only samples with a 5 % weight loss temperature below 220 °C show significant increased YI values, due to decomposition of some additive.

The temperature dependency during compounding and the influence of the particle size was investigated and it has been revealed that the efficiency of the lead additive is hardly affected by these changes. The results express a good solubility or at least a transformation process of the additive during processing in the polymer melt. The lead structure undergoes a maximum threshold concentration, which expresses the additives solubility limit. Exceeding this threshold leads to a haze increase, caused by the formed superstructures[3, 113]. The general good solubility of the lead structure enables compounding at lower temperatures, which in the end prevents decomposition of the additives.

Finally, by testing the lead structure, in a polypropylene copolymer resin it has been demonstrated that the novel library of nucleating and clarifying agents can be applied to common market relevant PP resins.

This chapter showed, that the substitution pattern on the benzylidene ‘wings’ influences the solubility and the final performance of the additives. Here as well, no sound tendencies could be drawn. In general, the overall chemical structure heavily influences the stacking and arrangement of the molecules. This triggers the overall network formation process and the lateral growth rate of the formed fibrils. These two parameters in turn determine the nucleation density which is induced by the additives. Therefore, the outcome of these experiments is that the overall chemical structure and the ability to form fine narrow networks is important to induce an as small as possible fibrillar scaffold.

7. Conclusion and Outlook

The present thesis dealt with the design, development and screening of novel nucleating and clarifying agents for polypropylene. The investigated family of dibenzylidene-*L*-gulonic acid derivatives represents in a historical context a further development in the long lasting search for highly efficient nucleating and or clarifying agents based on sugar acetals [53–56]. The major advantage of this class is having an additional modifiable functional group giving access towards different molecule geometries and thus different possible active surfaces compared to sorbitol based derivatives. The versatile chemistry and the broad range of available 'tails' gives access towards a huge library of structures, which allows to determine the relation between structure, properties, performance and geometries.

The underlying results revealed that not all C_6-polyols are capable to undergo a diacetalization reaction. Dibenzylidene-*L*-gulonic acid derivatives have been identified as the ideal model structure to develop a whole library, which allows targeted derivatization not only on the benzylidene 'wings', but also on the terminal moiety. The obtained 'library' delivered additives with customized thermal properties. These properties allowed to analyze the importance of melting and recrystallization of the pure additive in order to build up a network in the polymer melt. Indeed, all of the obtained novel additives induced nucleation and specific derivatives improved the optical properties of isotactic polypropylene as well. Unlike the typical α-phase nucleation of sugar acetals, a special derivative of this family has been identified as a 'hybrid' nucleating agent, inducing a mixture of α- and β-polymorphs. Depending on the overall chemical structure, derivatives of this family confirmed both common ('soluble' and 'dispersion' type) mechanisms for nucleating and clarifying iPP. The soluble derivatives showed a pronounced nanofibrillar network formation, allowing the induction of a high nucleation density. The identified lead structures enabled to achieve comparable results to some of the common nucleating and clarifying agents, although there is room for further improvement to reach the level of the state of the art derivatives. Nevertheless, the aim to gain further insights into a potential structure activity relation was achieved, as some important parameter governing nucleation could be identified.

Currently, future research will still depend on the known trial and error approach. A possible route to potential guidelines could be to focus on the additive geometry and the lattice match between additive and polypropylene. The stacking distance seems to be an important factor. The novel developed additives enable to vary the distance by insertion of different substituents on the 'tail'.

The potential key step to investigate is the lateral growth rate of the additive fibrils. By gaining a better understanding of the properties and conditions affecting this parameter, it might be possible to influence the development of the fibrils in a controlled way. This in the end enables to design an ultra-fine scaffold, which induces outstanding nucleation and clarification. Therefore, the additive fibrils need to form networks that do not exceed the wavelength of visible light.

Furthermore, having demonstrated the effectiveness of the novel additives in iPP, the question remains, whether they can be applied in other semi-crystalline polymers as well. Transferability

to the common used high-density polyethylene (HDPE) would solve the problem of a lack of transparency of the material. Considering the high nucleation and crystal growth rate, the nucleation of HDPE remains a challenging topic. However, by understanding the lateral growth rate one could trigger the growth rate of the additive network, enabling the adaption to the specific needs for nucleating HDPE.

In addition, the possibility to induce the β-form of iPP could advantageously be explored further. Potential efficient β-inducing nucleating agents with high dispersibility due to solubility would enable the development of iPP with interesting properties.

8. Summary

The topic of the present thesis was the design, development and evaluation of novel nucleating and clarifying agents for isotactic polypropylene. The focus was on the identification of structure-activity relationships, allowing to gain further insights into the nucleating and clarifying phenomena.

At first, it was necessary to identify a suitable substance class, which allowed for systematic variation of the chemical structure of the additives. Therefore, dibenzylidenesorbitol (DBS) and its derivatives functioned as a comparison system to develop similar structures. It turned out that most likely, due to the configuration of the hydroxyl groups, not all polyols consisting of a C_6 'backbone' are capable to undergo a diacetalization reaction. Dibenzylidene-*L*-gulonic acid (DBGAc) derivatives were identified as model structures and a broad 'library' of derivatives became accessible. The chemical structure was varied systematically by modifications on the 'tail' and different substitution pattern on the benzylidene 'wings'. A 'library', comprising of 34 derivatives, was synthesized to study structure-property relationships.

In a second step, the thermal properties of all additives were investigated setwise. Most of the additives, except for the DBGAc (**6**) derivatives, featured sufficient temperature stability under the commonly applied processing conditions of iPP at around 220 °C. Depending on the overall chemical structure and mainly influenced by the terminal functional group, the additives revealed two different thermal behaviors. The DBGAcMeE (**5**) and DBGA-*n* (**8**) derivatives predominantly exhibit a distinct melting and crystallization point, whereas most of the DBGAc (**6**) and DBGA (**7**) derivatives decompose subsequently during the melting process. It was found out that, by selection of the 'tail', the overall thermal behavior is determined and by varying the substitution pattern on the 'wings', slight stability improvements can be achieved.

The whole 'library' of dibenzylidene-*L*-gulonic acid derivatives was screened with regard to their ability to nucleate and clarify iPP in the concentration range from 0.03 to 0.60 wt%. The influence of the molecular structure on crystallization temperature and optical properties haze and clarity was discussed setwise. All derivatives were found to nucleate iPP with different levels of efficiency and selected derivatives were even found to improve haze and clarity values of injection-molded samples.

The most efficient nucleating agent, namely 3,5:4,6-bis-(3,5-dimethylbenzylidene)-*L*-gulonic acid methyl ester (**5d**), was capable to increase the crystallization temperature of iPP from 113.4 °C to 131.0 °C. The most efficient clarifying agent, namely 3,5:4,6-bis-(3,4-dimethylbenzylidene)-*L*-gulonic amide (**7c**), was capable to reduce the haze value from 63.9 % to 22.8 % and improve clarity from 44.1 % to 94.4 %. Both derivatives reached their best results at a concentration level of 0.30 wt%, but several derivatives were found to reach their top performance at the maximum applied loading level. For example 3,5:4,6-bis-(4-propylbenzylidene)-*L*-gulonic amide (**7h**) reduced the haze value by 37.7 % at a concentration of 0.60 wt%.

The opportunity to combine different functionalities by choosing different 'wings' and 'tails' enables to somehow design molecules with desired properties and different efficiencies on

crystallization temperature and optical properties. The variation revealed some basic structure property relations. Depending on the 'tail', the additives efficiency to clarify iPP was found to follow the tendency of DBGA (**7**) > DBGA-*n* (**8**) > DBGAcMeE (**5**) > DBGAc (**6**). In addition, the alkyl chain length of the DBGA-*n* derivatives influenced the additives efficiency as well and in certain cases, specific derivatives showed improved optical properties with decreasing alkyl chain length. However, the nucleation and clarification performance of the additives strongly depends on the substituents and the overall chemical structure.

Detailed experiments on selected derivatives were conducted to further explore the mechanism of action of the novel nucleating and clarifying agents. Besides typical α-nucleating and clarifying agents, 3,5:4,6-bis-(3,4-dimethylbenzylidene)-*L*-gulonic methyl amide (**8.1c**) was surprisingly found to be a 'hybrid' nucleating agent. The calculated k-value of 0.30 at a concentration of 0.60 wt% indicates that the α-phase is still the predominant one. To our knowledge, it is the first time that a dibenzylidene acetal based nucleating agent induces the β-phase and exhibits a good solubility in iPP, which is an outstanding property for β-nucleating agents.

The dissolution and recrystallization behavior of selected compounds was investigated via optical microscopy and rheology, revealing different phase behaviors in the iPP melt. Most of the additives were found to be highly soluble in the melt, only the DBGAc (**6**) set was found to be insoluble and to decompose partly during processing. Depending on the substitution pattern, the insoluble additives were able to induce nucleation by providing a finely dispersed particulate surface. All other derivatives bearing a different 'tail', as DBGAcMeE (**5**), DBGA (**7**) and DBGA-*n* (**8**), were at least soluble in the iPP melt and assembled into fibrillar networks upon cooling to provide a surface which induced nucleation and clarification. The overall chemical structure influenced heavily the fineness and density of the formed network. This was ultimately held responsible to determine the clarification potential of the additive. Especially the two most efficient clarifying agents, namely 3,5:4,6-bis-(3,4-dimethylbenzylidene)-*L*-gulonic amide (**7c**) and 3,5:4,6-bis-(4-propylbenzylidene)-*L*-gulonic amide (**7h**), were found to provide a nearly invisible network in the polymer melt. In addition, by having access to different melting and recrystallization profiles of the pure additives, it was possible to investigate the influence of the melting and recrystallization point on the nucleation process. As the fineness of the fibrils was held responsible, the lateral growth rate of the additive fibrils might be a decisive factor. The lateral growth rate, in turn, is likely to be influenced heavily by the overall molecular structure.

In a further step, the nucleation density was studied by optical microscopy on the basis of the induced spherulitic size in compression-molded samples, and in thin-sections of injection-molded samples. The experimental results in general revealed overall reduced spherulite sizes and matching increased nucleation efficiencies.

In a last step, the efficiency of the lead structure, namely 3,5:4,6-bis-(3,4-dimethylbenzylidene)-*L*-gulonic amide (**7c**), was evaluated under varied conditions, such as compounding temperature, additive particle size and different polypropylene resin types. The results showed

that the novel nucleating and clarifying additives are likely to be applied independently of the processing conditions.

For the first time, dibenzylidene sorbitol like structures were investigated systematically regarding their nucleation and clarifying ability, taking into account the influence of different functional ‘tails’ in combination with different substitution pattern on the benzylidene ‘wings’. As a general learning, the results demonstrate that the individual chemical structure and even minor changes have a significant impact on the performance of the respective additives. The common mechanism of nucleating and clarifying agents was confirmed, but it was not possible to reveal structure-property relations, which allow the design of a perfectly matching clarifying agent. Nevertheless, the results based on this ‘library’ of additives provide prerequisites to support future research to derive preliminary structure-performance relationships and may enable to draw empirical guidelines for the design of even better nucleating and clarifying agents.

9. Zusammenfassung

Das Ziel dieser Dissertation war die Identifizierung, Entwicklung und Evaluierung von neuen Nukleierungsmitteln und Transparenzverstärkern für isotaktisches Polypropylen. Der Fokus der Untersuchungen lag auf der Aufklärung von Struktur-Wirkungsbeziehungen, um einen tieferen Einblick in das zu Grunde liegende Phänomen der Nukleierung und Transparenzverstärkung zu erlangen.

Zuerst war es notwendig eine geeignete Substanzklasse zu identifizieren, welche eine systematische Variation der chemischen Struktur des Additivs ermöglichte. Um ähnliche Strukturen zu entwickeln, wurden die Transparenzverstärker aus der Produktfamilie der Dibenzylidensorbitole (DBS) als Vergleichssystem herangezogen. Wie sich herausstellte ist es vermutlich aufgrund der Konfiguration der Hydroxylgruppen nicht möglich alle Polyole, die aus einem C_6-Rückgrat bestehen, einer zweifachen Acetalisierung zu unterziehen. Derivate der Dibenzyliden-*L*-gulonsäure konnten jedoch als Modellstruktur identifiziert werden. Auf deren Basis war es möglich eine umfangreiche Molekül-Bibliothek zu synthetisieren. Anhand von Modifikationen am funktionalen Säurerest und durch die Wahl verschiedener Substitutionsmuster an den beiden Benzyliden-Resten wurde die chemische Struktur systematisch variiert. Es wurden 34 Strukturen synthetisiert, um deren Struktur–Eigenschaftsbeziehungen zu studieren.

In einem zweiten Schritt wurden die thermischen Eigenschaften aller Substanzen anhand von Gruppen untersucht. Die meisten Substanzen wiesen eine ausreichende Temperaturstabilität unter den üblichen Verarbeitungsbedingungen von iPP bei ca. 220 °C auf. Nur die DBGAc (**6**) Derivate stellten eine Ausnahme dar. Abhängig von der jeweiligen chemischen Struktur und vor allem der funktionellen Endgruppe zeigten die Moleküle zwei unterschiedliche thermische Verhaltensweisen. Die DBGAcMeE (**5**) und DBGA-*n* (**8**) Derivate zeigen überwiegend einen ausgeprägten Schmelz- und Kristallisationspunkt, wohingegen die meisten DBGAc (**6**) und DBGA (**7**) Derivate gleich nach dem Schmelzvorgang in die Zersetzung übergehen. Es zeigte sich, dass die Wahl der funktionellen Endgruppe das thermische Verhalten der Moleküle bestimmt und sich durch Variation der Substitutionsmuster Stabilitätsverbesserungen erzielen lassen.

Die nukleierungs- und/oder transparenzverstärkende Wirkung der neuen Dibenzyliden-*L*-gulonsäure Derivate in isotaktischem Polypropylen wurde in einem Konzentrationsbereich von 0.03 bis 0.60 Gew.% untersucht. Der Einfluss der molekularen Struktur auf die Kristallisationstemperatur und die optischen Eigenschaften *Trübung* (Haze) und *Bildschärfe* (Clarity) wurden gruppenweise diskutiert. Alle Derivate nukleieren iPP, jedoch mit unterschiedlicher Effektivität und ausgewählte Derivate zeigten sogar eine Verbesserung der Trübungs- und Bildschärfewerte von spritzgegossenen Mustern.

Das wirksamste Nukleierungsmittel, nämlich 3,5:4,6-bis-(3,5-Dimethylbenzyliden)-*L*-gulonsäuremethylester (**5d**), war in der Lage die Kristallisationstemperatur von iPP von 113.4 °C auf 131.0 °C zu erhöhen. Der effizienteste Transparenzverstärker, 3,5:4,6-bis-(3,4-Dimethylbenzyliden)-*L*-gulonsäureamid (**7c**), war in der Lage den Trübungswert von 63.9 % auf 22.8 % zu reduzieren und den Bildschärfewert von 44.1 % auf 94.4 % zu erhöhen. Beide

Derivate erzielten ihre besten Ergebnisse bei einer Konzentration von 0.30 Gew.%. Dennoch wurden die besten Ergebnisse von zahlreichen Derivaten erst bei der höchsten verwendeten Konzentration erreicht. Als gutes Beispiel dient 3,5:4,6-bis-(4-Propylbenzyliden)-*L*-gulonsäureamid (**7h**), welches den Trübungswert um 37.7 % bei einer verwendeten Konzentration von 0.60 Gew.% reduziert.

Die Möglichkeit verschiedene Funktionalitäten durch die Wahl verschiedener Benzylidensubstituenten und funktionaler Endgruppen zu kombinieren, erlaubt es gezielt Moleküle mit gewünschten Eigenschaften und verschiedenen Wirksamkeiten in Bezug auf die Kristallisationstemperatur und die optischen Eigenschaften zu entwickeln. Die Variationen zeigten einige grundsätzliche Struktur-Eigenschaftsbeziehungen. Die Fähigkeit der Additive die optischen Eigenschaften von iPP zu verbessern folgt der Tendenz: DBGA (**7**) > DBGA-*n* (**8**) > DBGAcMeE (**5**) > DBGAc (**6**), ist jedoch abhängig von der funktionellen Endgruppe. Zusätzlich konnte festgestellt werden, dass auch die Kettenlänge der Alkylgruppe der DBGA-*n* Derivate die Effizienz der Additive beeinflusst und bestimmte Derivate die optischen Eigenschaften einiger Additiv/Polymer-Mischungen mit abnehmender Kettenlänge der Additivderivate verbessern. Allerdings hängt die nukleierungs- und transparenzverstärkende Wirkung stark von dem Substitutionsmuster und der allgemeinen Struktur der Additive ab.

Um den Wirkungsmechanismus der neuen Nukleierungsmittel und Transparenzverstärker besser zu verstehen, wurden detaillierte Untersuchungen an ausgewählten Derivaten durchgeführt. Röntgenographische Untersuchungen führten zu dem Ergebnis, dass die meisten der neuen Additive die α-Phase des PP induzieren. Dennoch zeigte überraschenderweise das Additiv 3,5:4,6-bis-(3,4-Dimethylbenzyliden)-*L*-gulonsäuremethylamid (**8.1c**), dass es eine Mischform aus α- und β-Phase induziert. Anhand des k-Wertes von 0.30 sieht man, dass die α-Phase jedoch noch überwiegt. Unseres Wissens nach ist es das erste Mal, dass dibenzylidenacetalbasierte Nukleierungsmittel die β-Phase anregen und zugleich eine gute Löslichkeit aufweisen.

Löslichkeits- und Rekristallisationsversuche von ausgewählten Substanzen wurde anhand von optischer Polarisationsmikroskopie und mittels Rheologie untersucht und zeigten unterschiedliche Phasenverhalten in der iPP Schmelze. Die meisten Additive besitzen eine gute Löslichkeit in der Schmelze, wobei die DBGAc (**6**) Derivate eine Ausnahme darstellen. Sie sind unlöslich und zersetzen sich teilweise während der Verarbeitung. Je nach Substitutionsmuster sind die unlöslichen Additive in der Lage den Nukleierungsprozess auszulösen, indem sie eine fein verteilte partikuläre Oberfläche erzeugen. Alle anderen Derivate, welche eine andere funktionelle Gruppe tragen, wie DBGAcMeE (**5**), DBGA (**7**) und DBGA-*n* (**8**), sind löslich in der iPP Schmelze und bilden ein feinfaseriges Netzwerk beim Abkühlen der Schmelze. Dieses Netzwerk bietet eine Oberfläche an der die Nukleierung beginnen kann. Es konnte festgestellt werden, dass die Feinheit und Dichte des erzeugten Netzwerkes durch die allgemeine chemische Struktur beeinflusst wird. Diese Tatsache wurde als Hauptursache für die transparenzverbessernde Wirkung des Additivs identifiziert. Vor allem für die beiden effizientesten Transparenzverstärker, nämlich 3,5:4,6-bis-(3,4-Dimethylbenzyliden)-*L*-gulonsäureamid (**7c**) und 3,5:4,6-bis-(4-Propylbenzyliden)-*L*-gulonsäureamid (**7h**), sind die gebildeten Netzwerke so fein, dass sie nur sehr schwer nachgewiesen werden konnten.

Zusätzlich konnte durch den Zugriff auf verschiedene Schmelz- und Rekristallisationsprofile der reinen Additive der Einfluss des Schmelz- und Rekristallisationspunktes auf den Nukleierungsprozess untersucht werden. Da die Feinheit des Netzwerkes wichtig zu sein scheint, ist auch die laterale Wachstumsrate des Additivnetzwerkes ein wichtiger Faktor. Diese wiederum scheint maßgeblich von der allgemeinen chemischen Struktur der Additive beeinflusst zu werden.

In einem weiteren Schritt wurde die Nukleierungsdichte auf Grundlage der Sphärolithgröße anhand von Polarisationsmikroskopischen Untersuchungen an formgepressten Proben und anhand von Dünnschnitten aus Spritzgusskörpern untersucht. Die Experimente bestätigen überwiegend bekannte Befunde, wie reduzierte Sphärolithgrößen und erhöhte Nukleierungseffizienzen.

Die Leitstruktur, 3,5:4,6-bis-(3,4-Dimethylbenzyliden)-*L*-gulonsäureamid (**7c**) wurde zusätzlich unter abgewandelten Bedingungen und in einem andren Polymertyp verarbeitet. Dabei wurden verschiedene Verarbeitungstemperaturen am Extruder, verschiedene Partikelgrößen, sowie ein anderer Polypropylen Typ untersucht. Die Ergebnisse deuten darauf hin, dass die neuen Nukleierungsmittel und Transparenzverstärker weitgehend unabhängig von den Prozessbedingungen verwendet werden können.

Zum ersten Mal wurden Sorbitol-ähnliche Strukturen anhand ihrer nukleierungs- und transparenzverstärkenden Wirkung unter Berücksichtigung des Einflusses verschiedener funktioneller Reste in Kombination mit verschiedenen Substitutionsmustern an den Benzyliden-Resten systematisch untersucht. Generell zeigen die Ergebnisse, dass die individuelle chemische Struktur und kleinste Veränderungen derer einen wesentlichen Einfluss auf die Wirksamkeit der jeweiligen Additive haben. Der allgemein bekannte Wirkungsmechanismus von Nukleierungsmitteln und Transparenzverstärkern konnte bestätigt werden, jedoch war es nicht möglich Struktur-Eigenschaftsbeziehungen aufzudecken, welche die Entwicklung eins idealen Transparenzverstärkers erlauben. Nichtsdestotrotz, liefern die Ergebnisse eine Grundlage für die zukünftige Erforschung von Struktur-Eigenschaftsbeziehungen und die Entwicklung von besseren Nukleierungsmitteln und Transparenzverstärkern.

10. Experimental Part

10.1. General remarks

10.1.1.Chemicals and Solvents

Chemicals and Solvents

All chemicals and solvents were used as received without further purification, if not stated otherwise. Demineralized water was obtained directly from the tab. For nuclear magnetic resonance (NMR) measurements deuterated solvents from Merck were employed.

Materials

The polymers used were isotactic polypropylene homopolymer, Moplen® HP 500 N (MFR = 12 g/10 min, M_n = 47 kg/mol, M_w = 393 kg/mol) and a random propylene copolymer, Moplen® RP 310 M (MFR 8.5 g/10 min) from Lyondell Basell. Isotactic polypropylene homopolymer Moplen® HP 500 N was used in powder form (< 1000 μm) as received from Ultrapolymers. Polypropylene random copolymer Moplen® RP 310 M was freeze milled in a Retsch ZM 200 before use. Both PP polymer types are slightly stabilized. Additional stabilization was done with 0.1 wt% Irganox® 1010, 0.1 wt% Irgafos® 168 and 0.1 wt% Ca-stearate before compounding.

The clarifying agents 1,3:2,4-bis(3,4-dimethylbenzylidene)sorbitol (**DMDBS**, Millad® 3988, CAS: 135861-56-2) and 1,2,3-trideoxy-4,6:5,7-bis-O-[(4-propylphenyl)methylene]-nonitol (**TBPMN**, Millad® NX 8000, CAS: 882073-43-0) were used as received from Milliken Chemical. The clarifying agent 1,3,5-tris(2,2-dimethylpropionylamino)benzene (Irgaclear® **XT** 386, CAS: 745070-61-5) was used as received from BASF. The clarifying agent proprietary mixture containing lithium 2,2'-methylenebis(2,4-di-tert-butylphenyl)phosphate and one further organic compound (ADK Stab **NA 71**, CAS: 85209-93-4) and the nucleating agent sodium 2,2'-methylene-bis-(2,4-di-tert-butylphenyl)-phosphate (ADK Stab **NA 11** UH, CAS: 85209-91-2) were used as received from Adeka Corporation. All further additives were synthesized according to general procedures described below.

10.1.2.Analytical Methods

Nuclear magnetic resonance spectrometry

Nuclear magnetic resonance *(NMR)* experiments ^{1}H-NMR and ^{13}C-NMR spectra were recorded on a Bruker Advance III, 400 MHz spectrometer at 26 °C at 400 MHz resp. 100 MHz. Chemical shifts (δ) are quoted (ppm) and are relative to tetramethylsilane (TMS) (δ = 0 ppm) as the internal standard or the residual solvent peak in dimethyl sulfoxide (DMSO-d_6) (δ 2.50 ppm, ^{1}H; δ 39.52 ppm, ^{13}C). All the deuterated NMR solvents were purchased from *Merck*. Multiplicities are indicated by *s* (singlet), *d* (doublet), *t* (triplet), *q* (quartet), *quint* (quintet), *m* (multiplet), *b* (broad), *dd* (doublet of doublet) and *dt* (doublet of triplet). Scalar coupling constants, *J*, are reported in Hertz (Hz). The assignments were verified using HSQC 2D-experiments if necessary.

Thin-layer chromatography

Analytical thin-layer chromatography (*TLC*) was performed on Merck silica gel plates (aluminum sheets precoated with silica (60 F_{254})). As mobile phase ethyl acetate – hexane (1:5) or ethyl acetate – hexane (4:1) were used. Visualization was accomplished with UV light at 254 nm or with Seebach's solution stain (2.5 g phosphomolybdic acid, 1 g $Ce(SO_4)_2$, 6 mL conc. H_2SO_4, 60 mL H_2O) with subsequent heating in hot air flow, unless other noted.

Mass spectrometry

High resolution mass spectra (*HR-MS*) were performed on an instrument from Thermo Scientific™ (GC: TRACE™ 1310; MSD: QExtractive GC). The details belonging to each device component can be taken from Table 10-1.

Table 10-1 Instrument data of HR-MS device

Device component	Description
Column	DB-1MS; 15 m; Id 0.25 mm; 0.1 mm Film; Fa. Agilent
Ionization	EI+; 40 - 1000 amu; 280 °C CI- Reactant gas methane; 40 - 1000 amu
Carrier Gas	Helium at 15 kPa; Split 20:1
Heat rate	T 1 = 60 °C; IT 1 = 0 min; HR 1 = 10 °C/ min T 2 = 340 °C; IT 2 = 240 min; HR 2 = 0 °C/ min
Injection	1 μl
Preparation	Solve in approx. 3 % in *N*,*N*-Dimethylformamide If necessary solve in a mixture of *N*,*N*-Dimethylformamide / *N*-Methyl-*N*-(trimethylsilyl)-trifluoracetamide (MSTFA) = 1 / 1 for 1 h at 80 °C

Thermal analysis

Thermogravimetric analysis (*TGA*) was measured under nitrogen atmosphere in an alumina 70 μl crucible on a Mettler Toledo TGA 1 (SF) and data were recorded with a standard heating rate of 10 K/min in a temperature range from 30 to 450 °C. The sample weight was about 10 mg. Decomposition temperatures of the pure additive refer to the temperature at 5 % weight loss ($T_{-5\ wt\%}$). Differential scanning calorimetry (*DSC*) decomposition experiments were performed in a single heating run from 30 to 450 °C on a Mettler Toledo DSC 821 under nitrogen in a glass 100 μl crucible with a heating rate of 3 K/min. Melting temperature (T_m) refers to the peak temperature and decomposition temperature ($T_{dec.}$) to the onset temperature. The investigated temperature range for a two-cycle heating-cooling experiment of the pure additive was selected according to the corresponding data obtained by TGA analysis and DSC decomposition measurements. The experiment was performed on a Mettler Toledo DSC 823e under nitrogen atmosphere in an alumina 40 μl crucible with a standard heating or cooling rate of 10 K/min. The sample weight was about 10 mg. Melting temperatures (T_m^1, T_m^2) and crystallization temperatures (T_c^1, T_c^2) refer to the peak temperatures. Upper numbers indicate the heating/cooling round. In case of subsequent decomposition after melting the melting

temperature obtained from the DSC decomposition experiment was used as T_m of the pure additive.

Differential scanning calorimetry (*DSC*) of the polymer compound was performed on a Mettler Toledo DSC 3+ under nitrogen atmosphere in an alumina 40ul crucible with a standard heating or cooling rate of 10 K/min. Prior to recording of thermograms, the samples were held at 230 °C for 5 min to erase "thermal history" and prevent self-seeding of iPP. Each analysis refers to a two-cycle heating-cooling experiment. The sample weight was about 10 mg. Reported melting ($T_{m,p}$) and crystallization temperatures ($T_{c,p}$) refer to the peak temperatures of 2nd heating and 1st crystallization run in the corresponding thermograms. The degree of crystallinity of the polymer was calculated from the enthalpy of fusion (ΔH_m), derived from the endothermic melting peak, adopting a value of 209 J/g (ΔH_m^0) [145] for 100 % crystalline isotactic polypropylene.

The reported values are based on values from single measurements. For validation, a series of 5 measurements each has been performed with the 'control' iPP homopolymer and iPP/DMDBS (0.30 wt%). For iPP homopolymer an average $T_{c,p}$ of 113.78 °C with a standard deviation of 0.28 °C has been determined. In case of the nucleated sample an average $T_{c,p}$ of 130.87 °C with a standard deviation of 0.39 °C has been calculated.

Rheology

A Discovery hybrid rheometer (HR-3, TA Instruments) was used to measure the temperature dependency of the absolute value of the complex viscosity of various compounds in the range of 110 – 240 °C. Disk-shaped specimens (25 mm diameter, 1 mm thickness) punched from injection-molded plaques were used. Characterization was conducted with a parallel-plate setup (r = 12.5 mm, h = 0.8 mm). Each specimen was initially heated to 240 °C and held for 5 min to achieve thermal equilibrium. A 2 % strain was applied at an oscillation frequency of 10 rad/s, and the temperature was subsequently decreased at a rate of 2 °C/min until solidification of iPP occurred. Inaccurate, erroneous measurements during solidification prior to 110 °C are hidden.

Optical properties

The standard optical characteristics 'transmission', 'haze' and 'clarity' were measured for the injection-molded discs with a 'Haze-Gard Plus' instrument (BYK Gardner GmbH), which conforms to ASTM D-1003 [156]. Total transmittance is the ratio of total transmitted light to incident light. It is reduced by reflectance and absorbance. Haze is defined as that portion of visible light that is scattered at wider angles ($2.5° < \theta < 90°$) and is a measure for the turbidity of a sample. Clarity, usually refers to the scattering contribution at small angles ($\theta < 2.5°$) and is related to the sharpness of an object when viewed through the sample [58, 157, 158]. The reported values are the average of at least three measured samples. Typically, the standard deviations for the measured three samples were below 0.5 % for transmission, haze and clarity. Deviations likely result from the additive distribution and the sample surface. The standard deviation for two independent processing steps of the 'control' material was found to be in the following range: transmission ~0.5 %, haze ~2.0 % and clarity ~1.5 %.

Optical microscopy

Optical microscopy combined with heating and cooling experiments was carried out with a Leica DMLM microscope equipped with a Leica Heating Stage 350. The heating stage is connected to a control transformer and for heating purposes low voltage is used. Heating and cooling rate is about 10 K/min. The microscope was equipped with a Leica DFC 450 camera and micrographs were taken between crossed polarizers. Otherwise optical microscopy was carried out with an Olympus BX 53 microscope and micrographs were taken between crossed polarizers.

β-Content

Wide-angle X-ray scattering (*WAXS*) 2D patterns were recorded with a Xenocs Xeuss SAXS/WAXS system with a GeniX 3D Ultra low divergence source (wavelength Cu K_α (λ = 1.54 Å)), and a Pilatus 300K Detector from Dectris. The sample-to-detector distance was calibrated using silver behenate. 2D spectra were converted into 1D scattering curves. According to standard procedures described in literature, the content of the β-crystal modification was calculated form X-ray data employing the relation:

$$k = \frac{H_{\beta(300)}}{H_{\beta(300)} + H_{\alpha(110)} + H_{\alpha(040)} + H_{\alpha(130)}} \qquad (1)$$

Measurements were done with 1.0 mm thick injection-molded iPP plaques comprising, if not stated otherwise, a standard amount of 0.30 wt% of the various additives.

Yellowness index

Yellowness was measured for the injection-molded discs with a CM-5 Spectrophotometer (Konica Minolta), which conforms to ASTM E313 [159].

Scanning electron microscopy

Scanning electron microscopy (SEM) images were taken on a Zeiss, DSM 982 GENIMI operating at 3.0 kV. Samples of the xerogel (0.1 wt% additive/*n*-octanol) were prepared by drying the gel in air for several days and then sputter-coated with a 15 nm layer of chromium using a QUORUM EMS150T S.

High Temperature Gel Permeation Chromatography (HT-GPC)

HT-GPC analyses were performed on an Agilent PL-GPC 220 High Temperature GPC System equipped with an IR detector (Modell IR 4, PolymerChar). The PP sample was dissolved at a concentration of 2.0 mg/mL in 1,2,4-Trichlorobezene at 160 °C. The dissolution time prior to injection was 4 h. The injection volume was 200 μL and the chromatographic separation was performed using an Agilent PLgel Olexis Guard (50 x 7.5 mm) as precolumn and three Agilent PLgel Olexis (300 x 7.5 mm) columns at a flow rate of 1.0 mL/min and a temperature of 150 °C.

10.1.3.Methods

Methodology of parallel reaction station

All test series were performed in 150 mL injection vials, which could be closed with alumina crimp caps. The caps have a predetermined breaking point at about 1.0 bar. For heating a 6.5 cm high aluminum block with an adapted radius for a Heidolph magnetic stirrer was used. The aluminum blocks contain five deep (5.0 cm) bores with the diameter of the reaction vessels and one drill for the temperature sensor. Reagents were weighted in and a 2.5 mm magnetic stirrer was added, before the vessels were closed with the caps. All temperatures relate to the temperature of the heating blocks.

Gel Preparation

The relevant additive sample (0.010 g) was weighted into a capped test tube and filled up to 1.000 g with *n*-octanol. The sample was sonicated and heated up until a clear solution in the heat flow of a heating gun. The solution was cooled to room temperature for ~1 h and the tube was inverted. Gelation was considered successful if no sample flow occurred.

Sample Preparation

Previous to compounding, various mixtures of stabilizers, additives and powdery iPP were dry blended in a plastic bag and shaken for 2 min until sufficient distribution. Due to the three compounding cycles and the fact, that the used isotactic polypropylene type (Moplen® HP 500 N) is only minimal stabilized additional stabilization (0.1 wt% Irgafos ® 168, 0.1 wt% Irganox® 1010, 0.1 wt% Calcium stearate) was added. The range of additive contents varies between 0.03 and 0.60 wt%. It has to be noted that the reported concentrations refer to the respective initial weight fraction of the additive in the sample. Slight deviations may have developed during processing of the samples.

Compounding

Mixtures of powdered iPP (Moplen® HP 500 N), Irganox® 1010, Irgafos® 168, Ca-stearate and 0.03 wt %, 0.15 wt%, 0.30 wt%, 0.45 wt%, 0.60 wt% of the respective additive were compounded at 100 rpm in three cycles in a single screw extruder (Weber ET20, 20 mm, 25D) at 220 °C, if not stated otherwise. Afterwards the mixtures were discharged. 'Control' samples were treated in a similar way.

Figure 10-1 Quick compression type screw with two mixing sections (1x4 and 1x2) and decompression zone [160].

Additional experiments have been conducted on a lab scale twin screw extruder (Thermo Scientific™ Process 11, 11 mm, 40D), which setup is comparable to typical industrial used twin screw extruders.

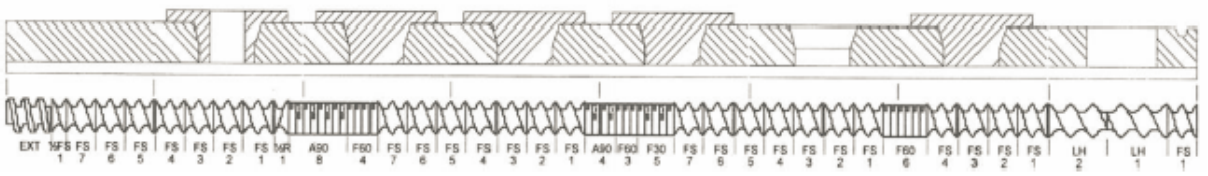

Figure 10-2 Screw configuration of the Process 11 twin screw extruder [161].

Injection molding

Injection molding was performed with an Arburg Allrounder 2200 S 250-60 (22 mm, 20D). The previously pelletized, compounded granulate was melted at 220 °C and injection-molded in a polished droplet formed mold. The mold temperature was at about 50 °C. The collected test specimen had the following form (Figure 10-3) and a thickness of 1.0 mm. About 10-20 samples were injection-molded.

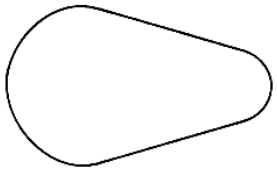

Figure 10-3 Dimensions of injection-molded plaques (thickness 1.0 mm, 6.0 mm height, 4.0 mm width)

Film Preparation

Films for optical microscopy were prepared by melt-compression molding previously compounded material between microscope slide and cover glass. Therefore the samples were cut with a razor blade and were held for 120 sec at 220 °C, weighted with 4 kg. Followed by quenching to room temperature.

Microtome

Thin sections were prepared with a Leica RM 2245 Semi-Automated Rotary Microtome. Therefore 10 μm thin sections were cut orthogonal to the molding direction.

10.2. Synthesis

10.2.1.Procedure for the preparation of *L*-Gulonic acid gamma lactone (2)

L-Gulonic acid gamma lactone (**2**)

A solution of 23.1 g (0.13 mol) *L*-ascorbic acid (**1**) and 0.1 g Corlite in 170.0 g water was hydrogenated over 3.0 g of 5 % Ru/Al_2O_3 (H213 B/D) in a hydrogenator at 50 °C, 30-40 bar hydrogen pressure and 1300 rpm for 6 h. After steady uptake of hydrogen, the reaction was cooled down and the catalyst was removed by filtration over celite. Water was removed by lyophilisation to yield 22.66 g (97 %) of a white fluffy powder, which was pure by NMR. On recrystallization of the sample from water, crystalline material was obtained and identical to commercial [162] L-gulonic acid gamma lactone (**2**). m.p.: 186.6 °C; lit.[162]: 187-190 °C; $[\alpha]_D^{19}$: + 55° (c= 4, H_2O); ^{1}H-NMR (400 MHz, DMSO-d_6): δ = 3.44-3.55 (m, 2, -CH_2); 3.71-3.77 (m, 1, -CH); 4.16-4.24 (m, 2, -CH); 4.43-4.45 (q, 1, -CH); 4.66 (t, 1, -OH); 4.97-4.98(d, 1, -OH); 5.33-5.34 (d, 1, -OH); 5.78-5.80 (d, 1, -OH).

10.2.2.Procedure for the preparation of benzaldehyde dimethyl acetal derivatives (4)

General procedure [102, 103]

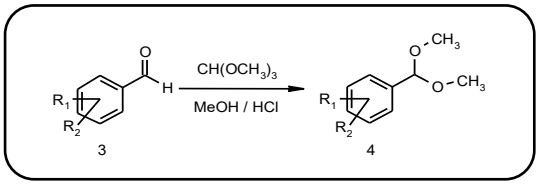

A round bottomed flask, equipped with heating bath, condenser and a stirrer, was charged with trimethylorthoformiate (6.00 Eq.), dry methanol (500 mL/mol), concentrated hydrochloric acid (0.11 Eq.) and the relevant substituted benzaldehyde (**3**, 1.00 Eq.). The solution was stirred for approximately 24 h at 40 °C and in between at room temperature until TLC showed full conversion of the starting material. A saturated sodium carbonate solution (50 mL/mol) was added to the reaction mixture. The formed precipitate was filtered off and the liquid phase was extracted with petroleum benzene (3 x 100 mL). The combined organic phases were dried over sodium sulfate, filtered off and the organic layer was evaporated to yield the relevant substituted benzaldehyde dimethyl acetal (**4**).

4-Methylbenzaldehyde dimethyl acetal (**4b**)

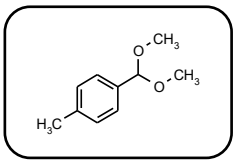

According to the general procedure 4-methylbenzaldehyde (**3b**) 0.208 mol, 25.00 g) was treated with trimethylorthoformiate (1.248 mol, 136.53 mL) and concentrated hydrochloric acid (0.023 mol, 1.89 mL). General workup yielded the product **4b** as a clear liquid (31.1 g, 90 %). R_f = 0.80 (ethyl acetate – hexane 1:5); ^{1}H-NMR (400 MHz, DMSO-d_6): δ = 2.30 (s, 3, -CH_3); 3.21 (s, 6, -OCH_3); 5.33 (s, 1, -OCHO-); 7.17-7.28 (m, 4, aromatic).

3,4-Dimethylbenzaldehyde dimethyl acetal (**4c**)

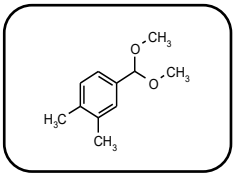

According to the general procedure 3,4-dimethylbenzaldehyde (**3c**) (0.186 mol, 25.00 g) was treated with trimethylorthoformiate (1.118 mol, 122.29 mL) and concentrated hydrochloric acid (0.021 mol, 1.79 mL). General workup yielded the product **4c** as a clear liquid (32.2 g, 96 %). R_f = 0.81 (ethyl acetate – hexane 1:5); ^{1}H-NMR (400 MHz, DMSO-d_6): δ = 2.21 (s, 3, -CH_3); 2.22 (s, 3, -CH_3); 3.21 (s, 6, -OCH_3); 5.29 (s, 1, -OCHO-); 7.07-7.14 (m, 3, aromatic).

3,5-Dimethylbenzaldehyde dimethyl acetal (**4d**)

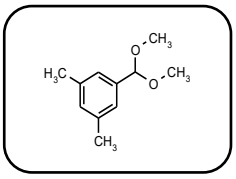

According to the general procedure 3,5-dimethylbenzaldehyde (**3d**) (0.186 mol, 25.00 g) was treated with trimethylorthoformiate (1.118 mol, 122.29 mL) and concentrated hydrochloric acid (0.021 mol, 1.70 mL). General workup yielded the product **4d** as a clear liquid (27.4 g, 82 %). R_f = 0.83 (ethyl acetate – hexane 1:5); ^{1}H-NMR (400 MHz, DMSO-d_6): δ = 2.27 (s, 3, -CH_3); 2.27 (s, 3, -CH_3); 3.22 (s, 6, -OCH_3); 5.28 (s, 1, -OCHO-); 6.95-6.98 (m, 3, aromatic).

2,4-Dimethylbenzaldehyde dimethyl acetal (**4e**)

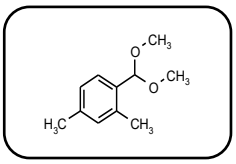

According to the general procedure 2,4-dimethylbenzaldehyde (**3e**) (0.186 mol, 25.00 g) was treated with trimethylorthoformiate (1.118 mol, 122.29 mL) and concentrated hydrochloric acid (0.21 mol, 1.70 mL). General workup yielded the product **4e** as a clear liquid (30.6 g, 91 %). R_f = 0.80 (ethyl acetate – hexane 1:5); ^{1}H-NMR (400 MHz, DMSO-d_6): δ = 2.25 (s, 3, -CH_3); 2.26 (s, 3, -CH_3); 3.21 (s, 6, -OCH_3); 5.41 (s, 1, -OCHO-); 6.97-6.99 (t, 2, aromatic); 7.29-7.32 (d, 1, aromatic).

2,5-Dimethylbenzaldehyde dimethyl acetal (**4f**)

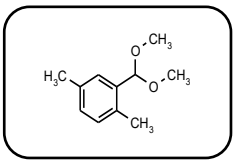

According to the general procedure 2,5-dimethylbenzaldehyde (**3f**) (0.186 mol, 25.00 g) was treated with trimethylorthoformiate (1.118 mol, 122.29 mL) and concentrated hydrochloric acid (0.021 mol, 1.70 mL). General workup yielded the product **4f** as a clear liquid (29.8 g, 89 %). R_f = 0.80 (ethyl acetate – hexane 1:5); ^{1}H-NMR (400 MHz, DMSO-d_6): δ = 2.25 (s, 3, -CH_3); 2.27 (s, 3, -CH_3); 3.21 (s, 6, -OCH_3); 5.41 (s, 1, -OCHO-); 7.02-7.07 (m, 2, aromatic); 7.24 (s, 1, aromatic).

2,6-Dimethylbenzaldehyde dimethyl acetal (**4g**)

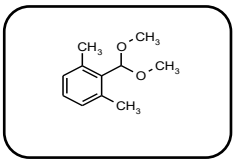

According to the general procedure 2,6-dimethylbenzaldehyde (**3g**) (0.186 mol, 25.00 g) was treated with trimethylorthoformiate (1.118 mol, 122.29 mL) and concentrated hydrochloric acid (0.021 mol, 1.70 mL). General workup yielded the product **4g** as a clear liquid (30.12 g, 90 %). R_f = 0.80 (ethyl acetate – hexane 1:5); ^{1}H-NMR (400 MHz, DMSO-d_6): δ = 2.37 (s, 6, -CH_3); 3.32 (s, 6, -OCH_3); 5.48 (s, 1, -OCHO-); 6.96-6.98 (d, 2, aromatic); 7.06-7.10 (m, 1, aromatic).

4-Propylbenzaldehyde dimethyl acetal (**4.1h**)

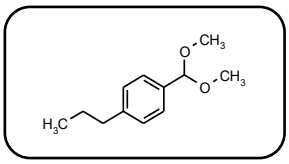

According to the general procedure 4-propylbenzaldehyde (**3h**) (0.169 mol, 25.00 g) was treated with trimethylorthoformiate (1.012 mol, 110.74 mL) and concentrated hydrochloric acid (0.019 mol, 1.55 mL). General workup yielded the product **4.1h** as a clear liquid (31.5 g, 96 %). R_f = 0.74 (ethyl acetate – hexane 1:5); ^{1}H-NMR (400 MHz, DMSO-d_6): δ = 0.86-0.90 (t, 3, -CH_3); 1.54-1.63 (m, 2, -CH_2); 2.53-2.57 (t, 2, -CH_2); 3.22 (s, 6, -OCH_3); 5.34 (s, 1, -OCHO-); 7.17-7.19 (d, 2, aromatic); 7.28-7.29 (d, 2, aromatic).

4-Isobutylbenzaldehyde dimethyl acetal (**4i**)

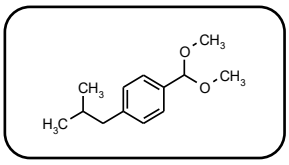

According to the general procedure 4-isobutylbenzaldehyde (**3i**) (0.154 mol, 25.00 g) was treated with trimethylorthoformiate (0.925 mol, 101.15 mL) and concentrated hydrochloric acid (0.017 mol, 1.40 mL). General workup yielded the product **4i** as a clear liquid (28.2 g, 88 %). R_f = 0.78 (ethyl acetate – hexane 1:5); ^{1}H-NMR (400 MHz, DMSO-d_6): δ = 0.84 (s, 3, -CH_3); 0.86 (s, 3, -CH_3); 1.77-1.87 (m, 1, -CH); 2.43-2.45 (d, 2, -CH_2); 3.22 (s, 6, -OCH_3); 5.34 (s, 1, -OCHO-); 7.14-7.16 (d, 2, aromatic); 7.27-7.29 (d, 2, aromatic).

10.2.3.Procedure for the preparation of 3,5:4,6-dibenzylidene-*L*-gulonic acid alkyl ester derivatives (5)

General procedure [99–101]

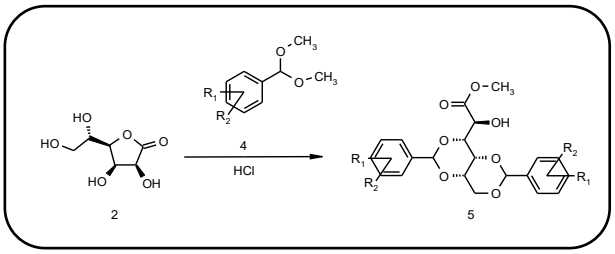

A round bottomed flask, equipped with a mechanical stirrer, was charged with *L*-gulonic acid gamma lactone (**2**) (1.00 Eq.), relevant substituted benzaldehyde dimethyl acetal (**4**) (4.00 Eq.), concentrated hydrochloric acid (0.40 Eq.) The suspension was stirred for about 24 h at room temperature. The formed participate was diluted with acetonitrile (725 mL/mol) for better stirring and availability of unreacted starting material. The suspension was stirred until TLC showed full consumption of the starting material. The product was filtered off and washed with water (3 x 100 mL) and then with diethyl ether (3 x 100 mL). The product was dried under vacuum at 110 °C for 12 h to yield the relevant substituted 3,5:4,6-dibenzylidene-L-gulonic acid methyl ester (**5**).

3,5:4,6-Dibenzylidene-L-gulonic acid methyl ester (**5a**)

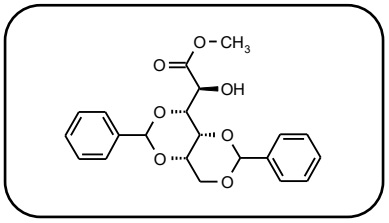

According to the general procedure *L*-gulonic acid gamma lactone (**2**, 0.067 mol, 11.88 g) was reacted with the relevant substituted benzaldehyde dimethyl acetal (**4a**, 0.267 mol, 40.02 mL) and concentrated hydrochloric acid (0.027 mol, 2.21 mL). For better dilution 50.00 mL acetonitrile were added. General workup yielded the product **5a** as a white powder (22.72 g, 88 %). R_f = 0.70 (ethyl acetate – hexane 4:1); ^{1}H-NMR (400 MHz, DMSO-

d_6): δ = 3.63 (s, 3, -OCH_3); 4.02-4.30 (m, 6, -CH,-CH_2); 5.69 (s, 1, -OCHO-); 5.70 (s, 1, -OCHO-); 6.11-6.13 (d, *J* = 6.1 Hz, -OH); 7.36-7.48 (m, 10, aromatic); ^{13}C-NMR (100 MHz, DMSO-d6): δ = 52.0 (1, -OCH_3); 68.1; 69.7; 70.2; 78.7 (5, -CH-, -CH_2-); 99.5; 99.7 (2, -OCHO-); 126.4; 126.5; 128.46; 128.49; 129.1; 129.2; 138.5; 139.0 (12, aromatic); 173.2 (1, -CO_2-); HRMS (EI): Calculated for $C_{21}H_{21}O_7$ $[M-H]^+$ 385.1287; found 385.1282; TGA: $T_{-5\ wt\%}$ = 269.17 °C; DSC: T_m = 210.79 °C, $T_{dec.}$ = 291.34 °C; T_m^1 = 206.40 °C (-129.12 J/g); T_c^1 = 185.50 °C (98.22 J/g); T_m^2 = 203.25 °C (-102.45 J/g); T_c^2 = 160.28 °C (86.47 J/g).

3,5:4,6-di-(4-Methylbenzylidene)-*L*-gulonic acid methyl ester (**5b**)

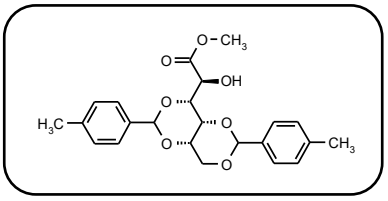

According to the general procedure *L*-gulonic acid gamma lactone (**2**, 0.012 mol, 2.14 g) was reacted with the relevant substituted benzaldehyde dimethyl acetal (**4b**, 0.048 mol, 8.09 mL) and concentrated hydrochloric acid (0.005 mol, 0.40 mL). For better dilution 10.00 mL acetonitrile were added. General workup yielded the product **5b** as a white powder (4.53 g, 91 %). R_f = 0.78 (ethyl acetate – hexane 4:1); ^{1}H-NMR (400 MHz, DMSO-d_6): δ = 2.30 (s, 3, -CH_3); 2.31 (s, 3, -CH_3); 3.62 (s, 3, -OCH_3); 3.98-4.28 (m, 6, -CH,-CH_2); 5.63 (s, 1, -OCHO-); 5.64 (s, 1, -OCHO-); 6.08-6.10 (d, *J* = 6.1 Hz, -OH); 7.17-7.35 (m, 8, aromatic); ^{13}C-NMR (100 MHz, DMSO-d_6): δ = 21.3 (2, -CH_3); 51.9 (1, -OCH_3); 68.1; 69.6; 70.1; 78.7 (5, -CH-, -CH_2-); 99.6; 99.8 (2, -OCHO-); 126.4; 126.5; 128.9; 129.0 (8, -CH-, aromatic); 135.7; 136.2; 138.3; 138.4 (12, aromatic); 173.3 (1, -CO_2-); HRMS (EI): Calculated for $C_{23}H_{25}O_7$ $[M-H]^+$ 413.1600, found 413.1594; TGA: $T_{-5\ wt\%}$ = 281.31 °C; DSC: T_m = 220.15 °C, $T_{dec.}$ = 278.38 °C; T_m^1 = 226.12 °C (-131.16 J/g); T_c^1 = 167.02 °C (62.37 J/g); T_m^2 = 213.54 °C (-61.69 J/g); T_c^2 = 151.13 °C (21.60 J/g).

3,5:4,6-bis-(3,4-Dimethylbenzylidene)-*L*-gulonic acid methyl ester (**5c**)

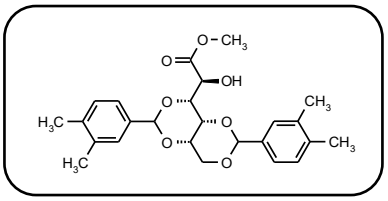

According to the general procedure *L*-gulonic acid gamma lactone (**2**, 0.069 mol, 12.35 g) was reacted with the relevant substituted benzaldehyde dimethyl acetal (**4c**, 0.277 mol, 50.71 mL) and concentrated hydrochloric acid (0.028 mol, 2.30 mL). For better dilution 50.00 mL acetonitrile were added. General workup yielded the product **5c** as a white powder (30.69 g, 93 %). R_f = 0.82 (ethyl acetate – hexane 4:1); ^{1}H-NMR (400 MHz, DMSO-d_6): δ = 2.22 (s, 6, -CH_3); 2.23 (s, 6, -CH_3); 3.62 (s, 3, -OCH_3); 3.96-4.27 (m, 6, -CH,-CH_2); 5.60 (s, 2, -OCHO-); 6.07-6.08 (d, *J* = 6.1 Hz, -OH); 7.07-7.22 (m, 6, aromatic); ^{13}C-NMR (100 MHz, DMSO-d_6): δ = 19.7; 19.9 (4, -CH_3); 51.9 (1, -OCH_3); 68.05; 68.11; 69.6; 70.2; 78.8 (5, -CH-, -CH_2-); 99.7; 99.9 (2, -OCHO-); 123.9; 124.0; 127.5; 127.6; 129.45; 129.47; 136.07; 136.11; 136.6; 136.97; 137.03 (12, aromatic); 173.3 (1, -CO_2-); HRMS (EI): Calculated for $C_{25}H_{29}O_7$ $[M-H]^+$ 441.1913, found 441.1910; TGA: $T_{-5wt\%}$ = 292.34 °C; DSC: T_m = 250.07 °C, $T_{dec.}$ = 298.80 °C; T_m^1 = 249.40 °C (-112.78 J/g); T_c^1 = 195.11 °C (51.93 J/g); T_m^2 = 232.96 °C (-57.88 J/g); T_c^2 = 166.70 °C (21.35 J/g).

3,5:4,6-bis-(3,5-Dimethylbenzylidene)-*L*-gulonic acid methyl ester (**5d**)

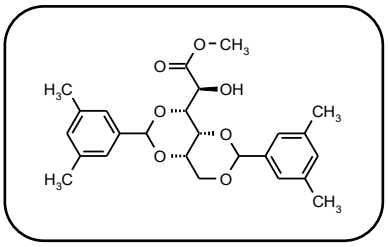

According to the general procedure *L*-gulonic acid gamma lactone (**2**, 0.042 mol, 7.41 g) was reacted with the relevant substituted benzaldehyde dimethyl acetal (**4d**, 0.152 mol, 27.79 mL) and concentrated hydrochloric acid (0.017 mol, 1.38 mL). For better dilution 30.00 mL acetonitrile were added. General workup yielded the product **5d** as a white powder (16.78 g, 91 %). R_f = 0.84 (ethyl acetate – hexane 4:1); ^{1}H-NMR (400 MHz, DMSO-d_6): δ = 2.27 (s, 6, -CH_3); 2.28 (s, 6, -CH_3); 3.64 (s, 3, -OCH_3); 3.96-4.24 (m, 6, -CH,-CH_2); 5.60 (s, 2, -OCHO-); 6.09-6.10 (d, *J* = 6.1 Hz, -OH); 6.98; (s, 4, aromatic); 7.06 (s, 2, aromatic); ^{13}C-NMR (100 MHz, DMSO-d_6): δ = 21.39; 21.41 (4, -CH_3); 51.9 (1, -OCH_3); 68.0; 68.2; 69.6; 70.2; 78.8 (5, -CH-, -CH_2-); 99.7; 100.0 (2, -OCHO-); 124.2; 124.3; 130.4; 137.4; 138.4; 138.9 (12, aromatic); 173.4 (1, -CO_2-); HRMS (EI): Calculated for $C_{25}H_{29}O_7$ $[M-H]^+$ 441.1913, found 441.1907; TGA: $T_{-5wt\,\%}$ = 277.12 °C; DSC: T_m = 264.92 °C; $T_{dec.}$ = 282.53 °C; T_m^1 = 271.68 °C (-147.78 J/g); T_c^1 = 194.30 °C (24.11 J/g); T_m^2 = 242.27 °C (16.76 J/g).

3,5:4,6-bis-(2,4-Dimethylbenzylidene)-*L*-gulonic acid methyl ester (**5e**)

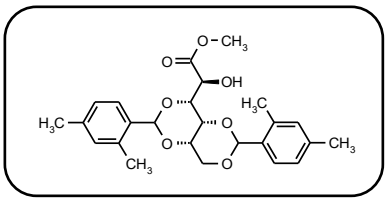

According to the general procedure *L*-gulonic acid gamma lactone (**2**, 0.042 mol, 7.41 g) was reacted with the relevant substituted benzaldehyde dimethyl acetal (**4e**, 0.166 mol, 30.43 mL) and concentrated hydrochloric acid (0.017 mol, 1.38 mL). For better dilution 30.00 mL acetonitrile were added. General workup yielded the product **5e** as a white powder (16.56 g, 90 %). R_f = 0.81 (ethyl acetate – hexane 4:1); ^{1}H-NMR (400 MHz, DMSO-d_6): δ = 2.23 (s, 3, CH_3); 2.25-2.26 (d, 6, -CH_3); 2.34 (s, 3, -CH_3); 3.57 (s, 3, -OCH_3); 3.97-4.20 (m, 6, -CH,-CH_2); 5.71 (d, 2, -OCHO-); 6.01-6.03 (d, *J* = 6.0 Hz, -OH); 6.97-7.00 (t, 4, aromatic); 7.34-7.38 (t, 2, aromatic); ^{13}C-NMR (100 MHz, DMSO-d_6): δ = 18.7; 21.2 (4, -CH_3); 51.9 (1, -OCH_3); 68.1; 68.2; 69.7; 70.1; 78.8 (5, -CH-, -CH_2-); 98.6; 99.4 (2, -OCHO-); 126.21; 126.23; 126.3; 126.8; 131.3; 131.4; 133.6; 134.1; 136.3; 136.4; 138.1; 138.2 (12, aromatic); 173.3 (1, -CO_2-); HRMS (EI): Calculated for $C_{25}H_{29}O_7$ $[M-H]^+$ 441.1913, found 441.1906; TGA: $T_{-5\,wt\%}$ = 295.61 °C; DSC: T_m = 230.08 °C, 247.24 °C; $T_{dec.}$ = 304.31 °C; T_m^1 = 232.64 °C (-70.05 J/g), 242.98 °C (-41.02 J/g); T_c^1 = 242.98 °C (-41.02 J/g); T_m^2 = 212.63 °C (-20.44 J/g).

3,5:4,6-bis-(2,5-Dimethylbenzylidene)-*L*-gulonic acid methyl ester (**5f**)

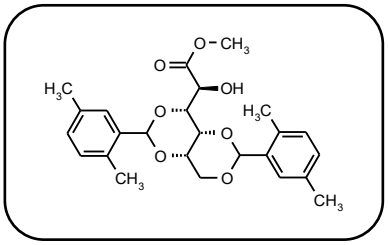

According to the general procedure *L*-gulonic acid gamma lactone (**2**, 0.041 mol, 7.36 g) was reacted with the relevant substituted benzaldehyde dimethyl acetal (**4f**, 0.165 mol, 30.20 mL) and concentrated hydrochloric acid (0.017 mol, 1.37 mL). For better dilution 30.00 mL acetonitrile were added. General workup yielded the product **5f** as a white powder (15.00 g, 82 %). R_f = 0.81 (ethyl acetate – hexane 4:1); ^{1}H-NMR (400 MHz, DMSO-d_6): δ = 2.23 (s, 3, -CH_3); 2.27 (s, 6, -CH_3); 2.34 (s, 3, -CH_3); 3.58 (s, 3, -OCH_3); 4.00-4.22 (m, 6, -CH,-CH_2); 5.73 (s, 1, -OCHO-); 5.74 (s, 1, -OCHO-); 6.03-6.04 (d, *J* = 6.0 Hz, -OH); 7.05-7.07 (d,

4, aromatic); 7.31-7.33 (d, 2, aromatic); ^{13}C-NMR (100 MHz, DMSO-d_6): δ = 18.3; 21.2 (4, -CH_3); 51.9 (1, -OCH_3); 68.2; 69.7; 70.2; 78.8 (5, -CH-, -CH_2-); 98.6; 99.4 (2, -OCHO-); 126.9; 127.4; 129.5; 130.6; 130.7; 133.3; 133.4; 134.55; 134.57; 136.1; 136.6 (12, aromatic); 173.3 (1, -CO_2-); HRMS (EI): Calculated for $C_{25}H_{29}O_7$ $[M-H]^+$ 441.1913, found 441.1909; TGA: $T_{-5\ wt\%}$ = 284.25 °C; DSC: T_m = 233.03 °C, 241.59 °C; $T_{dec.}$ = 241.21 °C; T_m^1 = 233.04 °C (-75.91 J/g), 244.88 °C (-100.43 J/g); T_c^1 = 211.12 °C (90.99 J/g); T_m^2 = 236.14 °C (-87.85 J/g); T_c^2 = 202.30 °C (72.33 J/g).

3,5:4,6-di-(4-Propylbenzylidene)-*L*-gulonic acid methyl ester (**5.1h**)

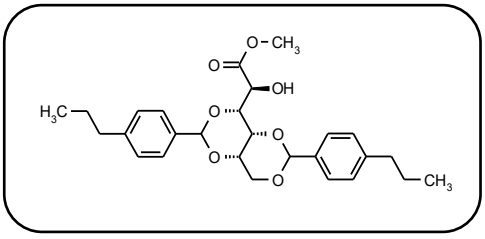

According to the general procedure *L*-gulonic acid gamma lactone (**2**, 0.013 mol, 2.24 g) was reacted with the relevant substituted benzaldehyde dimethyl acetal (**4.1h,** 0.050 mol, 9.89 mL) and concentrated hydrochloric acid (0.005 mol, 0.42 mL). For better dilution 10.00 mL acetonitrile were added. General workup yielded the product **5.1h** as a white powder (4.91 g, 81 %). R_f = 0.83 (ethyl acetate – hexane 4:1); ^{1}H-NMR (400 MHz, DMSO-d_6): δ = 0.85-0.90 (m, 6, -CH_3); 1.52-1.62 (m, 4, -CH_2-); 2.52-2.57 (m, 4, -CH_2-); 3.62 (s, 3, -OCH_3); 3.98-4.28 (m, 6, -CH,-CH_2); 5.64 (s, 1, -OCHO-); 5.65 (s, 1, -OCHO-); 6.09-6.10 (d, *J* = 6.1 Hz, -OH); 7.17-7.21 (t, 4, aromatic); 7.27-7.29 (d, 2, aromatic); 7.36-7.38 (d, 2, aromatic); ^{13}C-NMR (100 MHz, DMSO-d_6): δ = 14.1 (2, -CH_3); 24.5; 24.6 (2, -CH_2-); 37.5; 37.6 (2, -CH_2-); 52.0 (1, -OCH_3); 68.06; 68.09; 69.7; 70.1; 78.7 (5, -CH-, -CH_2-); 99.6; 99.8 (2, -OCHO-); 126.3; 126.5; 128.4; 136.0; 136.5; 143.0; 143.1 (12, aromatic); 173.2 (1, -CO_2-); HRMS (EI): Calculated for $C_{27}H_{33}O_7$ $[M-H]^+$ 469.2226, found 469.2216; TGA: $T_{-5\ wt\%}$ = 289.06 °C; DSC: T_m = 189.49 °C; $T_{dec.}$ = 311.55 °C; T_m^1 = 198.11 °C (-13.56 J/g), 207.08 °C (-99.34 J/g); T_c^1 = 179.61 °C (92.00 J/g); T_m^2 = 205.56 °C (-92.28 J/g); T_c^2 = 176.61 °C (82.17 J/g).

3,5:4,6-di-(4-Propylbenzylidene)-*L*-gulonic acid ethyl ester (**5.2h**)

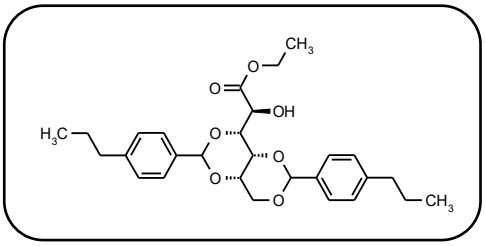

According to the general procedure *L*-gulonic acid gamma lactone (**2**, 0.021 mol, 3.75 g) was reacted with the commercial 4-propylbenzaldehyde diethyl acetal (**4.2h**, 0.084 mol, 20.00 mL) and concentrated hydrochloric acid (0.008 mol, 0.70 mL). For better dilution 15.00 mL acetonitrile were added. General workup yielded the product **5.2h** as a white powder (8.21 g, 81 %). R_f = 0.85 (ethyl acetate – hexane 4:1); ^{1}H-NMR (400 MHz, DMSO-d_6): δ = 0.85-0.90 (q, 6, -CH_3); 1.11-1.15 (t, 3, -OCH_2-CH_3) 1.52-1.62 (m, 4, -CH_2-); 2.52-2.57 (m, 4, -CH_2-); 3.98-4.25 (m, 8, -CH,-CH_2, -OCH_2-); 5.64 (s, 1, -OCHO-); 5.65 (s, 1, -OCHO-); 6.04-6.05 (d, *J* = 6.0 Hz, -OH); 7.17-7.21 (t, 4, aromatic); 7.28-7.30 (d, 2, aromatic); 7.36-7.38 (d, 2, aromatic); ^{13}C-NMR (100 MHz, DMSO-d_6): δ = 14.0; 14.1; 14.5 (3, -CH_3, -OCH_2-CH_3); 24.5; 24.6 (2, -CH_2-); 37.4; 37.5 (2, -CH_2-); 60.5; 68.09; 68.12; 69.7; 70.1; 78.8 (5, -CH-, -CH_2-, -OCH_2-); 99.5; 99.8 (2, -OCHO-); 126.3; 126.5; 128.3; 128.4; 136.0; 136.5; 143.0; 143.1 (12, aromatic); 172.8 (1, -CO_2-); HRMS (EI): Calculated for $C_{28}H_{35}O_7$ $[M-H]^+$ 483.2383, found 483.2375; TGA: $T_{-5\ wt\%}$ = 305.17 °C; DSC:

T_m = 217.30 °C (-12.25 J/g), 346.21 °C (-121.85 J/g); $T_{dec.}$ = 311.68 °C; T_m^1 = 202.27 °C (-111.61 J/g).

3,5:4,6-di-(4-Isobutylbenzylidene)-*L*-gulonic acid methyl ester (**5i**)

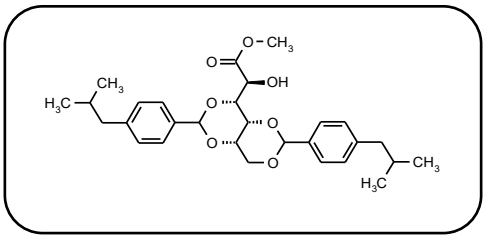

According to the general procedure *L*-gulonic acid gamma lactone (**2**, 0.034 mol, 6.02 g) was reacted with the relevant substituted benzaldehyde dimethyl acetal (**4i**, 0.135 mol, 28.56 mL) and concentrated hydrochloric acid (0.014 mol, 1.12 mL). For better dilution 25.00 mL acetonitrile were added. General workup yielded the product **5i** as a white powder (9.88 g, 59 %). R_f = 0.85 (ethyl acetate – hexane 4:1); ^{1}H-NMR (400 MHz, DMSO-d_6): δ = 0.84 (d, 6, -CH_3); 0.86 (d, 6 –CH_3); 1.78-1.86 (m, 2, -CH-); 2.43-2.46 (q, 4, -CH_2-); 3.63 (s, 3, -OCH_3); 3.99-4.29 (m, 6, -CH,-CH_2); 5.65 (s, 1, -OCHO-); 5.66 (s, 1, -OCHO-); 6.09-6.11 (d, *J* = 6.1 Hz, -OH); 7.14-7.18 (t, 4, aromatic); 7.28-7.29 (d, 2, aromatic); 7.36-7.38 (d, 2, aromatic); ^{13}C-NMR (100 MHz, DMSO-d_6): δ = 22.6 (4, -CH_3); 30.1 (2, -CH-); 44.81; 44.83 (2, -CH_2-); 52.0 (1, -OCH_3); 68.1; 69.7; 70.2; 78.7 (5, -CH-, -CH_2-); 99.6; 99.8 (2, -OCHO-); 126.2; 126.3; 129.0; 136.0; 136.5; 142.0; 142.1 (12, aromatic); 173.2 (1, -CO_2-); HRMS (EI): Calculated for $C_{29}H_{37}O_7$ $[M-H]^+$ 497.2539, found 497.2532; TGA: $T_{-5\ wt\%}$ = 310.01 °C; DSC: T_m = 162.78 °C, 194.48 °C; $T_{dec.}$ = 311.46 °C; T_m^1 = 163.86 °C (-35.53 J/g); 293.54 °C (-68.93 J/g); 192.78 °C (-12.33 J/g).

10.2.4.Procedure for the preparation of 3,5:4,6-dibenzylidene-*L*-gulonic acid derivatives (6)

General procedure [101]

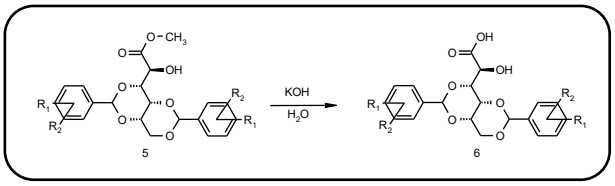

A round bottomed flask, equipped with a heating bath, condenser and a stirrer, was charged with the relevant 3,5:4,6-dibenzylidene-*L*-gulonic acid methyl ester (**5**) (1.00 Eq.), potassium hydroxide (4.00 Eq.) and water (5.13 L/mol). The suspension was stirred for about 16 h at 80 °C and in between at room temperature until TLC showed full conversion of the starting material. Hydrochloric acid (2 N) was added until pH 2. The product was filtered off and washed with water (3 x 100 mL). The product was dried under vacuum at 110 °C for 12 h to yield the relevant substituted 3,5:4,6-dibenzylidene-*L*-gulonic acid (**6**).

3,5:4,6-Dibenzylidene-*L*-gulonic acid (**6a**)

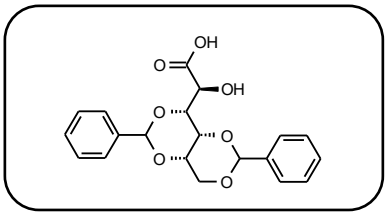

According to the general procedure relevant 3,5:4,6-dibenzylidene-*L*-gulonic acid methyl ester (**5a**, 0.013 mol, 5.00 g) was treated with KOH (0.065 mol, 3.63 g) in 65.00 mL water. General workup yielded the product **6a** as a white powder (4.45 g, 92 %). R_f = 0.11 (ethyl acetate – hexane 4:1); ^{1}H-NMR (400 MHz, DMSO-d_6): δ = 4.00-4.23 (m, 6, -CH,-CH_2);

5.69 (s, 1, -OCHO-); 5.70 (s, 1, -OCHO-); 7.36-7.49 (m, 10, aromatic); ^{13}C-NMR (100 MHz, DMSO-d_6): δ = 68.2; 69.7; 70.2; 78.9 (5, -CH-, -CH_2-); 99.7 (2, -OCHO-); 126.6; 128.5; 129.1; 129.2; 138.6; 139.0 (12, aromatic); 173.2 (1, -CO_2-); HRMS (EI): Calculated for $C_{26}H_{35}O_7Si_2$ $[M\text{-}H]^+$ 515.1921, found 515.1918; TGA: $T_{-5\,wt\%}$ = 212.68 °C; DSC: T_m = 188.62 °C; $T_{dec.}$ = 222.12 °C; $T_m{}^1$ = 206.61 °C (-222.74 J/g).

3,5:4,6-di-(4-Methylbenzylidene)-*L*-gulonic acid (**6b**)

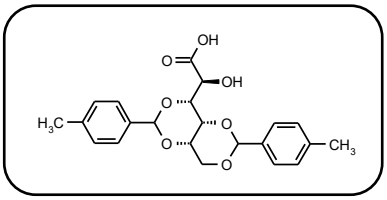

According to the general procedure relevant 3,5:4,6-dibenzylidene-*L*-gulonic acid methyl ester (**5b**, 0.012 mol, 5.00 g) was treated with KOH (0.060 mol, 3.38 g) in 60.00 mL water. General workup yielded the product **6b** as a white powder (4.55 g, 94 %). R_f = 0.03 (ethyl acetate – hexane 4:1); ^{1}H-NMR (400 MHz, DMSO-d_6): δ = 2.30 (s, 3, -CH_3); 2.31 (s, 3, -CH_3); 3.96-4.20 (m, 6, -CH,-CH_2); 5.63 (s, 2, -OCHO-); 7.16-7.36 (m, 8, aromatic); ^{13}C-NMR (100 MHz, DMSO-d_6): δ = 21.3 (2, -CH_3); 68.2; 69.7; 70.2; 78.9 (5, -CH-, -CH_2-); 99.8 (2, -OCHO-); 126.49; 126.53; 128.92; 128.93; 135.8; 136.3; 138.3; 138.4 (12, aromatic); 174.3 (1, -CO_2-); HRMS (EI): Calculated for $C_{28}H_{39}O_7Si_2$ $[M\text{-}H]^+$ 543.2234, found 543.2228; TGA: $T_{-5\,wt\%}$ = 213.64 °C; DSC: T_m = 191.95 °C; $T_{dec.}$ = 201.30 °C.

3,5:4,6-bis-(3,4-Dimethylbenzylidene)-*L*-gulonic acid (**6c**)

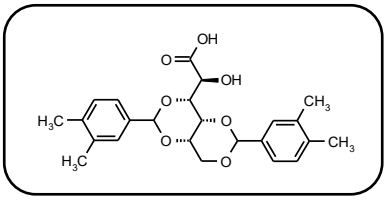

According to the general procedure relevant 3,5:4,6-dibenzylidene-*L*-gulonic acid methyl ester (**5c**, 0.011 mol, 5.00 g) was treated with KOH (0.057 mol, 3.17 g) in 55.00 mL water. General workup yielded the product **6c** as a white powder (4.80 g, 99 %). R_f = 0.08 (ethyl acetate – hexane 4:1); ^{1}H-NMR (400 MHz, DMSO-d_6): δ = 2.21 (s, 6, -CH_3); 2.23 (s, 6, -CH_3); 3.86-4.15 (m, 6, -CH,-CH_2); 5.55 (s, 1, -OCHO-); 5.56 (s, 1, -OCHO); 7.10-7.22 (m, 6, aromatic); ^{13}C-NMR (100 MHz, DMSO-d_6): δ = 19.7; 19.88; 19.90 (4, -CH_3); 68.7; 68.8; 69.7; 70.3; 79.3 (5, -CH-, -CH_2-); 99.9; 100.0 (2, -OCHO-); 124.0; 124.2; 127.6; 127.7; 129.4; 129.4; 136.0; 136.1; 136.4; 136.7; 136.9; 137.0 (12, aromatic); 174.5 (1, -CO_2-); HRMS (EI): Calculated for $C_{30}H_{43}O_7Si_2$ $[M\text{-}H]^+$ 571.2547, found 571.2551; TGA: $T_{-5\,wt\%}$ = 213.15 °C; DSC: T_m = 187.14 °C; $T_{dec.}$ = 191.68 °C.

3,5:4,6-bis-(3,5-Dimethylbenzylidene)-*L*-gulonic acid (**6d**)

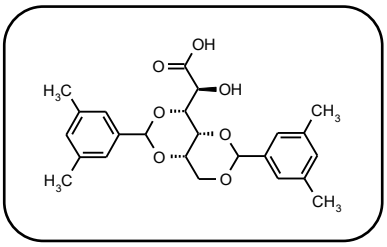

According to the general procedure relevant 3,5:4,6-dibenzylidene-*L*-gulonic acid methyl ester (**5d**, 0.011 mol, 5.00 g) was treated with KOH (0.057 mol, 3.17 g) in 55.00 mL water. General workup yielded the product **6d** as a white powder (4.79 g, 99 %). R_f = 0.11 (ethyl acetate – hexane 4:1); ^{1}H-NMR (400 MHz, DMSO-d_6): δ = 2.27 (s, 6, -CH_3); 2.29 (s, 6, -CH_3); 3.91-4.17 (m, 6, -CH,-CH_2); 5.58 (s, 2, -OCHO-); 6.99-7.08 (s, 6, aromatic); ^{13}C-NMR (100 MHz, DMSO-d_6): δ = 21.4 (4, -CH_3); 68.4; 69.6; 70.3; 79.1 (5, -CH-, -CH_2-); 100.0 (2, -OCHO-); 124.3; 124.4; 130.4; 137.4; 138.6; 139.0 (12, aromatic); 174.4 (1, -CO_2-); HRMS

(EI): Calculated for $C_{30}H_{43}O_7Si_2$ $[M-H]^+$ 571.2547, found 571.2548; TGA: $T_{-5\,wt\%}$ = 236.26 °C; DSC: T_m = 219.14 °C; $T_{dec.}$ = 222.02 °C.

3,5:4,6-bis-(2,4-Dimethylbenzylidene)-*L*-gulonic acid (**6e**)

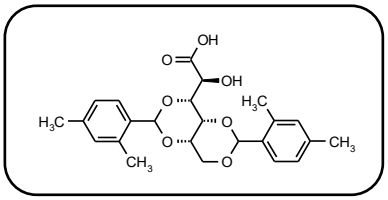

According to the general procedure relevant 3,5:4,6-dibenzylidene-*L*-gulonic acid methyl ester (**5e**, 0.011 mol, 5.00 g) was treated with KOH (0.057 mol, 3.17 g) in 55.00 mL water. General workup yielded the product **6e** as a white powder (4.44 g, 92 %). R_f = 0.09 (ethyl acetate – hexane 4:1); ^{1}H-NMR (400 MHz, DMSO-d_6): δ = 2.25-2.28 (d, 9, -CH_3); 2.34 (s, 3, -CH_3); 3.95-4.19 (m, 6, -CH,-CH_2); 5.70 (s, 2, -OCHO-); 6.97-6.99 (d, 4, aromatic); 7.36-7.38 (d, 2, aromatic); ^{13}C-NMR (100 MHz, DMSO-d_6): δ = 18.9; 19.0; 21.2 (4, -CH_3); 68.2; 68.3; 69.8; 70.2; 79.0 (5, -CH-, -CH_2-); 98.9; 99.3 (2, -OCHO-); 126.1; 126.2; 126.5; 126.7; 131.3; 131.4; 133.7; 134.2; 136.4; 136.5; 138.1 (12, aromatic); 174.4 (1, -CO_2-); HRMS (EI): Calculated for $C_{30}H_{43}O_7Si_2$ $[M-H]^+$ 571.2547, found 571.2550; TGA: $T_{-5\,wt\%}$ = 207.74 °C; DSC: T_m = 177.04 °C; $T_{dec.}$ = 193.45 °C.

3,5:4,6-bis-(2,5-Dimethylbenzylidene)-*L*-gulonic acid *(***6f**)

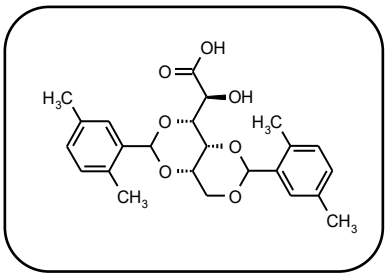

According to the general procedure relevant 3,5:4,6-dibenzylidene-*L*-gulonic acid methyl ester (**5f**, 0.011 mol, 5.00 g) was treated with KOH (0.057 mol, 3.17 g) in 55.00 mL water. General workup yielded the product **6f** as a white powder (4.71 g, 97 %). R_f = 0.09 (ethyl acetate – hexane 4:1); ^{1}H-NMR (400 MHz, DMSO-d_6): δ = 2.27 (s, 6, -CH_3); 2.30 (s, 3, -CH_3); 2.34 (s, 3, -CH_3); 3.74-4.15 (m, 6, -CH,-CH_2); 5.64 (s, 1, -OCHO-); 5.66 (s, 1, -OCHO-); 7.03-7.05 (d, 4, aromatic); 7.33 (d, 2, aromatic); ^{13}C-NMR (100 MHz, DMSO-d_6): δ =18.6; 18.7; 21.1 (4, -CH_3); 69.3; 69.4; 69.9; 70.5; 80.0 (5, -CH-, -CH_2-); 99.1; 99.2 (2, -OCHO-); 127.3; 127.4; 129.3; 130.5; 130.6; 133.4; 133.5; 134.3; 134.4; 136.6; 136.8 (12, aromatic); 174.5 (1, -CO_2-); HRMS (EI): Calculated for $C_{30}H_{43}O_7Si_2$ $[M-H]^+$ 571.2547, found 571.2553; TGA: $T_{-5\,wt\%}$ = 223.27 °C; DSC: T_m = 208.63 °C; $T_{dec.}$ = 211.64 °C.

3,5:4,6-di-(4-Propylbenzylidene)-*L*-gulonic acid (**6h**)

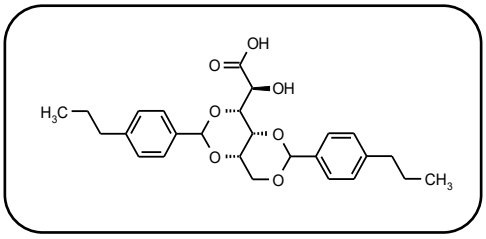

According to the general procedure relevant 3,5:4,6-dibenzylidene-*L*-gulonic acid methyl ester (**5.2h**, 0.010 mol, 5.00 g) was treated with KOH (0.052 mol, 2.89 g) in 50.00 mL water. General workup yielded the product **6h** as a white powder (4.70 g, 100 %). R_f = 0.09 (ethyl acetate – hexane 4:1); ^{1}H-NMR (400 MHz, DMSO-d_6): δ= 0.37 (t, 6, -CH_3); 1.55-1.60 (q, 4, -CH_2-); 2.54 (t, 4, -CH_2-); 3.84-4.14 (m, 6, -CH-, -CH_2-); 5.58 (s, 2, -OCHO-); 7.16-7.20 (t, 4, aromatic); 7.33-7.37 (t, 4, aromatic); ^{13}C-NMR (100 MHz, DMSO-d_6): δ= 14.0; 14.1 (2, -CH_3); 24.56; 24.59 (2, -CH_2-); 37.5 (2, -CH_2-); 69.1; 69.3; 69.8; 70.4; 80.0 (5, -CH-, -CH_2-); 99.8; 99.9 (2, -OCHO-); 126.5; 126.7; 128.25;

128.30; 136.4; 136.7; 142.9; 143.0 (12, aromatic); 174.6 (1, -CO_2-); HRMS (EI): Calculated for $C_{32}H_{47}O_7Si_2$ $[M\text{-}H]^+$ 599.2860, found 599.2868; TGA: $T_{-5\ wt\%}$ = 213.98 °C; DSC: T_m = 188.86 °C; $T_{dec.}$ = 190.44 °C.

3,5:4,6-di-(4-Isobutylbenzylidene)-*L*-gulonic acid (**6i**)

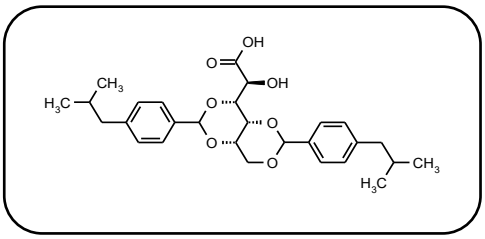

According to the general procedure relevant 3,5:4,6-dibenzylidene-*L*-gulonic acid methyl ester (**5i**, 0.010 mol, 5.00 g) was treated with KOH (0.050 mol, 2.81 g) in 50.00 g water. General workup yielded the product **6i** as a white powder (4.62 g, 95 %). R_f = 0.19 (ethyl acetate – hexane 4:1); ^{1}H-NMR (400 MHz, DMSO-d_6): δ = 0.84-0.86 (d, 12, -CH3); 1.79-1.85 (quint, 2, -CH-); 2.44-2.45 (d, 4, -CH_2-); 3.85-4.15 (m, 6, -CH-, -CH_2-); 5.59 (s, 2, -OCHO-); 7.13-7.16 (t, 4, aromatic); 7.34-7.37 (t, 4, aromatic); ^{13}C-NMR (100 MHz, DMSO-d_6): δ = 22.6 (4, -CH_3); 30.11; 30.13 (2, -CH-); 44.9 (2, -CH_2-); 69.3; 69.8; 70.5; 79.7 (5, -CH-, -CH_2-); 99.8; 99.9 (2, -OCHO-); 126.3; 126.6; 128.8; 128.9; 136.5; 136.7; 141.8; 141.9 (12, aromatic); 174.4 (1, -CO_2-); HRMS (EI): Calculated for $C_{34}H_{51}O_7Si_2$ $[M\text{-}H]^+$ 627.3173, found 627.3186; TGA: $T_{-5\ wt\%}$ = 202.00 °C; DSC: T_m = 185.50 °C; $T_{dec.}$ = 189.78 °C.

10.2.5. Procedure for the preparation of 3,5:4,6-dibenzylidene-*L*-gulonic amide derivatives (7)

General procedure [101, 104]

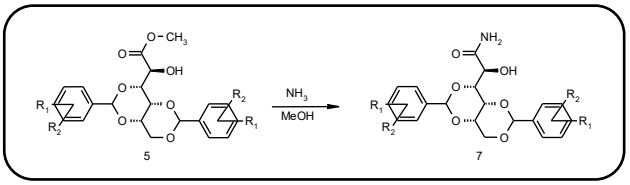

A beaded rim flask, equipped with aluminum heating block, magnetic stirrer and pressure seal was charged with the relevant 3,5:4,6-dibenzylidene-*L*-gluconic acid methyl ester (**5**) (1.00 Eq.) and ammonia in methanol (2 N) (7 Eq.). The suspension was stirred for about 16 h at 70 °C and overnight at room temperature until TLC showed full conversion of the starting material. The formed powder was isolated by filtration and washed with diethyl ether (3 x 100 mL). The product was dried under vacuum at 110 °C for 12 h to yield the relevant substituted 3,5:4,6-dibenzylidene-*L*-gulonic amid (**7**).

3,5:4,6-Dibenzylidene-*L*-gulonic amide (**7a**)

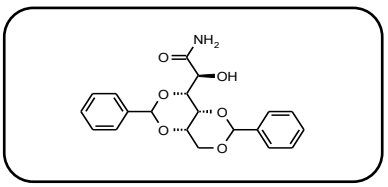

According to the general procedure relevant 3,5:4,6-dibenzylidene-*L*-gulonic acid methyl ester (**5a**, 0.026 mol, 10.00 g) was reacted with ammonia in methanol (0.776 mol, 110.92 mL). General workup yielded the product **7a** as a white powder (9.37 g, 98 %). R_f = 0.40 (ethyl acetate – hexane 4:1); ^{1}H-NMR (400 MHz, DMSO-d_6): δ = 3.98-4.23 (m, 6, -CH-, -CH_3-); 5.31-5.33 (d, 2, J = 5.3 Hz, -OH), 5.66 (s, 1, -OCHO-); 5.68 (s, 1, -OCHO-); 6.99 (bs, 1, -NH_2); 7.36-7.50 (m, 11, -NH_2, aromatic); ^{13}C-NMR (100 MHz, DMSO-d_6): δ = 68.3; 68.8; 69.8; 70.4; 79.0 (5, -CH, -CH_2-);

99.7; 99.9 (2, -OCHO-); 126.7; 128.4; 129.1; 129.1; 138.7; 139.1 (12, aromatic); 174.2 (1, -CON-); HRMS (EI): Calculated for $C_{20}H_{20}NO_6$ $[M\text{-}H]^+$ 370.1291, found 370.1282; TGA: $T_{-5\ wt\%}$ = 291.54 °C; DSC: T_m = 258.41 °C; $T_{dec.}$ = 280.76 °C; T_m^1 = 256.23 °C (-129.57 J/g); T_c^1 = 196.42 °C (59.72 J/g); T_m^2 = 244.50 °C (-57.11 J/g).

3,5:4,6-di-(4-Methylbenzylidene)-*L*-gulonic amide (**7b**)

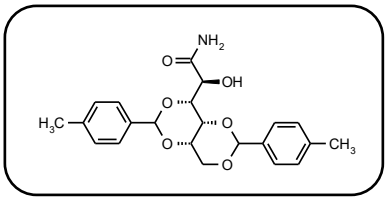

According to the general procedure relevant 3,5:4,6-dibenzylidene-*L*-gulonic acid methyl ester (**5b**, 0.012 mol, 5.00 g) was reacted with ammonia in methanol (0.362 mol, 51.70 mL). General workup yielded the product **7b** as a white powder (4.55 g, 94 %). R_f = 0.38 (ethyl acetate – hexane 4:1); ^{1}H-NMR (400 MHz, DMSO-d_6): δ= 2.30-2.31 (d, 6, -CH_3); 3.94-4.20 (m, 6, -CH-, -CH_2-); 5.27-5.29 (d, J = 5.3 Hz, 1, -OH); 5.61-5.63 (d, 2, -OCHO-); 6.99 (bs, 1, -NH_2); 7.16-7.37 (m, 8, aromatic); 7.43 (bs, 1, -NH_2); ^{13}C-NMR (100 MHz, DMSO-d_6): δ= 21.3 (2, -CH_3); 68.3; 68.8; 69.7; 70.4; 79.0 (5, -CH-, -CH_2-); 99.8; 99.9; (2, -OCHO-); 126.6; 128.9; 136.0; 136.3; 138.3 (12, aromatic); 174.3 (1, -CON-); HRMS (EI): Calculated for $C_{22}H_{24}NO_6$ $[M\text{-}H]^+$ 398.1604, found 398.1596; TGA: $T_{-5\ wt\%}$ = 291.25 °C; DSC: T_m = 239.60 °C; $T_{dec.}$ = 244.47 °C.

3,5:4,6-bis-(3,4-Dimethylbenzylidene)-*L*-gulonic amide (**7c**)

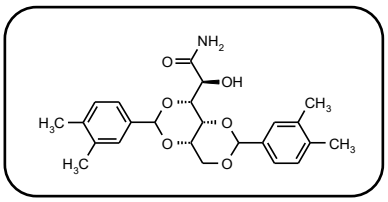

According to the general procedure relevant 3,5:4,6-dibenzylidene-*L*-gulonic acid methyl ester (**5c**, 0.094 mol, 41.78 g) was reacted with ammonia in methanol (3.493 mol, 0.5 L). General workup yielded the product **7c** as a white powder (39.55 g, 98 %). R_f = 0.43 (ethyl acetate – hexane 4:1); ^{1}H-NMR (400 MHz, DMSO-d_6): δ= 2.22-2.23 (bd, 12, -CH_3); 3.92-4.18 (m, 6, -CH-, -CH_2-); 5.26-5.28 (d, J = 5.3 Hz, 1, -OH); 5.57 (s, 1, -OCHO-); 5.59 (s, 1, -OCHO-); 6.99 (bs, 1, -NH_2); 7.10-7.24 (m, 6, aromatic); 7.43 (bs, 1, -NH_2); ^{13}C-NMR (100 MHz, DMSO-d_6): δ= 19.7; 19.9 (4, -CH_3); 68.3; 68.8; 69.7; 70.4; 79.1 (5, -CH-, -CH_2-); 99.9; 100.1 (2, -OCHO-); 124.2; 127.8; 129.3; 129.4; 136.0; 136.3; 136.6; 136.9; 137.0 (12, aromatic); 174.3 (1, -CON-); HRMS (EI): Calculated for $C_{24}H_{28}NO_6$ $[M\text{-}H]^+$ 426.1917, found 426.1913; TGA: $T_{-5\ wt\%}$ = 296.85 °C; DSC: T_m = 260.77 °C; $T_{dec.}$ = 263.17 °C; T_m^1 = 244.14 °C (-6.73 J/g).

3,5:4,6-bis-(3,5-Dimethylbenzylidene)-*L*-gulonic amide (**7d**)

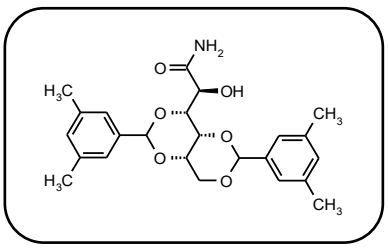

According to the general procedure relevant 3,5:4,6-dibenzylidene-*L*-gulonic acid methyl ester (**5d**, 0.016 mol, 7.00 g) was reacted with ammonia in methanol (0.475 mol, 67.80 mL). General workup yielded the product **7d** as a white powder (6.37 g, 94 %). R_f = 0.58 (ethyl acetate – hexane 4:1); ^{1}H-NMR (400 MHz, DMSO-d_6): δ = 2.27-2-28 (d, 12, -CH_3); 3.92-4.18 (m, 6, -CH-, -CH_2-); 5.29-5.31 (d, J = 5.3 Hz, 1, -OH); 5.56 (s, 1, -OCHO-); 5.58 (s, 1, -OCHO-); 6.98-7.08 (m, 7, -NH_2, aromatic); 7.46 (bs, 1, -NH_2); ^{13}C-NMR (100 MHz, DMSO-d_6): δ= 21.4 (4, -CH_3); 68.3; 68.8; 69.7; 70.4; 79.1 (5, -CH-; -CH_2-); 100.1; 100.1 (2, -OCHO-); 124.5; 124.6; 130.3; 130.4; 137.30; 137.32; 138.7; 139.0 (12, aromatic); 174.3 (1, -CON-);

HRMS (EI): Calculated for $C_{24}H_{28}NO_6$ $[M-H]^+$ 426.1917, found 426.1913; TGA: $T_{-5\ wt\%}$ = 309.06 °C; DSC: T_m = 277.91 °C; $T_{dec.}$ = 280.47 °C.

3,5:4,6-bis-(2,4-Dimethylbenzylidene)-*L*-gulonic amide (**7e**)

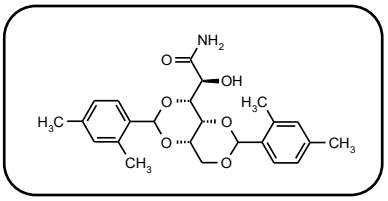

According to the general procedure relevant 3,5:4,6-dibenzylidene-*L*-gulonic acid methyl ester (**5e**, 0.016 mol, 7.00 g) was reacted with ammonia in methanol (0.475 mol, 67.80 mL). General workup yielded the product **7e** as a white powder (6.56 g, 97 %). R_f = 0.49 (ethyl acetate – hexane 4:1); ^{1}H-NMR (400 MHz, DMSO-d_6): δ= 2.25-2.26 (d, 6, -CH_3); 2.28 (s, 3, -CH_3); 2.35 (s, 3, -CH_3); 3.93-4.20 (m, 6, -CH-,-CH_2-); 5.18-5.19 (d, J = 5.3 Hz, 1, -OH); 5.66 (s, 1, -OCHO-); 5.70 (s, 1, -OCHO-); 6.95-6.98 (m, 5, -NH_2, aromatic); 7.37-7.41 (t, 3, -NH_2, aromatic); ^{13}C-NMR (100 MHz, DMSO-d_6): δ= 19.0; 19.1; 21.2 (4, -CH_3); 68.3; 68.8; 69.9; 70.4; 79.1 (5, -CH-, -CH_2-); 98.9; 99.2 (2, -OCHO-); 126.07; 126.11; 126.5; 126.6; 131.26; 131.30; 133.9; 134.2; 136.49; 136.51; 138.00; 138.02 (12, aromatic); 174.4 (1, -CON-); HRMS (EI): Calculated for $C_{24}H_{28}NO_6$ $[M-H]^+$ 426.1917, found 426.1914; TGA: $T_{-5\ wt\%}$ = 284.74 °C; DSC: T_m = 221.80 °C; $T_{dec.}$ = 243.36 °C; T_m^1 = 229.73 °C (-125.10 J/g).

3,5:4,6-bis-(2,4-Dimethylbenzylidene)-*L*-gulonic amide (**7f**)

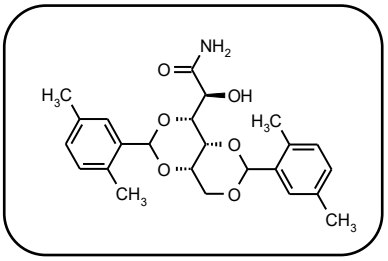

According to the general procedure relevant 3,5:4,6-dibenzylidene-*L*-gulonic acid methyl ester (**5f**, 0.011 mol, 5.00 g) was reacted with ammonia in methanol (0.339 mol, 48.43 mL). General workup yielded the product **7f** as a white powder (4.67 g, 97 %). R_f = 0.49 (ethyl acetate – hexane 4:1); ^{1}H-NMR (400 MHz, DMSO-d_6): δ= 2.26-2.27 (d, 9, -CH_3); 2.35 (s, 3, -CH_3); 3.95-4.22 (m, 6, -CH-, -CH_2-); 5.20-5.22 (d, J = 5.3 Hz, 1, -OH); 5.68 (s, 1, -OCHO-); 5.71 (s, 1, -OCHO-); 6.95 (bs, 1, -NH_2); 7.04-7.05 (d, 4, aromatic); 7.33-7.36 (d, 2, aromatic); 7.39 (bs, 1, -NH_2); ^{13}C-NMR (100 MHz, DMSO-d_6): δ= 18.6; 18.7; 21.1; 21.2 (4, -CH_3); 68.3; 68.8; 69.8; 70.5; 79.1 (5, -CH-, -CH_2-); 98.9; 99.2 (2, -OCHO-); 127.2; 127.3; 129.35; 129.38; 130.5; 130.6; 133.4; 133.5; 134.4; 134.5; 136.4; 136.7 (12, aromatic); 174.4 (1, -CON-); HRMS (EI): Calculated for $C_{24}H_{29}NO_6$ $[M]^+$ 427.1995, found 427.1989; TGA: $T_{-5\ wt\%}$ = 297.16 °C; DSC: T_m = 267.08 °C; $T_{dec.}$ = 274.69 °C; T_m^1 = 272.38 °C (-132.37 J/g).

3,5:4,6-di-(4-Propylbenzylidene)-*L*-gulonic amide (**7h**)

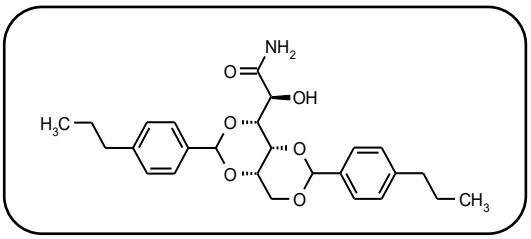

According to the general procedure relevant 3,5:4,6-dibenzylidene-*L*-gulonic acid ethyl ester (**5.2h**, 0.017 mol, 8.21 g) was reacted with ammonia in methanol (0.508 mol, 72.61 mL). General workup yielded the product **7h** as a white powder (6.89 g, 89 %). R_f = 0.54 (ethyl acetate – hexane 4:1); ^{1}H-NMR (400 MHz, DMSO-d_6): δ= 0.85-0.90 (t, 6, -CH_3); 1.53-1.62 (m, 4, -CH_2-); 2.53-2.57 (t, 4, -CH_2-); 3.94-4.20 (m, 6, -CH-, -CH_2-); 5.27-5.29 (d, J = 5.3 Hz, 1, -OH); 5.61 (s, 1, -OCHO-);

5.63 (s, 1, -OCHO-); 6.97 (bs, 1, -NH_2); 7.17-7.20 (t, 4, aromatic); 7.33-7.39 (m, 4, aromatic); 7.43 (bs, 1, -NH_2); ^{13}C-NMR (100 MHz, DMSO-d_6): δ = 14.03; 14.04 (2, -CH_3); 24.56; 24.58 (2, -CH_2-); 37.5 (2, -CH_2-); 68.3; 68.8; 69.8; 70.4; 79.0 (5, -CH-, -CH_2-); 99.8; 100.0 (2, -OCHO-); 126.6; 128.3; 136.2; 136.6; 142.98; 143.04 (12, aromatic); 174.3 (1, -CON-); HRMS (EI): Calculated for $C_{26}H_{32}NO_6$ $[M-H]^+$ 454.2230, found 454.2224; TGA: $T_{-5\ wt\%}$ = 287.60 °C; DSC: T_m = 223.16 °C; $T_{dec.}$ = 266.66 °C; T_m^1 = 224.52 °C (-134.02 J/g); T_c^1 = 171.44 °C (24.53 J/g); T_m^2 = 194.38 °C (-24.79 J/g); T_c^2 = 129.74 °C (5.55 J/g).

3,5:4,6-Di-(4-Isobutylbenzylidene)-*L*-gulonic amide (7**i**)

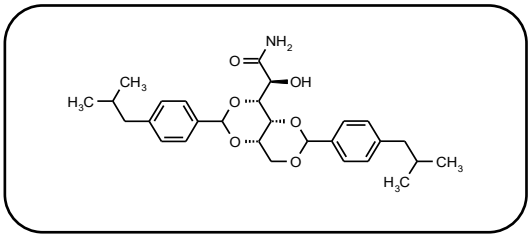

According to the general procedure relevant 3,5:4,6-dibenzylidene-*L*-gulonic acid methyl ester (**5i**, 0.009 mol, 4.50 g) was reacted with ammonia in methanol (0.271 mol, 38.68 mL). General workup yielded the product **7i** as a white powder (4.09 g, 94 %). R_f = 0.61 (ethyl acetate – hexane 4:1); ^{1}H-NMR (400 MHz, DMSO-d_6): δ= 0.84-0.86 (dd, 12, -CH_3); 1.78-1.86 (m, 2, -CH-); 2.43-2.46 (q, 4, -CH_2-); 3.94-4.20 (m, 6, -CH-, -CH_2-); 5.28-5.30 (d, J = 5.3 Hz, 1, -OH); 5.62 (s, 1, -OCHO-); 5.64 (s, 1, -OCHO-); 6.98 (bs, 1, -NH_2); 7.15 (t, 4, aromatic); 7.34-7.39 (m, 4, aromatic); 7.44 (bs, 1, -NH_2); ^{13}C-NMR (100 MHz, DMSO-d_6): δ=22.6 (4, -CH_3); 30.1 (2, -CH-); 44.8 (2, -CH_2-); 68.3; 68.8; 69.8; 70.4; 79.0 (5, -CH-, -CH_2-); 99.8; 100.0 (2, -OCHO-); 126.5; 128.9; 136.2; 136.6; 141.96; 142.02 (12, aromatic); 174.3 (1, -CON-); HRMS (EI): Calculated for $C_{28}H_{36}NO_6$ $[M-H]^+$ 482.2543, found 482.2534; TGA: $T_{-5\ wt\%}$ = 295.06 °C; DSC: T_m = 202.30 °C, 216.69 °C; $T_{dec.}$ = 263.53 °C; T_m^1 = 205.77 °C (-47.96 J/g), 216.57 °C (-52.57 J/g); T_c^1 = 134.96 °C (10.01 J/g).

10.2.6. Procedure for the preparation of 3,5:4,6-dibenzylidene-L-gulonic alkyl amide derivatives (8.1-6)

General procedure [101, 104]

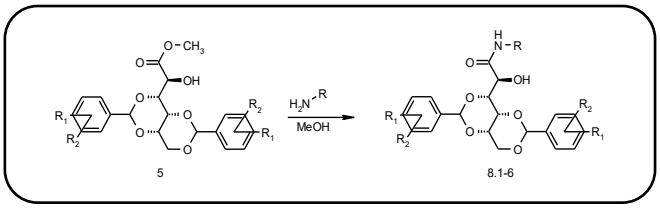

A 150 mL beaded rim flask, equipped with aluminum heating block, magnetic stirrer and pressure seal was charged with the relevant 3,5:4,6-dibenzylidene-*L*-gluconic acid methyl ester (**5**) (1.00 Eq.), relevant amine derivative in methanol (2 N) (15.00 Eq.) or the relevant amine derivative (8.00 Eq.) in methanol (0.75 L/mol) based on the amine derivative. The suspension was stirred for about 16 h at 70 °C and overnight at room temperature until TLC showed full conversion of the starting material. The formed powder was isolated by filtration and washed with diethyl ether (3 x 100 mL). The product was dried under vacuum at 110 °C for 12 h to yield the relevant substituted 3,5:4,6-dibenzylidene-*L*-gulonic alkyl amide (**8.1-6**).

3,5:4,6-Dibenzylidene-*L*-gulonic methyl amide (**8.1a**)

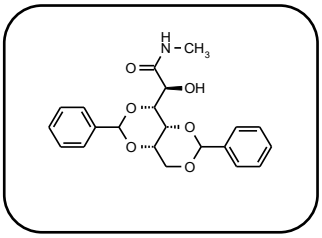

According to the general procedure 3,5:4,6-dibenzylidene-*L*-gulonic acid methyl ester (**5a**, 0.012 mol, 4.50 g) was reacted with methyl amine in methanol (2 N) (0.175 mol, 87.35 mL). General workup yielded the product **8.1a** as a white powder (4.32 g, 96 %). R_f = 0.44 (ethyl acetate – hexane 4:1); ^{1}H-NMR (400 MHz, DMSO-d_6): δ= 2.57-2.58 (d, 3, -CH_3); 3.99-4.23 (m, 6, -CH-, -CH_2-); 5.43 (bs, J = 5.4 Hz, 1, -OH); 5.66 (s, 1, -OCHO-); 5.69 (s, 1, -OCHO-); 7.37-7.50 (m, 10, aromatic); 7.99-8.00 (bd, 1, -NH-); ^{13}C-NMR (100 MHz, DMSO-d_6): δ= 25.9 (1, -CH_3); 68.6; 68.7, 69.7; 70.4; 78.9 (5, -CH-, -CH_2-); 99.6; 99.9 (2, -OCHO-); 125.2; 126.6; 126.7; 128.38; 128.41; 129.1; 138.7; 139.1 (12, aromatic); 172.6 (1, -CON-); HRMS (EI): Calculated for $C_{21}H_{22}NO_6$ [M-H]$^+$ 384.1441, found 384.1441; TGA: $T_{-5\ wt\%}$ = 278.14 °C; DSC: T_m = 272.46 °C; $T_{dec.}$ = 296.21 °C; T_m^1 = 263.29 °C (-5.40 J/g); T_c^1 = 262.82 °C (9.07 J/g); T_m^2 = 263.08 °C (-9.45 J/g); T_c^2 = 262.79 °C (12.30 J/g).

3,5:4,6-Dibenzylidene-*L*-gulonic ethyl amide (**8.2a**)

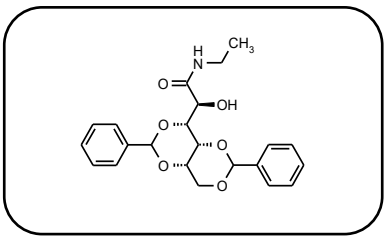

According to the general procedure in two 150 mL beaded rim flasks 3,5:4,6-dibenzylidene-*L*-gulonic acid methyl ester (**5a**, 0.013 mol, 5.00 g) was reacted with ethyl amine in methanol (2 N) (0.194 mol, 97.05 mL). General workup yielded the product **8.2a** as a white powder (4.90 g, 95 %). R_f = 0.49 (ethyl acetate – hexane 4:1); ^{1}H-NMR (400 MHz, DMSO-d_6): δ= 0.96 (t, 3, -CH_3); 2.97-3.07 (m, 1, -CH_2-); 3.07-3.17 (m, 1, -CH_2-); 3.98-4.24 (m, 6, -CH-, -CH_2-); 5.34-5.35 (d, J = 5.4 Hz, 1, -OH); 5.66 (s, 1, -OCHO-); 5.68 (s, 1, -OCHO-); 7.35-7.49 (m, 10, aromatic); 8.04 (t, 1, -NH-); ^{13}C-NMR (100 MHz, DMSO-d_6): δ=15.1 (1, -CH_3); 33.7 (1, -CH_2-); 68.6; 68.8, 69.8; 70.4; 79.0 (5, -CH-, -CH_2-); 99.5; 99.8 (2, -OCHO-); 126.5; 126.7; 128.3; 128.4; 129.0; 138.7; 139.0 (12, aromatic); 171.8 (1, -CON-); HRMS (EI): Calculated for $C_{22}H_{24}NO_6$ [M-H]$^+$ 398.1604, found 398.1597; TGA: $T_{-5\ wt\%}$ = 284.09 °C; DSC: T_m = 263.70 °C; $T_{dec.}$ = 308.45 °C; T_m^1 = 259.28 °C (-146.27 J/g); T_c^1 = 221.64 °C (111.55 J/g); T_m^2 = 255.55 °C (-105.20 J/g); T_c^2 = 208.98 °C (85.70 J/g).

3,5:4,6-Dibenzylidene-*L*-gulonic propyl amide (**8.3a**)

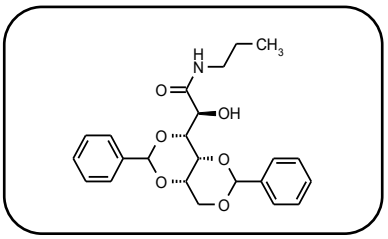

According to the general procedure 3,5:4,6-dibenzylidene-*L*-gulonic acid methyl ester (**5a**, 0.003 mol, 1.00 g) was reacted with propyl amine (0.021 mol, 1.70 mL) in methanol (15.75 mL). General workup yielded the product **8.3a** as a white powder (0.89 g, 84 %). R_f = 0.54 (ethyl acetate – hexane 4:1); ^{1}H-NMR (400 MHz, DMSO-d_6): δ= 0.74 (t, 3, -CH_3); 1.30-1.39 (m, 2, -CH_2-); 2.88-2.96 (m, 1, -CH_2-); 3.03-3.12 (m, 1, -CH_2-); 3.98-4.23 (m, 6, -CH-, -CH_2-); 5.33-5.35 (d, J = 5.3 Hz, 1, -OH); 5.65 (s, 1, -OCHO-); 5.68 (s, 1, -OCHO-); 7.35-7.50 (m, 10, aromatic); 8.02 (t, 1, -NH-); ^{13}C-NMR (100 MHz, DMSO-d_6): δ= 11.8 (1, -CH_3); 22.7 (2, -CH_2-); 68.7; 68.8; 69.8; 70.4; 79.0 (5, -CH-, -CH_2-); 99.6; 99.9 (2, -OCHO-); 126.6; 126.7; 128.3; 128.4; 129.1; 138.7; 139.1 (12, aromatic); 172.0 (1, -CON-); HRMS (EI): Calculated for

$C_{23}H_{26}NO_6$ [M-H]$^+$ 412.1760, found 412.1755; TGA: $T_{-5\ wt\%}$ = 269.29 °C; DSC: T_m = 263.71 °C; $T_{dec.}$ = 293.98 °C; T_m^1 = 260.33 °C (-131.00 J/g); T_c^1 = 219.26 °C (88.24 J/g); T_m^2 = 255.36 °C (-81.56 J/g); T_c^2 = 206.26 °C (60.37 J/g).

3,5:4,6-Dibenzylidene-*L*-gulonic butyl amide (**8.4a**)

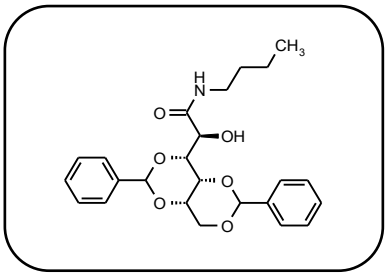

According to the general procedure 3,5:4,6-dibenzylidene-*L*-gulonic acid methyl ester (**5a**, 0.003 mol, 1.00 g) was reacted with butyl amine (0.021 mol, 2.05 mL) in methanol (15.75 mL). General workup yielded the product **8.4a** as a white powder (0.80 g, 83 %). R_f = 0.59 (ethyl acetate – hexane 4:1); ^{1}H-NMR (400 MHz, DMSO-d_6): δ= 0.74 (t, 3, -CH_3); 1.12-1.21 (m, 2, -CH_2-); 1.27-1.35 (m, 2, -CH_2-); 2.90-2.97 (m, 1, -CH_2-); 3.09-3.18 (m, 1, -CH_2-); 3.98-4.23 (m, 6, -CH-, -CH_2-); 5.32-5.34 (d, J = 5.3 Hz, 1, -OH); 5.65 (s, 1, -OCHO-); 5.68 (s, 1, -OCHO-); 7.34-7.50 (m, 10, aromatic); 8.00 (t, 1, -NH-); ^{13}C-NMR (100 MHz, DMSO-d_6): δ = 14.1 (1, -CH_3); 19.9 (1, -CH_2-); 31.7 (1, -CH_2-); 38.4 (1, -CH_2-); 68.7; 68.8; 69.8; 70.4; 79.0 (5, -OCHO-); 99.7; 99.9 (2, -OCHO-); 126.6; 126.7; 128.3; 128.4; 129.1; 138.7; 139.1 (12, aromatic); 172.0 (1, -CON-); HRMS (EI): Calculated for $C_{23}H_{28}NO_6$ [M-H]$^+$ 426.1917, found 426.1912; TGA: $T_{-5\ wt\%}$ = 295.46 °C; DSC: T_m = 246.82 °C; $T_{dec.}$ = 304.17 °C; T_m^1 = 242.50 °C (-135.04 J/g); T_c^1 = 213.80 °C (107.24 J/g); T_m^2 = 238.96 °C (-91.59 J/g); T_c^2 = 205.76 °C (90.00 J/g).

3,5:4,6-Dibenzylidene-*L*-gulonic octyl amide (**8.5a**)

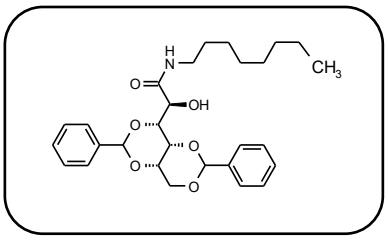

According to the general procedure 3,5:4,6-dibenzylidene-*L*-gulonic acid methyl ester (5**a**, 0.013 mol, 5.00 g) was reacted with octyl amine (0.104 mol, 17.15 mL) in methanol (78.00 mL). General workup yielded the product **8.5a** as a white powder (5.80 g, 93 %). R_f = 0.70 (ethyl acetate – hexane 4:1); ^{1}H-NMR (400 MHz, DMSO-d_6): δ= 0.84 (t, 3, -CH_3); 1.14-1.25 (m, 10, -CH_2-); 1.31-1.34 (m, 2, -CH_2-); s.89-2.97 (m, 1, -CH_2-); 3.07-3.16 (m, 1, -CH_2-); 3.98-4.23 (m, 6, -CH-, -CH_2-); 5.32-5.33 (d, J = 5.3 Hz, 1, -OH); 5.65 (s, 1, -OCHO-); 5.68 (s, 1, -OCHO-); 7.34-7.50 (m, 10, aromatic); 8.00 (t, 1, -NH-); ^{13}C-NMR (100 MHz, DMSO-d_6): δ = 14.4 (1, -CH_3); 22.6; 26.8; 29.0; 29.2; 29.6; 31.8; 38.8 (7, -CH_2-); 68.7; 68.8; 69.8; 70.4; 79.0 (5, -CH-, -CH_2-); 99.6; 99.9 (2, -OCHO-); 126.6; 126.7; 128.3; 128.4; 129.0; 129.1; 138.7; 139.0 (10, aromatic); 171.9 (1, -CON-); HRMS (EI): Calculated for $C_{28}H_{36}NO_6$ [M-H]$^+$ 482.2543, found 482.2534; TGA: $T_{-5\ wt\%}$ = 320.52 °C; DSC: T_m = 208.64 °C; $T_{dec.}$ = 305.11 °C; T_m^1 = 205.93 °C (-110.54 J/g); T_c^1 = 167.67 °C (72.52 J/g); T_m^2 = 200.11 °C (-60.10 J/g); T_c^2 = 162.81 °C (49.16 J/g).

3,5:4,6-Dibenzylidene-*L*-gulonic dodecyl amide (**8.6a**)

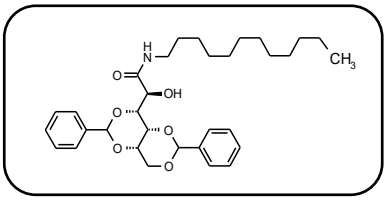

According to the general procedure 3,5:4,6-dibenzylidene-*L*-gulonic acid methyl ester (**5a**, 0.004 mol, 1.50 g) was reacted with dodecyl amine (0.031 mol, 7.20 mL) in methanol (23.25 mL). General workup yielded the product **8.6a** as a white powder (1.58 g, 75 %). R_f = 0.75 (ethyl acetate – hexane 4:1); ^{1}H-NMR (400 MHz, DMSO-d_6): δ= 0.85 (t, 3, -CH_3); 1.13-1.32 (m, 20, -CH_2-); 2.89-2.97 (m, 1, -CH_2-); 3.08-3.16 (m, 1, -CH_2-); 3.98-4.23 (m, 6, -CH-, -CH_2-); 5.32-5.33 (d, J = 5.3 Hz, 1, -OH); 5.65 (s, 1, -OCHO-); 5.68 (s, 1, -OCHO-); 7.34-7.49 (m, 10, aromatic); 8.00 (t, 1, -NH-); ^{13}C-NMR (100 MHz, DMSO-d_6): δ=14.4 (1, -CH_3); 22.6; 26.8; 29.2; 29.3; 29.4; 29.5; 29.5; 29.6; 31.8; 38.8 (11, -CH_2-); 68.7; 68.8; 69.8; 70.4; 79.0 (5, -CH-, -CH_2-); HRMS (EI): Calculated for $C_{32}H_{44}NO_6$ $[M-H]^+$ 538.3169, found 538.3167; TGA: $T_{-5\ wt\%}$ = 321.41 °C; DSC: T_m = 194.20 °C; $T_{dec.}$ = 274.75 °C; T_m^1 = 192.75 °C (-116.99 J/g); T_c^1 = 165.77 °C (36.78 J/g); T_m^2 = 166.53 °C (27.83 J/g); T_c^2 = 163.12 °C (28.15 J/g).

3,5:4,6-bis-(3,4-Dimethylbenzylidene)-*L*-gulonic methyl amide (**8.1c**)

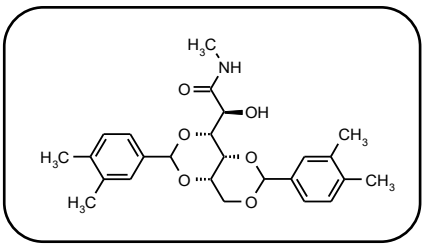

According to the general procedure 3,5:4,6-bis-(3,4-dimethylbenzylidene)-L-gulonic acid methyl ester (**5c**, 0.009 mol, 3.80 g) was reacted with methyl amine in methanol (2 N) (0.123 mol, 64.41 mL). General workup yielded the product **8.1c** as a white powder (3.57 g, 94 %). R_f = 0.00-0.10 (ethyl acetate – hexane 4:1); ^{1}H-NMR (400 MHz, DMSO-d_6): δ= 2.21-2.23 (bd, 12, -CH_3); 2.56-2.57 (d, 3, -CH_3); 3.92-4.18 (m, 6, -CH-, -CH_2-); 5.35-5.37 (d, J = 5.3 Hz, 1, -OH); 5.55 (s, 1, -OCHO-); 5.59 (s, 1, -OCHO-); 7.12-7.23 (m, 6, aromatic); 7.98-7.99 (bd, 1, -NH-); HRMS (EI): Calculated for $C_{25}H_{30}NO_6$ $(M-H)^+$ 440.2073, found 440.2066; TGA: $T_{-5\ wt\%}$ = 305.55 °C; DSC: T_m = 315.38 °C; $T_{dec.}$ = 239.43 °C, 328.97 °C.

3,5:4,6-bis-(3,4-Dimethylbenzylidene)-*L*-gulonic ethyl amide (**8.2c**)

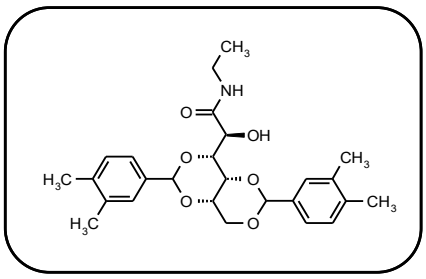

According to the general procedure 3,5:4,6-bis-(3,4-dimethylbenzylidene)-L-gulonic acid methyl ester (**5c**, 0.009 mol, 3.80 g) was reacted with ethyl amine in methanol (2 N) (0.123 mol, 64.41 mL). General workup yielded the product **8.2c** as a white powder (3.72 g, 95 %). R_f = 0.00 (ethyl acetate – hexane 4:1); ^{1}H-NMR (400 MHz, DMSO-d_6): δ =0.96-1.00 (t, 3, -CH_3); 2.21-2.23 (m, 12, -CH_3); 2.98-3.17 (m, 2, -CH_2-); 3.92-4.16 (m, 6, -CH-, -CH_2-); 5.30 (bd, J = 5.3 Hz, 1, -OH); 5.57 (s, 1, -OCHO-); 5.59 (s, 1, -OCHO-); 7.11-7.22 (m, 6, aromatic); 8.05 (t, 1, -NH-); HRMS (EI): Calculated for $C_{26}H_{32}NO_6$ $(M-H)^+$ 454.2230, found 454.2225; TGA: $T_{-5\ wt\%}$ = 296.72 °C; DSC: T_m = 303.10 °C; $T_{dec.}$ = 152.92 °C, 321.03 °C.

3,5:4,6-di-(4-Propylbenzylidene)-*L*-gulonic methyl amide (**8.1h**)

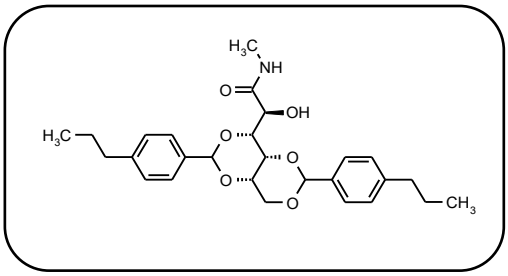

According to the general procedure 3,5:4,6-di-(4-propylbenzylidene)-L-gulonic acid ethyl ester (**5.2h**, 0.008 mol, 4.00 g) was reacted with ethyl amine in methanol (2 N) (0.124 mol, 61.91 mL). General workup yielded the product **8.1h** as a white powder (3.61 g, 93 %). R_f = 0.61 (ethyl acetate – hexane 4:1); ^{1}H-NMR (400 MHz, DMSO-d6): δ = 0.85-0.90 (t, 6, -CH_3); 1.53-1.62 (m, 4, -CH_2-); 2.53-2.56 (m, 7, -CH_2-, -CH_3); 3.94-4.20 (m, 6, -CH-, -CH_2-); 5.37-5.39 (d, J = 5.3 Hz, 1, -OH); 5.60 (s, 1, -OCHO-); 5.63 (s, 1, -OCHO-); 7.17-7.20 (m, 4, aromatic); 7.31-7.33 (d, 2, aromatic); 7.37-7.39 (d, s, aromatic); 7.96-7.97 (bd, 1, -NH-); HRMS (EI): Calculated for $C_{27}H_{34}NO_6$ $(M-H)^+$ 468.2386, found 468.2378; TGA: $T_{5\ wt\%}$ = 298.71 °C; DSC: T_m = 214.97 °C, 253.19 °C; $T_{dec.}$ = 303.82 °C; T_m^1 = 221.31 °C (-12.21 J/g), 251.12 °C (-124.49 J/g); T_c^1 = 231.07 °C (105.35 J/g); T_m^2 = 249.34 °C (-103.41 J/g); T_c^2 = 230.65 °C (97.29 J/g).

3,5:4,6-di-(4-Propylbenzylidene)-*L*-gulonic ethyl amide (**8.2h**)

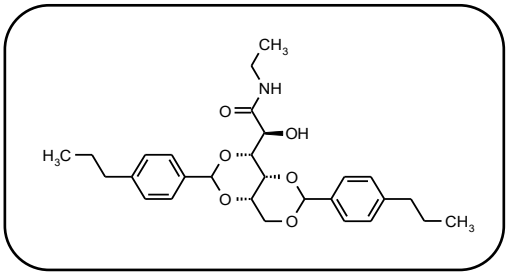

According to the general procedure 3,5:4,6-di-(4-propylbenzylidene)-L-gulonic acid ethyl ester (**5.2h**, 0.008 mol, 4.00 g) was reacted with ethyl amine in methanol (2 N) (0.124 mol, 61.91 mL). General workup yielded the product **8.2h** as a white powder (3.67 g, 92 %). R_f = 0.59 (ethyl acetate – hexane 4:1); ^{1}H-NMR (400 MHz, DMSO-d_6): δ = 0.85-0.89 (m, 6, -CH_3); 0.96 (t, 3, -CH_3); 1.52-1.62 (m, 4, -CH_2-); 2.52-2.57 (m, 4, -CH_2-); 2.95-3.04 (m, 1, -CH_2-); 3.08-3.14 (m, 1, -CH_2-); 5.30-5.32 (d, 1, -OH); 5.61 (s, 1, -OCHO-); 5.63 (s, 1, -OCHO-); 7.18 (t, 4, aromatic); 7.31-7.33 (d, 2, aromatic); 7.37-7.39 (d, 2, aromatic); 8.02 (t, 1, -NH-);HRMS (EI): Calculated for $C_{28}H_{36}NO_6$ $[M-H]^+$ 482.2543, found 482.2533; TGA: $T_{5\ wt\%}$ = 314.76 °C; DSC: T_m = 246.12 °C; $T_{dec.}$ = 315.76 °C; T_m^1 = 240.97 °C (-90.59 J/g); T_c^1 = 172.99 °C (19.54 J/g); T_m^2 = 208.63 °C (-14.54 J/g).

Appendix

Gelation test for the tested additives (1.0 wt% in *n*-Octanol)

5a	5b	5c	5d	5e	5f	5h	5i
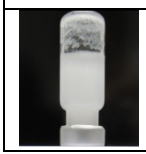							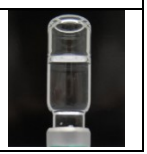

6a	6b	6c	6d	6e	6f	6h	6i
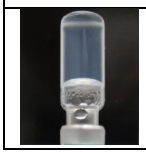							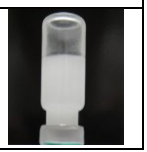

7a	7b	7c	7d	7e	7f	7h	7i
							

8.1a	8.2a	8.3a	8.4a	8.5a	8.6a
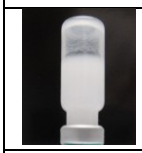					

8.1c	8.2c	8.1h	8.2h
			

DMDBS	TBPMN
	

β-phase content (k-value)

	wt%								
#	0	0.01	0.02	0.03	0.15	0.30	0.45	0.60	0.75
Control	0.04	-	-	-	-	-	-	-	-
DMDBS	-	-	-	0.05	0.04	0.03	0.02	0.02	-
TBPMN	-		-	-	-	0.04	-	-	-
NA 11	-	-	-	-	-	0.03	-	-	-
NA 71	-	-	-	-	-	0.03	-	-	-
XT	-			-	-	0.03	-	-	-
5a	-	-	-	-	-	0.05	-	-	-
5b	-	-	-	-	-	0.05	-	-	-
5c	-	-	-	-	-	0.06	-	0.04	0.04
5d	-	-	-	-	-	0.08	-	-	-
5e	-	-	-	-	-	0.06	-	-	-
5f	-	-	-	-	-	0.04	-	-	-
5h	-	-	-	-	-	0.02	-	-	-
5i	-	-	-	-	-	0.05	-	-	-
6a	-	-	-	-	-	0.05	-	-	-
6b	-	-	-	-	-	0.03	-	-	-
6c	-	-	-	-	-	0.03	-	0.03	-
6d	-	-	-	-	-	0.03	-	-	-
6e	-	-	-	-	-	0.03	-	-	-
6f	-	-	-	-	-	0.04	-	-	-
6h	-	-	-	-	-	0.04	-	-	-
6i	-	-	-	-	-	0.03	-	-	-
7a	-	-	-	-	-	0.06	-	-	-
7b	-	-	-	-	-	0.03	-	-	-
7c	-	-	-	-	-	0.03	-	0.03	-
7d	-	-	-	-	-	0.03	-	-	-
7e	-	-	-	-	-	0.04	-	-	-
7f	-	-	-	-	-	0.04	-	-	-
7h	-	-	-	-	-	0.04	-	0.05	-
7i	-	-	-	-	-	0.04	-	-	-
8.1a	-	-	-	-	-	0.04	-	0.05	-
8.2a	-	-	-	-	-	0.04	-	0.04	-
8.3a	-	-	-	-	-	0.05	-	0.06	-
8.4a	-	-	-	-	-	0.04	-	0.05	-
8.5a	-	-	-	-	-	0.04	-	0.04	-
8.6a	-	-	-	-	-	0.05	-	0.04	-
8.1c	-	-	-	0.08	0.13	0.18	0.27	0.30	-
8.1h	-	-	-	-	-	0.04	-	0.04	-
8.2c	-	-	-	-	-	0.04	-	0.03	-
8.2h	-	-	-	-	-	0.05	-	0.04	-

Nucleation Efficiency

	wt%								
#	0	0.01	0.02	0.03	0.15	0.30	0.45	0.60	0.75
Control	0 %	-	-	-	-	-	-	-	-
DMDBS	-	-	-	0	60	64	65	67	-
TBPMN	-		-	4	25	66	71	72	-
NA 11	-	-	-	42	57	61	63	65	-
NA 71	-	-	-	35	62	65	70	72	-
XT	-	46	47	49	37	43	46	45	-
5a	-	-	-	3	3	4	26	49	-
5b	-	-	-	9	8	37	46	40	-
5c	-	-	-	4	10	56	53	56	56
5d	-	-	-	11	55	65	64	46	-
5e	-	-	-	4	1	23	37	34	-
5f	-	-	-	8	8	7	10	39	-
5h	-	-	-	5	5	6	8	8	-
5i	-	-	-	4	7	5	7	6	-
6a	-	-	-	3	14	22	39	41	-
6b	-	-	-	5	10	26	34	29	-
6c	-	-	-	9	13	31	42	39	-
6d	-	-	-	7	10	32	44	43	-
6e	-	-	-	6	34	40	38	22	-
6f	-	-	-	7	13	14	16	18	-
6h	-	-	-	7	12	15	15	18	-
6i	-	-	-	9	11	15	28	17	-
7a	-	-	-	7	23	48	26	36	-
7b	-	-	-	6	31	36	36	33	-
7c	-	-	-	0	40	39	37	34	-
7d	-	-	-	4	32	34	40	39	-
7e	-	-	-	0	1	33	33	56	-
7f	-	-	-	8	10	20	34	13	-
7h	-	-	-	4	15	33	30	32	-
7i	-	-	-	5	8	9	36	50	-
8.1a	-	-	-	13	14	55	53	53	-
8.2a	-	-	-	4	10	11	36	36	-
8.3a	-	-	-	6	10	31	42	40	-
8.4a	-	-	-	6	10	11	47	46	-
8.5a	-	-	-	10	11	13	5	6	-
8.6a	-	-	-	10	11	13	17	17	-
8.1c	-	-	-	7	40	42	37	41	-
8.1h	-	-	-	6	7	46	50	49	-
8.2c	-	-	-	6	47	34	40	32	-
8.2h	-	-	-	11	12	29	63	65	-

Micrographs

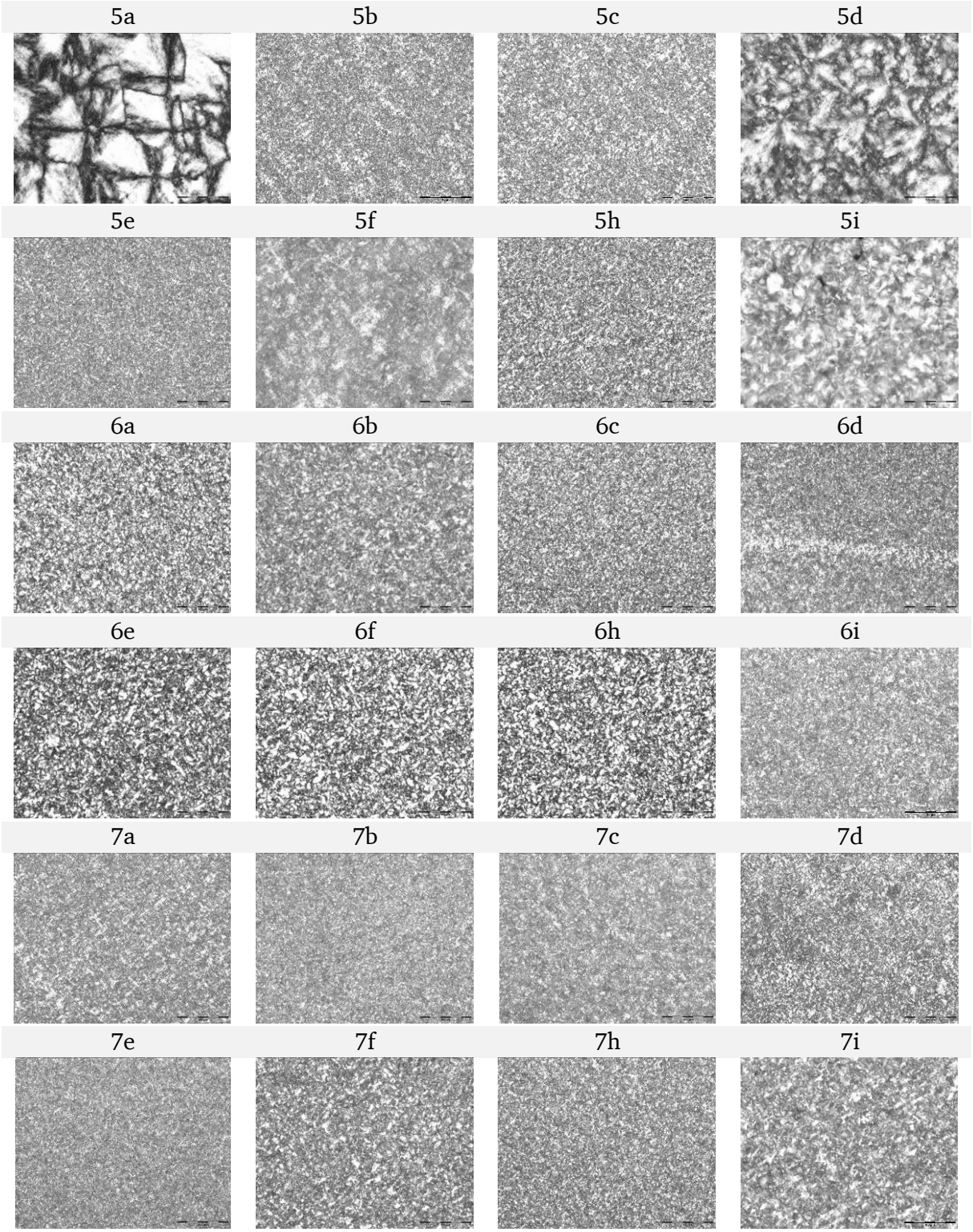

Figure A-1 Polarized optical micrographs of melt-compression-molded iPP films. Concentration: 0.60 wt% of the respective additive 5 or 6 and 0.30 wt% of the respective additive 7. Scale bar 100 µm.

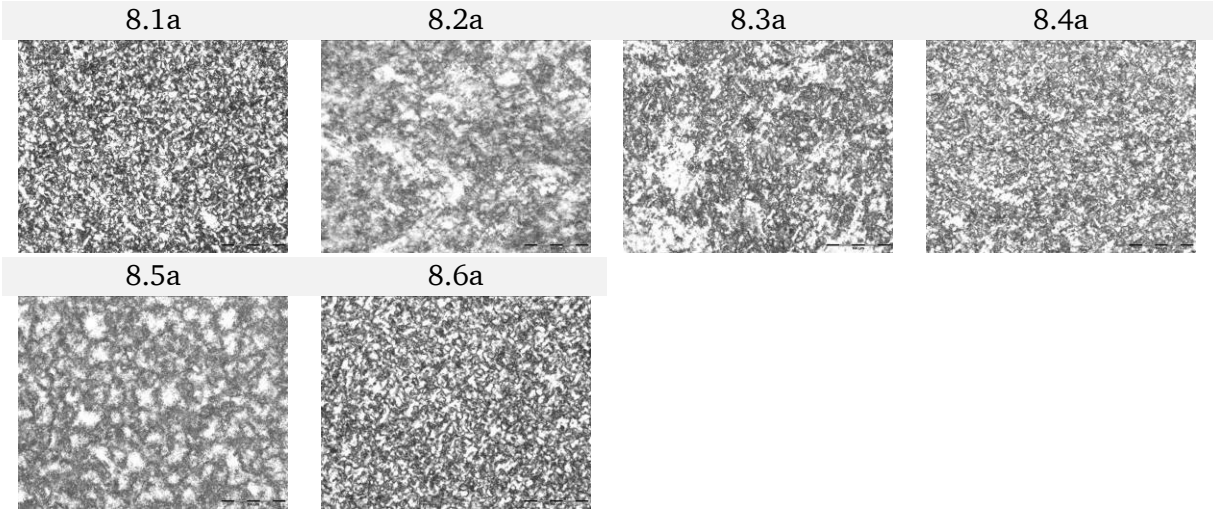

Figure A-2 Polarized optical micrographs of melt-compression-molded iPP films. Concentration: 0.60 wt% of the respective additive 8. Scale bar 100 µm.

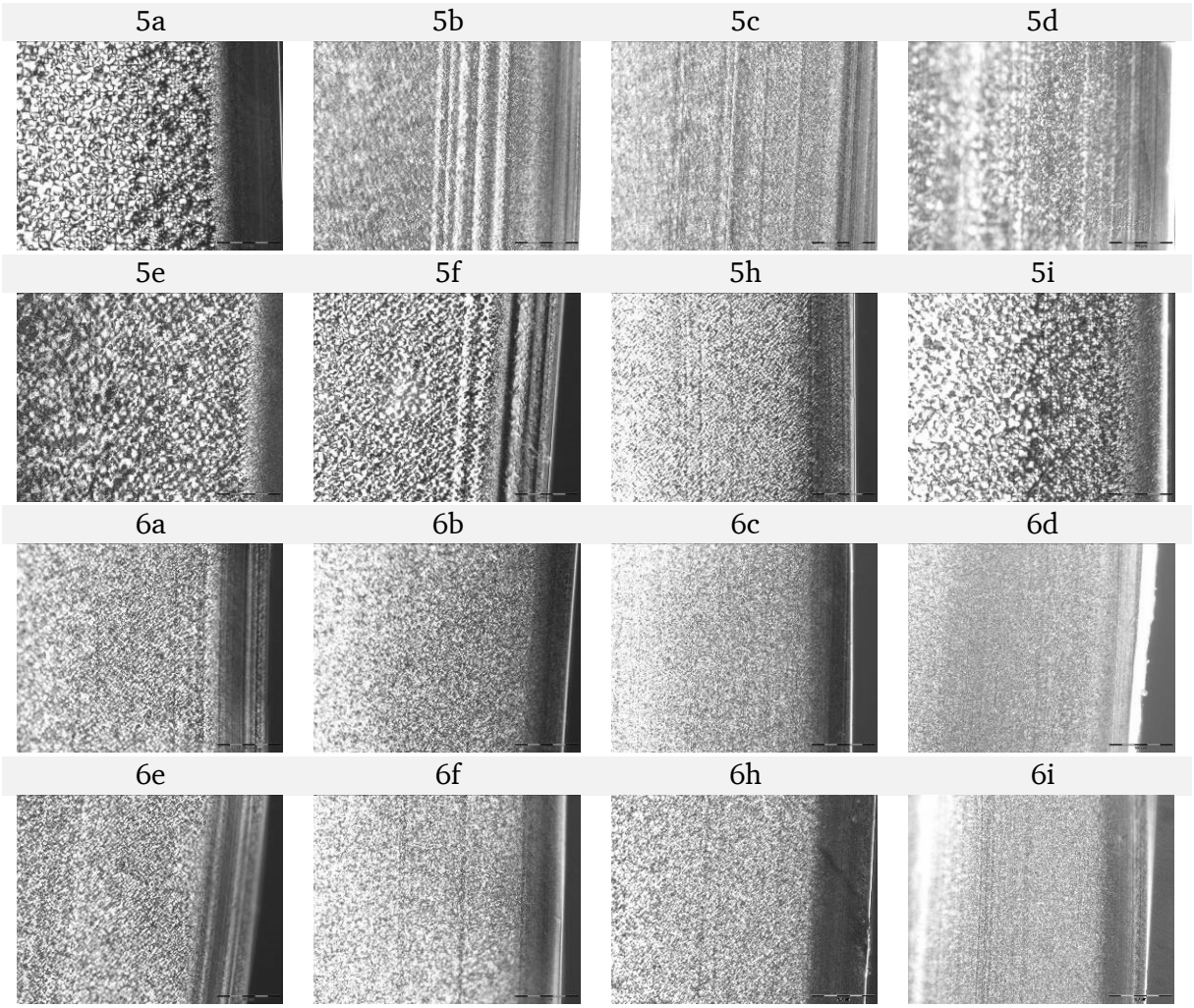

Figure A-3 Polarized optical micrographs of 10 µm thin-sections of 1.0 mm injection-molded iPP plaques. Concentration: 0.60 wt% of the respective additive 5 or 6. Scale bar 100 µm.

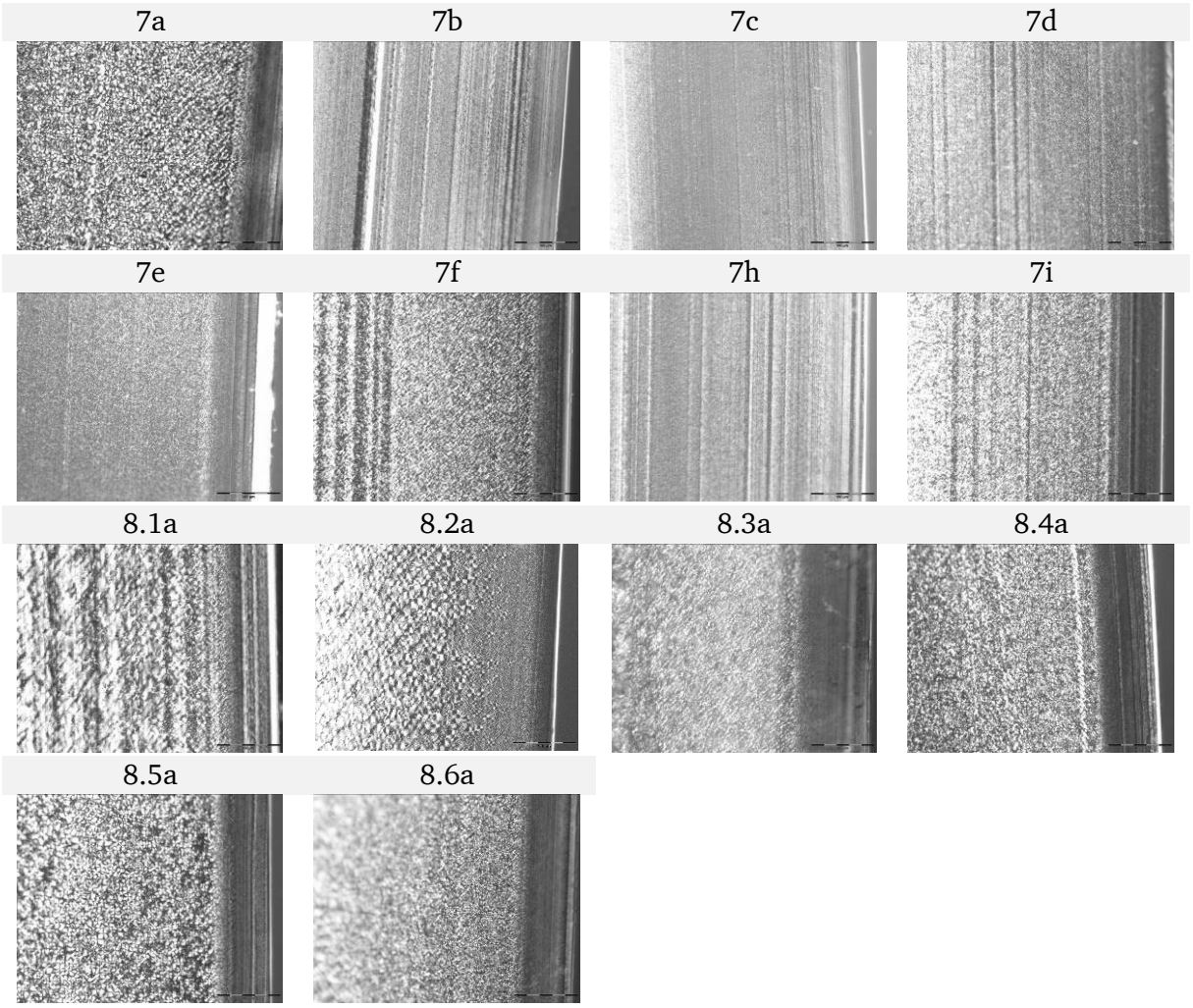

Figure A-4 Polarized optical micrographs of 10 µm thin-sections of 1.0 mm injection-molded iPP plaques. Concentration: 0.30 wt% of the respective additive 7 and 0.60 wt% of the respective additive 8. Scale bar 100 µm.

Crystallinity

	wt%								
#	0	0.01	0.02	0.03	0.15	0.30	0.45	0.60	0.75
Control	44.0 %	-	-	-	-	-	-	-	-
DMDBS	-	-	-	42.5	50.5	50.7	48.9	51.3	-
TBPMN	-		-	45.5	46.5	50.0	50.8	50.9	-
NA 11	-	-	-	48.6	49.9	45.8	49.7	50.8	-
NA 71	-	-	-	44.5	50.7	49.7	50.6	51.7	-
XT	-	49.7	50.9	51.0	49.7	51.2	49.7	49.9	-
5a	-	-	-	46.1	46.9	47.2	47.6	46.8	-
5b	-	-	-	45.0	47.1	47.3	48.3	48.6	-
5c	-	-	-	45.5	45.8	47.9	47.7	50.4	50.3
5d	-	-	-	45.4	48.3	48.8	48.8	47.6	-
5e	-	-	-	46.2	45.4	47.6	47.1	49.7	-
5f	-	-	-	48.2	46.5	46.2	45.6	48.2	-
5h	-	-	-	44.7	47.3	45.3	44.2	24.2	-
5i	-	-	-	46.4	46.5	46.8	46.8	48.0	-
6a	-	-	-	44.0	45.9	47.8	49.5	46.9	-
6b	-	-	-	45.3	49.3	45.6	47.4	45.6	-
6c	-	-	-	48.4	46.9	46.7	49.0	46.1	-
6d	-	-	-	46.5	48.9	50.8	49.6	50.0	-
6e	-	-	-	46.4	49.5	49.6	46.5	47.2	-
6f	-	-	-	42.8	44.4	43.8	44.2	35.9	-
6h	-	-	-	43.4	44.9	42.7	42.8	38.7	-
6i	-	-	-	48.3	45.8	47.2	46.2	50.0	-
7a	-	-	-	43.5	48.1	46.8	46.5	45.4	-
7b	-	-	-	46.3	47.7	50.0	49.1	48.6	-
7c	-	-	-	46.3	50.6	49.6	49.8	50.0	-
7d	-	-	-	46.4	47.6	48.2	50.1	48.7	-
7e	-	-	-	45.4	46.0	44.1	47.3	47.8	-
7f	-	-	-	48.5	47.0	47.3	45.9	46.4	-
7h	-	-	-	46.9	46.5	47.8	49.1	50.0	-
7i	-	-	-	46.1	45.5	45.0	47.8	49.7	-
8.1a	-	-	-	45.2	46.2	47.3	46.6	46.0	-
8.2a	-	-	-	39.8	48.0	46.1	47.1	44.8	-
8.3a	-	-	-	45.8	46.5	48.3	47.6	47.0	-
8.4a	-	-	-	45.3	45.4	45.7	48.2	47.8	-
8.5a	-	-	-	45.8	47.7	45.7	46.0	45.4	-
8.6a	-	-	-	44.4	43.9	46.9	45.7	46.5	-
8.1c	-	-	-	48.5	51.9	50.5	50.7	49.7	-
8.1h	-	-	-	43.0	45.5	46.8	51.9	48.5	-
8.2c	-	-	-	46.9	50.3	47.8	46.1	47.9	-
8.2h	-	-	-	46.7	45.1	49.2	50.7	49.6	-

Yellowness Index

	wt%								
#	0	0.01	0.02	0.03	0.15	0.30	0.45	0.60	0.75
Control	2.20	-	-	-	-	-	-	-	-
DMDBS	-	-	-	2.38	1.51	2.21	2.27	2.44	-
TBPMN	-		-	2.43	1.11	0.98	1.47	0.68	-
NA 11	-	-	-	2.35	2.17	2.07	2.15	2.29	-
NA 71	-	-	-	2.30	1.63	2.03	2.37	2.54	-
XT	-	1.43	1.85	1.73	1.90	1.80	1.94	2.21	-
5a	-	-	-	2.63	2.56	2.96	4.15	4.51	-
5b	-	-	-	2.50	2.58	2.74	2.48	2.47	-
5c	-	-	-	2.65	2.68	2.71	2.39	2.50	2.52
5d	-	-	-	2.67	2.71	2.90	8.32	6.84	-
5e	-	-	-	2.55	2.49	2.54	2.51	2.17	-
5f	-	-	-	1.71	2.56	2.50	2.61	2.60	-
5h	-	-	-	1.84	1.87	2.01	2.13	2.28	-
5i	-	-	-	2.47	2.56	2.47	2.56	2.61	-
6a	-	-	-	3.09	4.32	3.73	4.22	7.84	-
6b	-	-	-	2.80	4.23	3.57	4.37	7.45	-
6c	-	-	-	2.79	2.95	2.86	3.15	5.91	-
6d	-	-	-	2.71	3.18	2.85	2.52	3.77	-
6e	-	-	-	2.58	3.92	3.64	5.14	16.0	-
6f	-	-	-	2.76	6.24	9.60	9.30	6.26	-
6h	-	-	-	2.89	7.06	17.0	15.5	15.0	-
6i	-	-	-	2.83	7.68	15.1	11.3	7.99	-
7a	-	-	-	2.44	3.23	5.38	7.63	6.13	-
7b	-	-	-	2.56	1.80	2.44	3.26	3.75	-
7c	-	-	-	2.53	1.75	2.43	3.19	3.72	-
7d	-	-	-	2.48	1.59	3.01	3.31	3.64	-
7e	-	-	-	2.47	2.59	2.12	2.75	3.43	-
7f	-	-	-	2.49	2.70	3.04	3.93	4.62	-
7h	-	-	-	2.51	2.23	2.36	3.27	3.74	-
7i	-	-	-	2.67	2.77	2.85	2.66	3.58	-
8.1a	-	-	-	2.58	2.59	2.70	3.20	3.05	-
8.2a	-	-	-	2.79	2.73	2.83	2.23	2.20	-
8.3a	-	-	-	2.71	2.74	3.03	3.32	3.21	-
8.4a	-	-	-	2.74	2.74	3.14	3.24	3.24	-
8.5a	-	-	-	2.73	2.74	2.72	2.65	2.73	-
8.6a	-	-	-	2.79	2.75	2.77	2.70	2.73	-
8.1c	-	-	-	1.80	1.68	2.93	4.22	5.16	-
8.1h	-	-	-	1.76	1.82	1.60	1.52	1.78	-
8.2c	-	-	-	1.86	1.76	1.63	1.78	2.72	-
8.2h	-	-	-	2.53	2.65	2.65	2.44	2.63	-

List of abbreviations

aPP	Atactic polypropylene
CA	Clarifying agent
CI	Chemical ionization
copo	Copolymer
Conc.	Concentration
C_x	Number of carbon atoms in each molecule
DBS	Dibenzylidene sorbitol
DMDBS	Bis (3,4-dimethylbenzylidene) sorbitol
DSC	Differential scanning calorimetry
DBGA	Dibenzylidene-*L*-gulonic amide
DBGA-*n*	Dibenzylidene-*L*-gulonic alkyl amide
DBGAc	Dibenzylidene-*L*-gulonic acid
DBGAcMeE	Dibenzylidene-*L*-gulonic acid methyl ester
EDBS	Bis (4-ethylbenzylidene) sorbitol
EI	Electron ionization
G	Gel
GC	Gas chromatography
HBA	Hydrogen bond acceptor
HBD	Hydrogen bond donor
HDPE	High-density polyethylene
homo	Homopolymer
HR-MS	High resolution mass spectrometry
HSQC	Heteronuclear single quantum coherence
ΔH_m^0	Enthalpy of fusion of the totally crystalline polymer
iPP	Isotactic polypropylene
k	β-Phase content
LDPE	Low-density polyethylene
LMOGs	Low molecular-mass organic gelators

MBS		Monobenzylidene sorbitol
MDBS		Bis (4-methylbenzylidene) sorbitol
MFR	[g·10 min^{-1}]	Melt flow rate
M_n	[g·mol^{-1}]	Number average molecular weight
M_w	[g·mol^{-1}]	Weight average molecular weight
NA		Nucleating agent
NE		Nucleation efficiency
NMR		Nuclear magnetic resonance
OH		Hydroxyl
p		Para
P		Particulate
ppm		Parts per million
PA		Polyamide
PE		Polyethylene
PET		Polyethylene terephthalate
PS		Polystyrene
PTFE		Polytetrafluoroethylene
PP		Polypropylene
PVC		Polyvinyl chloride
PVCH		Poly (vinylcyclohexane)
raco		Random copolymer
rpm		Rounds per minute
S		Soluble
SALS		Small-angle light scattering
SAXS		Small-angle X-ray scattering
SEM		Scanning electron microscopy
sPP		Syndiotactic polypropylene
$T_{-5\ wt\%}$	[°C]	5 % weight loss temperature
$t_{1/2}$	[min]	Crystallization halftime

TBS		Tribenzylidene sorbitol
TBPMN		Tridesoxy-bis-*O*-[(4-propylphenyl) methylene]-nonitol
T_c	[°C]	Crystallization temperature
$T_{c,p}$	[°C]	Crystallization temperature, polymer
ΔT_0	[°C]	Degree of super-cooling / undercooling
tert		Tertiary
T_g	[°C]	Glass transition temperature
TGA		Thermogravimetric analysis
T_m^0	[°C]	Equilibrium melting point
T_m	[°C]	Melting temperature
$T_{m,p}$	[°C]	Melting temperature, polymer
TMS		Tetramethylsilane
TLC		Thin-layer chromatography
Trans.		Transmission
USD		United states dollar
UV		Ultraviolet
vS		Viscous solution
vs.		Versus
WAXD		Wide-angle X-ray diffraction
WAXS		Wide-angle X-ray scattering
wt%	[%]	Weight percent
X_c	[%]	Degree of crystallinity
YI	[-]	Yellowness index
α, β, γ		iPP crystal modifications
δ	[ppm]	Chemical shift
η^*	[Pa·s]	Shear viscosity

List of Figures

List of Tables

11. Literature Cited

1. Markets and Markets. *Nucleating & clarifying agents market to reach US$4.45 billion by 2026.* Additives for Polymers 2017; (2):11.

2. Zweifel H., editor. *Plastics Additives Handbook.* 6th Ed. Munich: Hanser Verlag; 2009.

3. Meeten G.H., editor. *Optical Properties of Polymers.* London: Elsevier Applied Science; 1986.

4. Bonte Y., Schweda R. *Polypropylen (PP).* Kunststoffe 2001; 91:262–6.

5. Pritchard G. *Plastics Additives:* An A-Z Reference. London: Chapman & Hall; 1997.

6. Kurja J., Mehl N. A. *Nucleating Agents for Semi-crystalline Polymers. In:* Zweifel H., editor. Plastics Additives Handbook. 6th Ed. Munich: Hanser Verlag; 2009.

7. AMI Consulting. *Global demand trends for polyolefins*. In: Polyolefins Additive 2017: International conference on polyolefin performance, compounding, blending and additives. Vienna, Austria; 2017.

8. Maier R.D., Kristiansen P.M. *Nukleierungsmittel und Transperenzverstärker. In:* Maier R.D., Schiller M., editors. Handbuch Kunststoff-Additive. 4., vollständig neu bearbeitete Auflage. München: Hanser; 2016.

9. *Clariant's latest Cesa products target clear PP and improved PET, PLA recycling.* Additives for Polymers 2017; (6):1–2.

10. Townsend Solutions. *Plastic Additives 9:* Nucleating and Clarifying Agents; Market Reports; 2017.

11. Pasquini N, editor. *Polypropylene handbook.* 2nd Ed. Munich: Hanser; 2005.

12. Maier C, Calafut T. *Polypropylene:* The Definitive User's Guide and Databook. Norwich: Plastics Design Library; 1998.

13. Gahleitner M, Paulik C. *Polypropylene.* Ullmann's Encyclopedia of Industrial Chemistry. Weinheim: Wiley-VCH; 2000.

14. Gedde U.W. *Polymer physics.* 2nd Ed. Dordrecht: Springer Science+Business Media; 1999.

15. Corradini P, Auriemma F, Rosa C de. *Crystals and Crystallinity in Polymeric Materials.* Accounts of Chemical Research 2006; 39(5):314–23.

16. Tjong S.C., Li R.K.Y., Cheung T. *Mechanical Behavior of $CaCO_3$ Particulate-Filled β-Crystalline Phase Polypropylene Composites.* Polymer Engineering & Science 1997; 37(1):166–72.

17. Varga J., Karger-Kocsis J. *Rules of Supermolecular Structure Formation in Sheared Isotactic Polypropylene Melts.* Journal of Polymer Science Part B: Polymer Physics 1996; 34(4):657–70.

18. Dragaun H., Hubeny H., Muschik H. *Shear-Induced β-Form Crystallization in Isotactic Polypropylene.* Journal of Polymer Science: Polymer Physics Edition 1977; 15(10):1779–89.

19. Leugering H.J., Kirsch G. *Beeinflussung der Kristallstruktur von isotaktischem Polypropylen durch Kristallisation aus orientierten Schmelzen.* Angewandte Makromolekulare Chemie 1973; 33(1):17–23.

20. Chen Y.-H., Mao Y.-M., Li Z.-M., Hsiao B.S. *Competitive Growth of α- and β-Crystals in β-Nucleated Isotactic Polypropylene under Shear Flow.* Macromolecules 2010; 43(16):6760–71.

21. Lovinger AJ, Chua J.O., Gryte C.C. *Studies on the α and β Forms of Isotactic Polypropylene by Crystallization in a Temperature Gradient.* Journal of Polymer Science: Polymer Physics Edition 1977; 15(4):641–56.

22. Turner-Jones A., Aizlewood J.M., Beckett D.R. *Crystalline Forms of Isotactic Polypropylene.* Macromolecular Chemistry and Physics 1964; 75(1):134–58.

23. Campbell R.A., Phillips P.J., Lin J.S. *The gamma phase of high-molecular-weight polypropylene:* 1. Morphological aspects. Polymer 1993; 34(23):4809–16.

24. Mezghani, K., Phillips, P.J. *The Morphology of the Gamma Form of Isotactic Polypropylene at 200 MPA.* Society of Plastics Engineers 1996; conference proceedings - ANTEC 1996.

25. Varga J., Ehrenstein G.W., Schlarb A.K. *Vibration welding of alpha and beta isotactic polypropylenes:* Mechanical properties and structure. Express Polymer Letters 2008; 2(3):148–56.

26. Luo F., Geng C., Wang K., Deng H., Chen F., Fu Q. et al. *New Understanding in Tuning Toughness of β-Polypropylene:* The Role of β-Nucleated Crystalline Morphology. Macromolecules 2009; 42(23):9325–31.

27. Varga J. *β-Modification of Isotactic Polypropylene:* Preparation, Structure, Processing, Properties and Application. Journal of Macromolecular Science, Part B: Physics 2002; 41(4-6):1121–71.

28. Romankiewicz A., Sterzynski T., Brostow W. *Structural characterization of α- and β-nucleated isotactic polypropylene.* Polymer International 2004; 53(12):2086–91.

29. Leugering H.J. *Einfluß der Kristallstruktur und der Überstruktur auf einige Eigenschaften von Polypropylen.* Macormoleculare Chemie 1967; 109(1):204–16.

30. Mathieu C., Thierry A., Wittmann J.C., Lotz B. *Specificity and Versatility of Nucleating Agents Toward Isotactic Polypropylene Crystal Phases.* Journal of Polymer Science Part B: Polymer Physics 2002; 40(22):2504–15.

31. Libster D., Aserin A., Garti N. *A novel dispersion method comprising a nucleating agent solubilized in a microemulsion, in polymeric matrix:* I. Dispersion method and polymer characterization. Journal of Colloid and Interface Science 2006; 299(1):172–81.

32. Mohmeyer N., Schmidt H.-W., Kristiansen P.M., Altstädt V. *Influence of Chemical Structure and Solubility of Bisamide Additives on the Nucleation of Isotactic Polypropylene and the Improvement of Its Charge Storage Properties.* Macromolecules 2006; 39(17):5760–7.

33. van Krevelen D.W., te Nijenhuis K., editors. *Properties of Polymers.* 4th Ed. Amsterdam: Elsevier Sc ience; 2009.

34. Galeski A. *Nucleation. In:* Karger-Kocsis J, editor. Polypropylene: An A-Z reference. Dordrecht: Springer Netherlands; 2012.

35. van Krevelen D.W., te Nijenhuis K. *Crystallisation and Recrystallisation. In:* van Krevelen D.W., te Nijenhuis K., editors. Properties of Polymers. 4th Ed. Amsterdam: Elsevier Sc ience; 2009.

36. Hoffmann K., Huber G., Mäder D. *Nucleating and Clarifying Agents for Polyolefins.* Macromolecular Symposia 2001; 176(1):83–92.

37. Beck H.N., Ledbetter H.D. *DTA Study of Heterogeneous Nucleation of Crystallization in Polypropylene.* Journal of Applied Polymer Science 1965; 9(6):2131–42.

38. Binsbergen F., Delange B. *Heterogeneous nucleation in the crystallization of polyolefins:* Part 2. Kinetics of crystallization of nucleated polypropylene. Polymer 1970; 11(6):309–32.

39. Fairgrieve S. *Nucleating Agents.* London; 2005. Rapra Review Report 187.

40. Beck H.N. *Heterogeneous Nucleating Agents for Polypropylene Crystallization.* Journal of Applied Polymer Science 1967; 11(5):673–85.

41. Binsbergen F.L. *Heterogeneous nucleation of crystallization.* Progress in Solid State Chemistry 1973; 8:189–238.

42. Binsbergen F.L. *Heterogeneous nucleation in the crystallization of polyolefins:* Part 1. Chemical and physical nature of nucleating agents. Polymer 1970; 11(5):253–67.

43. Zhao X.E., Dotson D.L., inventors; Milliken & Company. *Bicyclo[2.2.1]heptane dicarbocylate salts as Polyolefin Nucleators.* US 6,465,551. 2002.

44. Dotson D.L., inventor; Milliken & Company. *Disodium hexahydrophthalate salt compositions and nucleated polymers comprising such compositions.* US 6,562,890. 2003.

45. Blomenhofer M., Ganzleben S., Hanft D., Schmidt H.-W., Kristiansen M., Smith P. et al. *"Designer" Nucleating Agents for Polypropylene.* Macromolecules 2005; 38(9):3688–95.

46. Schmidt H.-W., Blomenhofer M., Stoll K., Meier H.-R., inventors; CIBA Specialty Chemicals Corporation. *Resin compositons.* US 2007/0149663. 2007.

47. Takahashi M., Tobita E., inventors; Asahi Denka Kogyo Kabushiki Kaisha. *Crystalline Polymer Composition.* US 6,184,275. 2001.

48. Nakahara Y., Akutsu M., Haruna T., Takahashi M., inventors. *Bis-Phenol Phosphates as Clarifiers for Polyolefin Resins.* US 4,463,113. 1984.

49. Sherman LM. *New Clarifiers & Nucleators:* They Make Polypropylene Run Clearer and Faster. Plastics Technology 2002; 7:44.

50. Lee D.-H., Yoon K.-B. *Effect of Polycyclopentene on Crystallization of Isotactic Polypropylene.* Journal of Applied Polymer Science 1994; 54:1507–11.

51. Bernland K., Smith P. *Nucleating Polymer Crystallization with Poly(tetrafluoroethylene) Nanofibrils.* Journal of Applied Polymer Science 2009; 114(1):281–7.

52. Okesola B.O., Vieira V.M.P., Cornwell D.J., Whitelaw N.K., Smith D.K. *1,3:2,4-Dibenzylidene-D-sorbitol (DBS) and its derivatives - efficient, versatile and industrially-relevant low-molecular-weight gelators with over 100 years of history and a bright future.* Soft Matter 2015; 11(24):4768–87.

53. Hamada K, Uchiyama H, inventors; E.C. Chemical Industries & Co, Ltd.; C. Itoh & Co., Ltd.,. *Polyolefin Plastic Compositions.* US 4,016,118. 1977.

54. Toshiaki K., Tomio N., inventors; New Japan Chemical Company Ltd. *Modification of Polypropylene.* JP 53117044. 1978.

55. Rekers J.W., inventor; Milliken Research Coropration. *Bis(3,4-dialkylbenzylidene)sorbitol acetals and compostions containing same.* US 5,049,605. 1991.

56. Xie C., Li J., Rieth L.R., Smith J.A., Anderson J.D.O., Waybright S.M. et al., inventors; Milliken & Company. *Method of nucleating a polyolefin compositon with acetal-based compounds.* US 7,157,510. 2007.

57. Millner O.E., Clarke R.P., Titus G.R., inventors; Becton Dickinson and Company. *Clarifiers for polyolefins and polyolefin compositions containing same.* EP 0463588. 1992.

58. Pukánszky B. *Optical clarity of polypropylene products. In:* Karger-Kocsis J, editor. Polypropylene: An A-Z reference. Dordrecht: Springer Netherlands; 2012. p. 554–61.

59. Nagarajan K., Levon K., Myerson A.S. *Nucleating Agents in Polypropylene.* Journal of Thermal Analysis and Calorimetry 2000; 59:497–508.

60. Shepard T.A., Delsorbo C.R., Louth R.M., Walborn J.L., Norman D.A., Harvey N.G. et al. *Self-Organization and Polyolefin Nucleation Efficacy of 1,3:2,4-Di-p-Methylbenzylidene Sorbitol.* Journal of Polymer Science Part B: Polymer Physics 1997; 35(16):2617–28.

61. Thierry A., Straupé C., Lotz B., Wittmann J.C. *Physical gelation: a path towards 'ideal' dispersion of additives in polymers.* Polymer communications 1990; 31(8):299–301.

62. Lotz B., Thierry A. *Polymer Crystals: Epitaxial Growth. In:* Buschow K.H.J., Chan R.W., Flemings M.C., Ilschner B., editors. Encyclopedia of Materials: Science and Technology. Amsterdam: Elsevier; 2001. p. 7267–72.

63. Wittmann JC, Lotz B. *Epitaxial Crystallization of Polymers on Organic and Polymeric Substrates.* Progress in Polymer Science 1990; 15(6):909–48.

64. Lotz B., Wittmann J.-C. *Epitaxy of helical polyolefins: Polymer blends and polymer-nucleating agent systems.* Macromolecular Chemistry and Physics 1984; 185(9):2043–52.

65. Mathieu C., Thierry A., Wittmann J.C., Lotz B. *"Multiple" nucleation of the (010) contact face of isotactic polypropylene, α phase.* Polymer 2000; 41(19):7241–53.

66. Zhang Y.-F., Xin Z. *Effects of substituted aromatic heterocyclic phosphate salts on properties, crystallization, and melting behaviors of isotactic polypropylene.* Journal of Applied Polymer Science 2006; 100(6):4868–74.

67. Yoshimoto S., Ueda T., Yamanaka K., Kawaguchi A., Tobita E., Haruna T. *Epitaxial act of sodium 2,2′-methylene-bis-(4,6-di-t-butylphenylene)phosphate on isotactic polypropylene.* Polymer 2001; 42(23):9627–31.

68. Libster D, Aserin A., Garti N. *Advanced nucleating agents for polypropylene.* Polymers for Advanced Technologies 2007; 18(9):685–95.

69. Lipp J., Shuster M., Terry A.E., Cohen Y. *Fibril Formation of 1,3:2,4-Di(3,4-dimethylbenzylidene) Sorbitol in a Polypropylene Melt.* Langmuir 2006; 22(14):6398–402.

70. Thierry A, Straupé C., Wittmann J.-C., Lotz B. *Organogelators and Polymer Crystallisation.* Macromolecular Symposia 2006; 241(1):103–10.

71. Fillon B., Lotz B., Thierry A., Wittmann J.C. *Self-Nucleation and Enhanced Nucleation of Polymers. Definition of a Convenient Calorimetric "Efficiency Scale" and Evaluation of*

Nucleating Additives in Isotactic Polypropylene (α Phase). Journal of Polymer Science Part B: Polymer Physics 1993; 31(10):1395–405.

72. Kristiansen M., Werner M., Tervoort T., Smith P., Blomenhofer M., Schmidt H.-W. *The Binary System Isotactic Polypropylene/Bis(3,4-dimethylbenzylidene)sorbitol: Phase Behavior, Nucleation, and Optical Properties.* Macromolecules 2003; 36(14):5150–6.

73. Marco C., Ellis G., Gómez M.A., Arribas J.M. *Comparative study of the nucleation activity of third-generation sorbitol-based nucleating agents for isotactic polypropylene.* Journal of Applied Polymer Science 2002; 84(13):2440–50.

74. Thierry A., Fillon B., Straupé C., Lotz B., Wittmann J.C. *Polymer nucleating agents: Efficiency scale and impact of physical gelation.* Solidification Processes in Polymers 1992; 87:28–31.

75. Kim C.Y., Kim Y.C., Kim S.C. *Temperature Dependence of the Nucleation Effect of Sorbitol Derivatives on Polypropylene Crystallization.* Polymer Engineering and Science 1993; 33(22):1445–51.

76. Garg S.N., Stein R.S., Su T.K., Tabar R.J., Misra A. *Light Scattering Studies of Nucleation of Polypropylene. In:* Family F., Landau D.P., editors. Kinetics of aggregation and gelation. Amesterdam: North-Holland; 1984. p. 229–34.

77. Bernland K., Tervoort T., Smith P. *Phase behavior and optical- and mechanical properties of the binary system isotactic polypropylene and the nucleating/clarifying agent 1,2,3-trideoxy-4,6:5,7-bis-O-[(4-propylphenyl) methylene]-nonitol.* Polymer 2009; 50(11):2460–4.

78. Bernland K., Goossens J.G.P., Smith P., Tervoort T.A. *On Clarification of Haze in Polypropylene.* Journal of Polymer Science Part B: Polymer Physics 2016; 54(9):865–74.

79. Tenma M, Yamaguchi M. *Structure and properties of injection-molded polypropylene with sorbitol-based clarifier.* Polym. Eng. Sci. 2007; 47(9):1441–6.

80. Smith T.L., Masilamani D., Bui L.K., Khanna Y.P., Bray R.G., Hammond W.B. et al. *The Mechanism of Action of Sugar Acetals as Nucleating Agents for Polypropylene.* Macromolecules 1994; 27(12):3147–55.

81. Millner O., Titus G. *Becton Dickinson Scientists Employ Computational Chemistry to Design Clarifying Additives for Polypropylene.* Chemical Design Automation News 1990; 5(10).

82. Marco C., Ellis G., Gómez M.A., Arribas J.M. *Analysis of the Dynamic Crystallisation of Isotactic Polypropylene/ α-Nucleating Agent Systems by DSC.* Journal of Thermal Analysis and Calorimetry 2002; 68(1):61–74.

83. Weidinger A., Hermans P.H. *On the Determination of the Crystalline Fraction of Polyethylenes from X-Ray Diffraction.* Macromolecular Chemistry and Physics 1961; 50(1):98–115.

84. Gahleitner M., Grein C., Kheirandish S., Wolfschwenger J. *Nucleation of Polypropylene Homo- and Copolymers.* International Polymer Processing 2011; 26(1):2–20.

85. Yamasaki S., Tsutsumi H. *The Dependence of the Polarity of Solvents on 1,3:2,4-Di-O-benzylidene-D-sorbitol Gel.* Bulletin of the Chemical Society of Japan 1995; 68(1):123–7.

86. Yamasaki S., Ohashi Y., Tsutsumi H., Tsujii K. *The Aggregated Higher-Structure of 1,3:2,4-Di-O-benzylidene-D-sorbitol in Organic Gels.* Bulletin of the Chemical Society of Japan 1995; 68(1):146–51.

87. Raluca S., Ott C., Sulca N., Lungu A., Iovu H. *Functionalized D-Sorbitol-Based Organogelators for Dental Materials (I).* Materiale Plastice 2009; 46(3):230–5.

88. Watase M., Nakatani Y., Itagaki H. *On the Origin of the Formation and Stability of Physical Gels of Di-O-benzylidene-D-sorbitol.* The Journal of Physical Chemistry B 1999; 103(13):2366–73.

89. Watase M, Itagaki H. *Thermal and Rheological Properties of Physical Gels Formed from Benzylidene-D-sorbitol Derivatives.* Bulletin of the Chemical Society of Japan 1998; 71(6):1457–66.

90. Smith D.K. *Molecular gels - underpinning nanoscale materials with organic chemistry.* Tetrahedron 2007; 63(31):7283–4.

91. Muro-Small M.L., Chen J., McNeil A.J. *Dissolution Parameters Reveal Role of Structure and Solvent in Molecular Gelation.* Langmuir 2011; 27(21):13248–53.

92. Rohner S.S., Ruiz-Olles J., Smith D.K. *Speed versus stability – structure-activity effects on the assembly of two-component gels.* RSC Advances 2015; 5(34):27190–6.

93. Den P.F., Feng Y.Q., Xu F.H., Song J. *Synthesis of Organic Gelatores Based on Acetal Condensed from Sorbitol and Derived Benzaldehyde and the Properties of Gels Prepared from Various Solvents.* Fine Chemicals 2007; 24(11):1056–60.

94. Neanu C., Lascu A., Csunderlik C. *Synthesis of Benzylidene Acetals of N-Acetyl-N-Methyl Glucamine.* Revue Roumaine de Chimie 2007; 52(8-9):869–74.

95. Shing T.K.M. *Enantiospecific Synthesis of D-mannono-* δ*-lactam from Vitamin C.* Journal of the Chemical Society, Chemical Communications 1988; (18):1221.

96. Andrews G.C., Crawford T.C., Bacon B.E. *Stereoselective, Catalytic Reduction of L-Ascorbic Acid: A Convenient Synthesis of L-gulono-1,4-lactone.* The Journal of Organic Chemistry 1981; 46(14):2976–7.

97. Liu Z., Yoshihara A., Wormald M.R., Jenkinson S.F., Gibson V., Izumori K. et al. *L-Fucose from Vitamin C with Only Acetonide Protection.* Org Lett 2014; 16(21):5663–5.

98. Soriano D.S., Meserole C.A., Mulcahy F.M. *Catalytic Hydrogenation of L-Ascorbic Acid (Vitamin C): A Stereoselective Process for the Production of L-Gulono-1, 4-Lactone.* Synthetic Communications 1995; 25(20):3263–5.

99. Crawford TC, Breitenbach R. *New Syntheses of L-Ascorbic Acid (Vitamin C).* Journal of the Chemical Society, Chemical Communications 1979; (9):388.

100. Crawford T.C., inventor; Pfizer Inc. *Process for preparing 3,5:4,6-protected derivatives of L- or D-gulonic acid, their use in preparing 2-keto-L- or D-gulonic acid or thier esters of L- or D-ascorbic acid, and certain novel 2-nitrato-gulonate intermediates.* EP 0000243. 1978.

101. Ōhashi K., Kikuchi Y., Yamazaki S., Nishizawa Y., Takaishi N., inventors; Kao Corporation. *Dibenzylidenated Polyhydric Alcohol Derivative.* JP H0267285. 1990.

102. Lee D., Williamson C.L., Chan L., Taylor M.S. *Regioselective, Borinic Acid-Catalyzed Monoacylation, Sulfonylation and Alkylation of Diols and Carbohydrates: Expansion of Substrate Scope and Mechanistic Studies.* J Am Chem Soc 2012; 134(19):8260–7.

103. Flamigni L., Ventura B., Tasior M., Becherer T., Langhals H., Gryko D.T. *New and Efficient Arrays for Photoinduced Charge Separation Based on Perylene Bisimide and Corroles.* Chemistry A European Journal 2008; 14(1):169–83.

104. Menche D., Hassfeld J., Li J., Rudolph S. *Total Synthesis of Archazolid A.* J Am Chem Soc 2007; 129(19):6100–1.

105. Alperstein D., Knani D. *In silico studies of 1,3(R):2,4(S)-dibenzylidene-D-sorbitol as a gelator for polypropylene.* Polymers for Advanced Technologies 2013; 24(4):391–7.

106. Li J., Fan K., Guan X., Yu Y., Song J. *Self-Assembly Mechanism of 1,3:2,4-Di(3,4-dichlorobenzylidene)-D-sorbitol and Control of the Supramolecular Chirality.* Langmuir 2014; 30(44):13422–9.

107. Song J., Sun H., Sun S., Feng R. *Synthesis and Gel Properties of Sorbitol Derivative Gelators.* Transactions of Tianjin University 2013; 19(5):319–25.

108. Tenma M., Mieda N., Takamatsu S., Yamaguchi M. *Structure and Properties for Transparent Polypropylene Containing Sorbitol-Based Clarifier.* Journal of Polymer Science Part B: Polymer Physics 2008; 46(1):41–7.

109. Hanabusa K., Tange J., Taguchi Y., Koyama Toshiki, Shirai H. *Small molecular gelling agents to harden organic liquids: alkylamide of N-benzyloxycarbonyl-L-valyl-L-valine.* Journal of the Chemical Society, Chemical Communications 1993; (4):390–2.

110. Tolinski M. *Additives for Polyolefins:* Getting the most out of Polypropylene, Polyethylene, and TPO. 2nd Ed.: Plastics Design Library - Elsevier; 2015.

111. Padden F.J., Keith H.D. *Spherulitic Crystallization in Polypropylene.* Journal of Applied Physics 1959; 30(10):1479–84.

112. Menyhárd A., Gahleitner M., Varga J., Bernreitner K., Jääskeläinen P., Øysæd H. et al. *The influence of nucleus density on optical properties in nucleated isotactic polypropylene.* European Polymer Journal 2009; 45(11):3138–48.

113. Horváth Z., Gyarmati B., Menyhárd A., Doshev P., Gahleitner M., Varga J. et al. *The role of solubility and critical temperatures for the efficiency of sorbitol clarifiers in polypropylene.* RSC Advances 2014; 4(38):19737–45.

114. Marco C., Ellis G., Gómez M.A., Arribas J.M. *Analysis of the Isothermal Crystallization of Isotactic Polypropylene Nucleated with Sorbitol Derivatives.* Journal of Applied Polymer Science 2003; 88(9):2261–74.

115. Phillips R.A., Wolkowicz M.D. *Structure and Morphology. In:* Pasquini N, editor. Polypropylene handbook. 2nd Ed. Munich: Hanser; 2005.

116. Jacoby P. *The Use of Beta Nucleation to Improve the Properties and Lower the Cost of Polypropylene Geogrids. In:* Li G., Chen Y., Tang X., editors. Geosynthetics in Civil and Environmental Engineering. Berlin: Springer; 2009. p. 74–7.

117. Goldstein M., Michalik E.R. *Theory of Scattering by an Inhomogeneous Solid Possessing Fluctuations in Density and Anisotropy.* Journal of Applied Physics 1955; 26(12):1450–7.

118. Keane J.J., Stein R.S. *The scattering of light from thin polymer films. II. Scattering from polyethylene.* Journal of Polymer Science 1956; 20(95):327–50.

119. Stein R.S., Misra A., Yuasa T., Khambatta F. *Recent Studies of Light Scattering from Polymer Films.* Pure and Applied Chemistry 1977; 49(7).

120. Yoon D.Y., Stein R.S. *Effect of interference between anisotropic scattering entities on light scattering from polymer films. II. The correlation function approach.* Journal of Polymer Science: Polymer Physics Edition 1974; 12(4):735–61.

121. Zhao Y., Vaughan A.S., Sutton S.J., Swingler S.G. *On the crystallization, morphology and physical properties of a clarified propylene/ethylene copolymer.* Polymer 2001; 42(15):6587–97.

122. Abraham F., Ganzleben S., Hanft D., Smith P., Schmidt H.-W. *Synthesis and Structure of Efficiency Relations of 1,3,5-Benzenetrisamides as Nucleating Agents and Clarifiers for Isotactic Poly(propylene).* Macromolecular Chemistry and Physics 2010; 211(2):171–81.

123. Varga J., Mudra I., Ehrenstein G.W. *Highly active thermally stable β-nucleating agents for isotactic polypropylene.* Journal of Applied Polymer Science 1999; 74(10):2357–68.

124. Menyhárd A., Varga J., Molnár G. *Comparison of different -nucleators for isotactic polypropylene, characterisation by DSC and temperature-modulated DSC (TMDSC) measurements.* Journal of Thermal Analysis and Calorimetry 2006; 83(3):625–30.

125. Li J.X., Cheung W.L. *Pimelic acid-based nucleating agents for hexagonal crystalline polypropylene.* Journal of Vinyl and Additive Technology 1997; 3(2):151–6.

126. Kristiansen P.M., Gress A., Smith P., Hanft D., Schmidt H.-W. *Phase behavior, nucleation and optical properties of the binary system isotactic polypropylene/N,N′,N″-tris-isopentyl-1,3,5-benzene-tricarboxamide.* Polymer 2006; 47(1):249–53.

127. Abraham F., Schmidt H.-W. *1,3,5-Benzenetrisamide based nucleating agents for poly(vinylidene fluoride).* Polymer 2010; 51(4):913–21.

128. Meijer-Vissers T., Goossens H. *The Influence of the Cooling Rate on the Nucleation Efficiency of Isotactic Poly(propylene) with Bis(3,4-dimethylbenzylidene)sorbitol.* Macromolecular Symposia 2013; 330(1):150–65.

129. Marco C., Gómez M.A., Ellis G., Arribas J.M. *Highly Efficient Nucleating Additive for Isotactic Polypropylene Studied by Differential Scanning Calorimetry.* Journal of Applied Polymer Science 2002; 84(9):1669–79.

130. Lamberti G. *Isotactic polypropylene crystallization: Analysis and modeling.* European Polymer Journal 2011; 47(5):1097–112.

131. Ma Z., Steenbakkers R.J.A., Giboz J., Peters G.W.M. *Using rheometry to determine nucleation density in a colored system containing a nucleating agent.* Rheologica Acta 2011; 50(11-12):909–15.

132. de Santis F., Pantani R. *Nucleation density and growth rate of polypropylene measured by calorimetric experiments.* Journal of Thermal Analysis and Calorimetry 2013; 112(3):1481–8.

133. Menyhárd A., Bredács M., Simon G., Horváth Z. *Determination of Nucleus Density in Semicrystalline Polymers from Nonisothermal Crystallization Curves.* Macromolecules 2015; 48(8):2561–9.

134. Chen J.-H., Chang Y.-L. *Isothermal Crystallization Kinetics and Morphology Development of Isotactic Polypropylene Blends with Atactic Polypropylene.* Journal of Applied Polymer Science 2007; 103(2):1093–104.

135. Mubarak Y., Harkin-Jones E., Martin P.J., Ahmad M. *Crystallization of Isotactic Polypropylene: Comparison Between alpha and beta Growth Rates*. In: 58th Society of Plastics Engineers - ANTEC; 2000.

136. Avrami M. *Kinetics of Phase Change. I General Theory.* The Journal of Chemical Physics 1939; 7(12):1103–12.

137. Avrami M. *Kinetics of Phase Change. II Transformation‐Time Relations for Random Distribution of Nuclei.* The Journal of Chemical Physics 1940; 8(2):212–24.

138. Lamberti G. *A direct way to determine iPP density nucleation from DSC isothermal measurements.* Polymer Bulletin 2004; 52(6):443–9.

139. Kantz M.R., Newman H.D., Stigale F.H. *The Skin-Core Morphology and Structure-Property Relationships in Injection-Molded Polypropylene.* Journal of Applied Polymer Science 1972; 16(5):1249–60.

140. Bai H., Wang Y., Song B., Li Y., Liu L. *Detecting Crystallization Structure Evolution of Polypropylene Injection‐Molded Bar Induced by Nucleating Agent.* Polymer Engineering & Science 2008; 48(8):1532–41.

141. Norton D.R., Keller A. *The spherulitic and lamellar morphology of melt-crystallized isotactic polypropylene.* Polymer 1985; 26(5):704–16.

142. Yeh C.F., Su A.C., Chen M., Sugimoto R. *Changes in Optical Texture of α-Spherulites of Isotactic Polypropylene upon Partial Melting and Recrystallization.* Journal of Polymer Research 1995; 2(3):139–46.

143. Awaya H. *Morphology of different types of isotactic polypropylene spherulites crystallized from melt.* Polymer 1988; 29(4):591–6.

144. Fraser G.V., Keller A., Odell J.A., Wills H.H. *The Influence of Nucleation Density and Cooling Rate on Crystallization of Polyethylene from the Melt.* Journal of Applied Polymer Science 1978; 22(10):2979–89.

145. Brandrup J., Immergut E.H., Grulke E.A. *Polymer handbook.* 4th Ed. New York: Wiley-Interscience; 2004.

146. Jervis D.A. *Optical brighteners: improving the colour of plastics.* Plastics, Additives and Compounding 2003; 5(6):42–6.

147. Balzano L., Portale G., Peters G.W.M., Rastogi S. *Thermoreversible DMDBS Phase Separation in iPP: The Effects of Flow on the Morphology.* Macromolecules 2008; 41(14):5350–5.

148. Housmans J.-W., Gahleitner M., Peters G.W.M., Meijer H.E.H. *Structure–property relations in molded, nucleated isotactic polypropylene.* Polymer 2009; 50(10):2304–19.

149. Wang K., Mai K., Zeng H. *Isothermal Crystallization Behavior and Melting Characteristics of Injection Sample of Nucleated Polypropylene.* Journal of Applied Polymer Science 2000; 78(14):2547–53.

150. Mercier J.P. *Nucleation in Polymer Crystallization: A Physical or a Chemical mechanism?* Polymer Engineering & Science 1990; 30(5):270–8.

151. Seven K.M., Cogen J.M., Gilchrist J.F. *Nucleating Agents for High-Density Polyethylene - A Review.* Polymer Engineering & Science 2016; 56(5):541–54.

152. Simanke A.G., Azeredo AP de, de Lemos C., Mauler R.S. *Influence of nucleating agent on the crystallization kinetics and morphology of polypropylene.* Polímeros 2016; 26(2):152–60.

153. Failla M.D., Lucas J.C., Mandelkern L. *Supermolecular Structure of Random Copolymers of Ethylene.* Macromolecules 1994; 27(6):1334–7.

154. Hosier I.L., Alamo R.G., Lin J.S. *Lamellar morphology of random metallocene propylene copolymers studied by atomic force microscopy.* Polymer 2004; 45(10):3441–55.

155. Poon B., Rogunova M., Chum S.P., Hiltner A., Baer E. *Classification of Homogeneous Copolymers of Propylene and 1-Octene Based on Comonomer Content.* Journal of Polymer Science Part B: Polymer Physics 2004; 42(23):4357–70.

156. ASTM D 1003. *Standard Test Method for Haze and Luminous Transmittance of Transparent Plastics*.

157. Willmouth F.M. *Transparency, Translucenncy and Gloss. In:* Meeten G.H., editor. Optical Properties of Polymers. London: Elsevier Applied Science; 1986. p. 265–333.

158. BYK-Gardner GmbH. *Haze-gard plus:* Operating Instructions.

159. ASTM E313. *Standard Practice for Calculating Yellowness and Whiteness Indices from Instrumentally Measured Color Coordinates*.

160. Hoechst AG. *Schematische Darstellung verschiedener Plastifizierschnecken f. Weber-Einschneckenextruder ET 20-25D*.

161. Thermo Fisher Scientific Inc. *Process 11:* Handbook.

162. Sigma-Aldrich. *L-Gulonic acid γ-lactone (95%):* #310301.

Felix Budde 18. Mai 2018

Flörsheimer Str. 8

60326 Frankfurt am Main

Erklärung

Ich erkläre hiermit, dass ich meine Dissertation selbstständig und nur mit den angegebenen Hilfsmitteln angefertigt habe und noch keinen Promotionsversuch unternommen habe.

Felix Budde

Felix Budde 18. Mai 2018

Flörsheimer Str. 8

60326 Frankfurt am Main

Erklärung der Übereinstimmung

Ich erkläre hiermit, dass die elektronische Version der Doktorarbeit mit der schriftlichen Version übereinstimmt. Die elektronische Version liegt dem Prüfungssekretariat vor.

Felix Budde

Curriculum Vitae

Name:	Felix Budde
Date of Birth:	24.01.1988
Place of Birth:	Beckum (North-Rhine Westphalia)
Nationality:	German

EDUCATION

11/2014 – 12/2017	Clariant Produkte (Deutschland) GmbH, Frankfurt a. M. PhD Thesis: “Development of novel nucleating and clarifying agents for polypropylene”
02/2015 – 12/2017	Fraunhofer Institute for Structural Durability and System Reliability LBF, Darmstadt
02/2014 – 05/2014	Clariant Produkte (Deutschland) GmbH, Frankfurt a. M. Master Thesis: “Beiträge zur Synthese aktiver und passiver Sauerstoffbarrieren auf organischer Basis für Polymere“
04/2012 – 05/2014	Heinrich-Heine-University, Düsseldorf Master of Science Business Chemistry
11/2011 – 03/2012	Henkel AG & Co. KGaA, Düsseldorf Bachelor Thesis: “Einfluss von Formel- und Prozessparametern auf das Herstell- und Applikationsverhalten von Toilettenreinigerprodukten”
10/2008 – 03/2012	Heinrich-Heine-University, Düsseldorf Bachelor of Science Business Chemistry
08/1998 – 06/2008	Gymnasium Laurentianum, Warendorf Abitur

Felix Budde